A Three-Dimensional Numerical Model for Predicting Pollutant and Sediment Transport Using an Eulerian-Lagrangian Marker Particle Technique

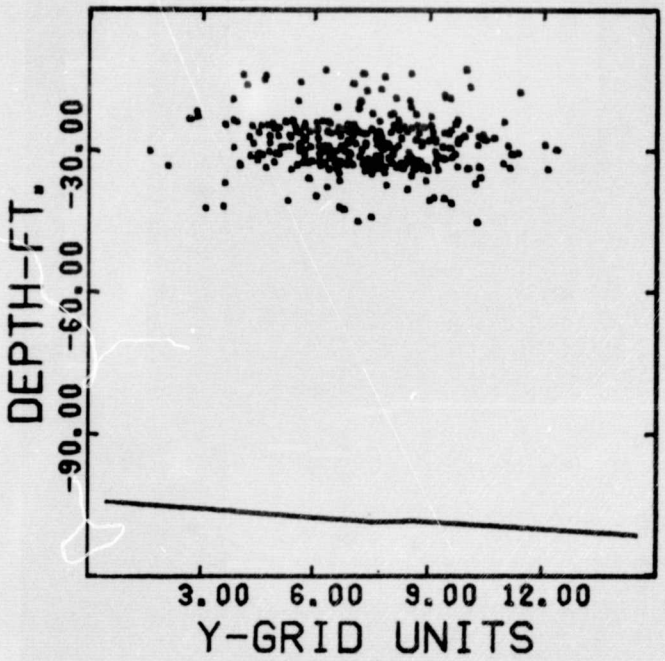

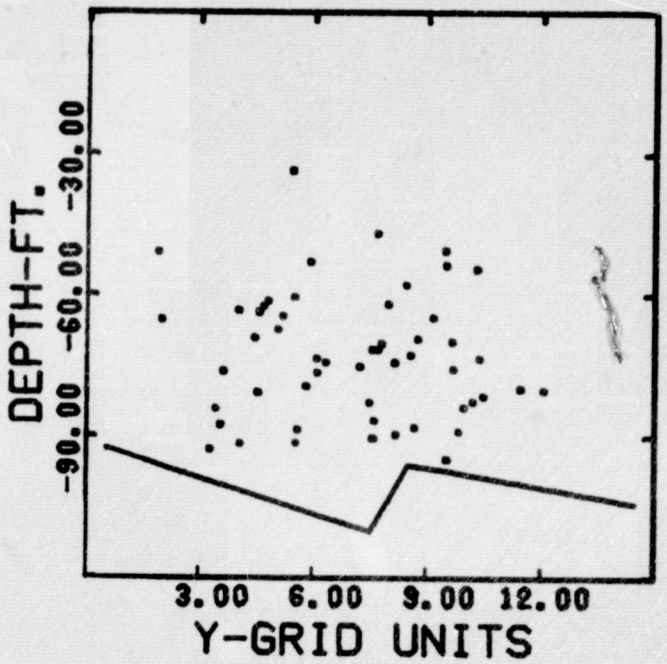

Danny Pavish
Malcolm Spaulding

DEPARTMENT OF OCEAN ENGINEERING
UNIVERSITY OF RHODE ISLAND KINGSTON, R. I. 02881

JULY 1977

INTERIM REPORT

TITLED

DEVELOPMENT AND APPLICATION OF A THREE DIMENSIONAL NUMERICAL MODEL FOR PREDICTING POLLUTANT AND SEDIMENT TRANSPORT USING AN EULERIAN-LAGRANGIAN MARKER PARTICLE TECHNIQUE

BY:

DANNY L. PAVISH

MALCOLM L. SPAULDING

OCEAN ENGINEERING DEPARTMENT

UNIVERSITY OF RHODE ISLAND

KINGSTON, RHODE ISLAND 02881

SPONSORED BY:

NATIONAL AERONAUTICS AND SPACE ADMINISTRATION

GRANT NSG 1008

LANGLEY RESEARCH CENTER

HAMPTON, VIRGINIA 23665

ABSTRACT

A computer coded Lagrangian marker particle in Eulerian finite difference cell solution to the three dimensional incompressible mass transport equation, Water Advective Particle in Cell Technique, WAPIC, was developed, verified against analytic solutions, and subsequently applied in the prediction of long term transport of a suspended sediment cloud resulting from an instantaneous dredge spoil release. Numerical results from WAPIC were verified against analytic solutions to the three dimensional incompressible mass transport equation for turbulent diffusion and advection of Gaussian dye releases in unbounded uniform and uniformly sheared uni-directional flow, and for steady-uniform plug channel flow. WAPIC was utilized to simulate an analytic solution for non-equilibrium sediment dropout from an initially vertically uniform particle distribution in one dimensional turbulent channel flow. Predicted sediment fallout rates and vertical concentration values, as a function of downstream distance were within an absolute accuracy of four percent of the analytic values.

The coastal zone mass transport version of the WAPIC algorithm employs a finite difference grid network which horizontally translates with the mean particle motion and expands with the dispersive growth of the marker particle cloud. The cartesian vertical co-ordinate of the three dimensional mass transport equation was transformed into dimensionless space, and then rearranged into flux

conservative, pseudo total velocity form, in order to allow adaptation to flow situations with a time and spatially varying bottom topography and free surface. A velocity processor was developed for the interpolation of velocities from a vertically averaged two dimensional velocity field of a tidally driven finite difference hydrodynamic numerical model. The transformed version of WAPIC was then coupled to the hydrodynamic velocity field by the velocity processor, and utilized to predict the long term diffusion and advection of dilute neutrally and negatively buoyant suspended sediment clouds resulting from an instantaneous release of barged dredge spoil at Brown's Ledge in Rhode Island Sound.

ACKNOWLEDGEMENTS

The author is indebted to many generous people who kindly offered their time and consideration, thus making this work possible. I wish to thank first of all, the members of my thesis committee, Dr. Malcolm Spaulding, Dr. Frank M. White, and Dr. Roger B. Dowdell. In particular the author wishes to thank: Dr. Spaulding, my admirable thesis advisor, who introduced me to field of numerical modeling, and provided many patient hours of discussion, critical insight, and hard work; Dr. Frank White who provided much needed assitance and discussion; Steve Hurlburt who developed the velocity processing program and provided the Rhode Island Sound two dimensional tidal velocity data ; Craig Swanson who provided valuable programming and computer graphics assistance; Dr. Clem Griscom of the Coastal Marine Resources Center; Sheldon Pratt of the Graduate School of Oceanography; the many people of the University of Rhode Island Academic Computer Center, specifically David Clayton, Roger Greenall, and Frank Caraccia; and Mrs. Leanne Mc Cullough, Mrs. Donna Gardiner of of the Dept. of Ocean Engineering, and Mrs. Virginia Obrien of the Office of Engineering Research who helped prepare sections of the manuscript. Last but not least, I wish to thank my steadfast colleague, Robert B. Gordon, to whom I owe much for his personal energy, insight, thought provoking discussions, and for introducing me to the works of Csanady, Roache, Leendertse, Hess, and

many others. This work was sponsored by a grant from the National Aeronautics and Space Administration, Langley Research Center, Hampton, Virginia.

TABLE OF CONTENTS

LIST OF TABLES

LIST OF FIGURES

LIST OF SYMBOLS

x	Horizontal Major Axis, X-Coordinate, Subscript
y	Horizontal Major Axis, Y-Coordinate, Subscript
z	Vertical Major Axis, Z-Coordinate, Subscript
η	Vertically Transformed Dimensionless Coordinate
t, T	Time
A	Viscous Drag Coefficient in Watson's Equation
C_o	Initial Average Concentration
c, c_i, c'	Mean, Instantaneous, Deviation from Mean, Value of Concentration
C_3	Skewness Coefficient
C_h	Chezy Coefficient
c_m	Manning Friction Factor
E	Excess Coefficient
h	Depth at M.S.L.
H	Total Depth = $h + \epsilon$
k	Von Karman Constant
K_x, K_y, K_z	x, y, z, Turbulent Diffusion or Dispersion Coefficients
l_x	Length scale of particle cloud
M_r	Moment Number Counter
n, N	Summation Counter
P_N, B_m	$\frac{n\pi}{H}$, $\frac{m\pi}{W}$, Width and Variable Summation Parameters
r	Summation Counter
R	Particle Radius

$R_{U_{i(t)}}$	Lagrangian Auto Correlation Coefficient
S	Pressure Drag Coefficient in Watson's Equation
t_L	Lagrangian Time Scale
V_o	Steady Uniform X-Current Velocity
u', v', w'	X, Y, Z Turbulent Deviations from Mean Velocity
U, V, W, ω	x, y, z, η Mean Advective Velocities
U_D, V_D, W_D, ω_D	x, y, z, η Turbulent Diffusion Velocities
U_T, V_T, W_T, ω_T	x, y, z, η Total Pseudo Transport Velocities
U_T^P, V_T^P, W_T^P, ω_T^P	x, y, z, η Total Pseudo Particle Velocities
U_T, V_T, W_T	x, y, z, Average Particle Velocity
W_S, ω_S	z, η Particle Settling Velocities
WH	Wave Height
WL	Wave Length
WT	Wave Period
α_n	Real Root of Transcendental Equation
α_p	Adjustable Coefficient for Calculating K_z
β	Dimensionless Fall Velocity
β_p	Adjustable Coefficient for Calculating K_z
Δ	Finite Difference Increment
$\vec{\nabla}$	Divergence Vector Operator
∂	Excess Coefficient
γ_2	Skewness Coefficient

∂	Partial Derivative Operator x, y, z, System
δ	Partial Derivative Operator x, y, η System
ϵ	Energy Dissipation Coefficient
ξ	Tide Height Relative to Mean Sea Level
η_p	Adjustable Coefficient for Calculating K_z
μ	Dynamic Viscosity
ρ_{FL}, ρ_p	Mass Density Fluid, Particle
σ_x, σ_y, σ_z	x, y, z, Standard Deviation
σ_{xo}, σ_{yo}, $\sigma_{z.o}$	x, y, z Initial Standard Deviations
τ	Lagrangian Time Lag
φ_3^2	Time of Shear Effect
Ω_y, Ω_z	Shear Rate of X-velocity in y, z Directions
ω	Dimensionless Vertical Velocity

I. INTRODUCTION & STATEMENT OF PROBLEM

Presently studies are in progress at the University of Rhode Island under the sponsorship of the U. S. Army Corps of Engineers concerning the feasibility and ecological impacts of the dumping of barged wastes in coastal areas such as Brown's Ledge. (1,2,3) From 1967 to 1970 approximately 8.2 million cubic yards of dredge spoil was deposited within a one square nautical mile site, four miles south of Newport, in Rhode Island Sound. The work of Saila, Pratt, and Polgar states that, within the limits of bathymetry measurements, practically little or no spoil was suspended during or after the disposal operation (2). Presently there is concern that sediment suspended in the water column by vertical turbulence during and after the disposal operation may drift into Rhode Island Sound recreation areas. As a coastal zone management tool, the following work attempts to numerically model the long term transport (1hr. - 2 day) of such wastes in the water column. WAPIC, a Lagrangian marker particle in Eulerian cell technique has been developed for simulating dilute sediment and particulate transport in a tidally dominated coastal zone environment.

A literature review by Johnson (4) of the U. S. Army Corps of Engineers Waterways Experiment station, states - " Very little mathematical modeling of the physical fate of dredged material disposed of in an aquatic environment has been undertaken." Pertinent to this study are the

mathematical models of Koh and Chang (5) and Krishnappan (6), which consider the short term fate of the waste release cloud as it drops from the surface until it collects on the bottom. Disposal of dredged sediment or bottom material in the coastal zone is accomplished with barges. While dredged waste is normally released by an instantaneous hopper release, sewage sludges are pumped in a liquid slurry through a pipe while the barge is under way, and acids and other chemicals are released continuously in the wake of a moving barge. Koh and Chang produced a numerical model designed to simulate all three of the previously mentioned modes of discharge. Barge disposal of dredged sediment in Rhode Island Sound was done by an instantaneous dumping in relatively shallow coastal areas of depths between 90-110 feet (1). Of interest is Koh and Chang's treatment of the instantaneous dumping operation.

Their model assumes that the descent of the waste cloud takes place in three stages, each stage being governed by a different mechanism. They are-

1. Convective cloud descent and entrainment
2. Cloud collapse
3. Long term cloud transport & settling (Figure 1-1)

During the first stage the negatively buoyant cloud descends and entrains water until neutral buoyancy is achieved. The assumption is made that the sediment laden cloud can be treated as a liquid of equivalent density falling through a less dense ambient medium. The sediment

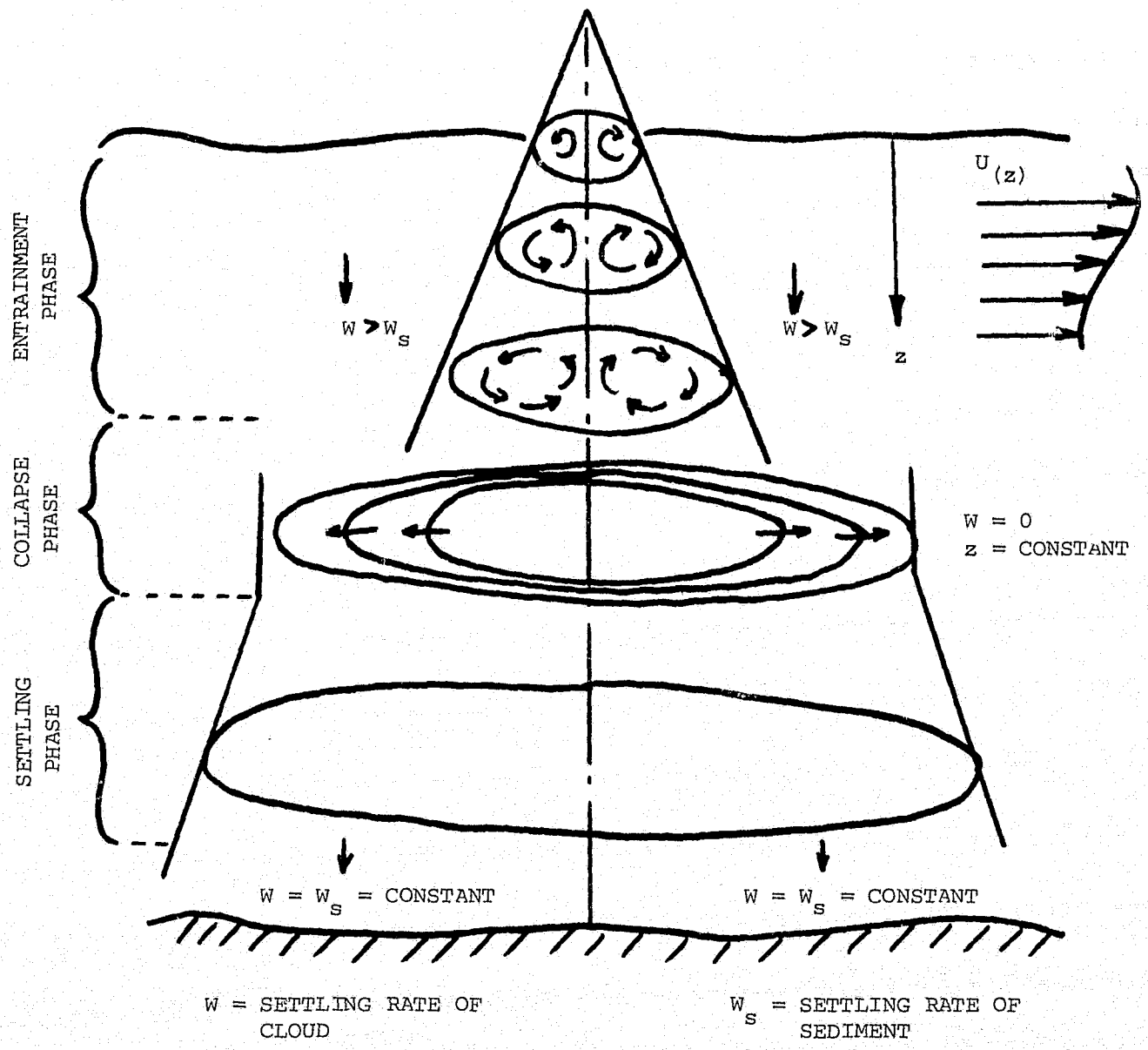

FIGURE 1.1 Koh and Chang's Mechanisms For Short Term Fallout of a Barged Instantaneous Waste Release

cloud which is now neutrally buoyant spreads horizontally at a constant vertical position due to liquid entrainment, in what is called the collapse stage. The assumption is made that the governing mechanism is the difference in hydrostatic pressure between the cloud and the ambient fluid. After the horizontal spreading stops the cloud of sediment particles undergoes vertical settling, and long term horizontal advection by the ambient current and turbulent diffusion due to this field. Koh and Chang's model assumes that the ambient current field is horizontally unidirectional and steady, and may vary in magnitude only in the vertical direction.

Krishnappan (6) developed a model for the determination of the size and height of a mound of sediment from an instantaneous release of dredge spoil in deep water with a turbulent one dimensional steady flow field. Laboratory experiments in still water showed that, the motion of uniformly sized particles can be treated in two stages, the initial entrainment phase, and the final settling phase. During the entrainment phase, the size of the particle cloud grows due to entrainment of ambient liquid while descent velocity decreases. During the settling phase, the fall velocity of the cloud is the same as the average settling velocity of the individual particles inside the cloud. In this stage, the cloud grows horizontally due to ambient turbulence, until it lands on the bottom.

Krishnappan disagrees with the assumptions used by Koh and Chang in the first stage, and also stated that the

collapse stage was unnecessary. Laboratory experiments showed that, during the entrainment or convective descent stage, the waste cloud must not be treated as a higher density liquid moving in an ambient fluid, but as a particle-liquid cloud or slurry moving through the water column. Results showed that the particle-liquid cloud did not increase in size throughout its first stage, while a liquid cloud of equivalent density continuously increases in horizontal size. The former grows until it reaches a constant size after which the cloud settles with decreasing velocity until it moves with the settling velocity of its particles. (Figure 1-2) His results further demonstrate that, when the depth of the water is less than a thousand meters, the settling phase will not occur. Thus in the Great Lakes or in shallow estuarine or coastal zone waters, the possiblities that the settling phase may occur are rare, and the entrainment phase will dominate until the particle cloud lands on the bottom. He states -

" Consequently models such as Koh and Chang's which devote considerable attention to the long term transport phase are unnecessarily elaborate."

The physical insight derived from Krishanppan's work is that barged sedimentary waste that is dumped instantaneously in relatively shallow water, such as Rhode Island Sound waters, falls to the bottom in the "entrainment phase" with very little if any of the spoil remaining in the water column within a few hours of the disposal operation. Observations by Saila et. al. (1)

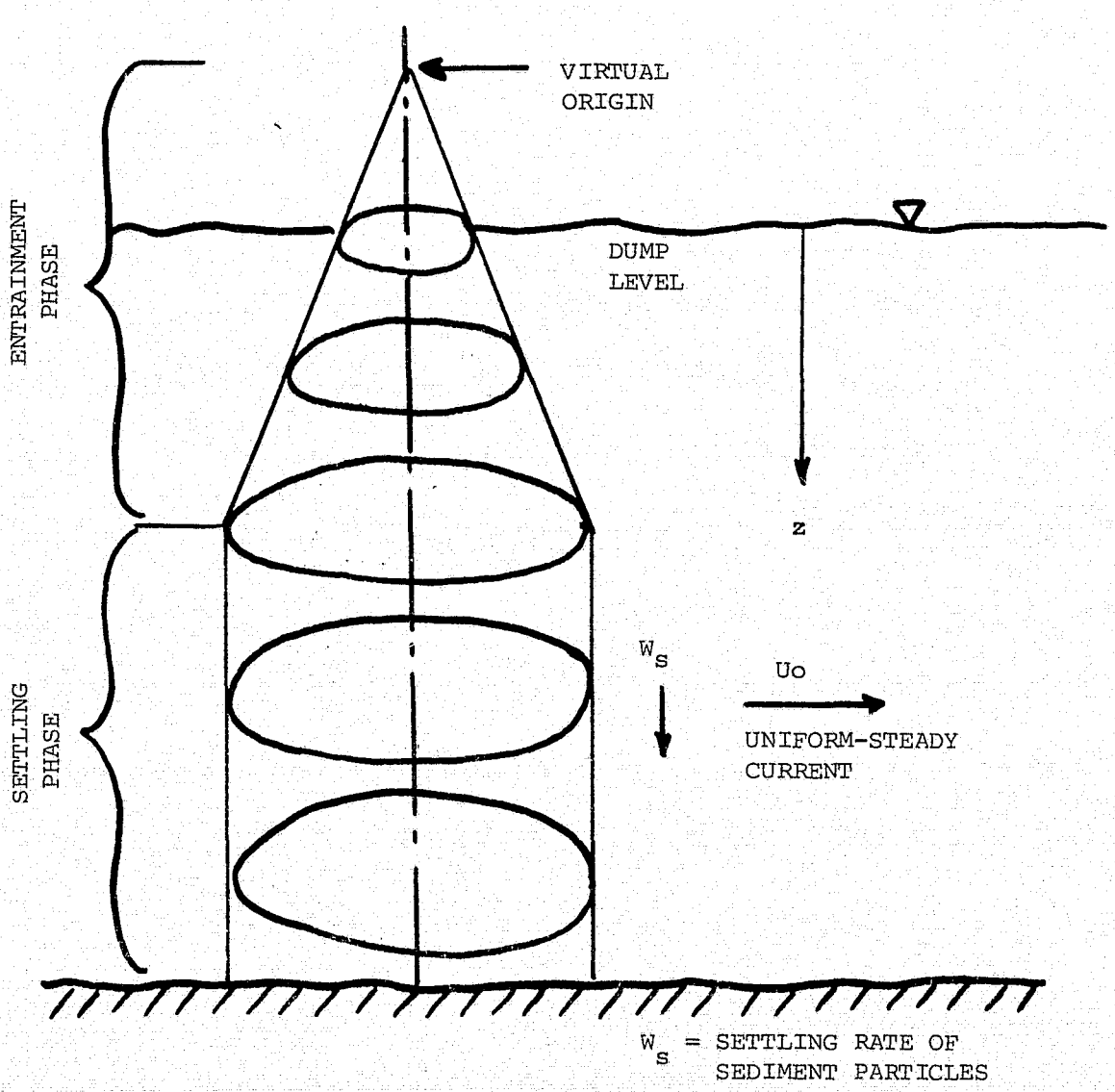

FIGURE 1.2 Krishnappan's Mechanisms For Short Term Fallout of a Barged Instantaneous Waste Release

support this conclusion.

Indeed a very conservative engineering estimate, in Rhode Island Sound waters, can be made assuming that a maximum of 1-5 % of the total spoil volume remains entrained in dilute form in the water column immediately following the disposal operation by the action of ambient turbulence. This cloud of sedimentary particles possessing near neutral buoyancy with still water settling rates of 0.001 to 0.03 ft/sec (for particle diameters ranging from 0.00005 to 0.00028 ft.) may remain in a water column 60 to 150 ft. deep for a time span of one to twenty four hours. Should the ambient turbulence be great enough to overcome the particle settling rates, the particles may be treated as if they were neutrally buoyant parcels of fluid. This cloud of visible turbidity will convect and diffuse with the ambient tidal and wind drift currents and turbulence to background levels.

The question might be asked - Why develop a long term transport model for this 1-5 % of the dredged waste which may remain in the water column ? Isn't this amount of material too miniscule to demand simulation ? The answer is no. First of all, this single barge disposal is repeated at least a hundred times to deposit three million cubic yards of sediment. Thus 1-5 barge loads of sediment waste will be entrained by the ambient current field, and advected and diffused across the coastal shelf, during this period of disposal operations. These dredged bottom sediments contain entrained pollutants in the form of

anaerobic sediments, heavy metals, PCB'S, etc. . Thus a biological oceanographer might be interested in the dispersal pattern of this cloud across the shelf as the particles eventually settle to the bottom. A single long term sediment transport simulation may provide estimates of the fallout patterns of this sediment and the entrained pollutants, ie., to demonstrate over what area the benthic environment is contaminated by the disposal operation.

A prediction of fallout or dispersal patterns of dilute suspended sedimentary particles in a turbulent tidally driven advective field requires the use of a three dimensional mass transport model of WAPIC'S capability. What is required is the ability to model the dispersal and settling patterns of non-buoyant dilute particulate matter in a coastal or estuarine environment.

A shortcoming of both Koh and Chang's and Krishnappan's work is the lack of proper treatment of the long term mass transport of the suspended plume by the spatial and temporally varying mean turbulent velocity field. In tidally driven waters such as Rhode Island Sound, the horizontal ambient velocity field is a complicated function of space and time. A cloud of suspended sediment particles will drift and diffuse with the tidal currents into areas where the flow field varies in magnitude and direction, from that found at the initial dump site. A long term transport treatment of suspended sediment in turbulent tidally dominated environment requires the coupling of a hydrodynamic velocity field with

a mass transport model. Spaulding and Hurlburt (8) and Hunter and Spaulding (7) have successfully coupled a two dimensional vertically averaged hydrodynamic model to two and three dimensional mass transport models, respectively, for predicting transport of neutrally buoyant dissolved constituents in Narragansett Bay and Rhode Island Sound waters respectively. Since these techniques are strictly Eulerian mass transport models, these methods cannot describe the settling or deposition patterns of discrete particles with varying settling rates. The following work is directed towards developing a numerical model for long term simulation (1hr. to 2 day) of sedimentary transport and deposition in estuarine and coastal waters. No effort has been made to improve upon Koh and Chang's and Krishnappan's 'short term' treatment of the descent of the dense sediment cloud to the bottom.

WAPIC, a three dimensional Lagrangian marker particle in Eulerian cell technique has been developed to simulate the long term transport and advection of dilute sedimentary and pollutant waste particles in the coastal zone and estuarine environment.

II. HISTORY of WAPIC

During the last ten years a considerable amount of work has been done in the area of mathematical modeling of transport phenomena in coastal and estuarine waters (9,10). Usually these numerical models make the assumption that the particulate or pollutant mass is dilute within the flow field. Numerical mass transport models for estuarine or coastal zone waters are concerned with water quality parameters such as dissolved oxygen (DO), biochemical oxygen demand (BOD), coliform decay, and larval growth rates and transport. (7,11,12)

Models have been developed that solve the incompressible mass transport equation in either one, two, or three dimensions. The solution viewpoint may be either purely Eulerian, Lagrangian, or a combination Eulerian-Lagrangian. In the ideal Lagrangian approach, the fluid or flow field is assumed to be divided into numerous finite size zones each of which represents a parcel of fluid. This mesh of cells flows along as the fluid flows in a manner characterized by the approximation to the partial differential equation of mass transport (Harlow (13)). Pure Lagrangian models for estuarine or tidal pollutant transport have been developed by Fischer (14), and Wallis (15). These models seem to enjoy success when a complicated flow field may be broken up into one dimensional segments or volumes.

The pure Eulerian scheme, divides the fluid field into a fixed mesh of cells or elements. This mesh is fixed in

space, and the fluid and particulates move through the mesh. The Eulerian schemes may be subdivided into two types of solution procedures, the finite difference and finite element methods. The finite difference schemes divide the regime into rectangular grids with the dependent variables defined at either the cell corners, centers or faces. The partial differentials are linearly approximated across these grids (16). Finite difference schemes may be further subdivided into the explicit and implicit methods of solution advancement in time. The explicit solution technique solves algebraically for the new value of the dependent variable from the previous value (16). The implicit techniques solves for the new value at time $t + \Delta t$ using advanced time values, requiring the use of iterative or Gaussian elimination techniques (16). Recently, in the field of estuarine pollutant transport modeling, two dimensional models have been popular, where the third dimensional independent variable has been removed by integration techniques (11,17,18). The alternating direction implicit technique, ADI, has also enjoyed success in two dimensional hydrodynamic and mass transport models by Leendertse (19), Hess and White (18), and Spaulding (20). The ADI method has been utilized by Hunter and Spaulding (7) in a three dimensional model for coliform decay and transport in the Providence River .

The second type of Eulerian scheme, the finite element technique, seems particularly well suited for modeling mass transport in situations with complicated boundaries that

finite difference techniques might find difficult to resolve. This method divides the zone of flow into triangular or quadrilateral elementsments with the dependent variables defined at the nodes of the triangles. A popular finite element technique solution technique is the Galerkin method of weighted residuals. A review and explanation of this solution technique may be found in the works of Wang (21), and Leimkuhler (22). Leimkuhler has recently completed a two dimensional vertically averaged finite element model for simulating sediment transport in Massachusetts Bay. Krone and Ariathurai (23) developed a one dimensional finite element model for determining sediment transport in the Savannah River estuary.

Interestingly, both finite element and finite difference Eulerian techniques share the following shortcomings in their computational procedures:

1. Fictitious diffusion

Fictitious diffusion is especially noticeable since each cell is forced to be homogeneous. When a material enters a cell all its properties are uniformly diffused throughout the Eulerian cell. The magnitude of this fictitious diffusion depends on the length and time scale of the numerical simulation.

2. Production of severly depressed concentration gradients upstream of point source waste loads.

3. Difficulty in handling scale dependent diffusion processes which are common in ocean and coastal zone regions.

4. Difficulty in representing an effluent of various particle sizes and density or buoyancy characteristics.

The steps leading to a practical solution to these problems which are inherent in pure Eulerian schemes for turbulent mass transport can be traced in the development of Lagrangian- Eulerian numerical methods.

In 1957, Evans and Harlow (24) of the Los Alamos Scientific Laboratory introduced the Particle in Cell, PIC, method. This numerical procedure was developed for the simulation of problems involving the dynamics of compressible fluids in two dimensions (13). This hybrid technique requires two computational meshes or systems one Eulerian, the other Lagrangian. The domain through which the fluid flows is a fixed Eulerian mesh of computational cells. The fluid or mass is represented by particles with physical mass, energy,and velocity (etc.) which move through the Eulerian mesh. As stated by Roache (16) concerning the PIC method - " The most unique aspect is that continuum flow is not modeled, rather a finite number of particles are used, their locations and velocities being traced by Lagrangian kinematics. They are not merely marker particles, but they participate in the calculation even when free surfaces and interfaces are present."

In 1963 the PIC method still had some shortcomings which had not been overcome (13). The PIC numerical method shared the Eulerian problem of resolving the detail of minute processes within the flow field, and a fixed grid system which could not overcome boundary difficulties. The

most severe limitation of the method that increased the difficulty of expanding the method to simulate three dimensional flow processes was the large computational storage requirements and run times required for the Lagrangian and Eulerian meshes. The development of larger and faster computational systems should allow the adaptation of the method to more complicated flow simulations.

The PIC method was strictly a solution technique for fluid dynamicists until Sklarew (25), in 1970, presented a paper detailing what shall be called the "pseudo total flux or velocity" method of solution for the turbulent mass transport equation. Sklarew's method allowed the adaptation of PIC for methods of solution to the turbulent three dimensional incompressible mass transport equation. The equation may be written in vector form as-

$$\frac{\partial c}{\partial t} + \vec{\nabla} \cdot Uc - \vec{\nabla}^2 \cdot (K_{ij} c) = 0 \qquad (2.1)$$

and may be rewritten as

$$\frac{\partial c}{\partial t} + \vec{\nabla} \cdot \left[(\vec{U} - K_{ij} \frac{\vec{\nabla} c}{c}) c \right] = 0 \qquad (2.2)$$

or

$$\frac{\partial c}{\partial t} + \vec{\nabla} \cdot [U_T c] = 0 \qquad (2.3)$$

where the pseudo total velocity vector is defined as

$$\vec{U}_t = \vec{U} + \vec{U}_D$$

$\vec{U}_D$ = Diffusion velocity vector (2.4)

$\vec{U}$ = Advective velocity vector

where $\vec{U}_T$ is the summation of the advective and diffusive velocity vectors, the the diffusion velocity being defined as

$$\vec{U}_D = \frac{-K_{ij}}{c} \vec{\nabla} c \qquad (2.5)$$

Given an externally supplied velocity vector U, each Lagrangian marker particle is moved explicitly in time with the total pseudo velocity, which is the summation of the advective and negative diffusion velocities. The diffusion velocity is calculated by the product of the marker particle concentration gradient across an Eulerian grid cell, divided by the concentraton at that positon, multiplied by the turbulent diffusion coefficient K_{ij} (Eq. 2.5).

In 1971 Hotchkiss (26) applied an explicit finite difference solution technique to the three dimensional incompressible Navier - Stokes equations to produce a time dependent advective atmospheric velocity field. Using Lagrangian marker particles and Sklarew's pseudo total velocity technique, an atmospheric heat and mass transport model was developed. Sklarew and Hotchkiss recognized, as did Hirt and Cook (27), that the treatment of minute detail of the sub flow field missed in the pure Eulerian schemes

could now be overcome. Gravity, viscous drag as a function of particulate diameter, direct particle deposition, reflection and scavenging from the boundaries could now be applied with the use of Lagrangian marker particles for simulation of airborne transport of pollutant particulates.

Recognizing the potential, Lange (28,29), Knox, Hardy, and Sherman (30) of the Lawrence Livermore Laboratory, coined a new phrase for this hybrid Eulerian - Lagrangian mass transport model, ADPIC. The Atmospheric Diffusion Particle in Cell technique was developed for prediction of atmospheric pollutant transport under complicated advective wind conditions, surface boundaries, and turbulence scales. This version of the PIC mass transport algorithm introduced an expanding grid system, borrowed from ALE, Alternating Lagrangian Eulerian technique, developed by Hirt et. al. (31) for simulating dynamics of high speed flow with complicated boundary conditons. This grid system could translate and expand with the marker particle cloud as it advected through space thus allowing greater resolution of particle cloud movement in space, and subsequently minimization of simulation computer time usage, since the simulation time step can be maximized. Scale dependent diffusion became a readily applicable feature by extracting a diffusion coefficient at each time step by use of the 4/3 power law equation which itself uses the horizontal standard deviations of the marker particle cloud. This feature will be explained in a subsequent chapter.

Knox et. al. (30) proposed the utilization of the

ADPIC technique for the physical fate prediction of dredge spoil and application to modeling of three dimensional transport of sediment in San Fransisco Bay. After an extensive review of the literature of numerical modeling of dredge spoil disposal, Johnson (4) recommended the use of the ADPIC technique for simulation of coastal zone and estuarine sediment and pollutant transport.

Spaulding (32) recognized the need for a three dimensional numerical model that was capable of handling the long term transport of discrete sedimentary particles in a coastal zone tidally dominated environment. WAPIC, Water Advective Particle in Cell Technique, a three dimensional explicit finite difference, pseudo total velocity solution to the turbulent mass transport equation was developed by Spaulding (32) in 1975 at the NASA Langley Research Center. The following work is a continuation of the adaptation of Harlow and Evan's PIC method and Sklarew's pseudo total velocity technique for solving mass transport problems in the coastal zone environment.

III. DEVELOPMENT OF EQUATIONS

A. Turbulent Advection Diffusion Equation

The incompressible ensemble time averaged three dimensional mass transport equation may be written as

$$\frac{\partial c}{\partial t} + U\frac{\partial c}{\partial x} + V\frac{\partial c}{\partial y} + W\frac{\partial c}{\partial z} = \frac{\partial}{\partial x}\left(K_x\frac{\partial c}{\partial x}\right) + \frac{\partial}{\partial y}\left(K_y\frac{\partial c}{\partial y}\right) + \frac{\partial}{\partial z}\left(K_z\frac{\partial c}{\partial z}\right) \tag{3.1}$$

U,V,W = x,y,z time and space averaged velocity components

K_x,K_y,K_z = x,y,z turbulent diffusion coefficients

c = Time and spatially averaged concentration

This equation assumes that the pollutant is dilute and neutrally buoyant and that the flux terms due to molecular diffusivity can be neglected since, in riverine,oceanic and atmospheric modeling of mass transport, these terms are typically two to three orders of magnitude smaller than the turbulent coefficients (17,33,35). For purposes of this work, the above equation also assumes that the fluid flow field may be specified by some time and spatially averaged velocity components and that the coefficients are time and spatially averaged "dispersion" coefficients which may be empirically or theoretically determined.

B. Addition of Particle Settling Velocity

In order to simulate the motion of a negatively

buoyant dilute constituent such as suspended sediment particles, Eq. 3.1 may be modified by the addition of the term

$$W_s \frac{\partial c}{\partial z}$$

which is the advective mass flux in the Z-direction due to the still water asymptotic particle settling velocity, Ws. The assumptions are made that the free fall particle settling velocity is constant in time and space for a given particle diameter and that the suspended constituent is dilute within the flow field. Equation 3.1 can now be rewritten

$$\frac{\partial c}{\partial t} + U\frac{\partial c}{\partial x} + V\frac{\partial c}{\partial y} + W\frac{\partial c}{\partial z} = \frac{\partial}{\partial x}\left(K_x \frac{\partial c}{\partial x}\right) + \frac{\partial}{\partial y}\left(K_y \frac{\partial c}{\partial y}\right) + \frac{\partial}{\partial z}\left(K_z \frac{\partial c}{\partial z}\right) - W_s \frac{\partial c}{\partial z} \qquad (3.2)$$

This equation, the turbulent incompressible three dimensional mass transport equation for negatively buoyant dilute particles is the basic equation around which the WAPIC solution method is constructed.

C. Flux Conservative Form

WAPIC employs the pseudo total velocity method which may be conceptualized as a flux conservative formulation of the three dimensional mass transport equation. Equation

3.2 may be rearranged -

$$\frac{\partial c}{\partial t} + \frac{\partial}{\partial x}\left(U - \frac{K_x}{c}\frac{\partial c}{\partial x}\right)c + \frac{\partial}{\partial y}\left(V - \frac{K_y}{c}\frac{\partial c}{\partial y}\right)c + \frac{\partial}{\partial z}\left(W + W_s - \frac{K_z}{c}\frac{\partial c}{\partial z}\right)c = 0 \qquad (3.3)$$

and rewritten as

$$\frac{\partial c}{\partial t} + \frac{\partial}{\partial x}(U_T c) + \frac{\partial}{\partial y}(V_T c) + \frac{\partial}{\partial z}(W_T c) = 0 \qquad (3.4)$$

where

$$U_T = U + U_D \qquad (3.5a)$$

$$V_T = V + V_D \qquad (3.5b)$$

$$W_T = W + W_S + W_D \qquad (3.5c)$$

and

$$U_D = -\frac{K_x}{c}\frac{\partial c}{\partial x} \qquad (3.6a)$$

$$V_D = -\frac{K_y}{c}\frac{\partial c}{\partial y} \qquad (3.6b)$$

$$W_D = -\frac{K_z}{c}\frac{\partial c}{\partial z} \qquad (3.6c)$$

where U_T, V_T, W_T, are defined as the pseudo total transport velocities. Equation 3.4 states that a particle is

advected with the mean motion of the fluid field and diffused with a velocity proportional to the concentration gradient surrounding that particle.

D. Transformation of the Vertical Coordinate

The numerical solution to Eq. 3.4 requires a uniform mesh of equivalent shape and volume finite difference cells throughout the three dimensional cartesian grid system. When this system of equal volume cells must be applied to two and three dimensional hydrodynamic velocity fields with time and spatially varying free surfaces and irregular bottom topography complications arise. In estuaries and coastal areas, the bottom topography may be irregular and will not fit a single rectangular mesh of equal volume cells, especially when that mesh of equal volume cells is translating and expanding in time beneath a free surface which is also rising and falling with space and time.

Following the method of Hunter and Spaulding (7), and Gordon (36), a solution is to non-dimensionalize the vertical coordinate in the three dimensional mass transport equation such that there is no lateral variation of the total vertical length. This technique allows the use of an expanding and translating Eulerian grid system in the X-Y plane, moving within a time and spatially varying bottom and free surface.

The complex grid system of Figure 3.1 in cartesian

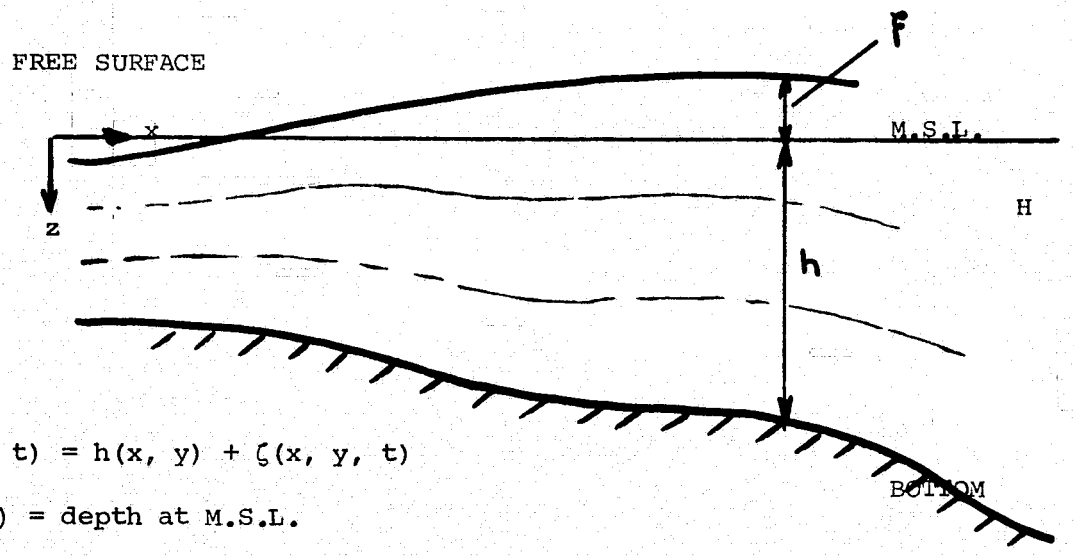

$H(x, y, t) = h(x, y) + \zeta(x, y, t)$

$h(x, y)$ = depth at M.S.L.

$\zeta(x, y, t)$ = free surface height above M.S.L. due to tidal variations

FIGURE 3.1 X-Z Cartesian View of "WAPIC" Grid Structure for Simulating Mass Transport in Tidal Waters

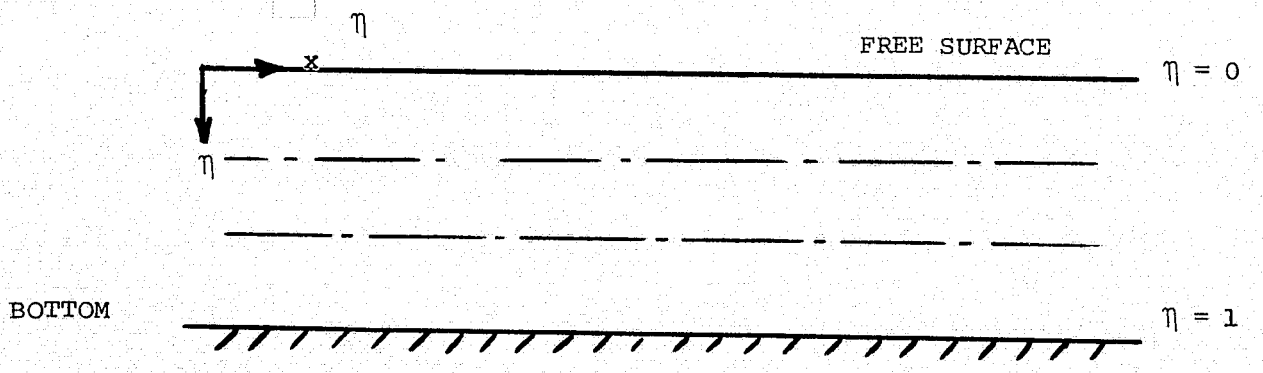

$$\eta(x, y, z, t) = \frac{z - \zeta(x, y, t)}{h(x, y) + \zeta(x, y, t)}$$

FIGURE 3.2 X-η Transformed Plane View of "WAPIC" Grid Structure

space can be transformed into an equal volume cell system in X-Y-η space, of Figure 3.2 . The transformation of the vertical coordinate proceeds from cartesian Z-space to dimensionless η space by setting the the value of η to 0, and -1 at the free surface and bottom respectively, (Figure 3.1) where

$$\eta(x,y,z,t) = \frac{z - \xi(x,y,t)}{H\ (x,\ y,\ t)} \tag{3.7}$$

$$H(x,\ y,\ t) = h(x,y) + \xi(x,\ y,\ t) \tag{3.8}$$

$$\eta(x,\ y,\ z,\ t) = \frac{z - \xi(x,\ y,\ t)}{h(x,y) + \xi(x,y,t)} \tag{3.9}$$

z = vertical coordinate (positive down)

$h(x,y)$ = depth at M.S.L.

$\xi(x,\ y,\ t)$ = free surface height above M.S.L. due to tidal variations

The procedure is to non-dimensionalize the three dimensional mass transport Eq. 3.4 in the Z-coordinate to dimensionless η-space using the following transformation identities after Gordon (36). The derivation of these identities may be found in Appendix A.

$$\frac{\partial}{\partial z}(\ ) = \frac{1}{H}\frac{\partial}{\partial \eta} \tag{3.10a}$$

$$\frac{\partial}{\partial t}(\ ) = \frac{\partial}{\partial t}(\ ) - \frac{1}{H}\left[(\eta + 1)\frac{\delta \xi}{\delta t}\right]\frac{\partial}{\partial \eta}(\ ) \tag{3.10b}$$

$$\frac{\partial}{\partial x}(\ ) = \frac{\delta}{\delta x}(\ ) - \frac{1}{H}\left[(\eta + 1)\frac{\delta \xi}{\delta x} + \eta \frac{\delta h}{\delta x}\right]\frac{\partial}{\partial \eta}(\ ) \qquad (3.10c)$$

$$\frac{\partial}{\partial y}(\ ) = \frac{\delta}{\delta y}(\ ) - \frac{1}{H}\left[(\eta + 1)\frac{\delta \xi}{\delta y} + \eta \frac{\delta h}{\delta y} + \eta \frac{\delta h}{\delta y}\right]\frac{\partial}{\partial \eta}(\ ) \qquad (3.10d)$$

Equation 3.4 was split into seven terms and transformed using the transform identities 3.10 a,b,c,d. The mathematics and assumptions utilized in the transformation are treated in detail in Appendix B. for the interested reader. The transformed pseudo total velocity form may be written as

$$\frac{\delta c}{\delta t} + \frac{\delta}{\delta x}[U_T c] + \frac{\delta}{\delta y}[V_T c] + \frac{\partial}{\partial \eta}[\omega_T c] = 0 \qquad (3.11)$$

Where U_T, V_T, ω_T, may be defined as

$$U_T = U - \frac{K_x}{c}\left[\frac{\delta c}{\delta x} - \frac{1}{H}\left[1 + \eta\right]\frac{\delta \xi}{\delta x} + \eta \frac{\delta h}{\delta x}\right]\frac{\partial c}{\partial \eta} \qquad (3.12)$$

$$V_T = V - \frac{K_y}{c}\left[\frac{\delta c}{\delta y} - \frac{1}{H}\left[1 + \eta\right]\frac{\delta \xi}{\delta y} + \eta \frac{\delta h}{\delta y}\right]\frac{\partial c}{\partial \eta} \qquad (3.13)$$

$$\omega_T = \omega - \frac{K_z}{H^2 C}\frac{\partial c}{\partial \eta} - \frac{\eta}{H}\left[U \frac{\delta h}{\delta x} - V \frac{\delta h}{\delta y}\right] + \omega_S \qquad (3.14)$$

$$\omega_S = \frac{1}{H}\{W_S - \{(\eta + 1)\frac{\delta\xi}{\delta t} + u[(\eta + 1)\frac{\delta\xi}{\delta x} + \eta\frac{\delta h}{\delta x}] + v[(\eta + 1)\frac{\delta\xi}{\delta y} + \eta\frac{\delta h}{\delta y}]\}\} \quad (3.15)$$

Equation 3.11, written in flux conservative form, may now handle the transport and deposition of Lagrangian marker particles in X-Y-η space.

The Eulerian three dimensional grid consists of equal volume cells throughout space, bounded at the free surface and bottom. The system may now take advective fluid velocities from an external source such as a two dimensional vertically averaged tidal hydrodynamic model, or a three dimensional tidal hydrodynamic model that utilizes the same transformation procedure (36). The WAPIC grid system can expand or translate in either the X or Y dimension but there can be no expansion or translation in the η-dimension due to the nature of the transformation.

IV. WAPIC ALGORITHM

The solution to the pseudo velocity equations is accomplished by a Lagrangian marker particle in Eulerian cell technique, utilizing Sklarew's total pseudo flux method. WAPIC employs a space staggered three dimensional Eulerian grid system composed of equal volume rectangular cells (Figure 4.1) Concentrations are defined at the center of the cells and the advection velocities, U, V, W and the diffusion velocities, U_D, V_D, W_D are defined at the center of the respective cell faces. Marker particles placed inside the Eulerian grid, which statistically represent the pollutant cloud are defined by their individual Lagrangian coordinates. A time cycle of the code can be divided into an Eulerian and Lagrangian step. Each step is explained as follows.

A. Eulerian Step

At the beginining of each time step, the concentrations, defined at the center of each cell, are used to calculate the diffusion velocities defined at the center of the cell faces. WAPIC employs a centered space finite difference approximation for the diffusion velocities. The finite difference forms for the diffusion velocities may be written in cartesian space, or in the vertically transformed dimensionless space.

1. Cartesian Finite Differences

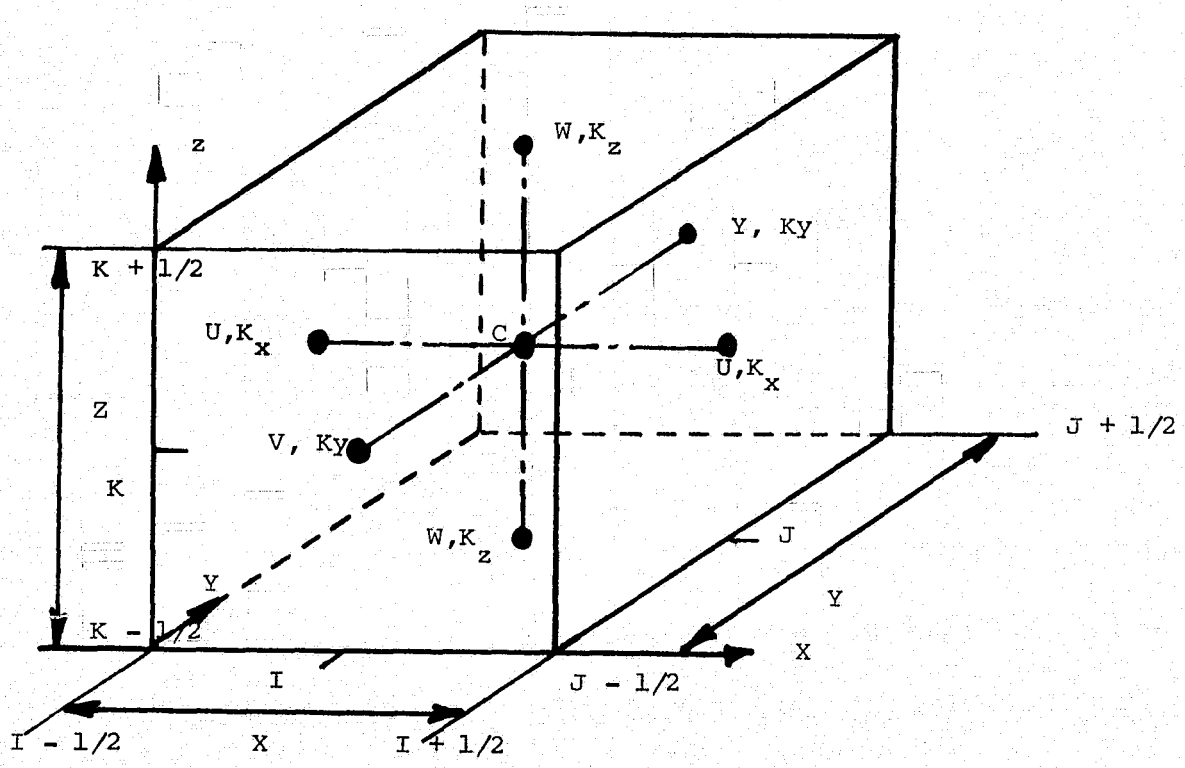

FIGURE 4.1 Three Dimensional Space Staggered Grid System

The cartesian form of the partial differential equation of mass transport is used to model unbounded and uniformly bounded mass transport in three dimensional X-Y-Z space. The partial differentials for the pseudo diffusion velocities (Eqs. 3.6-a,b,c,) are approximated by centered space finite difference formulations

$$U_D = \frac{-2K_x}{\left[C_{I+1,\,J,\,K} + C_{I,\,J,\,K}\right]} \frac{\left[C_{I+1,\,J,\,K} - C_{I,\,J,\,K}\right]}{\Delta x} \qquad (4.1)$$

$$V_D = \frac{-2K_y}{\left[C_{I,\,J+1,\,K} + C_{I,\,J,\,K}\right]} \frac{\left[C_{I,\,J+1,\,K} - C_{I,\,J,\,K}\right]}{\Delta y} \qquad (4.2)$$

$$W_D = \frac{-2K_z}{\left[C_{I,\,J,\,K+1} + C_{I,\,J,\,K}\right]} \frac{\left[C_{I,\,J,\,K+1} - C_{I,\,J,\,K}\right]}{\Delta z} \qquad (4.3)$$

The integer indicies, I, J, K, of the concentration field C, represent the three dimensional cell centers at which the concentration values are evaluated or defined. Since the concentration gradient in a given dimension is evaluated by the forward space approximation across cell centers from I to I+1, the diffusion velocity gradient is defined at the respective cell faces. These diffusion velocities are calculated throughout the the three dimensional space and then added to the externally supplied advection velocities, which also are defined at the grid faces, to yield the pseudo total velocities, U_T, V_T, W_T .

2. Transformed Finite Differences

As previously stated WAPIC utilizes the dimensionless

vertically transformed version of the pseudo total velocity equation, when simulating mass transport in a tidally dominated coastal zone environment which has a time and spatially varying free surface and irregular bottom topography. The turbulent diffusion velocities in Eqs. 3.12,13,14,15 are approximated by the forward space finite differences

$$U_D = \frac{-2K_x}{[C_{I+1,\,J,\,K} + C_{I,\,J,\,K}]} \left[\frac{(C_{I+1,\,J,\,K} - C_{I,\,J,\,K})}{\Delta x} - \frac{1}{H_{I,\,J}} \left[[1 + \eta] + \frac{[\xi_{I+1,\,J} - \xi_{I,\,J}]}{\Delta x} + \eta \frac{[h_{I+1,\,J} - h_{I,\,J}]}{\Delta x} \right] \right] \frac{[C_{I,\,J,\,\eta+1} - C_{I,\,J,\,\eta}]}{\Delta \eta} \quad (4.4)$$

$$V_D = \frac{-2K_y}{[C_{I,\,J+1,\,K} + C_{I,\,J,\,K}]} \left[\frac{(C_{I,\,J+1,\,K} - C_{I,\,J,\,K})}{\Delta y} - \frac{1}{H_{I,\,J}} \left[[1 + \eta] + \frac{[\xi_{I,\,J+1} - \xi_{I,\,J}]}{\Delta y} + \eta \frac{[h_{I,\,J+1} - h_{I,\,J}]}{\Delta y} \right] \right] \frac{[C_{I,\,J,\,\eta+1} - C_{I,\,J,\,\eta}]}{\Delta \eta} \quad (4.5)$$

$$\omega_D = \frac{-2K_z}{(H_{I,J})^2 [C_{I,\,J,\,K+1} - C_{I,\,J,\,K}]} \left[\frac{(C_{I,\,J,\,K+1} - C_{I,\,J,\,K})}{\Delta \eta} - \frac{\eta}{H_{I,\,J}} \left[U_{I,\,J,\,K} \frac{[h_{I+1,\,J} - h_{I,\,J}]}{\Delta x} - V_{I,\,J,\,K} \frac{[h_{I,\,J+1} - h_{I,\,J}]}{\Delta y} \right] \right] \quad (4.6)$$

$$\omega_S = \frac{1}{H_{I,J}}\left[W_S - \left[(\eta+1)\frac{[\xi^{n+1}_{I,J} - \xi^{n}_{I,J}]}{\Delta t} + U_{I,J,K}\left[(\eta+1)\frac{[\xi_{I+1,J} - \xi_{I,J}]}{\Delta x} + \eta\frac{[h_{I+1,J} - h_{I,J}]}{\Delta x}\right] + V_{I,J,K}\left[(\eta+1)\frac{[\xi_{I,J+1} - \xi_{I,J}]}{\Delta y} + \eta\frac{[h_{I,J+1} - h_{I,J}]}{\Delta y}\right]\right]\right] \quad (4.7)$$

As before, these diffusion velocities are then added to the externally supplied mass consistent advection field to yield the total pseudo velocities, Ut, Vt, Wt , in X-Y-N space.

B. Lagrangian step

Following the calculation of the pseudo total velocities throughout the Eulerian grid, each marker particle is advected in three space by the velocity field from time T to T +ΔT. Two methods of advance are employed

1. Pure Explicit
2. Time Centered Iterative

both using a bilinear weighting scheme to interpolate velocities for particles inside the grids. These procedures are as follows.

1. Explicit Formulation

The explicit formulation is used for simulation of mass transport of Lagrangian marker particles in steady undirectional or uniformly sheared flow fields (non curved

streamlines). Each marker particle within the Eulerian grid is transported from time T to T +ΔT, a distance in X-Y-Z space UΔt, VΔt, WΔt, respectively. respectively. The new Lagrangian coordinates become

$$x_{NEW} = x_{OLD} + U_T^P \Delta t \qquad (4.8a)$$

$$y_{NEW} = y_{OLD} + V_T^P \Delta t \qquad (4.8b)$$

$$z_{NEW} = z_{OLD} + W_T^P \Delta t \qquad (4.8c)$$

where U_T^P , V_T^P , W_T^P are the bilinear weighted velocities for each particle. The bilinear velocity weighting method is popularly used in the MAC method (16,27) for interpolating marker particle velocities in an Eulerian velocity grid. Figure 4.2 details a two dimensional example for determining the U_T^P, V_T^P, and W_T^P velocities for a particle within the space staggered grid system. This procedure was generalized to obtain a three dimensional bilinear weighted average. A given WAPIC grid may be surrounded by a maximum of 26 cells. (Figure 4.3) The WAPIC solution determines the particular cell in which the particle's coordinates are located, then divides that cell into eight equal volume octants, and finds the octant in which the particle is located. (Figure 4.4) Each marker particle is assigned a "fictitious" volume equal to the volume of an Eulerian grid cell. This fictitious volume may overlap into a maximum of eight surrounding grid cells.

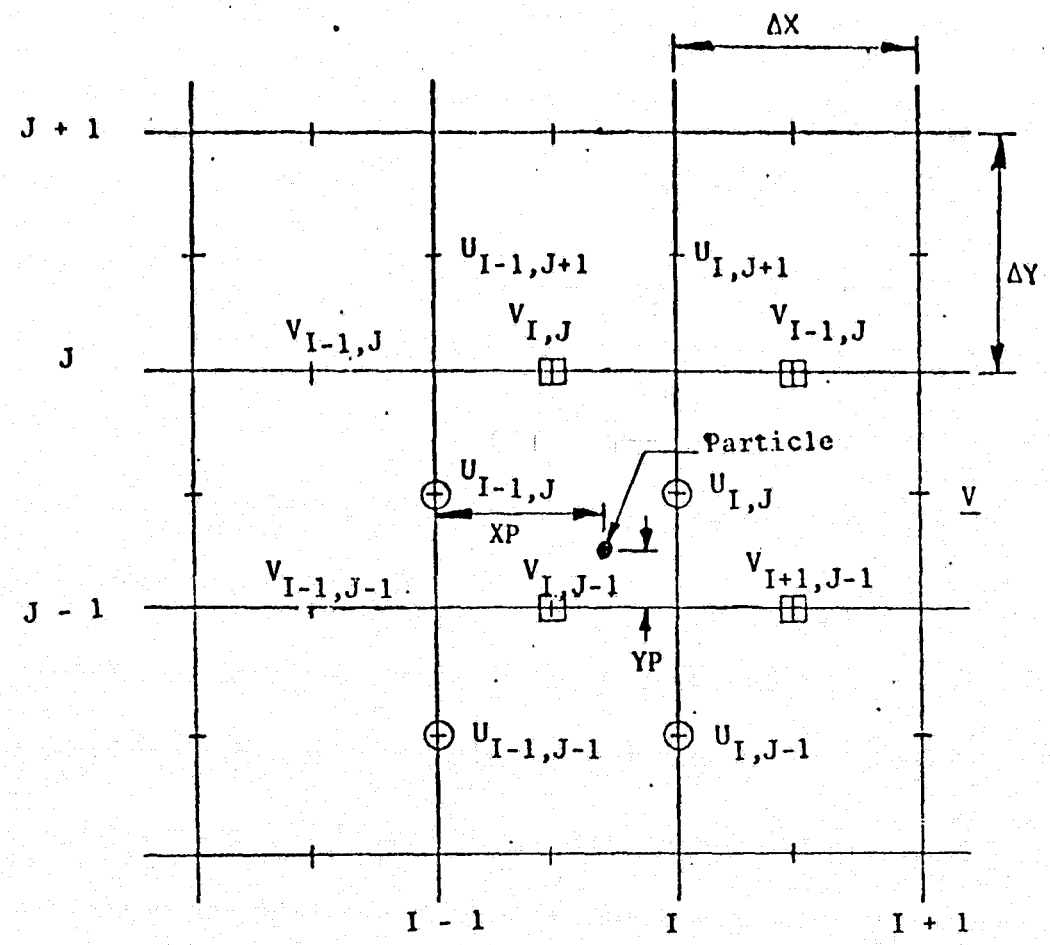

X DIRECTED VELOCITY (Up) AT PARTICLE POSITION

$$U1 = \frac{XP}{\Delta X}(U_{I,J} - U_{I-1,J}) + U_{I-1,J}$$

$$U2 = \frac{XP}{\Delta X}(U_{I,J-1} - U_{I-1,J-1}) + U_{I-1,J-1}$$

$$U_p = \frac{(YP + \Delta Y/2)}{\Delta Y}(U1 - U2) + U2$$

Y DIRECTED VELOCITY (Vp) AT PARTICLE POSITION

$$V1 = \frac{YP}{\Delta Y}(V_{I,J} - V_{I,J-1}) + V_{I,J-1}$$

$$V2 = \frac{YP}{\Delta Y}(V_{I+1,J} - V_{I+1,J-1}) + V_{I+1,J-1}$$

$$V_p = \frac{(XP - \Delta X/2)}{\Delta X}(V2 - V1) + V1$$

FIGURE 4.2 Two Dimensional Bilinear Weighting Scheme for Velocity Interpolation . . . . . .

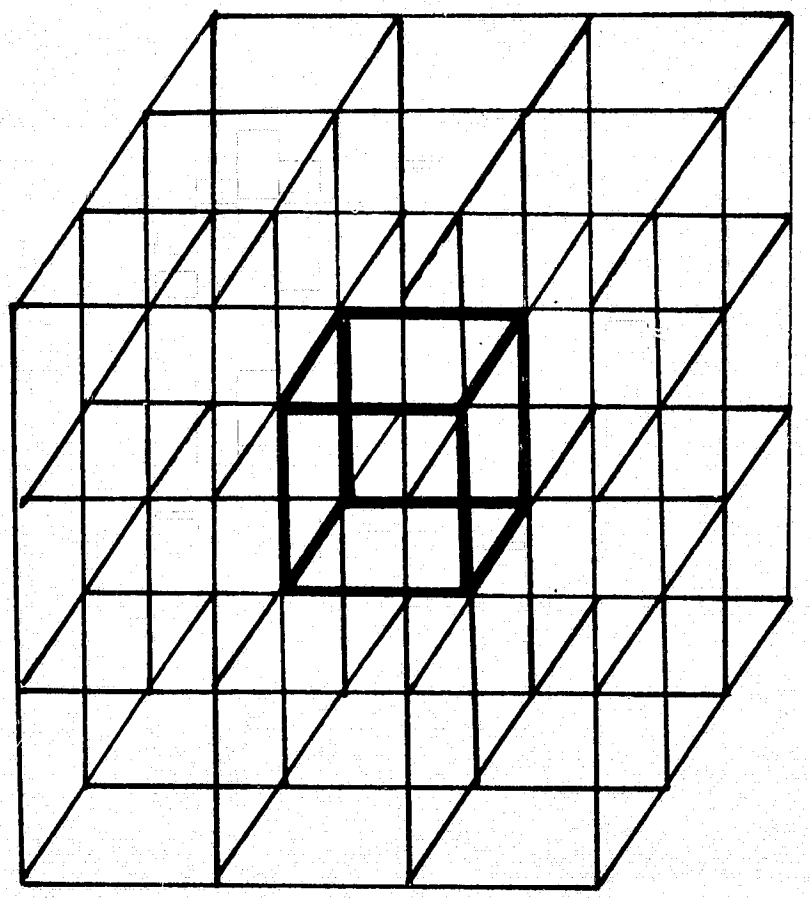

FIGURE 4.3 3 x 3 Eulerian Grid Cell Matrix

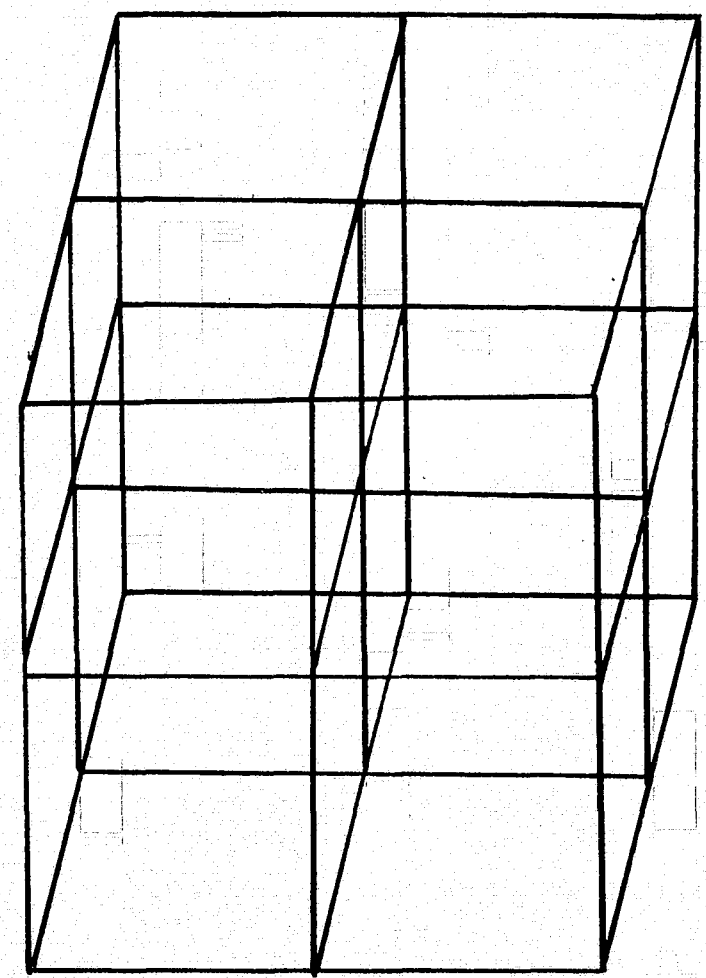

FIGURE 4.4 Eight Octants of a Three Dimensional Eulerian Grid Cell

Thus a particle's velocity is determined by a three dimensional weight of the nearest, eight, surrounding pseudo total velocities. Figure 4.5 details planar X-Y, X-Z, Y-Z views of the eight surrounding velocities used in the three dimensional bilinear scheme.

2. Iterative Time Centered Approach

The explicit particle movement technique with the bilinear weighting scheme was verified by Lange (28,29) against simple analytic diffusion cases in unbounded uniform and uniformly sheared flows to within 5.0 % accuracy of concentration prediction. When the streamlines of the flow field are curved, neutrally buoyant marker particles tend to develop trajectories not co-incident with streamlines of the flow field (37). This interpolation error inherent in an explicit scheme with a bilinear velocity weighting technique, may be corrected by decreasing the calculational time step ΔT, however at the expense of increased computational time.

Forester (37) proposed an iterative time centered approach for prediction of marker particle motion in curved flow fields. Instead of employing equations 4.8a,b,c to predict particle movement, the following procedure is employed:

$$x_{NEW} = x_{OLD} + (U_T^{pOLD} + U_T^{pNEW})\,\Delta t/2 \qquad (4.9)$$

where U_T^{pnew}, V_T^{pnew} W_T^{pnew}, represent the bilinear weighted particle velocities at the new position. The method

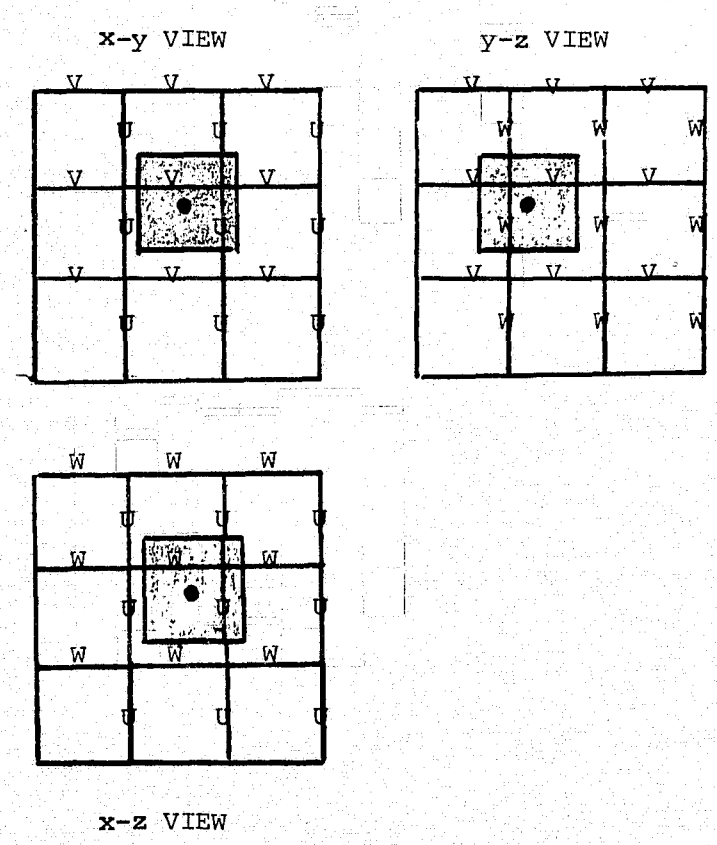

FIGURE 4.5 Fictitious Volume of a Lagrangian Particle Inside the Three Dimensional Eulerian Velocity Field

employs an iteration procedure where each distance estimate is used to produce a bilinear weighted particle velocity at the new position. Using Eq. 4.9 and the new particle velocity at that position, a new position is calculated and is tested for convergence against the previous position.

As an illustration of the utility of this technique, a two dimensional uniform circular vortex field was specified with a shear rate of $du/dy = -0.0004\ sec^{1}$, and $dv/dx = 0.0004\ sec^{1}$ with minimum and maximum velocities of -1.0 and 1.0 ft/sec in each dimension respectively. The WAPIC grid consisted of a 10x10 X-Y matrix, thus specifying a time step of 250 for grid lengths in X and Y of 500 ft., using a Courant dynamic stability time step restriction for accuracy of particle motion prediction. (Figure 4.6) When employing the non-iterative explicit bilinear weighted movement technique a massless marker particle placed in the circular vortex field was found to eventually spiral out of the field. (Figure 4.7) When using Forester's time centered iterative approach, a particle placed in the same initial position in the vortex field, showed a precise circular trajectory.

When the time centered iterative procedure is not employed for predicting particle transport in flow situatins with an eddy or vortex structure and a Courant time step limitation is used with the bilinear velocity interpolation scheme for particle motion, the deduction can be made that the mass or particles within the eddy will be accelerated out of the flow field prematurely. For

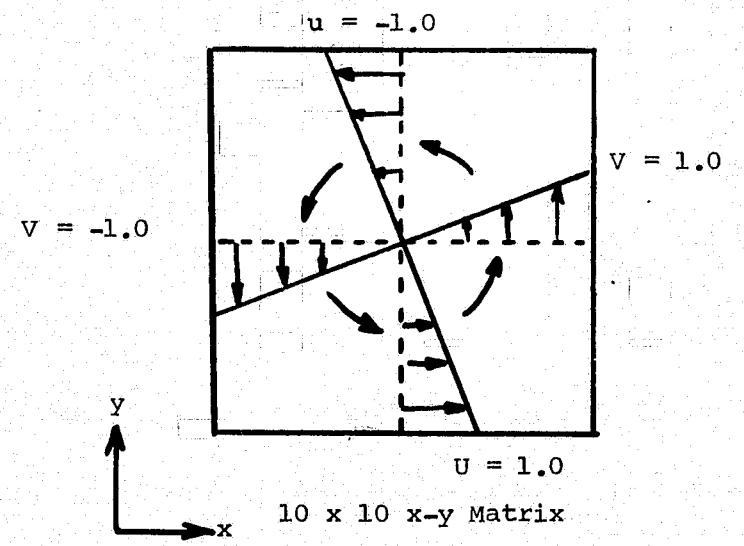

OPERATING PARAMETERS

$x, y = 500$ ft.

$K_x, K_y = 0.0$

$(U,V)_{MAX} = 1.0$ ft/sec

$(U,V)_{MIN} = -1.0$ ft/sec

$t = 250$ sec

$$\frac{\partial u}{\partial y} = \frac{\partial v}{\partial x} = \pm 4 \times 10^{-4} \text{ sec}^{-1}$$

$$W_z = \text{VORTICITY} = \frac{1}{2}\left(\frac{\partial u}{\partial y} - \frac{\partial v}{\partial x}\right) = -4 \times 10^{-4} \text{ sec}^{-1}$$

FIGURE 4.6 WAPIC Two Dimensional Velocity Distribution for a Uniform Circular Vortex Motion

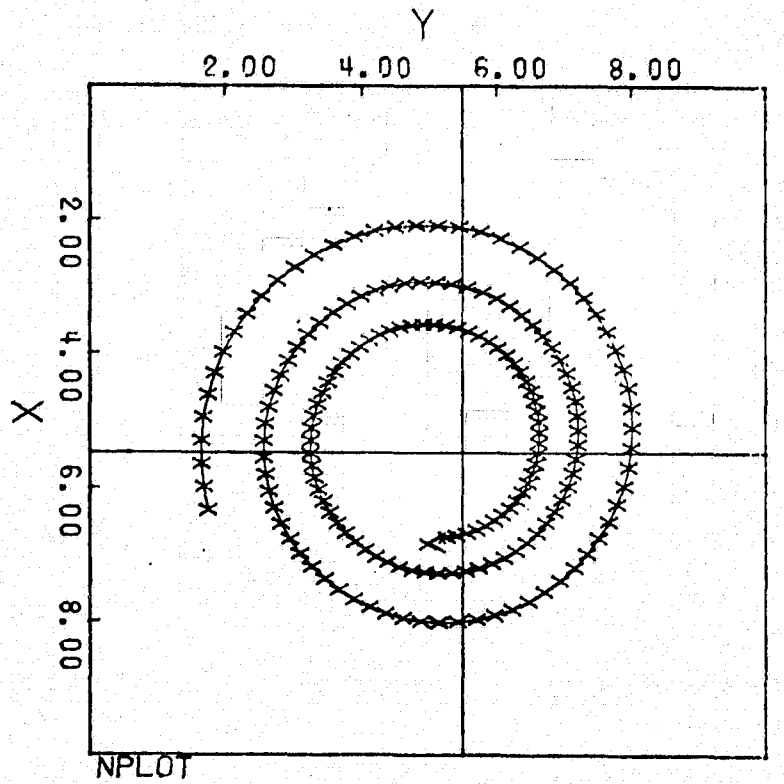

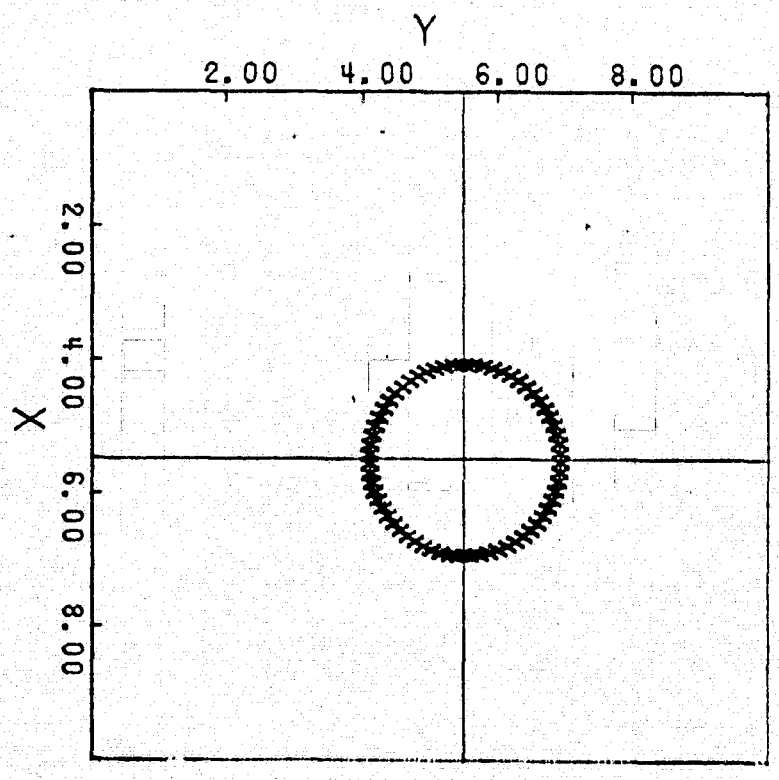

PARTICLE TRAJECTORIES INSIDE A CIRCULAR VORTEX FIELD

WITHOUT AND WITH

TIME CENTERED ITERATIVE TECHNIQUE FOR PARTICLE DISPLACEMENT

FIGURE 4.8 Particle Trajectories Inside a Uniform Circular Vortex Field. Demonstration of Time Centered Iterative Technique for Particle Displacement

modeling mass transport in complicated non uniform flow situations, the iterative time centered method requires much less time than a purely explicit technique for accurate prediction of particle motion. Exactly how much time will be saved for accuracy of particle motion prediction by using the iterative technique as opposed to the explicit technique is highly problem dependent. Results by Spaulding (32) for accuracy of prediction of particle trajectory in a uniform circular vortex field field indicate a factor of 3 to 5 decrease in computational time costs with Forester's implicit technique as compared to a purely explicit particle movement technique with the same Courant accuracy number.

C. Expanding and Translating Grid

The Lagrangian step contains the options of allowing selective expansion of the Eulerian grid system with the diffusive growth of the marker particle cloud and selective translation of the grid with the mean motion of the advected cloud, for any of the three dimensions in cartesian X-Y-Z space, and in the X-Y directions for the X-Y-η vertically non-dimensional coordinate system. Incorporation of this procedure permits maximum resolution of the marker particle concentration field with a minimum number of computational grids. The expansion and translation procedures which are particularly useful for

simulating instantaneous point releases in horizontally unbounded flow situations are developed in WAPIC as follows:

The expanding grid system can operate in any combination of the three dimensions. During the expansion step each particle is tested for placement within a certain distance of an outer grid system boundary. Should a particle reach a grid cell boundary in any given dimension, then each grid cell expands a specified percentage of grid cell length in that given dimension. Figure 4.8 illustrates an expansion in the X-direction for a 2x2 grid. As shown, the lower left hand corner of the grid is moved in the negative X-direction a distance one half of the grid cell length increase. WAPIC monitors the coordinates of this grid "origin" from time T=0, and updates its location in 3-space whenever there is an expansion or translation of the grid in succeeding time steps.

The grid translation procedure is designed to follow the mean motion of the marker particle cloud as it advects through space. At time T, an average particle velocity ($\bar{U}_p$, $\bar{V}_p$, $\bar{W}_p$) is calculated in each dimension, from the average values of the bilinear weighted particle velocities. The translation of the grid, in a given dimension, is achieved by moving each particle a distance U_p^* ΔT from the old particle position.

$$x_{NEW} = x_{OLD} + U_p \Delta t \qquad (4.10)$$

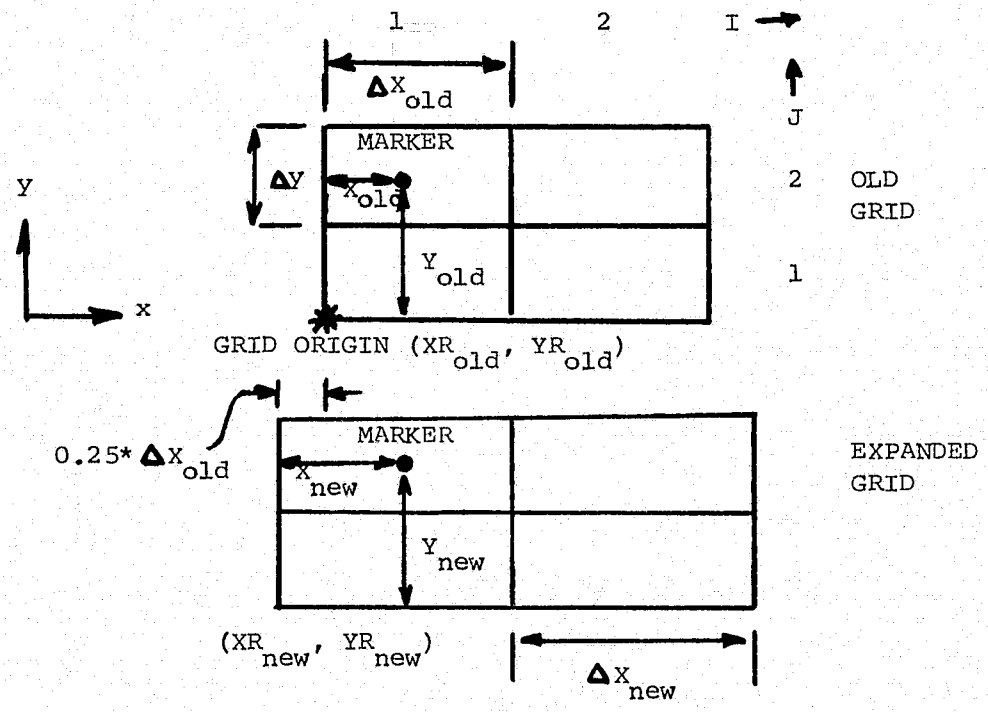

FRACTION OF GRID EXPANSION = 0.5

NEW X - POSITION OF MARKER PARTICLE

$$X_{new} = X_{old} + 0.5*(\text{FRACTION } \Delta X \text{ EXPANSION})*\Delta X_{old}$$

NEW X - POSITION OF EXPANDED GRID ORIGIN

$$XR_{new} = XR_{old} + XR_{old} - 0.5*(\text{FRACTION } \Delta X \text{ EXPANSION})*\Delta X_{old}$$

ΔX = X, Y GRID LENGTHS
X, Y = LAGRANGIAN COORDINATES OF MARKER
XR, YR = LAGRANGIAN COORDINATES OF ORIGIN

FIGURE 4.8 Nature of the WAPIC Expanding Grid Algorithm

and subsequently the origin (for example- in the X dimension) is moved

$$XR_{new} = XR_{old} + \bar{U}_p \Delta t \qquad (4.11)$$

D. Boundary Conditions

When the Eulerian grid no longer translates or expands in a given dimension, then boundary conditions must be employed in WAPIC for that given dimension. Because WAPIC is part Eulerian and part Lagrangian, boundary conditions are imposed on the Eulerian total pseudo velocity field, and on the Lagrangian marker particles within the field. Each three dimensional cell is assigned a boundary identification number for logical control of the pseudo velocity calculations and movement of Lagrangian marker particles within the given cell. Table 4.1 summarizes the cell types or classifications and the Eulerian and Lagrangian boundary conditions imposed within the cells.

1. Eulerian Boundary Conditions

As specified in Table 4.1, the Eulerian grid cells are classified into two groupings; these are -

(a) Vertical boundary cells (reflection, deposition, and erosion) whose cell faces lie on a horizontal plane boundary

(b) Horizontal cells (land, water, and open

CELL DESCRIPTION	EULERIAN BOUNDARY CONDITION	LAGRANGIAN BOUNDARY CONDITION
LAND CELL	NO FLUX $U_D = 0$	PARTICLE REFLECTION
WATER CELL	NONE	NONE
OPEN BOUNDARY	$U_D = 0$	PARTICLE REMOVAL
VERTICAL REFLECTION	$W_D \neq$ or $W_D = 0$	PARTICLE REFLECTION
VERTICAL DEPOSITION	$W_D \neq$ or $W_D = 0$	PARTICLE DEPOSITION
VERTICAL EROSION	SPECIFY BTM. SHEAR STRESS FOR EROSION	PARTICLE ENTRAINMENT

TABLE 4.1 Classification of Eulerian and Lagrangian Boundary Conditions

vertical plane boundaries) which are boundary and non-boundary cells not on a horizontal plane boundary.

Through the use of the vertical transformation, WAPIC can treat the complicated bottom topography and time varying free surface of estuarine and coastal hydrodynamic flows as uniform boundaries within the space staggered finite difference grid. Eulerian boundary conditions are imposed by controlling the calculation of the diffusion velocities throughout the grid. Consider the construction of a three dimensional (fixed) Eulerian grid with non-uniform lateral (Y) boundaries and a uniform free surface and bottom. Looking at a X-Z plane view, Figure 4.9, it is seen that the upper row of vertical velocities directly coincide with the boundary. Thus their diffusion velocities would be identically zero by the definition of no flux across a land or solid boundary. The lower row of vertical velocities which do not lie directly on the boundary have finite diffusion velocities by the forward space finite difference approximation. Following Lange's (28) assumption of constant marker particle flux at an open boundary (which rests on the assumption that the marker field is fully developed in the direction of the flow when it reaches the boundary), the diffusion velocities are set identically equal to zero for the left hand column of U-velocities. Figure 4.10 illustrates a horizontal plane view of the U-V diffusion velocity. For example, the diffusion velocities at U25 and U22 by the forward space finite difference Eq. 4.1 are zero. They do not have to be

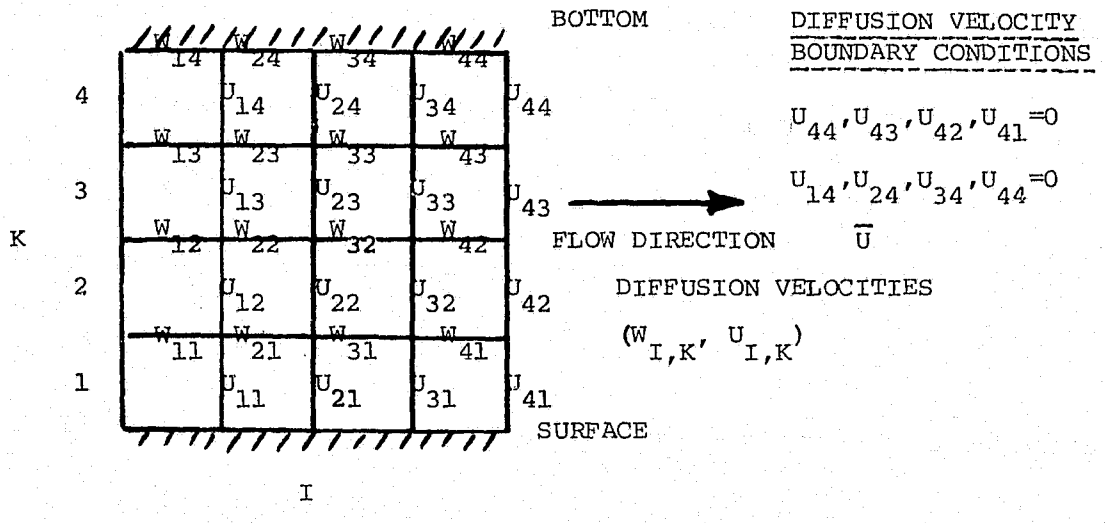

FIGURE 4.9 X-Z Planar View of Eulerian Diffusion Velocities and Boundary Conditions

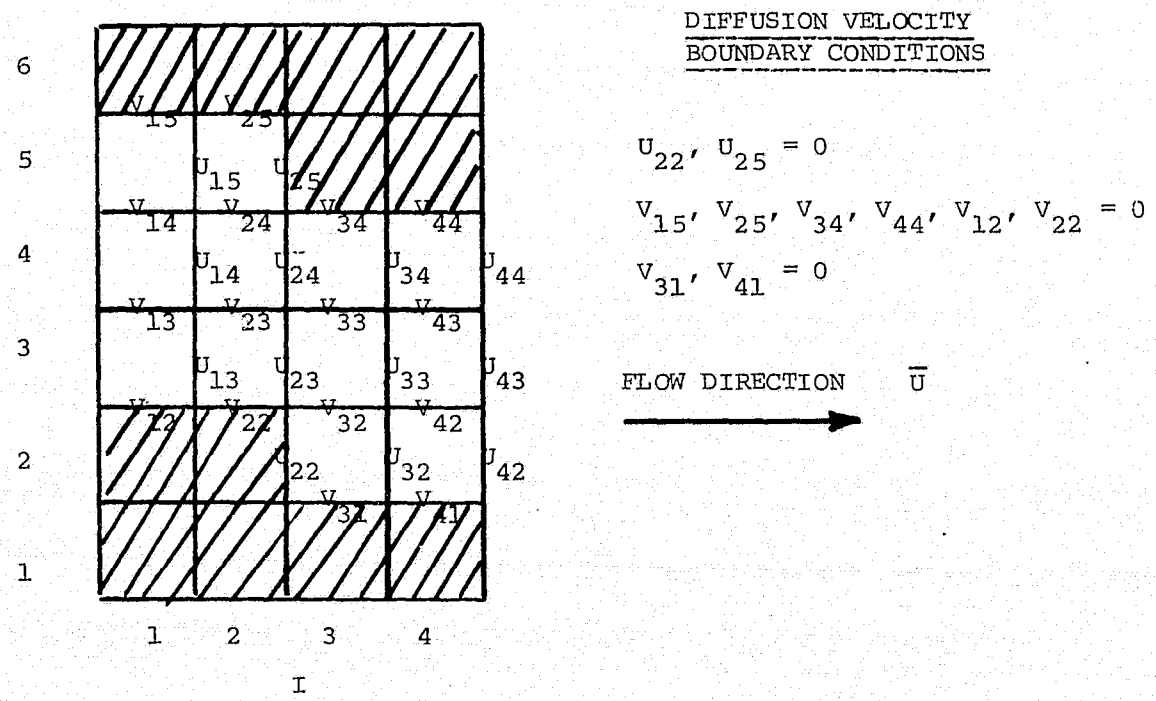

FIGURE 4.10 X-Y Planar View of Eulerian Diffusion Velocities and Boundary Conditions

equal to zero because the forward space concentration gradients can be finite by this definition, but are set to zero because they are located on the boundary. These assumptions are consistent with the no-flux assumption across a solid boundary.

Each marker particle is treated as though possessing a fictitious volume equal to a grid cell, centered at its coordinates. Should this fictitious volume overlap onto a horizontal land or open boundary cell, then the particle is either reflected or removed from the grid field. (Figure 4.11) A marker particle may penetrate halfway into a horizontal land or open boundary before the horizontal boundary conditions applies. For the purpose of vertical resolution of marker particle movement, a particle may penetrate as far as the cell face on which the vertical cell boundary is defined. Particles reaching a depositonal vertical boundary are removed from the field by setting their Z-coordinates to zero and storing the X-Y deposition coordinates.

E. Concentration Calculation

The final segment of the Lagrangian step is the calculation of the new concentration field from the new particle positions. Each marker is assigned a physical mass and a fictitious volume the size of one Eulerian grid cell. For a given marker particle, the WAPIC code locates

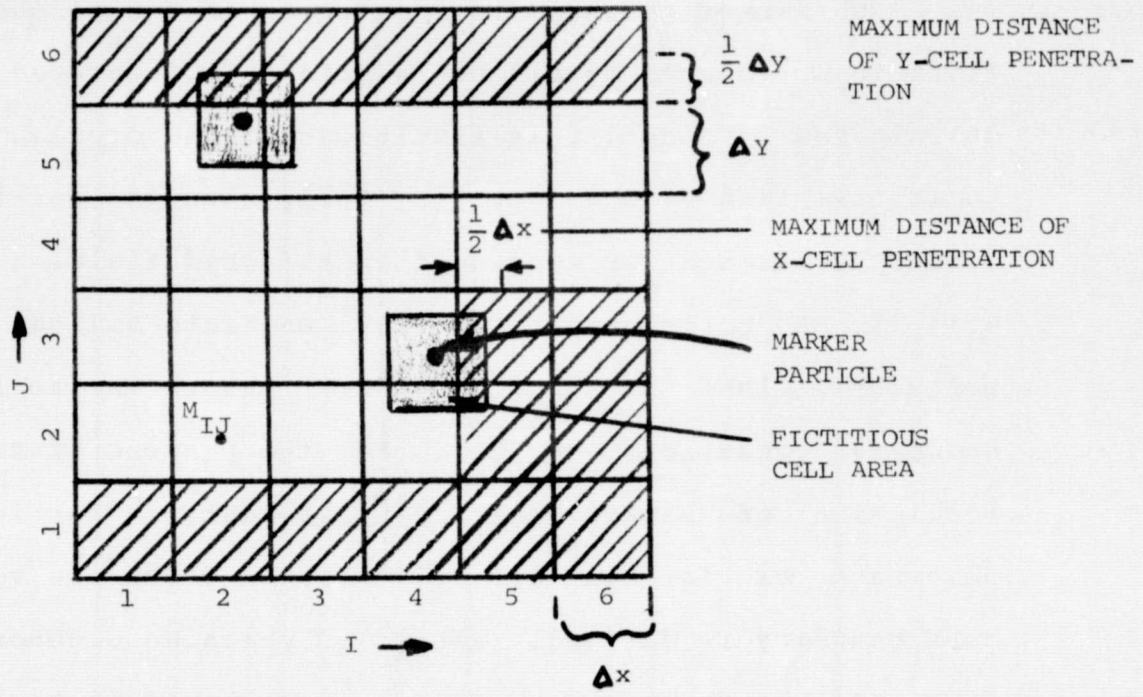

X, Y LAGRANGIAN PARTICLE COORDINATES

FIGURE 4.11 Two Dimensional X-Y View of Eulerian Grid and Lagrangian Marker Particle Reflection Procedure

the individual Eulerian cell and one of eight possible octants, of that cell, in which the particle's fictitious volume is located. Figure 4.12 details the concentration weighting scheme for a marker particle in a two dimensional grid system. WAPIC uses an extended version to allow for a third dimension. This mass sharing procedure is simply repeated for each particle in the field for calculation of the total cloud distribution of concentration in the grid system.

F. Two Dimensional Velocity Processor

The coupling of WAPIC to a two or three dimensional finite difference mesh Eulerian hydrodynamic velocity field requires the use of a "velocity processor". Since the WAPIC grid system is translating and expanding with the marker particle cloud as it advects with the tidal flow in a two dimensionally vertically averaged velocity field, the WAPIC Eulerian grid mesh points for velocities will not necessarily coincide with those of the externally supplied fixed Eulerian velocity field. Following the work of Dobson (38), a least squares surface fitting technique has been adopted to interpolate U and V horizontal velocities from a two dimensional space staggered finite difference grid system. The method employs the twelve nearest fixed grid neighbors (in the form of a cross) around the point of interest, and fits a quadratic surface of the type -

$$U_t = e_1 + e_2 X + e_3 Y + e_4 X^2 + e_5 XY + e_6 Y^2 \qquad (4.12)$$

e_n = Matrix Coefficients

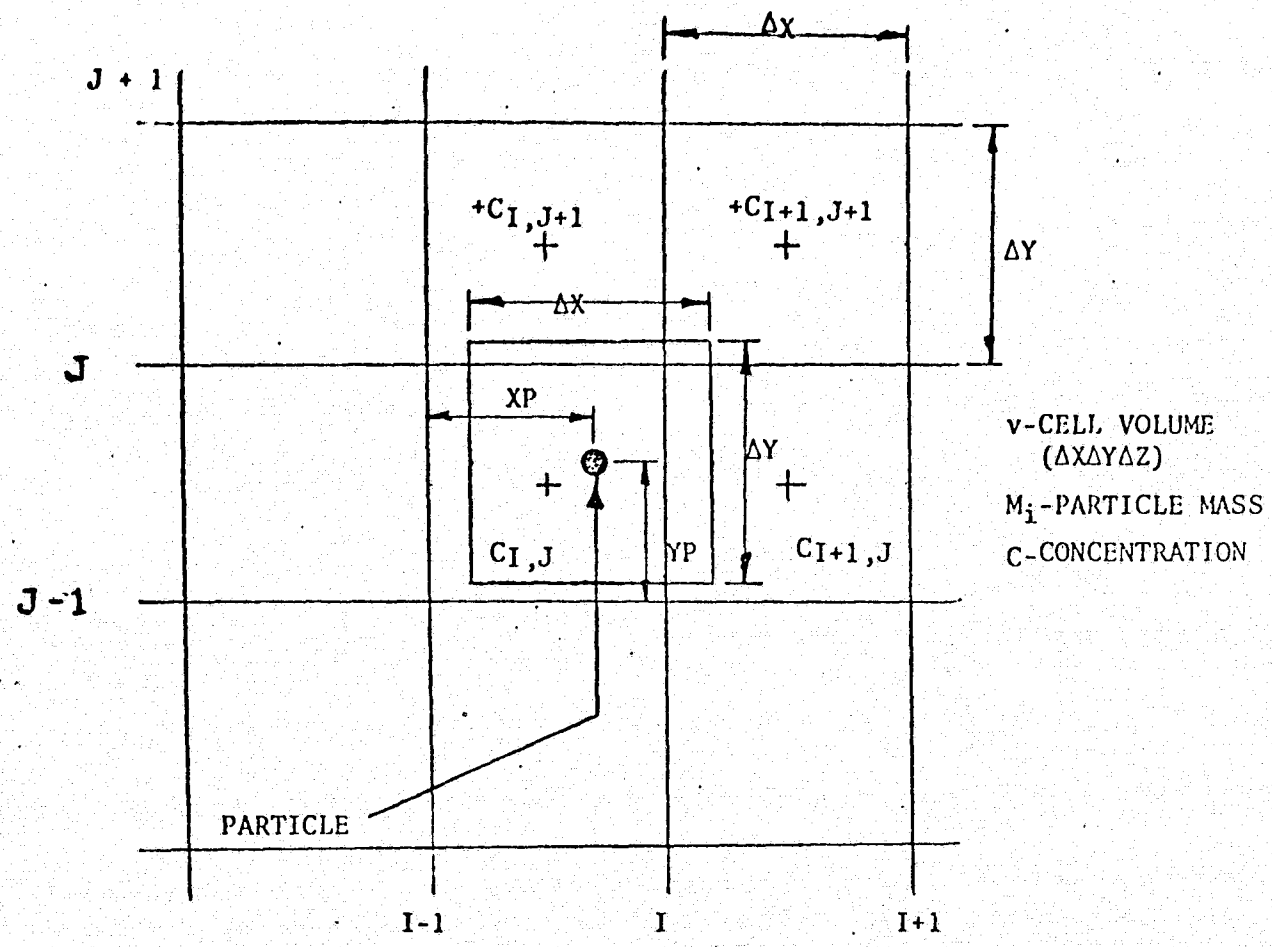

CONCENTRATION COMPUTATIONS

$$C_{I,J} = \frac{M}{v^2} (\Delta Z) \left(\frac{3\Delta X}{2} - XP\right) \left(\frac{3\Delta Y}{2} - YP\right)$$

$$C_{I+1,J} = \frac{M}{v^2} (\Delta Z) \left(XP - \frac{\Delta X}{2}\right) \left(\frac{3\Delta Y}{2} - YP\right)$$

$$C_{I+1,J+1} = \frac{M}{v^2} (\Delta Z) \left(XP - \frac{\Delta X}{2}\right) \left(YP - \frac{\Delta Y}{2}\right)$$

$$C_{I,J+1} = \frac{M}{v^2} (\Delta Z) \left(\frac{3\Delta X}{2} - XP\right) \left(YP - \frac{\Delta Y}{2}\right)$$

FIGURE 4.12 Two Dimensional X-Y View of Particle Concentration Weighting Scheme Inside the Eulerian Grid Matrix . . . . . .

The coefficients of this equation are determined by an analytic matrix solution procedure. (Figure 4.13) The velocity processor interpolates velocities from the fixed Eulerian system to the WAPIC mesh at each time step of the tidally driven transport simulation. This velocity interpolation technique is ideal when the WAPIC total grid mesh span is smaller than two or three hydrodynamic grid cells. When the WAPIC Eulerian grid grows to such a size that it is as large as a 4x4 tidal hydrodynamic field, then the surface fitting technique may produce discontinuities in the interpolated velocity field, if there are large variations in the velocity vector field. Should the expanding grid system encounter an island or outer boundary, expansion and translation is stopped and the twelve point surface fitting technique is replaced by a simple linear velocity extrapolation technique using the four nearest hydrodynamic grid neighbors to interpolate the velocity at the WAPIC grid point.

G. Particle Generation Procedures

WAPIC has three methods for locating marker particles within the Eulerian cells. These methods are as follows:

1. Instantaneous Gaussian Release

In general, turbulent Fickian diffusion from a point source in homogeneous uni-directional unbounded flow has a three dimensional Gaussian character (33). The concentration field can be described as exhibiting normal

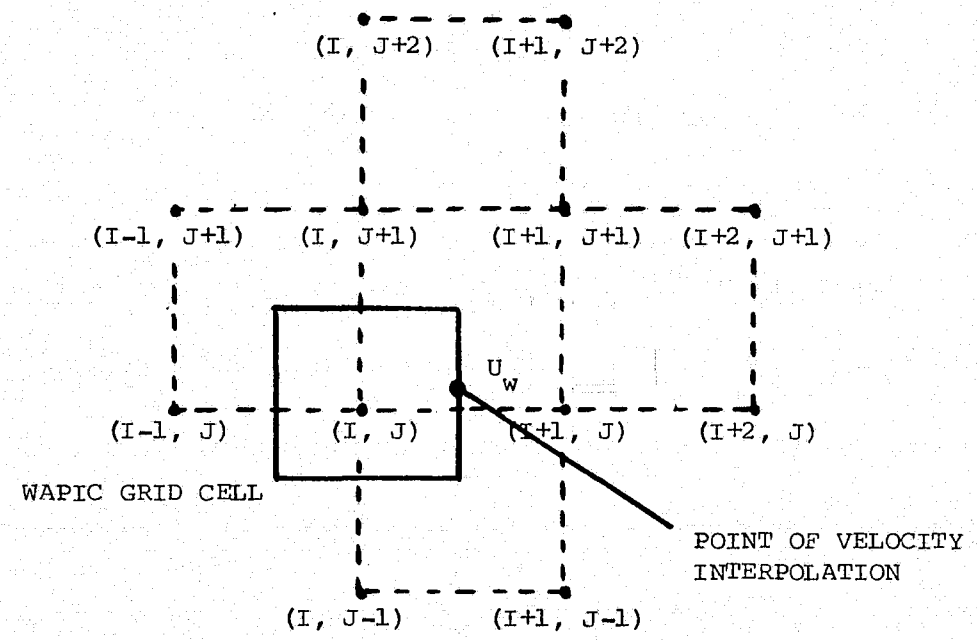

(I,J) LOCATION OF HYDRODYNAMIC VELOCITIES IN FIXED SPACE

U_w WAPIC ADVECTIVE VELOCITY ON TRANSLATING AND EXPANDING GRID

12 NEAREST FIXED GRID VELOCITIES (I,J) ARE USED TO FIT A SURFACE FOR THE INTERPOLATION OF THE VELOCITY AT U_w

FIGURE 4.13 Two Dimensional Velocity Processor Surface Fitting Interpolation Scheme

behavior around a maximum concentration. The assumption is made in the WAPIC procedure that the so called instantaneous point release, after a sufficient dispersion time, has some Gaussian character which can be described by its standard deviations about some mean position in cartesian space. The assumption is made that an initially finitely sized evenly distributed waste cloud such as the turbid plume from a dredge spoil disposal operaton can be represented in the long term dispersion phase as if it were a point release that had grown to a normal " Gaussian" concentration distribution in space.

Several experiments were conducted using Gaussian random number generators, similar to those used by Lange (28), to place the marker particles inside the Eulerian grid cells. These techniques proved to give particle distributions that displayed visual "bunching" or crowding around the major area of release center and required excessive computational time to place a large number of marker particle within the grid system. This problem was directly related to the quality of the Gaussian random number generators.

An alternative method was devised. This method specifies the number of particles to be placed in each ceil by using a Gaussian probability function. The assumption is made that 99.5% of the particles are within a range of ± 3*sigma (sigma= std. deviation from a given mean in three dimensional space). By specifying the three dimensional grid cell and standard deviation lengths and

the distance of each Eulerian grid cell from the mean particle position, the total number of particles per Eulerian grid cell can be determined by a simple analytic Gaussian function. A uniform random number generator is used (39) to locate the appropriate number of particles in each Eulerian grid cell. Should the need arise to utilize another type of initial distribution of marker particles, all that is necessary is to specify another analytic function that will specify the number of particles per Eulerian cell.

2. Continuous Gaussian Releases

A plume or continuous Gaussian release may be simulated by releasing a Gaussian particle distribution at the point source location for each succesive time step.

3. Uniform Random Distribution

The option has been included in WAPIC to fill any rectangular volume in the Eulerian grid with a uniform random marker particle distribution. This method may be useful in simulating the short term transport from an instantaneous plug or plane constituent release.

H. Particle Settling Velocities

The advantage of utilizing the PIC method for modeling transport of suspended sediment particles is that a spectrum of settling rates for particles within the cloud may be superimposed upon the advective and diffusive

particle velocities. The assumptions are made, for sake of simplicity and due to the lack of adequate field measurements of vertical density, that the water column is vertically well mixed in density and homogeneous with respect to vertical turbulence; and that a given Lagrangian marker particle statistically represents a given mass of sediment particles in the water column, all of equivalent density and still water asymptotic settling rate, Ws.

This particle settling rate is calculated by Watson's (40) empirically modified version of Rubey's (41) analytically derived still water settling law for sand grains.

$$W_S = \frac{(9A^2\mu^2 + (4/3)SR^3(\rho_p - \rho_{FL})\, g - 3A\mu)^{\frac{1}{2}}}{SR\rho_{FL}} \qquad (4.13)$$

S = pressure drag coefficient = 0.5303 dimensionless

A = viscous drag coefficient = 0.623 dimensionless

R = particle radius cm

W_S = settling velocity cm/sec

μ = fluid dynamic viscosity poise

ρ = mass density gm/cm^3

FL, P = subscripts for fluid or particle density

This vertical settling velocity is then added to the vertical advective and diffusive velocities to yield

$$W_T = W + W_D + W_S \tag{4.14}$$

or in dimensionless vertical velocity form

$$\omega_T = \omega + \omega_D + \omega_S \tag{4.15}$$

Using the above equation, a spectrum of particle settling rates can be represented by specifying sediment particle diameters and densities for the individual Lagrangian marker particles.

V. ACCUARCY PARAMETERS, PARTICLE-CELL RELATIONSHIPS

Since WAPIC is a Lagrangian particle in Eulerian finite difference cell technique, the questions may be asked: What effects do the relationships between the number of marker particles and the number of Eulerian cells used to resolve their distribution have on the accuracy and stability of WAPIC'S predictions? How well does WAPIC'S three dimensional Gaussian distribution procedure produce a truly normal cloud distribution? A discussion of the particle generation procedures and the accuracy and stability requirements of the particle in cell method follows.

A. Number of Eulerian Cells

A basic requirement for all methods that use Eulerian grid systems and finite difference or finite element procedures is that sufficient grids are utilized to resolve the concentration gradients of interest. In order to make an appropriate estimate of the number of Eulerian grid cells needed to resolve the normal concentration distribution in time and space, the technique employed by Lange (28) will be used.

Consider the one dimensional finite difference approximation to the diffusion velocity

$$U_{i+1/2} = - \frac{K_{x_{i+1/2}}}{c_{i+1/2}} \frac{[c_{i+1} - c_i]}{\Delta x} \qquad (5.1)$$

by dropping the subscript for the i+1/2 terms and expanding

Ci+1 and Ci in a Taylor series about i+1/2 to the first contributing term:

$$U_{series} = -\frac{K_x}{c\Delta x}\left[\frac{\partial c}{\partial x}\Delta x + \frac{1}{24}\frac{\partial^3 c}{\partial x^3}\Delta x^3 + H.O.T.\right] \qquad (5.2)$$

Expanding Eq. 5.2 and dropping the higher order terms yields

$$U_{F.D.} = -\frac{K_x}{c}\frac{\partial c}{\partial x} - \frac{K_x}{24}\frac{\Delta x^2}{c}\frac{\partial^3 c}{\partial x^3} \qquad (5.3)$$

The first term on the right hand side of Eq. 5.3 is the exact differential expression for the diffusivity velocity, and the second term is the first contributing error term. Taking the ratio of the WAPIC diffusion velocity approximation and the exact differential diffusion velocity yields

$$\frac{U_{F.D.}}{U_{EXACT}} = 1 + \left(\frac{\partial^3 c}{\partial x^3}\Big/\frac{\partial c}{\partial x}\right)\frac{\Delta x^2}{24} \qquad (5.4)$$

In order to obtain an estimate of the effect of Eulerian grid cell size on the diffusion velocity error term in Eq. 5.4, consider the simulation of a one dimensional Gaussian concentration distribution

$$c = \frac{Q}{\sigma}\left[-x^2/2\sigma^2\right] \qquad (5.5)$$

σ = Standard deviation

Q = Mass released

The first and third derivatives of Eq. 5.4 can be defined as

$$\frac{\partial c}{\partial x} = -\frac{Qx}{\sigma^3} e\,[-x^2/2\sigma^2] \tag{5.6}$$

$$\frac{\partial^3 c}{\partial x^3} = \frac{Qx}{\sigma^5}\left[3 - \frac{x^2}{\sigma^2}\right] e\,[-x^2/2\sigma^2] \tag{5.7}$$

Substitution of Eqs. 5.6 and 5.7 into Eq. 5.4 , yields

$$\frac{U_{F.D.}}{U_{EXACT}} = 1 - \frac{1}{24}\left(\frac{x^2}{\sigma^2} - 3\right)\frac{\Delta x^2}{\sigma^2} \tag{5.8}$$

Since 99% of all particles in a one dimensional Gaussian distribution lie within a distance x=3*sigma ,the substitution of x=3*sigma into Eq. 5.8, yields

$$\frac{U_{F.D.}}{U_{EXACT}} = 1 - \frac{\Delta x^2}{4\sigma^2} \tag{5.9}$$

For purpose of illustration, the substitution of sigma= ΔX or 2* ΔX in Eq. 5.9 yields a diffusion velocity error of 25% and 6.25 % respectively. This indicates that as more grid cells are used to resolve a given standard deviation of the Gaussian particle cloud, the WAPIC finite difference approximation becomes an increasingly better estimate of the exact analytic diffusion velocity.

B. Number of Particles Per Cell

The Lagrangian marker particles statistically represent the dissolved or suspended mass in the ambient flow field. Usually, for the case of numerical modeling of horizontal mass transport in estuarine and coastal areas, the turbulent diffusive transport is on the order of 0.1-5 % of the advective fluid velocities (35). When the particle cloud is small in relation to the scale of spatial variations in the advective velocity field, then the diffusive transport will govern the spread of the cloud about its center of mass, while the center of mass being transported with the mean velocity of the flow field. When the particulate cloud reaches into a field of velocity shear, then the advective velocities will dominate the spread of the particle cloud. Therefore, the more particles that can be used to represent a cloud or mass distribution in space, then the more finely can the diffusive mass transport process be simulated, provided that there is accurate resolution of the velocity field. However computer storage requirements and run time (run time is directly proportional to the number of marker particles) may place limits on the number of particles available for a given simulation.

WAPIC stores (IBM 370-155 , Fortran IV) the X,Y,Z coordinates and mass of each particle in one dimensional arrays. Figure 5.1 illustrates the minimum amount of storage (real*4) bytes required to handle these arrays

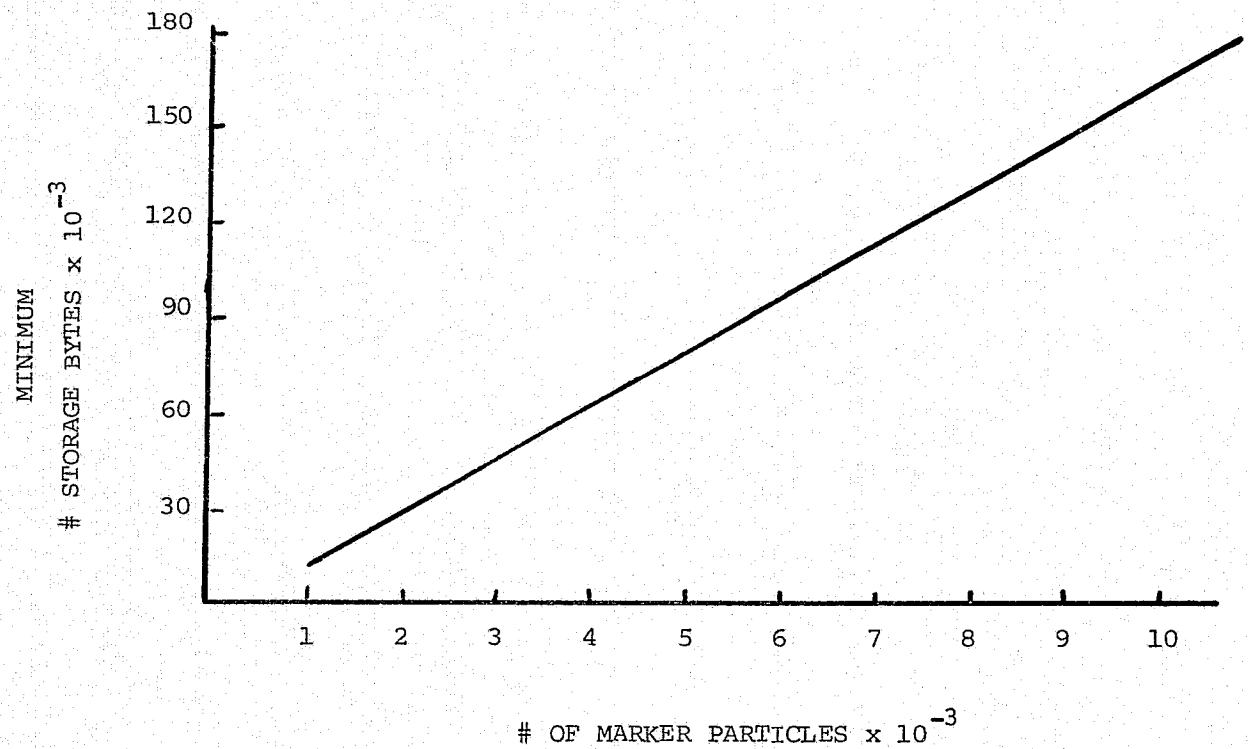

FIGURE 5.1 Minimum Three Dimensional Computer Storage Versus Number of Marker Particles

versus number of particles.

Assuming that the marker particle cloud is three dimensionally Gaussian, then the length or range of the cloud is approximately 6*sigma (3*sigma around the mean, where sigma is the standard deviation of the distribution). A ratio of sigma/dx of 2, (where sigma/dx equals the standard deviation to grid length ratio) provides a diffusion velocity with an approximate error of 6 % . Thus, if 6% error is acceptable, there will be required at least 12 grids (6x2) to represent the particle cloud in each dimension. Assume then that a 15x15x15 X-Y-Z Eulerian grid can resolve the concentration gradients within the Gaussian cloud. WAPIC utilizes three dimensional storage arrays for the Eulerian U, V, W velocities and concentration C and boundary cell flag M. Thus a 15x15x15 grid requires at least another

5x15x15x15x4 = 67.5 k bytes of real*4

Using Figure 5.1 and the above, for a Gaussian cloud of 5000 marker particles, at least 157.5 k storage bytes are required to accurately predict the three dimensional diffusion velocity.

As explained in Chapter IV. , WAPIC assigns a fictitious cell volume the size of an Eulerian grid to each marker particle. This technique allows the overlap of particle mass into its eight nearest neighboring cells, which tends to smooth the concentration field and thus the diffusion velocities. The question might be asked - How few marker particles per Eulerian cell, when using the

fictitious volume sharing scheme, will yield meaningful results for particle diffusion velocity calculations and therefore the diffusive spread of the particle cloud ? Lange (28) determined empirically that - " As few as one particle will obtain meaningful results. With fewer particles than that, ie. when particles have no neighbors around them, the diffusion velocity algorithm moves the particle to a center of an Eulerian cell and freezes it there."

C. Stability, Accuracy , Time Step Restrictions

Since WAPIC uses a finite difference Eulerian grid, it has a dynamic stability or time step restriction that states that the fastest moving particle can translate no more than one half a cell length in a given time step dt. This restriction is commonly used in vorticity transport solution techniques (16) and numerical tidal hydrodynamic models (17,18,42), and is defined for WAPIC'S uses as

$$\left[\frac{U_T \Delta t}{\Delta x}, \frac{V_T \Delta t}{\Delta y}, \frac{W_T \Delta t}{\Delta z}\right] \leq \frac{1}{2} \qquad (5.10)$$

where U_T , V_T , W_T are the Eulerian total pseudo transport velocities at time T, and ΔX, ΔY, ΔZ are the grid cell lengths. For purposes of this work the above time step restriction in Eq. 5.10 shall be called an accuracy

requirement, or accuracy number. Roache (16) states that PIC methods exhibit high frequency oscillations in the marker particle field which may be visualized as a type of instability in the solution procedure. The time step restriction acts to damp the amplitude of these marker particle oscillations in the Eulerian grid space. An example of this solution instability and the effect of the time step restriction will be demonstrated in a subsequent chapter.

As discussed in Chapter IV., should the user choose not to utilize the time centered iterative particle velocity interpolation technique and the flow field displays an eddy structure or curved streamlines, then the time step should be reduced below the value given by Eq. 5.10, for accuracy of particle motion prediction. The exact value of the time step needed is situation specific. The author recommends, though, that the time centered iterative technique be utilized, because of the substantial savings in reduced computational time for a specified accuracy of particle motion prediction (37).

D. Choosing a Standard Deviation - Grid Size Ratio

As discussed in Chapter IV., WAPIC simulates an instantaneous Gaussian release in space by using a normal distribution equation to specify the number of particles per Eulerian cell. A uniform random number generator

locates the individual particles in each Eulerian cell. The question was asked how well does this procedure produce a truly normal particle distribution? This question arises from the knowledge that the initial particle distribution influences the short and intermediate time concentration field when modeling mass transport in homogeneous turbulent unidirectional flow (33). Also, as mentioned previously, the ratio of the initial cloud standard deviation and grid spacing determines the accuracy of WAPIC'S diffusion velocity prediction. A rephrased question might be - How many marker particles are necessary to achieve a normal distribution with a given sigma/dx, (where again sigma/dx represents the ratio of the standard deviation to grid length), ratio that will allow accurate short and long term prediction of cloud dispersion ?

In order to achieve an accurate diffusion velocity and thus an intermediate and short term cloud disperson prediction, a sigma/dx ratio greater than one should be used, and preferably a ratio of two, which would be 94% accurate in the diffusion velocity approximation. As the ratio of sigma/dx increases beyond two, the computer storage and run time increase because the size of the Eulerian grid must increase. As in pure Eulerian schemes, a trade off exists between accuracy of prediction and computational costs.

Yevjevich (43) " provides a method for testing a particle distribution for normality. He provides two test criteria for a Gaussian or normal character

$$-0.10 < Cs < 0.10$$

and

$$-0.50 < E < 0.5$$

where Cs is the skewness coefficient and E is the excess coefficient of the particle distribution. The skewness coefficient is a measure of the asymmetry independent of the dimension of the variable, and is defined as the ratio of the third central moment to the second central moment to the 3/2 power.

$$C_s = \frac{M_3}{M_2^{3/2}} = \frac{M_3}{\sigma^3} \qquad (5.11)$$

M_2 = Second Moment

M_3 = Third Moment

C_s = Skewness Coefficient

where

$$M_r = \frac{1}{N} \sum_{i=1}^{N} (x_j - \bar{x})^r \qquad (5.12)$$

$\bar{x}$ = Mean

N = # Samples

M_r = Moment #

r = 1, 2, 3...

The excess coefficient is defined as the excess kurtosis relative to that of the normal distribution

$$E = \gamma_2 - 3 \qquad (5.13)$$

$$\gamma_2 = M_4/M_2^2 = M_4/\sigma^4 \qquad (5.14)$$

where a normal distribution is defined as having a kurtosis coefficient of 3. If E is negative then the distribution has a sharper peak than the normal distribution, and if E is positive then the inverse is true.

A procedure was written to test WAPIC'S Gaussian particle distribution scheme for ability to produce a "truly" normal distribution for varying numbers of particles at various sigma/dx ratios. Three dimensional "spherically normal" particle distributions were produced for sigma/dx ratios of 1.0 to 3.0 in increments of 0.25, using 1000 to 10000 particles in increments of 1000 for each ratio. The second, third and fourth moments around the mean were calculated, which allowed the calculation of the actual sigma/dx ratio, skewness coefficient and excess coefficient of each distribution.

Figure 5.2 illustrates the actual sigma/dx ratios derived from the estimated sigma/dx ratios at various particle numbers. From this figure the following approximations can be made.

1. Approximately 1000,1700,3000,4500 particles are needed to achieve an actual sigma/dx ratio of 1.0,1.25,1.5 and 1.75 respectively.

2. At estimated ratios greater than or equal to 2.0 more than 10000 particles are necessary to achieve an exact ratio agreement with the estimate.

3. At an estimated ratio of 2.0, there is little incentive to use more than 3000 particles, because there is very little change of slope in the actual line from 3000 to

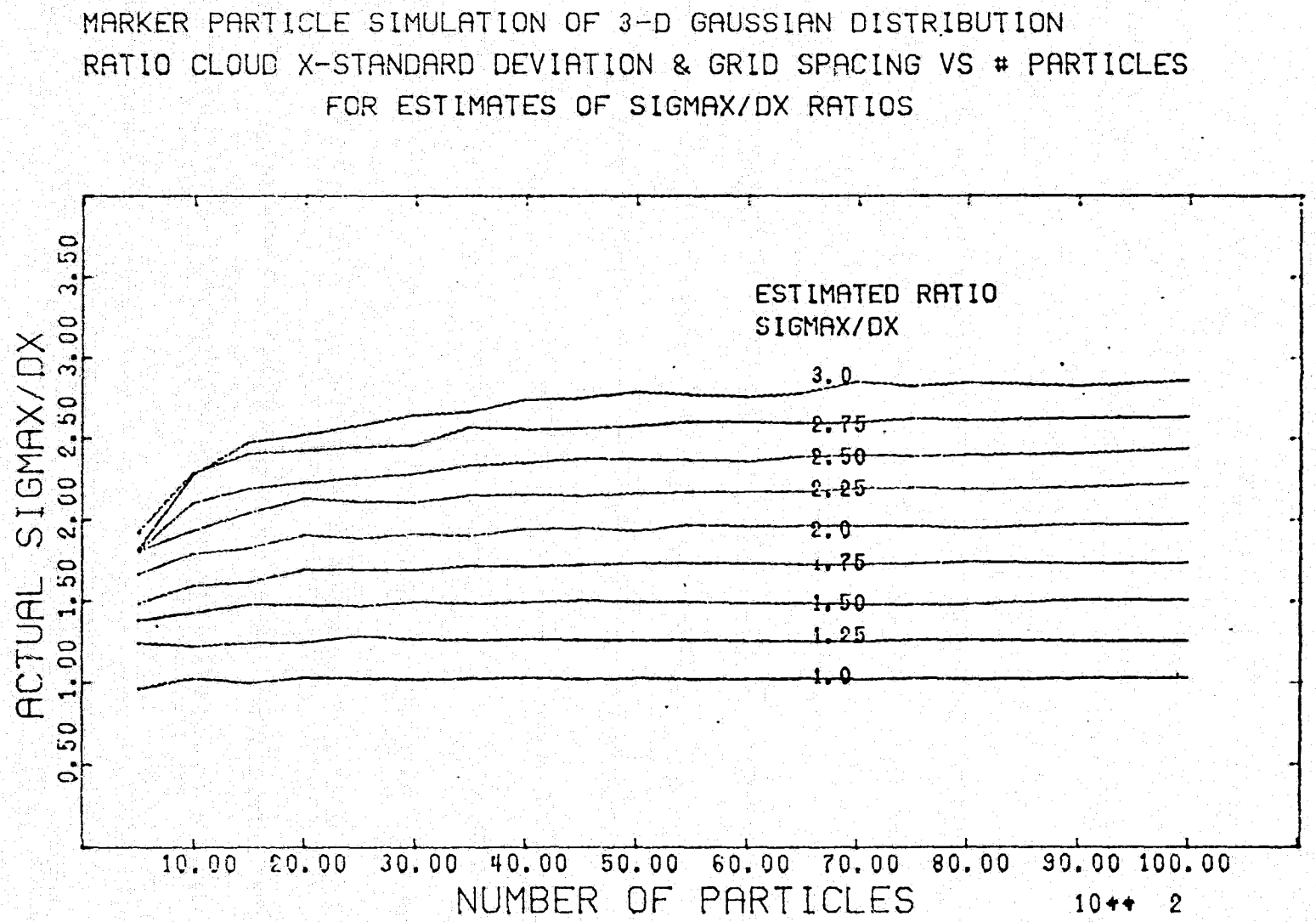

FIGURE 5.2 Actual Standard Deviation of WAPIC Particle Distribution Versus Number of Particles for Estimated Standard Deviation to Grid Length Ratio

10000 particles.

4. In order to achieve sigma/dx ratios greater than 2.0 within an accuracy of 10% more than 2000 particles are required.

Figure 5.3 illustrates a plot of the particle distribution X-skewness coefficients at sigma/dx ratios of 1.0,2.0,3.0 versus the number of marker particles. From this figure the conclusion is made that WAPIC'S procedure produces particle distributions well within the skewness constraints regardless of the number of particles and sigma/dx ratio, within the limits tested in this example.

Figure 5.4 illustrates a plot of the X-excess coefficients at sigma/dx ratios of 1.0,2.0,3.0 versus the number of marker particles. From this figure the following conclusions are drawn :

1. At sigma/dx ratio of 3.0, a negative excess kurtosis is produced when less than 3000 particles are used.

2. WAPIC'S procedure produces an excess coefficient for a normal distribution for sigma/dx ratios of 1.0 and 2.0, well within the range of excess of a normal distribution for sigma/dx ratios of 1.0 and 2.0 for all particle cases tested.

The method produces a normal distribution with a slight negative kurtosis (greater than -0.5) for particle numbers greater than 3000, indicating slightly higher concentration gradients in the center of the distribution.

In general, Figs. 5.3 and 5.4 illustrate the

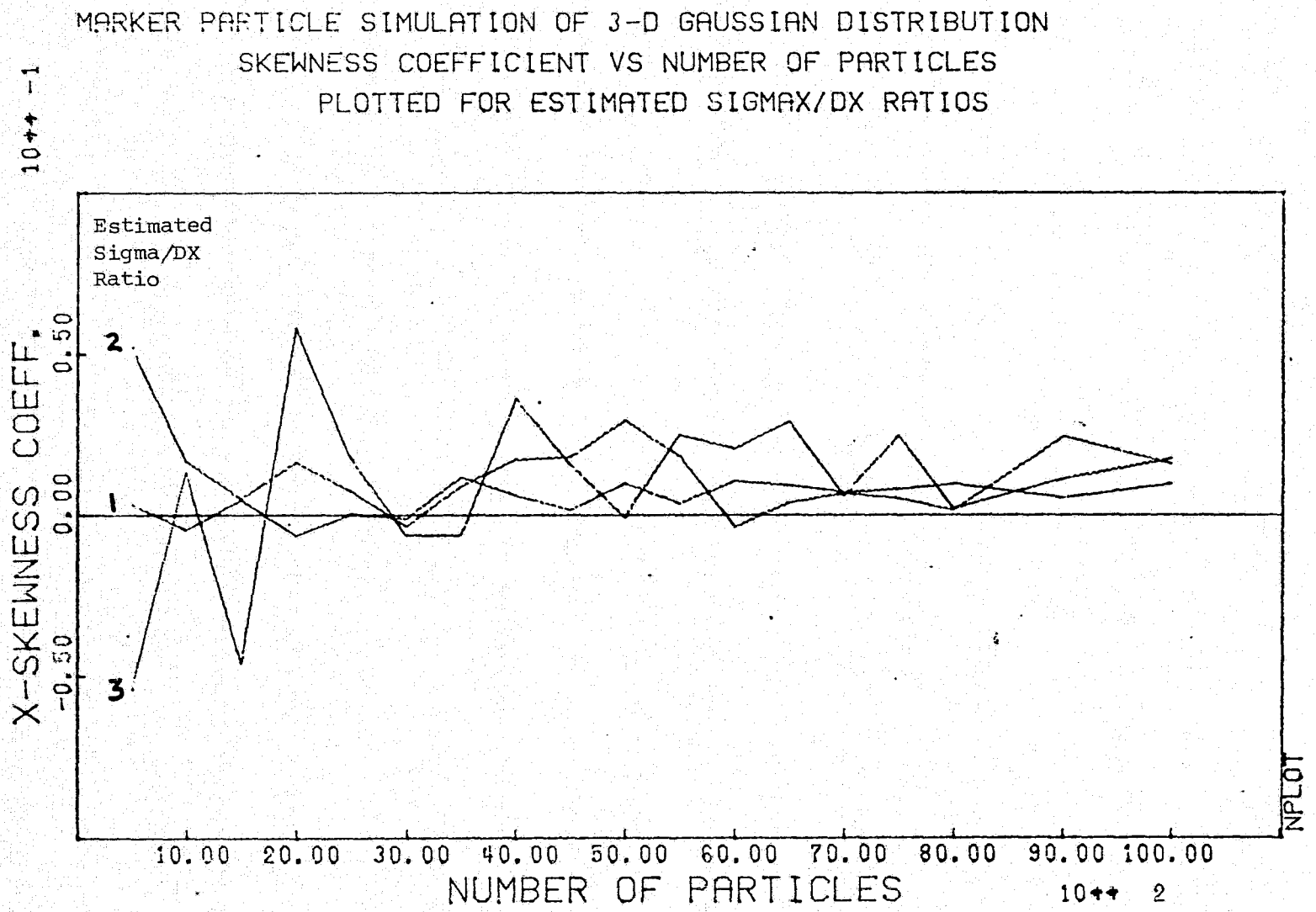

FIGURE 5.3 Skewness Coefficient of WAPIC Particle Distribution Versus Number of Particles for Estimated Standard Deviation to Grid Length Ratio

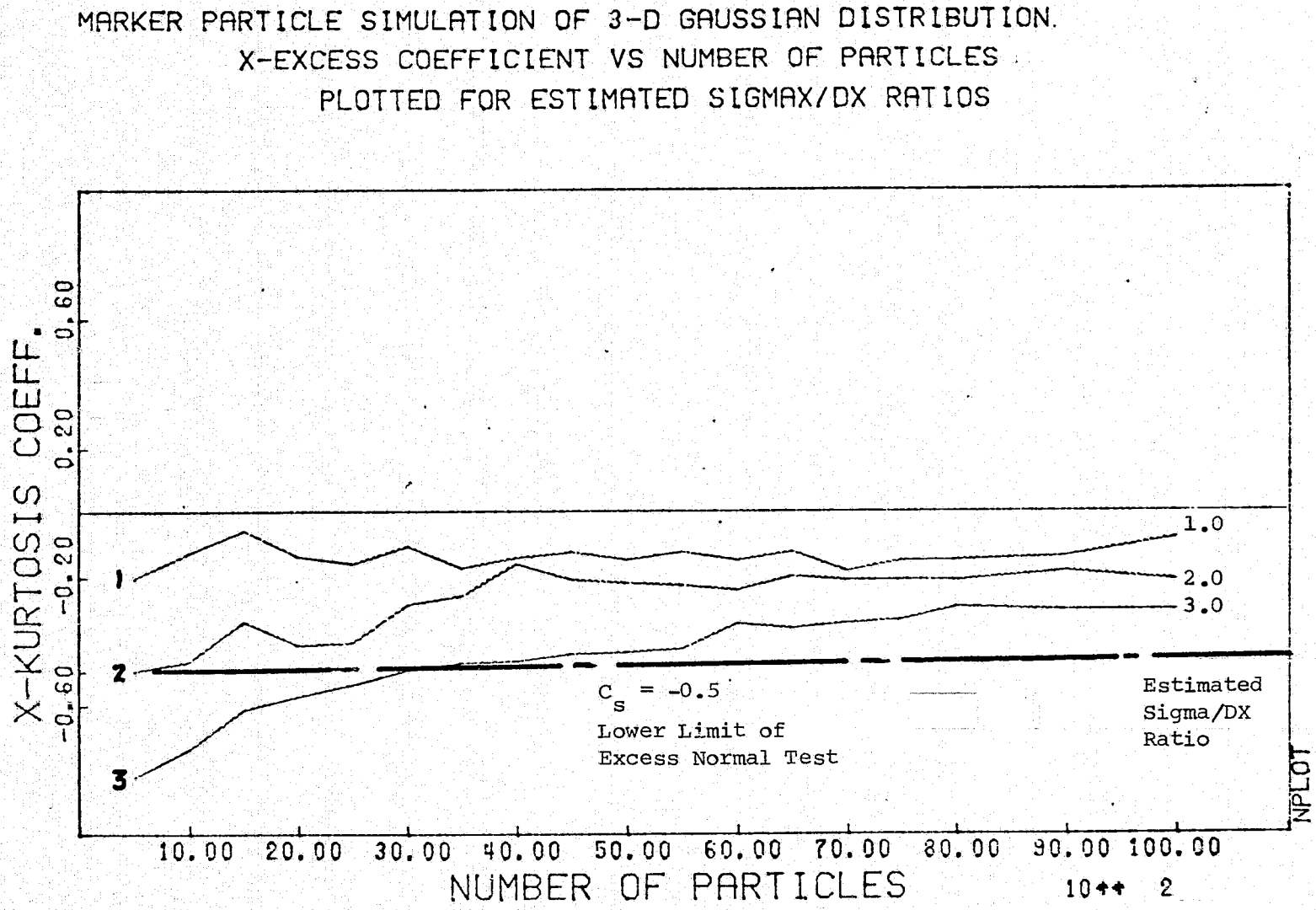

FIGURE 5.4 X-Excess Coefficient of WAPIC Particle Distribution Versus Number of Particles for Estimated Standard Deviation to Grid Length Ratio

effectiveness of WAPIC'S Gaussian particle distribution procedure in producing a "truly normal" distribution.

VI. TURBULENT DIFFUSION AND DISPERSION

A. Definition of Diffusion and Dispersion

Within the literature of numerical modeling of mass transport the processes responsible for net transport of dissolved or suspended constituents in a turbulent fluid, are advection, diffusion, and dispersion (4). Advection refers to the transport of some dissolved or suspended constituent by a spatially or time averaged velocity component.

A qualitative definition of diffusion and dispersion has been suggested by Holley (47) - " Let diffusion refer to transport in a given direction due to the difference between the true convection in that direction and the time average in that direction. Let dispersion refer to the transport in a given direction due to the uncertainty in a given direction due to the spatial average in that direction."

The turbulent ensemble time averaging of the mass transport equation produces a mean advective flux term and non linear advective terms of the form (4,17)

$$\frac{\partial}{\partial x_i} \overline{(U_i' \, c')} \quad i = 1, 2, 3 \tag{6.1}$$

This nonlinear advective term is impossible to specify at every given time and spatial point in a continuum. The assumption, which has physical validity, is that turbulent diffusion develops a " Gaussian" or normal concentration

distribution in space centered around a mean value in that given dimension of measurement (33). The linearizing assumption is made that

$$\frac{\partial}{\partial x_i} \overline{(U_i' c')} = \frac{\partial}{\partial x_i} K_i \frac{\partial c}{\partial x_i} \tag{6.2}$$

where

$$K_i \frac{\partial c}{\partial x_i} = \overline{(U_i' c')} \tag{6.3}$$

This allows the formidable time averaged values of the product of the deviations from the mean of the concentration and velocity field, to be replaced by the product of a constant coefficient and the gradient of the mean concentration.

In a similar manner, the three dimensional mass transport equation may be also spatially averaged with reference to deviations from the spatial mean velocity and concentrations. The gradients of the spatial average of the product of the deviations of concentration and velocities from the mean values are replaced by the product of an asymptotic "dispersion" coefficient and the spatially averaged mean concentration gradient.

The processes of turbulent diffusion and dispersion can be visualized as the "advective" transport by

components of velocity which deviate from the time and spatially averaged mean component of the velocity, ie. "turbulent velocity fluctuations." Assuming that the molecular diffusion scale is small compared to the scale of "turbulent" motions of a fluid particle, turbulent diffusion and dispersion do not exist; there is only advection of suspended mass by random velocity components (33). The terms turbulent diffusion and dispersion are mathematical descriptions for extra terms left over from the time and spatial averaging of the three dimensional mass transport equation.

Deterministic numerical mass transport models linearly simulate the turbulent transport of a suspended constituent through a distribution of finite grid cells or elements in space. Due to computer storage and computational time limitations, the numerical solution to the partial differential equation must be represented by discrete time steps across finite grid lengths. The continuum technique is to advance the initial concentration distribution through time across the finitely divided space domain. Numerical models thus employ both time and spatial averaging techniques to estimate a given level of constituent.

For the numerical modeling purposes of this work, Fickian diffusion and dispersion will be considered to be one and the same, as opposed to the definitions of Holley. In lieu of a more proper choice, the term turbulent diffusion will be used to describe the uncertainities in

the spatial and time averaged values of the mean advective and concentration field.

Thus K is a coefficient relating the uncertainty in the measurement of the advective velocity and concentration field due to time or spatial averaging the instantaneous flow and concentration field. Components of motion which have length and time scales smaller than that used by the numerical or analytic solution technique, may appear as as sub grid turbulence or may not appear at all. Turbulent advective motion with time and length scales greater than that used in the numerical system are difficult to specify within the field, and as will be discussed shortly, are approximated empirically by a scale dependent diffusion law.

Before presenting the methods for estimating diffusion coefficients , a discussion of " Fickian" diffusion and the "scale effect" in turbulent mass transfer would be informative.

B. Fickian Diffusion

As previously stated, the turbulent diffusion coefficient is used to replace the non linear terms of the form $d/dx(\overline{U_i c})$, which result from the averaging process. The popularly termed Reynold's shear stress analogy, employed by Von Karmann in 1934 (48) for a stationary homogeneous turbulent flow field, states that the rate of

transport of any characteristic of a fluid across a streamline (heat, salinity, silt, etc.) is proportional to the gradient of momentum (or of the given property) in the direction of transfer.

$$\frac{\overline{U_i' U_j'}}{\partial Uj/\partial x_i} = \frac{\overline{U_i' c'}}{\partial c/\partial x_i} = K_i = E_i \qquad (6.4)$$

This analogy allows turbulent diffusion to be defined in the same manner as molecular " Fickian" diffusion which has a " Gaussian" character (33).

C. Statistical Properties of Diffusion

The asymptotic Fickian description of turbulent eddy diffusivity assumes that the free stream turbulence has a stationary and homogeneous character. In the ocean, turbulence is not homogeneous or stationary. The observation was made (33), that eddies larger than the particulate cloud, advect it as whole, while smaller scale eddies produce a scattering of the cloud around its center of mass. As the cloud expands in size the boundaries between the eddies contributing to advection and those responsible for diffusion shift to larger scales. The cloud then goes through a short explosive expansion stage (33). The turbulent Fickian approach for describing cloud

expansion as a linear function of time fails to explain this behavior.

An alternate approach for describing the diffusion mechanism is the "stochastic" or statistical approach employed by Taylor (49). Taylor's equation for one dimensional diffusion in a turbulent stationary homogeneous mean flow field is defined as

$$\sigma_i^2(t) = 2\,U_i^2 \int_o^t (t-\tau)\, R_{U_i'(\tau)}\, d\tau \qquad (6.5)$$

where $\sigma_i(t)$ = the radius of inertia of the particle cloud, equal to the rms of instantaneous particle displacement $(\overline{x^2})^{\frac{1}{2}}$ and,

$$R_{U_i'(\tau)} = \overline{U_i'(t)\,U_i'(t+\tau)}/\overline{U_i'}^2 \qquad (6.6)$$

is the Lagrangian correlation coefficient of the particle velocity distributions taken over the interval T to T + ΔT;

where

τ = the time lag

$\overline{U_i'^2}$ = the mean squared instantaneous turbulent velocity in the i-direction.

Equation 6.5 describes the diffusion of a fluid particle about the mean position of the group. If the free stream turbulence is convected at a velocity Ui, then diffusion refers to the instantaneous displacement from a point moving with velocity Ui. a A general form of $\delta i(t)$ for all time t is difficult if not impossible obtain because of the functional dependence on the Lagrangian correlation coefficient. The Lagrangian correlation coefficient of the velocity field is independent of time for a stationary process and is an even function. This variable describes the "persistence" of the value once it is realized.

Equation 6.5 can be approximated, though, at the limits, $\tau=0$ and $\tau \rightarrow$ infinity. At a very small diffusion time $\tau \rightarrow 0$, where the $\lim_{\tau \rightarrow 0} R_{u_i'}(\tau) = 1$, Eq. 6.5 becomes

$$\sigma_i^2 (t) = \overline{U}_i'^2 \, \Delta t^2 \qquad (6.7)$$

This relationship states that at small diffusion times, the standard deviation of the particle cloud grows approximately linearly with time. This phase is called the linear phase, where the center of mass of the relatively small cloud meanders, with reference to a fixed frame, with the turbulent motion of the eddies. The cloud is so small

that the relative diffusion is due to sub-inertial range eddies.

When $\tau \rightarrow$ infinity, the so called asymptotic phase of diffusion, the cloud is large compared to the energy containing eddies. The center of gravity is no longer subject to displacement by turbulent eddies and is translated solely by the mean motion, the turbulent diffusion coefficient being defined as

$$\frac{1}{2}\frac{d\sigma i^2}{dt} = \overline{U}'^2 t_L = K_{i\ \text{Asymptotic}} \qquad (6.8)$$

t_L = Lagrangian time scale

where K_i, is a " Fickian" constant diffusion coefficient, and the standard deviation of the cloud grows as the square root of time.

During the intermediate stage of diffusion, $0 < \tau < \infty$, the relative diffusion is dominated by eddies on the order of the size of the cloud. Dimensional considerations by Batchelor (50,51), show that

$$\frac{1}{2}\frac{d\sigma_i^2}{dt} = \epsilon^{1/3}\sigma_i^{4/3} = K_i(t)_{\text{Intermediate}} \qquad (6.9)$$

Equation 6.9 states that the apparent eddy diffusivity is a non-linear function of time and increases with the 4/3

power of the cloud standard deviation. The validity of this relationship was first demonstrated by Stommel (52). Eq. 6.9 may be integrated to yield (33)

$$\sigma_i^{2/3} = \epsilon^{1/3} (t - t_o) \qquad (6.10)$$

In terms of time elapsed from the effective origin, t , the particulate cloud grows, or explodes, as $(t - t_o)^{3/2}$. This behavior, is in contrast, to the $(t)^{1/2}$ growth in the asymptotic Fickian diffusion stage, or in the initial linear growth stage. Csanady shows that the lifetime of this explosive stage is relatively short, or shorter than the lifetime of the energy containing eddies. As the cloud continues to grow the asymptotic diffusion stage is reached, where the cloud becomes large compared to the turbulent eddies. Csanady summarizes the governing mechanisms for horizontal cloud spread in the ocean:

" If the release of marked fluid takes place some distance from the shore, the field of turbulence surrounding the effluent may be expected to be horizontally homogeneous to a good approximation. Our theoretical results should therefore apply to such releases; in particular, if the initial cloud size is small compared to the typical horizontal eddy, a phase of accelerated relative (4/3 law) diffusion should be observable, during which the cloud grows non-linearly with time. The duration of this phase should be relatively short, and be followed by the asymptotic phase, where the cloud grows with the square

root of time."

Some striking support can be found for Csanady's observations in Sayre and Chang's work (53). They cite the experimental evidence of Yotasukura, et. al. (54), Glover (55), and Godfrey and Frederick (56), for longitudinal diffusion in homogeneous turbulent bounded channel flow: " In general the agreement for Fickian theory and experimental observations is poor in the early stages of diffusion, but tends to improve with increasing diffusion time or distance from the source." No comment was made about any attempt by Sayre and Chang to fit the initial data with a 4/3 type cloud growth law, though. They recommend that " The Gaussian or asymptotic turbulent diffusion mechanism be used for predicting diffusion at large times or distances from the source in flume diffusion studies. "

What these flume diffusion experiments could not ascertain is that when a dye patch becomes on the order of 1 kilometer or larger its diffusion rate increases sharply again, as if the 4/3 power was valid over a much larger range of eddy motion. Hunter and Spaulding (7) provide a review of attempts to validate the 4/3 law in the ocean, comparing the work of Yudelson (57), Okubo (58) and Koh and Chang (5). Figure 6.1 shows a comparison of Okubo's data and a least squares fit (composite) for diffusion coefficient versus length scale. Where the 4/3 law is

$$K_i = \epsilon_i l_i^n \quad i = x \text{ or } y \tag{6.11}$$

Hunter offers

$$K_i = 0.10\ l_i^{0.9983} \text{ in cm.} \qquad (6.12a)$$

$$K_i = 0.0059\ l_i^{0.9983} \text{ in feet} \qquad (6.12b)$$

This indicates a nearly a linear growth dependence for the diffusion coefficient with the cloud length scale. Indeed, a theoretical point source release which expands to the order of kilometers would experience a cascade of turbulent eddy sizes or scales of motion thus experiencing a multitude of linear asymptotic, and non-linear scale dependent diffusion phases. The practical utility of fitting a straight line to the above data obscures the cascade of cloud growth phases.

The discrepancies between simple statistical theory and actual diffusion theory are evident from the fact that turbulence in a flow field is not homogeneous, ie., many scales of eddy motion are present. As a particulate cloud expands, large turbulent eddy scales come into play. A constant eddy diffusivity plateau (asymptotic) is intermittently reached, and then surpassed as the cloud reaches into a larger scale flow structure, the cloud seeming to explode, growing with $(t-t_o.)^{3/2}$, for a relatively short time.

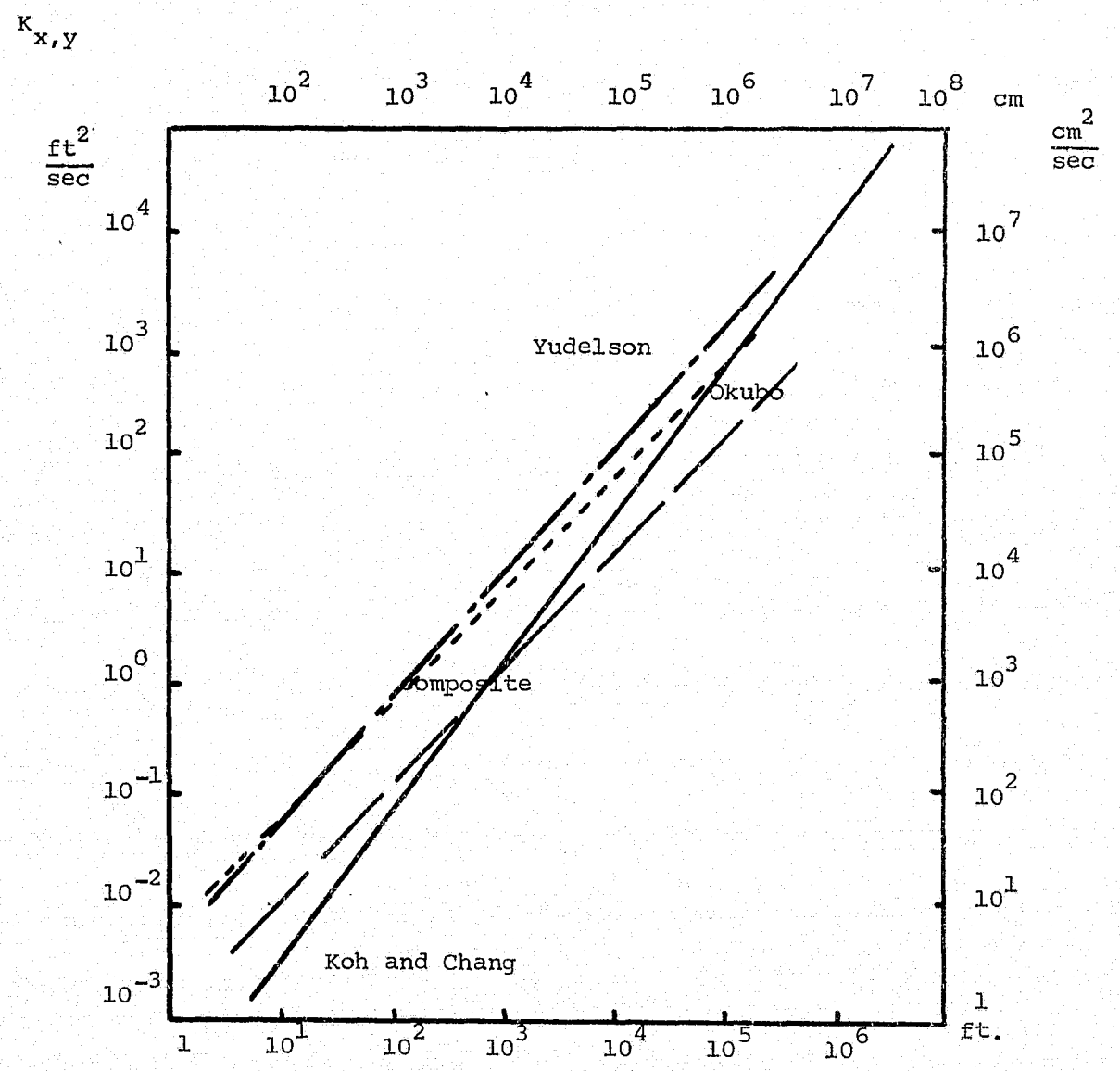

FIGURE 6.1 Offshore Diffusion Coefficient Relations

$K_{x,y}$ vs. l

If these larger scale flow structures can be regarded as a velocity shear of the mean flow field, then the increased cloud growth rates may be attributed to the non-uniformity of this field (33). As a practical measure Csanady recommends that the homogeneous turbulent mean velocity field model be retained and the use of empirical (4/3 law) data on cloud growth be used to predict diffusion coefficients.

D. Practical Calculation Methods

For practical use, in predicting transport of constituents in numerical models, diffusion might now be defined as the turbulent deviations in the mean velocity field due to the time and spatial averaging processes.

1. Horizontal Diffusion

The work of Elder (59) has been applied by Holley, Harleman, and Fischer (60) to estimate horizontal diffusion coefficients in the tidally dominated estuarine environment. Hunter and Spaulding adopted Elder's method with the addition of Leendertse's (61) formulation for the added effects on diffusion due to the wind.

$$K_i = K_i(\text{Elder}) + K_{WIND} \qquad (6.13a)$$

where the Elder diffusion coefficient relations approximate the observed spatial variations in the mean flow field in a

given dimension (shear) to the turbulent diffusion coefficients (popularly termed dispersion relations)

$$K_x = 5.93Hu^* = K_x = K_y \text{ Offshore} \tag{6.13b}$$

$$K_y = 0.23Hu^* = K_y \text{ Estuary} \tag{6.13c}$$

$$K_z = 0.06Hu^* \tag{6.13d}$$

and the added effects on the total diffusive transport due to the wind are approximated by a scale dependent 4/3 cloud growth law

$$K_{WIND} = .0059\, l_x^{0.9983} \tag{6.13e}$$

$$l_x = 3\sqrt{2\sigma_x\sigma_y} = l_y \tag{6.13f}$$

These modifications approximate the added effects of the wind in the form of turbulent eddies, surface drift currents, and predicts diffusion when the mean velocity in the tidally driven flow field is zero. A first order estimate of the length scale of the diffusing cloud might be the physical horizontal Fulerian grid size, or a typical vertical depth of the hydrodynamic field. Thus for a grid size equal to a nautical mile, (6800 ft.), a first guess for an asymptotic diffusion coefficient might be

$$K_{x,y} = 0.0059\ (6076)^{0.9987} = 40\ Ft^2/sec \tag{6.14}$$

The horizontal diffusion terms can then be calculated at points throughout the Fulerain grid using Elder's

relationships, (Eqs. 1) b,c,d), modified by the addition of a 4/3 power law to take in the added effects of the wind, (Eq. 6.13 e), as large scale turbulence within the flow field.

2. Vertical Diffusion and Sediment Transport

As stated by Hunter and Spaulding (7) - " Diffusion in the vertical direction is restrained by the bottom and the free surface, and by the magnitude of the vertical component of the flow, which is normally very small relative to the horizontal flow. Thus it has an effect several orders of magnitude smaller than that of horizontal diffusion. The latter, however, is still a small effect when diffusive transport is compared with advective transport. This is not likely to be the case in the vertical direction, since the vertical flow is also very small. Vertical diffusion and vertical advection are very closely related effects, since they are driven by the same force (instability). Since vertical diffusion is also highly dependent on wave action, it is likely to be more important than advection." Numerical mass transport schemes normally use diffusion alone to model vertical transport of constituents, because of ignorance of the vertical advective field.

The procedure is to calculate the vertical diffusion coefficient by a correlation with the Richardson number (7)

$$R_i = g/\rho \frac{d\rho}{dz} / 0.7(U/h)^2 \qquad (6.15)$$

where ρ = density of water
z = vertical level
h = total depth
U = horizontal velocity

which relates the stabilizing forces of the vertical stratification and the destabilizing forces of the lateral shear flow. Table 6.1 details a summary of the experimental values of the vertical diffusion coefficient in the ocean and Table 6.2 (from Spaulding (32)) details various attempts to correlate Kz with the Richardson number. Hunter and Spaulding applied Pritchard's equation (62) for calculating vertical diffusion in the Providence River.

$$K_z = \frac{\eta_\rho (U_z)^2}{H^3} (H - z^2) (1 + \beta_\rho R_i)^{-2} + \alpha_\rho z \frac{(H-z)}{H} \frac{WH}{WT} \text{EXP} \left(\frac{-2\pi z}{WL}\right) (1 + \beta_\rho R_i)^{-2} \quad (6.16)$$

where

η_ρ, β_ρ, α_ρ, are adjustable constants

R_i = Richardson #

z = distance downward from surface

H = total depth

WH = wave height

U_z = horizontal velocity at z

WT = wave period

WL = wave length

The problem with Eq. 6.16 is that the physical density field and wind field must be measured, and this may indeed be difficult when trying to estimate diffusion coefficients in offshore areas. In addition, the equation has only been

SUMMARY OF VALUES OF VERTICAL DIFFUSION COEFFICIENT K_z IN THE OCEAN (5)

Note: Molecular diffusivity for heat: 1.5×10^{-3} cm^2/sec (at 20°C, 1 atm)
salt: 1.3×10^{-5} cm^2/sec (at 20°C, 1 atm)

Current or oceanic region	Depth of layer (m)	Vertical Diffusion Coefficient K_z (cm^2/sec)	Reference	
Philippine Trench	5000-9788	2.0-3.2	Schmidt, 1917	*
Algerian Coast	0- 20	35-40	Schmidt, 1917	*
Mediterranean	0- 28	42	Schmidt, 1917	*
California Current	0- 200	30-40	McEwen, 1919	*
Caspian Sea	0- 100	1-3	Stockman, 1936	*
Barents Sea	-----	4-14	Subov, 1938	*
Bay of Biscay	0- 100	2-16	Fjeldstad, 1933	*
Equatorial Atlantic Ocean	0- 50	320	Defant, 1932	*
Randesfjord	0- 15	0.1-0.4	Jacobsen, 1913	*
Schultz Grund	0- 25	0.04-0.74	Jacobsen, 1913	*
Kuroshio	0- 200	30-80	Sverdrup-Staff, 1942	*
Kuroshio	0- 400	7-90	Suda, 1936	*
Southern Atlantic Ocean	400-1400	5-10	Defant, 1936	*
Arctic Ocean	200- 500	20-50	Sverdrup, 1933	*
Carribean Sea	500- 700	2.8	Seiwell, 1938	*
South Atlantic Ocean	3000-Bottom	4	Defant, 1936	*
South Atlantic Ocean	Near Bottom	4	Wattenberg, 1935	*
West Atlantic Trough (50°S to 10°N)	Near Bottom	7-50	Wüst, 1955	**
North Atlantic Indian Ocean Pacific Ocean	Near Bottom	4-30	Koczy, 1956	**
Tidal Channel (Mersey estuary and Irish Sea)	0- 20 (bottom)	2-40	Bowden, 1965 (with R_i from 0.1 to 2.0)	
Near Cape Kennedy, Florida	Surface Layer	19 (in August) 1.3 (in Summer	Carter and Okubo, 1965	
Bikini Lagoon	0- 50 (bottom)	260	Munk, Ewing and Revelle, 1949	
Coast of Denmark		0.05-1	Harremoes, 1967	***
California Coast		0.1-10	Foxworthy, Tibby and Barsom, 1966	***
-------	4	15-180 (at wind force 3-4)	Stommel and Woodcock, 1951	****

* As given by Defant, 1961
** As given by Bowden, 1962
*** As given by Harremoes, 1967
**** As given by Wiegel, 1964

TABLE 6.1 Summary of Values of Vertical Diffusion Coefficient K_z in the Ocean . . . . . (5)

SUMMARY OF FORMULAS ON CORRELATION OF VERTICAL DIFFUSION COEFFICIENT K_z WITH RICHARDSON'S NUMBER R_i (OR DENSITY GRADIENT ϵ) (Reference 5)

Note: K_{z0} : K_z at $R_i = 0$, i.e., the neutral case β : proportionality constant varies from case to case

Rossby and Montgomery (1935)*	$K_z = K_{z0}(1+\beta R_i)^{-1}$	
Rossby and Montgomery (1935)*	$K_z = K_{z0}(1+\beta R_i)^{-2}$	
Holzman (1943)*	$K_z = K_{z0}(1-\beta R_i)$	$R_i \leq \frac{1}{\beta}$
Yamamoto (1959)*	$K_z = K_{z0}(1-\beta R_i)^{1/2}$	$R_i \leq \frac{1}{\beta}$
Mamayev (1958)*	$K_z = K_{z0} e^{-\beta R_i}$	
Munk and Anderson (1948)**	$K_z = K_{z0}(1+\beta R_i)^{-3/2}$ $\beta = 3.33$ based upon data by Jacobsen (1913) and Taylor (1931)	
Harremoes (1968)	$K_z = 5 \times 10^{-3} \times \epsilon^{-2/3}$ cm^2/sec note: ϵ in m^{-1}; approximate experimental range $5\times10^{-9} < \epsilon < 15\times10^{-5}$ m^{-1}	
Kolesnikov, et al (1961)***	$K_z = K_{z\,min} + \frac{\beta}{\epsilon}$ in cm^2/sec $K_{z\,min}$ and β are empirically determined to be: $K_{z\,min} = 12$, $\beta = 8.3 \times 10^{-5}$ (1958 and 1960 observations) $K_{z\,min} = 2$, $\beta = 10.0 \times 10^{-5}$ (1959 observations)	
Koh and Fan (1969)	$K_z = 10^{-4}/\epsilon$ (K_z in cm^2/sec; ϵ in m^{-1}) $4 \times 10^{-7} \leq \epsilon \leq 10^{-2}$ m^{-1}	

* As given by Okubo (1962)
** As given by Bowden (1962)
*** The formulas presented in the translated version are apparently erroneous.

TABLE 6.2 Summary of Formulas on Correlation of Vertical Diffusion Coefficient K_z with the Richardson Number, R_i, (or density gradient) (5)

verified for the James River.

Csanady (33) remarks that the assumption that the vertical mean velocities and turbulence levels are small in comparison to those in the horizontal is true only when the wind is relatively light. He cites the existence of Langmuir circulations (after Langmuir, (63)). When strong winds are present (Langmuir circulations are invariably present for winds above 16 ft/sec), and in particular when the surface is strongly cooled, large scale horizontally aligned vortical flow structures, with axes parallel to the wind, sweep water downward from the surface to the first stable sheet (64,65). These are commonly known as windrows, being horizontally parallel rows of vortices having opposite rotational direction, with areas of upwelling and downwelling alternating between the rows. Foam and debris accumulate at the lines of confluence of the vortical rows. (Figure 6.2) Their exact physical mechanism is not known (66), but whatever the mechanism, they rapidly distribute a "marked fluid" over the vertical range from the surface to the first stable sheet (33).

This mode of transport is not a turbulent mechanism, but is an advective flux, and cannot be described by a Richardson type vertical diffusivity coefficient formulation. If Langmuir circulations are present, then the effect is to rapidly distribute a marked fluid from the surface down to the first stable sheet.

For more practical purposes of calculating sediment transport, a conservative estimate can be made, if no field

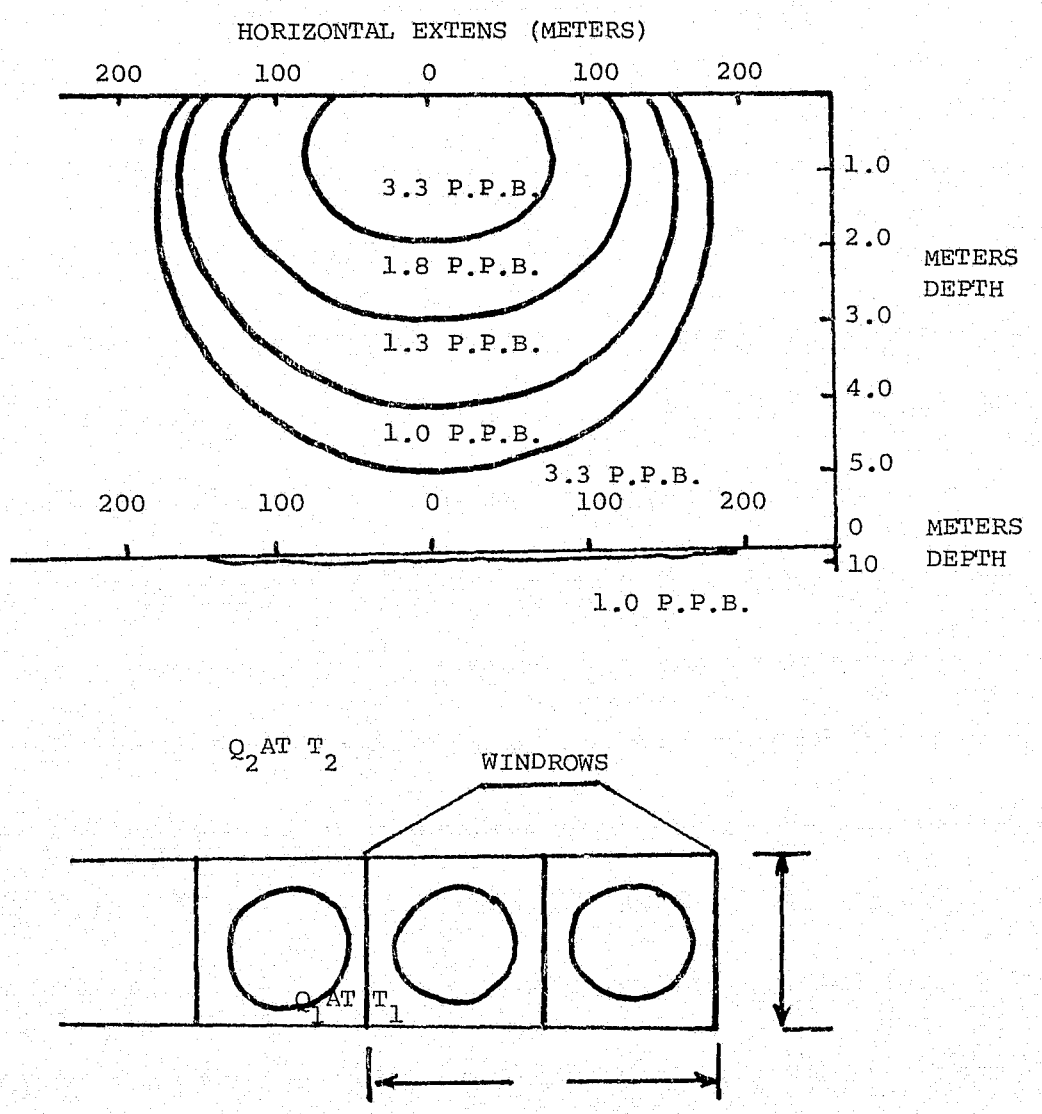

FIGURE 6.2 The Nature of Langmuir Circulations (Reference (33))

data is available, that the water column is well mixed, and a constant vertical eddy diffusivity can be be estimated by Eq. 6.13d, or others given by Hunter and Spaulding (7) in Table 6.1 . If enough data is present, the formulation of Pritchard, Eq. 6.16, may be used.

When considering the turbulent transport of non-buoyant sediment particles, the specification of the vertical turbulence level takes on new importance. Turbulence suspends the particles within the water column, just as dust particles are suspended by the " Brownian" random molecular motions.

For sedimentary particles, the rate of turbulent diffusive transport of mass of concentration c in the fluid, may be written

$$\beta K_z \frac{\partial^2 c}{\partial z^2} \qquad (6.17)$$

where beta is a constant on the order of unity, which is specific to a given constituent's physical characteristics, such as diameter and roughness. Experiments by Vanoi (44), later confirmed by Brush (45), and Milano (46), indicate that beta has a value equal to one for sediment grain diameters less than 0.2 mm. for a dilute suspension less than 3 % by weight of sediment.

In still, non-turbulent water, if it were not for vertical turbulence, negatively buoyant particles would drop out of the water cloumn with a nearly constant rate equal to the asymptotic free fall velocity. Murray (67)

demonstrated that the vertical turbulence levels produce oscillatory vertical particle motion for entrained sediment particles which in effect retards the fall out rate from that predicted by simple asymptotic free fall theory.

When trying to predict entrained sediment motion, WAPIC calculates a spatial-time averaged vertical diffusion velocity proportional to the product of the diffusion coefficient and the concentration gradient (see Eq. 3.6 c).

$$W_D = \frac{K_z}{c_{AVG}} \frac{\partial c}{\partial z} \tag{6.18}$$

A suspended particle is assumed to move with a vertical velocity which is the sum of the free fall settling velocity and the total vertical pseudo transport velocity. For purposes of illustration, assume that a channel 30 feet deep exists with a uniform Xdirected mean velocity of 1.0 ft/sec.

The diffusion coefficient may be estimated using a Manning coefficient of 0.020, and from Eq. 6.15-d, a Kz= 0.09 ft^2/sec. A particle of 0.000083 ft (0.0025 cm) mesh diameter with a specific density of 2.6 yields a settling velocity of 0.003 ft/sec from Rubey's modified settling law (Eq. 4.13) Assuming a vertical mixing length of 3.0 feet (a very conservative estimate, which equals 30ft/10 WAPIC vertical grids) a diffusion velocity may be approximated as

$$(W_D)_{MAX} = \frac{0.09\ Ft^2/sec}{3\ Ft.} = 0.35\ Ft/Sec \tag{6.19}$$

Indeed, this value is ten times larger than the sediment free fall velocity. A large diffusion coefficient with a corresponding small vertical settling velocity may result in large excursions for a WAPIC particle leading to oscillations in the vertical concentration field if the simulation time step (or vertical accuracy number) is not sufficiently small. This effect will be discussed in a section of the following chapter. The choice of vertical diffusion coefficient will help to determine the fallout rate in the simulation of sediment transport.

VII. VERIFICATION AGAINST ANALYTIC SOLUTIONS

Before WAPIC could be applied in the simulation of mass transport of sedimentary and pollutant materials in the coastal zone, some preliminary verification work was necessary. The purpose of the following studies was to test WAPIC and gain experience in the adaptation of WAPIC to various three dimensional mass transport situations. Five verification studies against analytic solutions to the mass transport equation were performed. The various operating parameters for each test case are summarized in Table 7.1 .

A. Unbounded Unidirectional Turbulent Flow Field

A spherically symmetric three dimensional Gaussian marker particle distribution was instantaneously released into a steady-uniform X-directed velocity field. Two thousand marker particles were placed, with a normal distribution in three space, within a 15x15x10 X-Y-Z Eulerian grid. A standard deviation to grid spacing ratio of 2.0 in the horizontal (X-Y) was utilized in order to approximate, to within 6% , the correct diffusion velocity, thus insuring the propagation of the initially spherical marker particle distribution in time. Uniform and time independent eddy diffusion coefficients were utilized.

CASE	FT X Y Z	TIME STEP t SEC	FT/SEC U. V. W.	BOUNDARY CONDITIONS GRID EXP. X Y Z	 GRID TRANSL. X Y Z	# GRIDS #X #Y #Z	NUMBER OF PARTICLES	INITIAL STANDARD DEVIATION FT. σ_{xo} X	 σ_{yo} Y	 σ_{zo} Z	DIFFUSION OR DISPERSION COEFT. FT^2/SEC K_x	 K_y	 K_z	MISCELLANEOUS OPERATING PARAMETERS
	500		1.0			15								
A.	500	250	0.0	Y Y Y	Y Y Y	15	2000	1000	1000	1.5	50.0	50.0	10001	$Q = 10^8$
	1.5		0.0			10								
	500		1.0			15								$\Omega_y = 0.0001$ sec^{-1}
B.	500	250	0.0	Y Y Y	Y Y Y	15	2000	1000	1000	1.5	50.0	50.0	0.0001	$U_o^y = 1.0$ FT/SEC AT CENTER OF CLOUD
	1.5		0.0			10								
	120		1.0			45								$T_{MAX} = 1930$ Secs.
C.	120	60.0	0.0	N N N	N N N	20	2816	240.0	240.0	3.0	50.0	50.0	.0001	$Q = 10^8$, $\frac{\delta Q}{\delta t} = 10^8$
	3.0		0.0			15								# PARTICLES/STEP = 88
	30		1.0			15								REFLECTION AT
D.	30	15.0	0.0	Y N N	Y N N	15	2000	60.	60.	2.0	25.	25.	.11	Y-Z BOUNDARIES
	2.0		0.0			15								W = 450 FT
														H = 30 FT
	240	60	1.0			15								MANNING COEFF. = 0.020
E.	30	30	0.0	N N N	Y N N	3	3000	NA	NA	NA	0.0	0.0	7.7	H = 30 FT
	2.0	20	0.0			3							EQUA	PARTICLE SETTLING RATES
														0.0005, 0.001, 0.005, 0.008
														0.01 FT/SEC
														REFLECTION AT SURFACE
														DEPOSITION AT BOTTOM

NA = DOES NOT APPLY Y = YES N = NO

Ω_y = SHEAR RATE (SEC^{-1})
H^y = DEPTH W = WIDTH
Q = MASS

TABLE 7.1 Operating Parameters for Verification Against Analytic Solutions

Comparison was made against a three dimensional analytic solution of the form, given by Quesada (68) -

$$c(x,y,z,t) = \frac{Q}{(2\pi)^{3/2}(\sigma_{xo}^2 + 2K_x t)^{1/2}(\sigma_{yo}^2 + 2K_y t)^{1/2}(\sigma_{zo}^2 + 2K_z t)^{1/2}}$$

$$x \text{ EXP } \left(- \frac{(x - U_o t)^2}{2(\sigma_{xo}^2 + 2K_x t)} - \frac{y^2}{2(\sigma_{yo}^2 + 2K_y t)} - \frac{z^2}{2(\sigma_{zo}^2 + 2K_z t)}\right) \quad (7.1)$$

$\sigma_{xo,yo,zo}$ = initial standard deviations
U_o = uniform steady current velocity
x,y,z = distances from initial center of mass of cloud
Q = mass
$K_{x,y,z}$ = asymptotic x,y,z turbulent diffusion coefficients

Equation 7.1 states that the standard deviations of the cloud particle distribution in a homogeneous turbulent steady flow field grow in a " Fickian " manner,

$$\sigma_x = (\sigma_{xo} + 2K_x t)^{1/2} \quad (7.2)$$

as the center of mass of the cloud moves downstream with the velocity U (33).

Figure 7.1 illustrates a two dimensional X-Y view of the WAPIC particle distribution at time T=0, and 10000 seconds. The axes of Figure 7.1 are in dimensionless X-Y grid units, where one grid unit = 500 length units. The center of mass of the cloud has translated a distance $U\Delta T$ = 10000 length units. Figure 7.2 details a direct quantitative comparison of WAPIC and the analytic solution for cloud concentration plotted as a function of downstream distance (in grid units) . The concentrations are

plotted for the cloud, at various times, along a line through the initial maximum concentration which is parallel to the downstream x axis. WAPIC concentration predictions are within an absolute value of 5 % of the analytic solution values.

An effort was made to illustrate the three dimensional diffusion process by producing two dimensional X-Y concentration contour plots at various Z-levels. Figures 7.3 and 7.4 illustrate analytic and WAPIC contours of concentration at times T=0,5000, and 10000 seconds. (Please ignore the difference in Z-levels in each corresponding frame of Figs. 7.2 and 7.3) This three dimensional unbounded diffusion study, verified WAPIC'S use of the translating and expanding grid options, and the approximation to the one dimensional diffusion velocity.

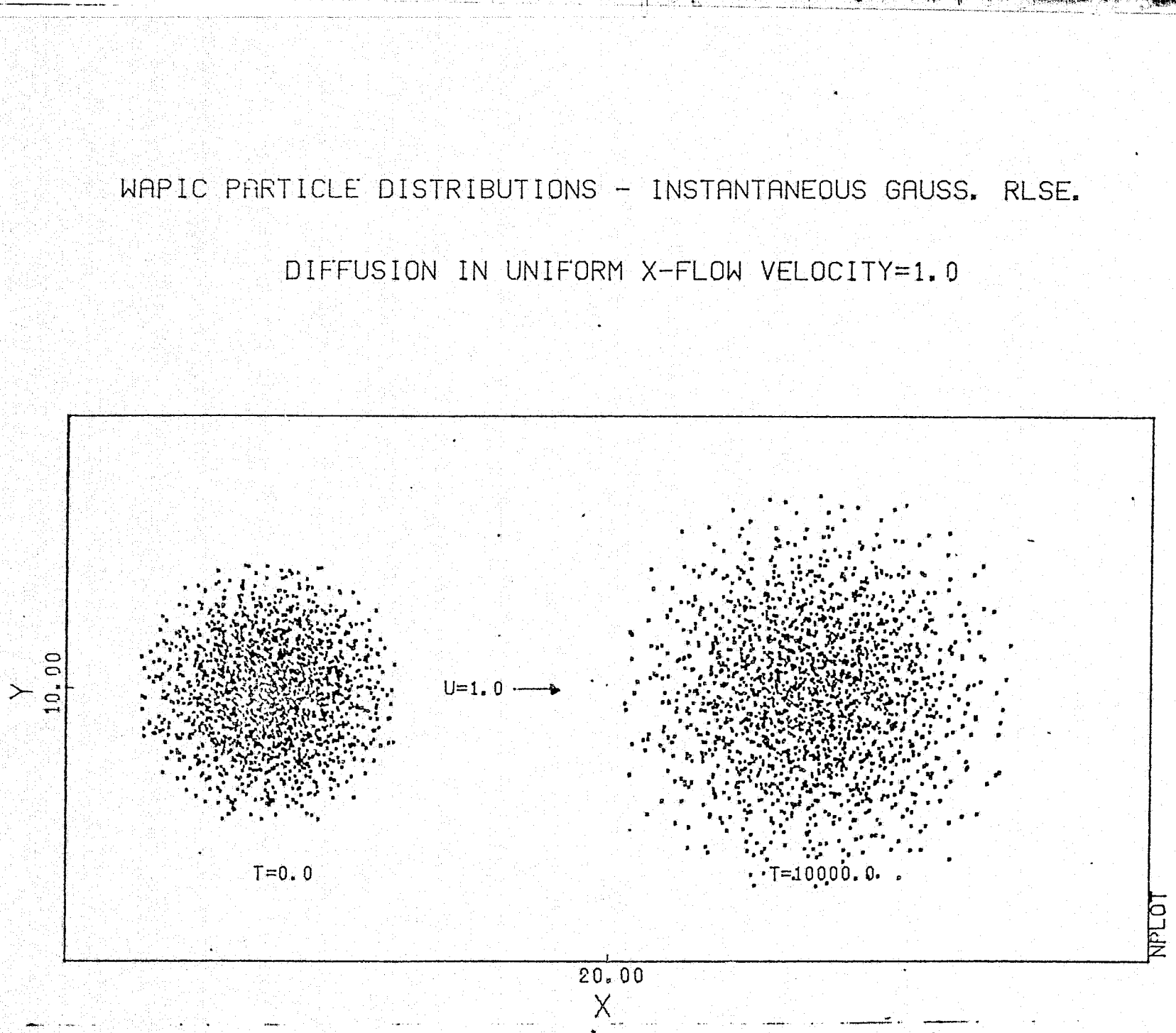

FIGURE 7.1 Two Dimensional Particle Distributions at Time T = 0, 10000 for Diffusion of an Initially Gaussian Release in a Unidirectional Steady Flow Field

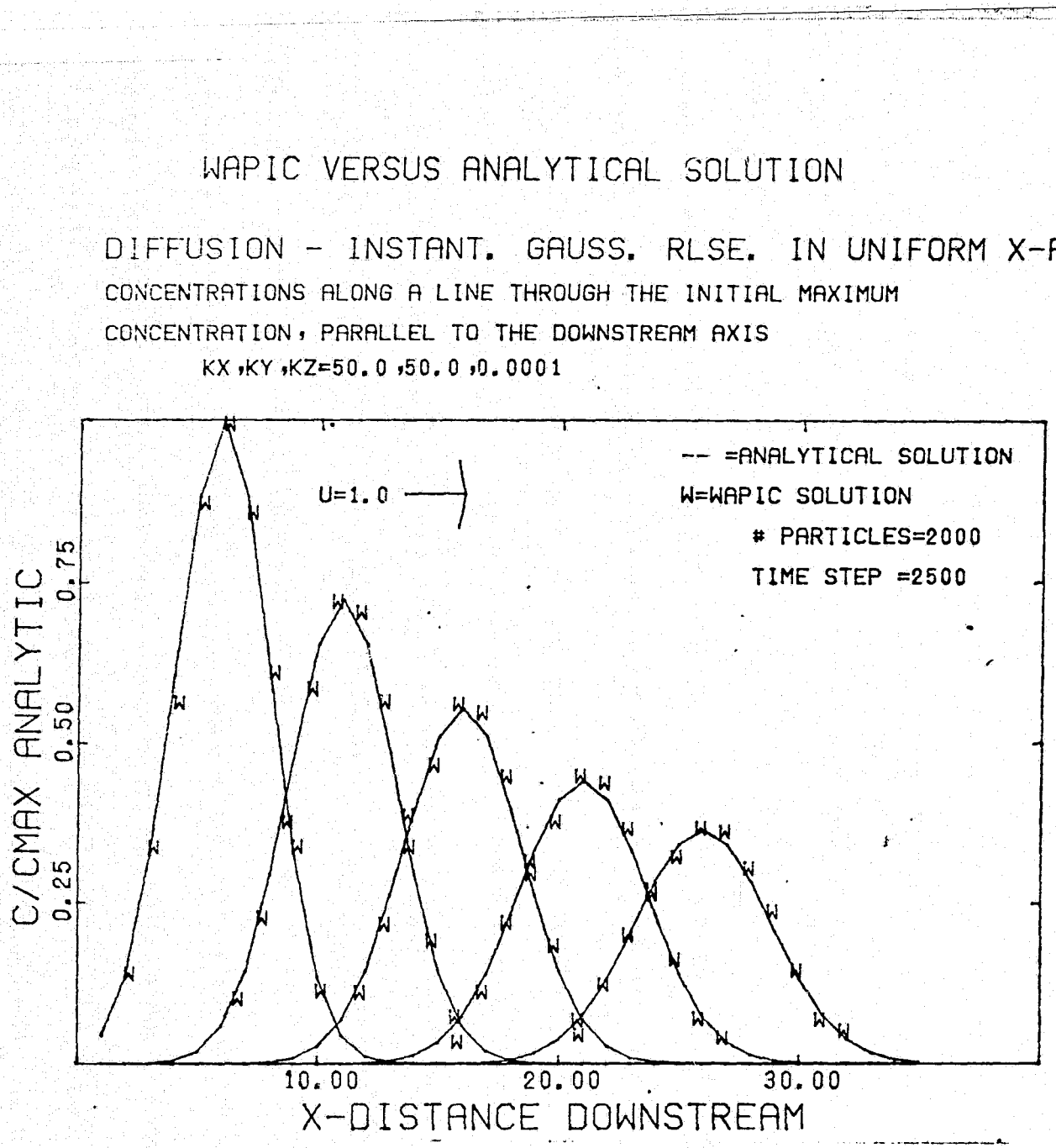

FIGURE 7.2 WAPIC Versus Analytic Solution, Diffusion an Initially Gaussian Release in a Unidirectional Flow Field, Concentrations Along a Line Through the Initial Maximum Value, Parallel to the Downstream Axis

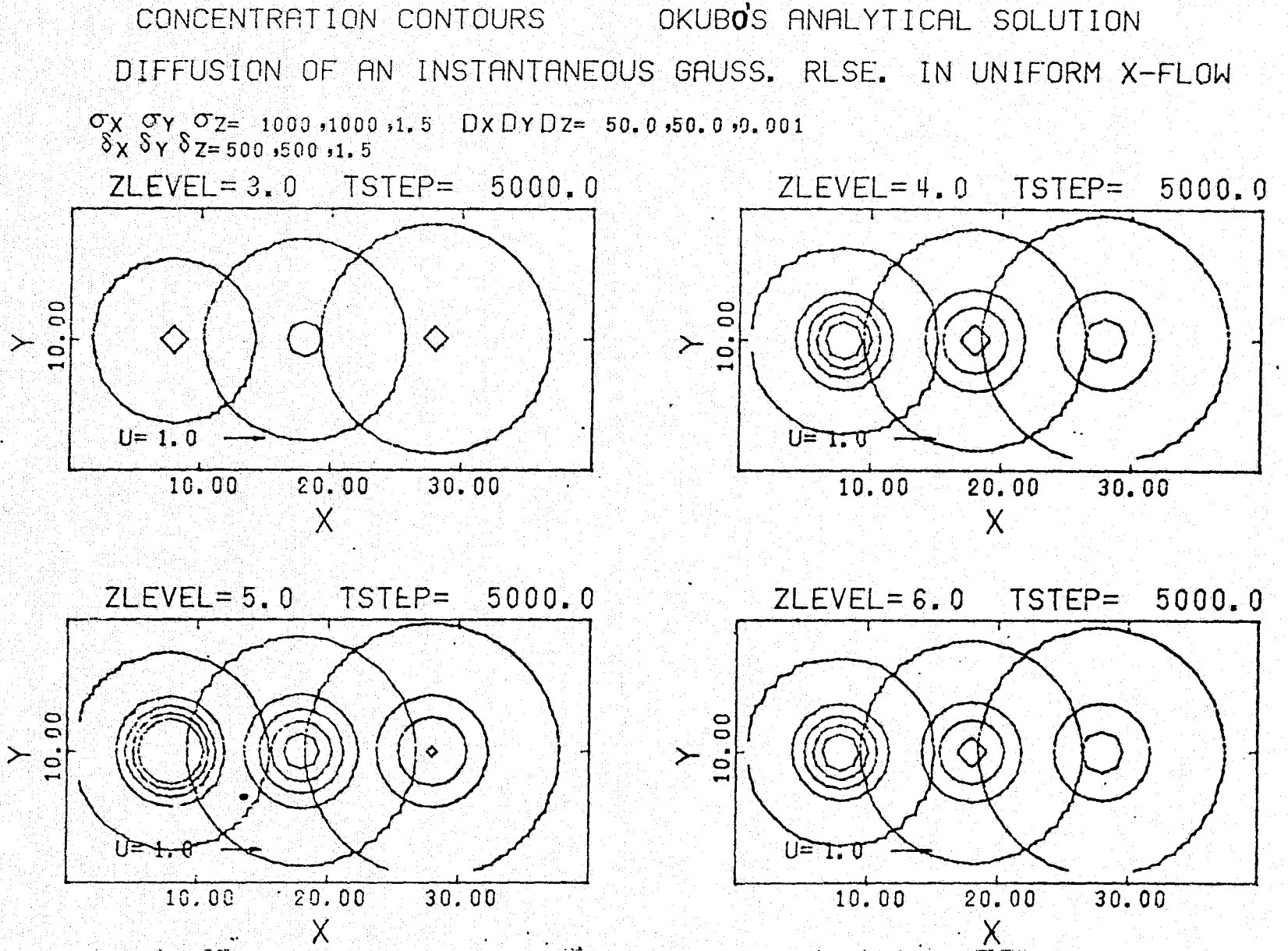

FIGURE 7.3 Concentration Contours, Okubo's Analytic Solution for Diffusion of an Instantaneous Gaussian Release in Uniform X-Flow

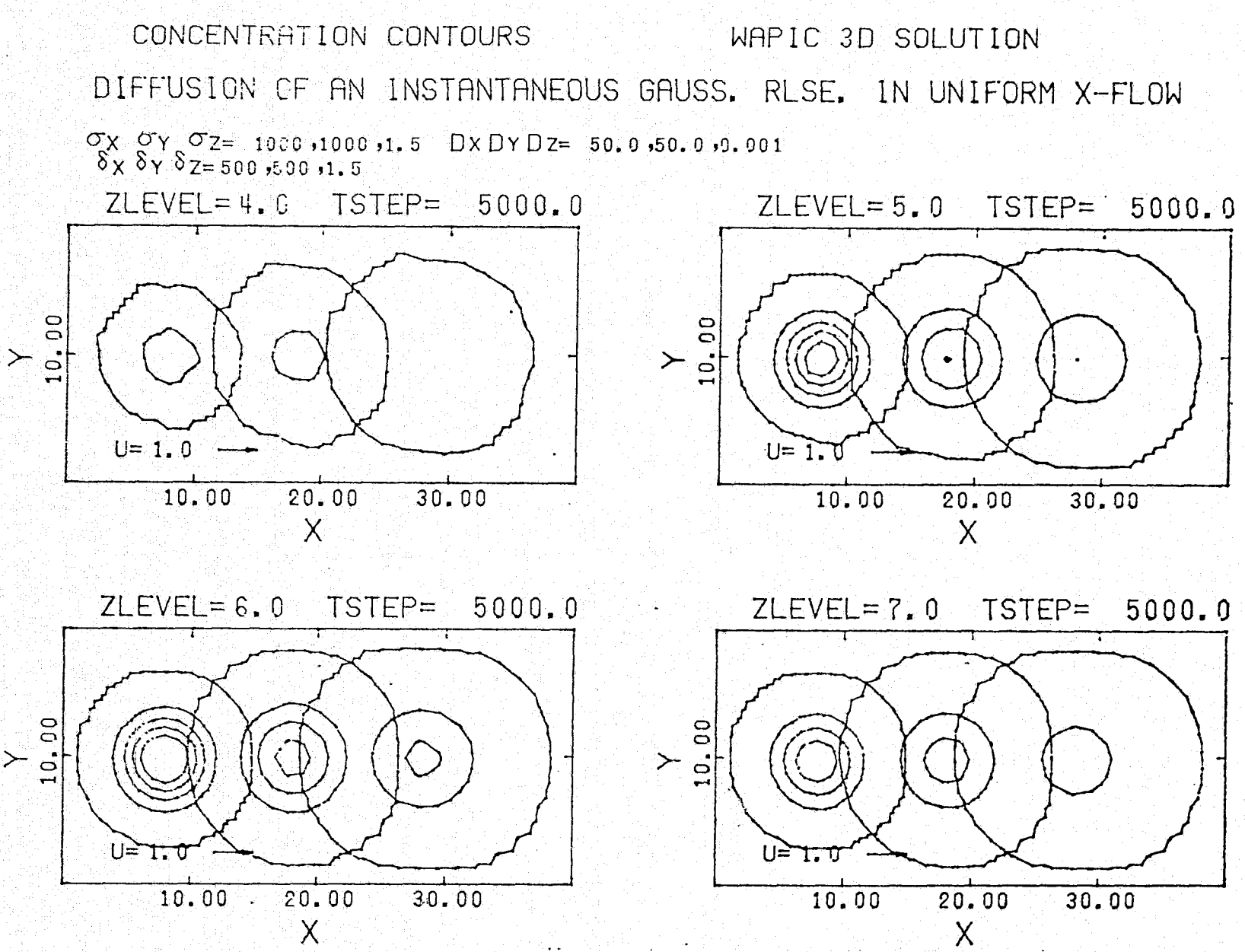

FIGURE 7.4 Concentration Contours, WAPIC Solution to Diffusion of an Instantaneous Gaussian Release in Uniform X-Flow

B. Diffusion in a Uniformly Sheared Flow Field

A three dimensional unidirectional velocity field with a uniform shear rate of du/dy = 0.0001 sec-1 , and a mean velocity of 1.0 ft/sec with a homogeneous turbulent field, was applied to study the shear effect on the diffusion and advection of an instantaneous Gaussian marker particle release.

Comparison was made against the analytic solutions of Carter and Okubo (69) and Okubo and Karweit (70), with the modification to represent the diffusion of a finite Gaussian release in space as opposed to a point release. The analytic equation is of the form

$$c(x,y,z,t) = \frac{Q}{(2\pi)^{3/2}(\sigma_{xo}^2 + 2K_x t)^{1/2}(\sigma_{yo}^2 + 2K_y t)^{1/2}(\sigma_{zo}^2 + 2K_z t)^{1/2}}$$

$$\text{EXP}\left(-\frac{1}{2}\left(\frac{(x - U_o t - \frac{1}{2}(\Omega_y y + \Omega_z z)t)^2}{(\sigma_{xo}^2 + 2K_x t)(1 + \varphi_3^2 t^2)} + \frac{y^2}{(\sigma_{yo}^2 + 2K_y t)}\right.\right.$$

$$\left.\left. + \frac{z^2}{(\sigma_{zo}^2 + 2K_z t)}\right)\right) \qquad (7.3)$$

where

$$\varphi_3^2 = \frac{1}{12}\left(\left(\Omega_y^2 \frac{K_y}{K_x}\right) + \left(\Omega_z^2 \frac{K_z}{K_x}\right)\right) \qquad (7.4)$$

The term φ^{-1} can be interpreted as the time at which the velocity shear begins to significantly affect the cloud's diffusion, or the time of the shear effect (70).

The shear effect can be seen in Figure 7.5, which illustrates a WAPIC two dimensional view of the particle distributions at time T=0 and 10000 seconds later. These plots show that the former Gaussian distribution is skewed to the side where the advection velocity is larger. The marker particle cloud disperses more (or skews) with the levels of higher X-directed velocities.

Figures 7.6 and 7.7, detail X-Y planar concentration contours at various Z-levels for the analytic and WAPIC solutions. Cloud concentrations are plotted at times T= 0,5000 and 10000 seconds. The observation is made that the concentration contours are stretched in the direction of increasing velocity, thus enhancing diffusion in the lateral, Y, direction. The WAPIC predicted concentration value are within an absolute value of 5 % of the analytic values at time T=10000.

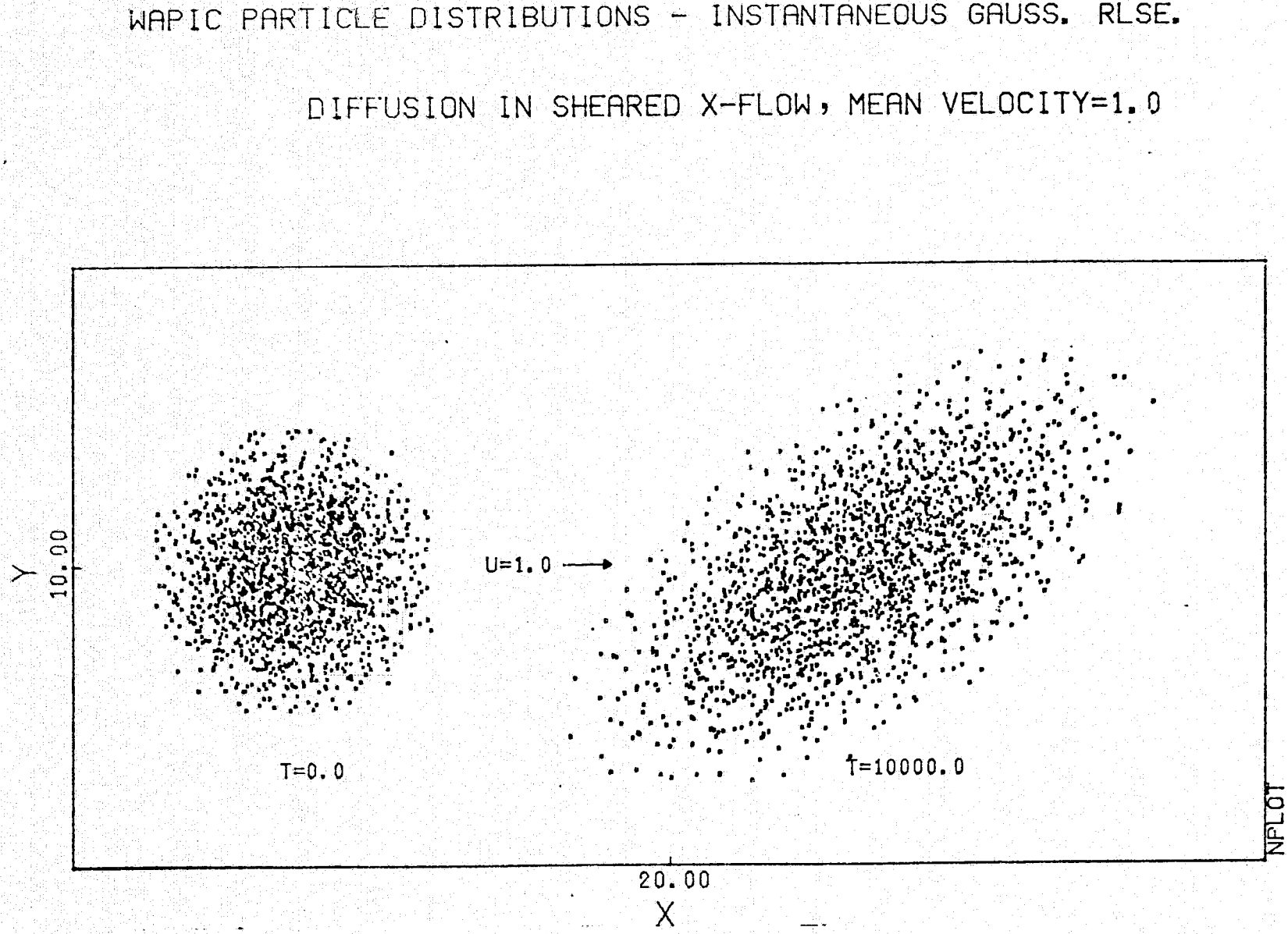

FIGURE 7.5 Two Dimensional Particle Distributions at Time T = 0, 10000 for Diffusion of an Initially Gaussian Release in a Unidirectional Steady Flow Field

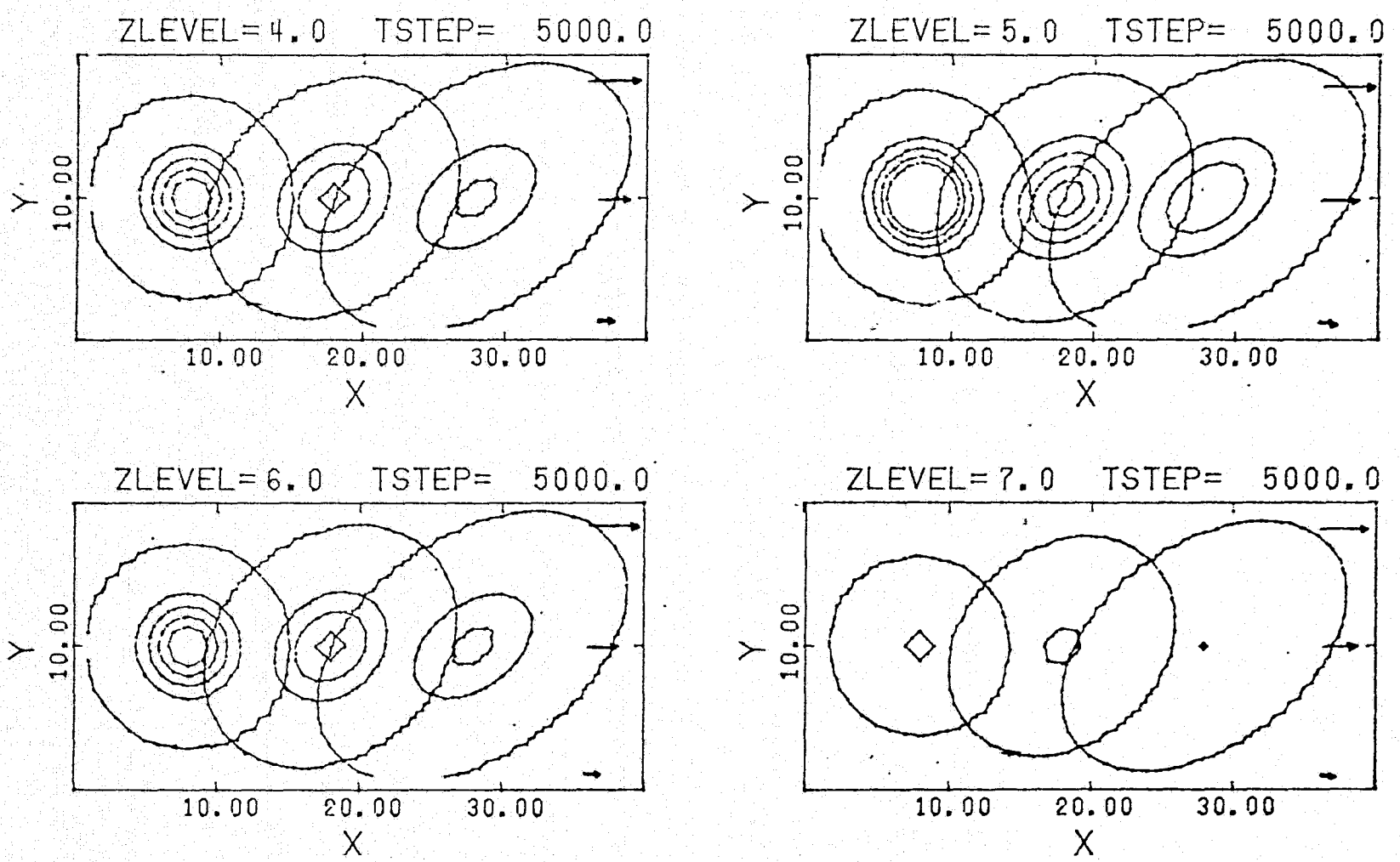

FIGURE 7.6 Concentration Contours, Okubo's Analytic Solution for Diffusion of an Initially Gaussian Release in Uniformly Sheared X-Flow

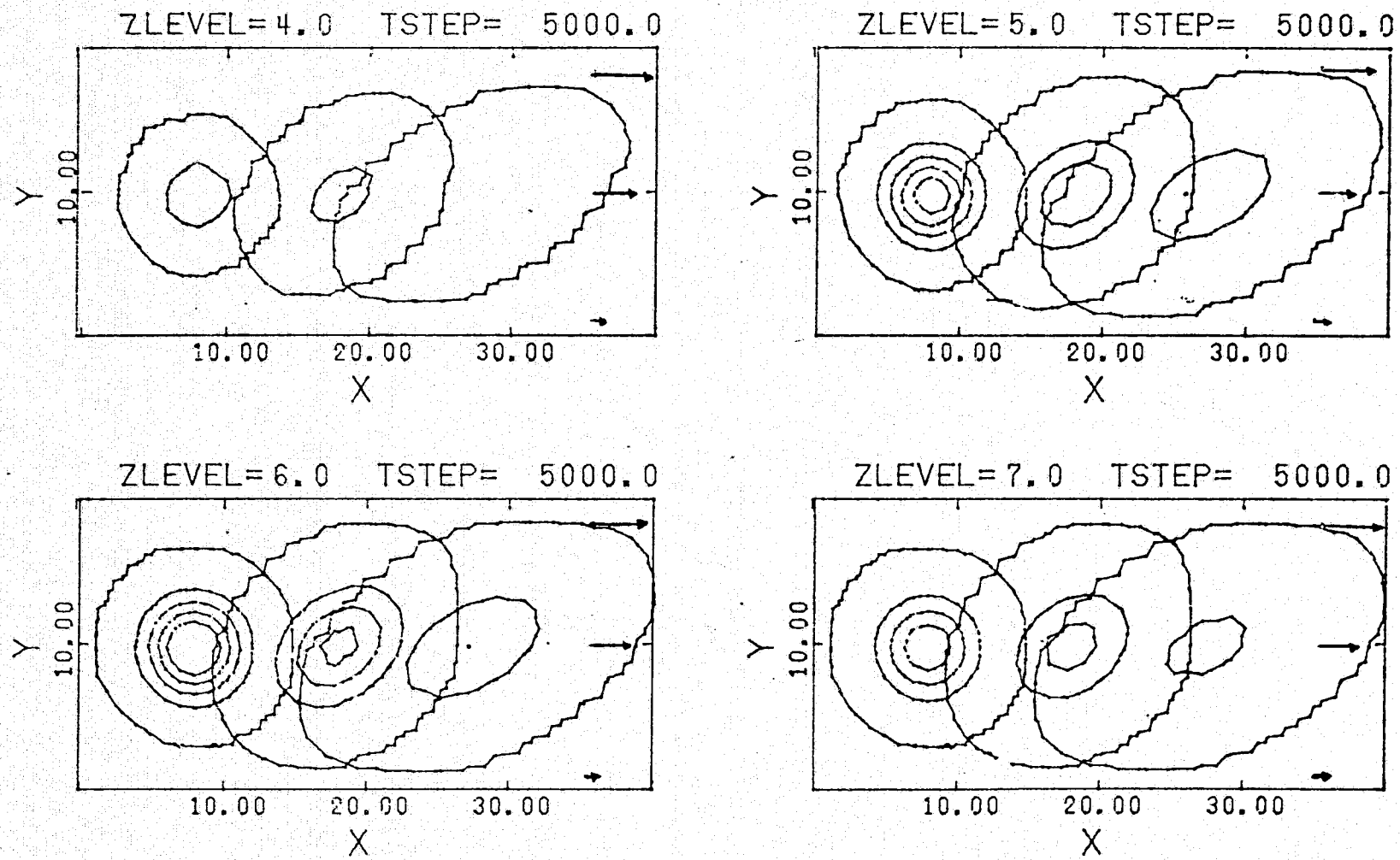

FIGURE 7.7 Concentration Contours, WAPIC Solution for Diffusion of an Initially Gaussian Release in Uniformly Sheared X-Flow

C. Diffusion of Continuous Gaussian Releases

A plume or continuous waste release in the long term transport phase may be simulated with WAPIC by releasing a Gaussian particle distribution at each time step (28,29). Okubo's analytic sclution for diffusion of a three dimensional instantaneous release in a uniform turbulent X-directed flow field, can be numerically integrated in time to yield a solution for the diffusion of a succession of point or Gaussian releases. Since the center of the waste or particle release is considered to be fixed in space, the WAPIC Eulerian grid will also be fixed in all three dimensions in the non-expanding, non-translating mode. Particles reaching the boundaries will be removed from the computational field.

An extremely large Eulerian grid of 45x20x15 X-Y-Z grid cells was required to perform a simulation of 1920 seconds, with a mean velocity of 1.0 ft/sec and a X-Y grid size of 120 ft. Approximately 88 marker particles were released per WAPIC time step. Horizontal standard deviation/grid spacing ratios of 2.0 were utilized. Figures 7.8 and 7.9 illustrate the concentration contour plots for the analytic and WAPIC plume simulation.

WAPIC shows correct plume concentration contour trend behavior, but shows irregular contour lines with considerably less diffusion along the outer fringes, relative to the analytic solution. Concentrations near the center of the WAPIC release were 3-4 times greater than

that found in the analytic solution. The reason for this poor behavior is that when using only 88 particles to represent each release, the particles tend to be clumped near the release point and not " Normally " distributed in space. This causes high concentration gradients and poor spread along the fringes of the release cloud where there are very few particles. As explained in Chapter V., this problem could have been overcome through the use of approximately 1000 or more marker particles per time step. But due to run and computer storage limitations, this would require at least 512k bytes of computer storage, to achieve an accurate comparison with the analytic solution. The inference can be made that the WAPIC method is not a practical method for simulating a continuous waste release unless the user has an extremely large, fast computer.

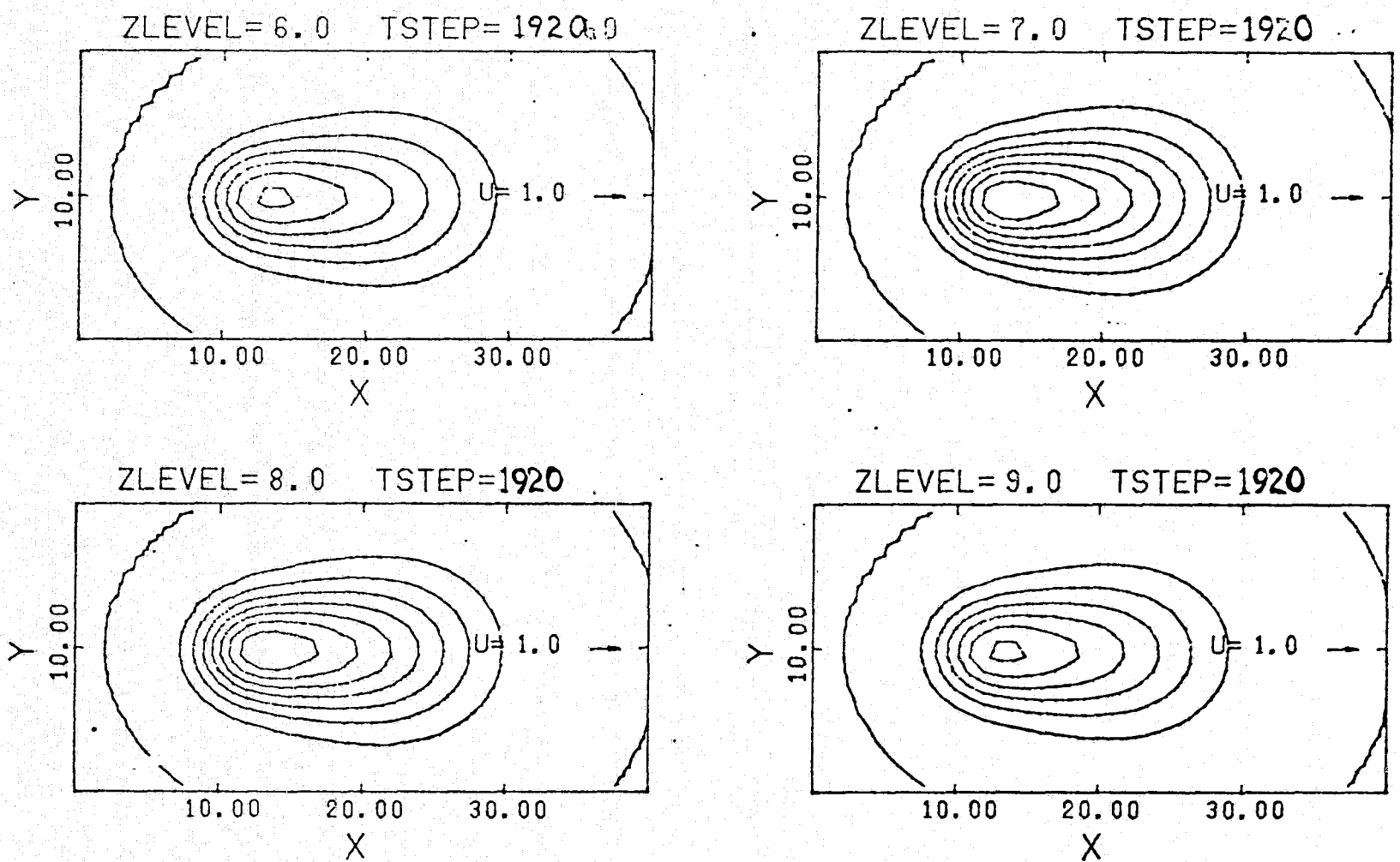

FIGURE 7.8 Concentration Contours, Analytic Solution for Diffusion of Continuous Gaussian Release in Uniform X-Flow

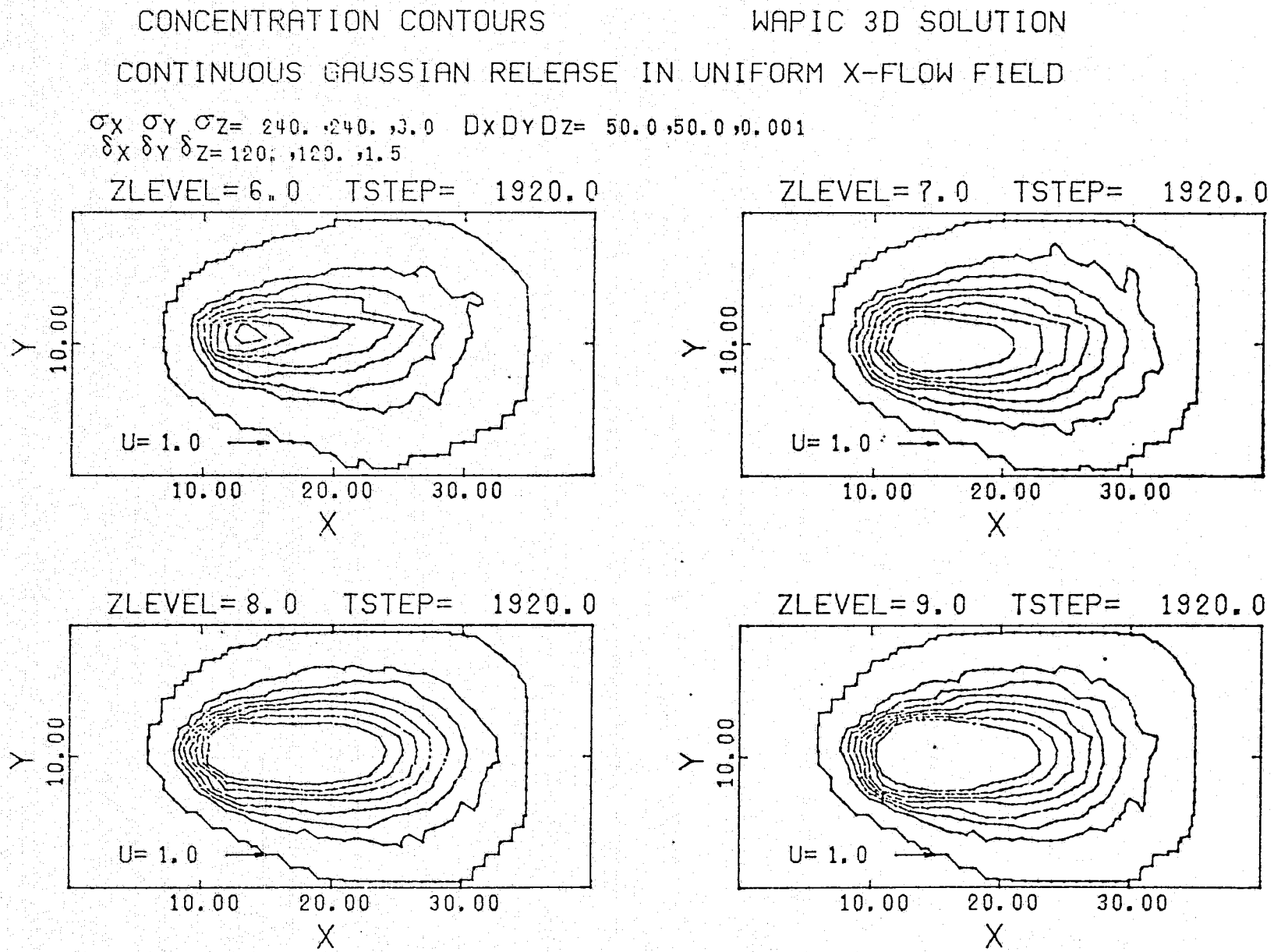

FIGURE 7.9 Concentration Contours, WAPIC Solution, for Diffusion of Continuous Gaussian Releases in Uniform X-Flow

D. Diffusion in Uniform Bounded Channel Flow

This simulation was performed to study WAPIC'S ability to model diffusion which is horizontally bounded, ie. reflecting boundaries. Analytic solutions are detailed in the works of Csanady (33), Wnek and Fochtman (71), and Cleary and Adrian (72). Csanady and Wnek utilize the method of images to approximate diffusion behavior at reflecting boundaries, while Cleary and Adrian use the integral transform approach, whose solution may be written as

$$C(x,y,z,t) = Q \frac{\exp\left(-\frac{(x - U_o t)^2}{4K_x t}\right)}{WH(4\pi K_x t)^{1/2}}$$

$$\times \left(1 + 2 \sum_{n=1}^{\infty} \exp\left(-P_N^2 K_z t\right) \cos\left(P_N z\right)\right) \qquad (7.5)$$

$$\times \left(1 + 2 \sum_{n=1}^{\infty} \exp\left(-\beta_M^2 K_y t\right) \cos\left(B_M y\right)\right)$$

where -

$$P_N = \frac{N\pi}{H} \quad B_M = \frac{M\pi}{W} \; N, \; M = 1, 2, 3...$$

H = depth, W = width

A channel 30 ft deep and 450 ft. wide with a uniform steady current field of 1.0 ft/sec was chosen as the experimental "apparatus" . The WAPIC Eulerian grid system was allowed to translate and expand only in the X-direction while the outer edges of the Y and Z grid dimensions became

the channel boundaries.

Cleary and Adrian's solution technique applies to diffusion from a point release. In order to simulate a Gaussian release at time T=0, the analytic solution had to be advanced in time 72 seconds, assuming a uniform turbulent flow field in the horizontal and vertical. This estimate follows from the Fickian turbulent diffusion relation

$$\sigma_x = (2K_x \Delta t)^{1/2} \tag{7.6}$$

for an instantaneous point release to grow to a given standard deviation.

Concentration contours for WAPIC and the analytic solution at different vertical levels for times T=0 and T=720 seconds later are given in Figures 7.10 and 7.11, respectively. The observation is made that the effect of the lateral boundary is to equivalence values of concentration in the lateral, Y, direction as the release moves downstream. For a line drawn through the center of the channel in the X-direction, concentrations agree within 5% . Along the walls the deviations are greater, in the 5-10% range. This large deviation can be attributed to the initial placement of the marker particles with reference to the channel center. The analytic solution has the point release placed exactly in the channel center, with a radially uniform concentration distribution, which results in symmetric reflective behavior at time T=720 seconds. Because WAPIC'S initial particle distribution is not

perfectly symmetric around the channel center, perfect lateral symmetry of concentration reflection is not possible.

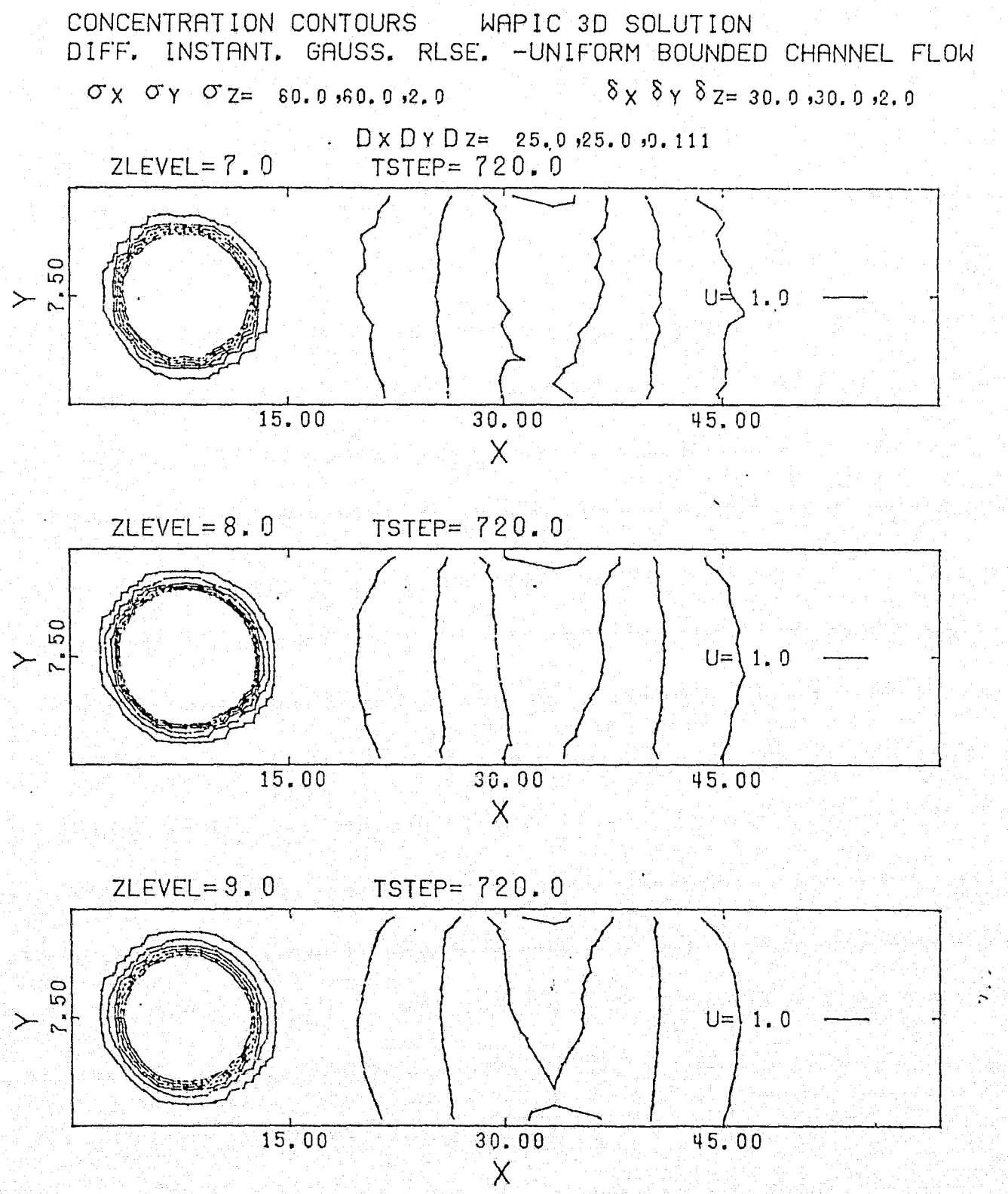

FIGURE 7.10 Concentration Contours, WAPIC Solution for Diffusion of an Instantaneous Gaussian Release in Uniform Bounded Channel Flow

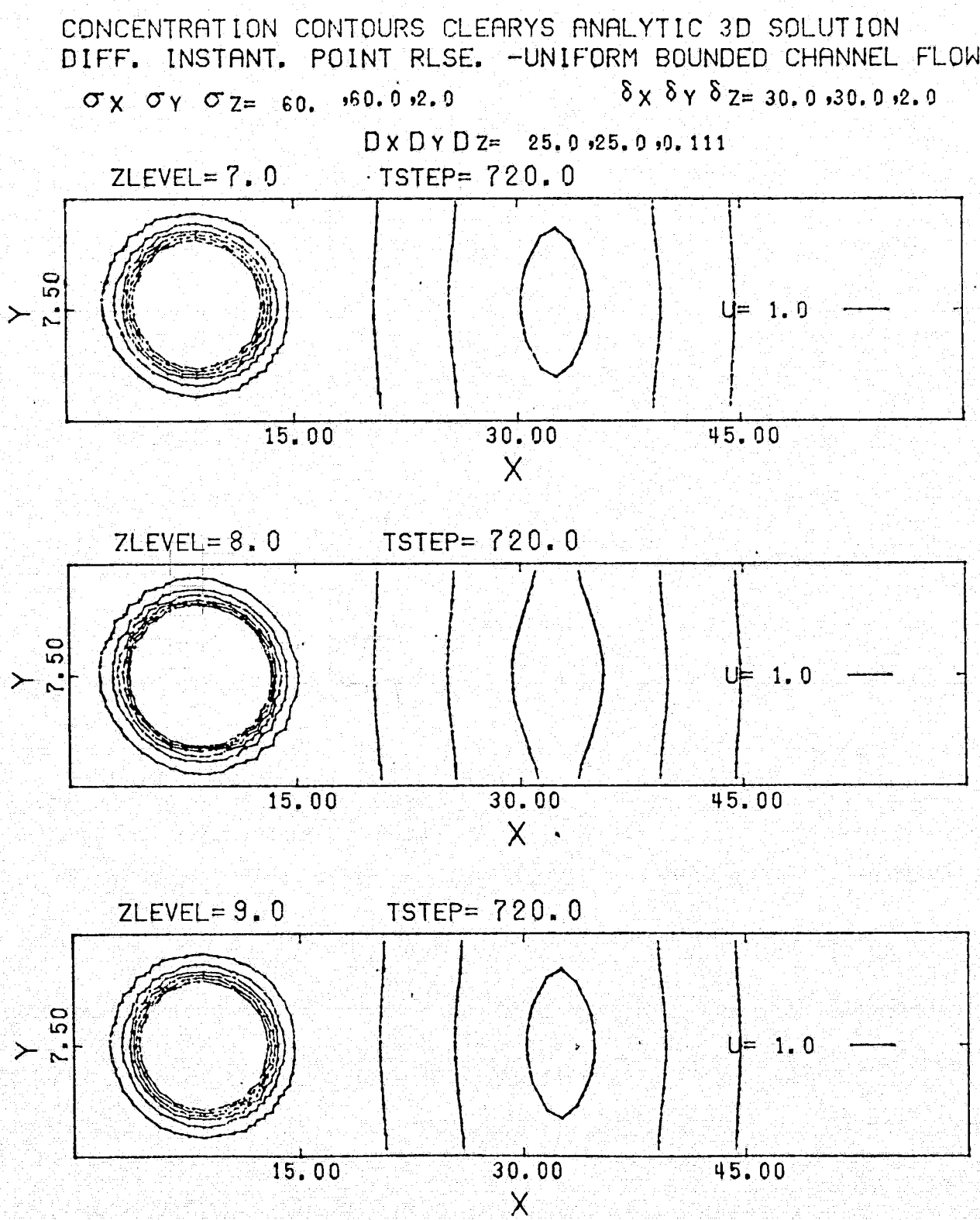

FIGURE 7.11 Concentration Contours, Cleary's Analytic Solution for Diffusion of an Instantaneous Gaussian Release in Uniform Bounded Channel Flow

E. Simulation of Sediment Transport in Stream Flow

Since WAPIC will be utilized to simulate the long term transport and fallout of suspended sediment in the coastal and estuarine environment, some preliminary testing of the pseudo total velocity method for treating turbulent settling was necessary. The decision was made to simulate the case of sediment fallout from an initially vertically uniform one dimensional concentration distribution in turbulent steady unidirectional channel flow. In 1943, Dobbins (73) derived an analytic formulation which successfully explained the observed vertical sediment distribution in steady one dimensional stream flow, in which the dilute suspended sediment was in equilibrium with the bed material. He also developed an analytic equation expressing concentration as a function of the vertical and horizontal downstream distances for an initially vertically uniform sediment distribution falling to zero concentration with the no scour bottom boundary condition. Sayre and Chang (53) integrated this equation over the vertical to obtain the vertically averaged concentration, or mass, remaining in the water column as a function of downstream distance.

A review of the equations and simplifying assumptions used by Dobbins to produce this solution would be instructive. Consider a turbulent unidirectional (X-Z) sediment laden flow field of singular settling velocity W_s, bounded by a uniform free surface and bottom boundary

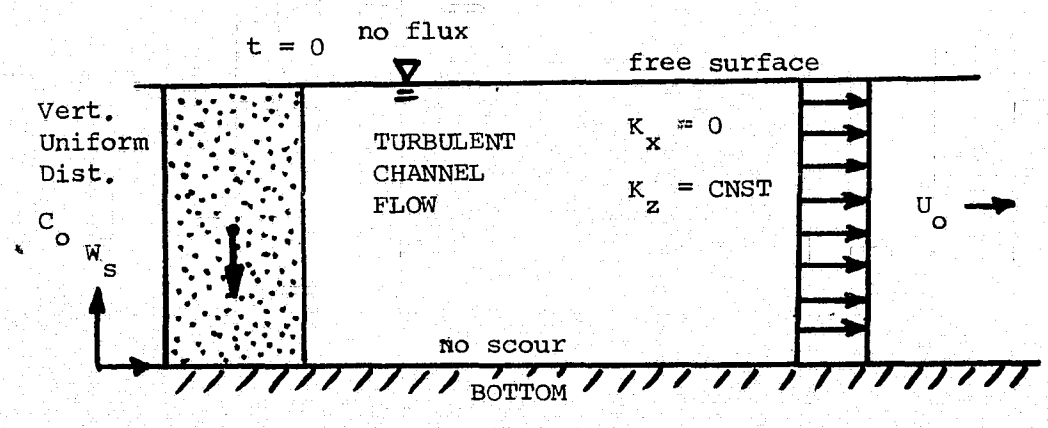

W_S = PARTICLE SETTLING VELOCITY

Dobbins assumes that the X-velocity distribution in the Z direction, though logarithmic and nearly parabolic, is approximately uniform across the vertical, and the vertical diffusion coefficient is uniform with depth and can be related to the bottom shear stress or shear velocity by

$$K_z = kHU^* \tag{7.7}$$

$$U^* = g^{\frac{1}{2}} U/C_h \tag{7.8}$$

$$C_h = 1.49H^{1/6}/C_m \tag{7.9}$$

where:

C_m = Manning Coefficient
C_h = Chezy Coefficient
k = Von Karmann Constant = 0.40
H = Hydraulic Radius or Depth
U* = Shear Velocity

Equation 7.7 relates the mathematical expression for vertical eddy diffusivity for a parabolic velocity distribution . Equations 7.8 and 7.9 are the Chezy expressions for relating shear velocity to a bottom friction coefficient, the Manning friction factor.

The two dimensional mass transport formulation may be written as

$$U\frac{\partial c}{\partial x} = K_z \frac{\partial^2 c}{\partial x^2} + K_x \frac{\partial^2 c}{\partial x^2} + W_s \frac{\partial c}{\partial x} \qquad (7.10)$$

Assuming that the longitudinal diffusion term is small in comparison with the vertical diffusion

$$U\frac{\partial c}{\partial x} = K_z \frac{\partial^2 c}{\partial z^2} + W_s \frac{\partial c}{\partial x} \qquad (7.11)$$

Since the fluid is moving with a uniform velocity, U , the Lagrangian viewpoint of an observer moving with the fluid-sediment parcel at velocity U is taken. The assumption is made that

$$U\frac{\partial c}{\partial x} = \frac{\partial c}{\partial t}$$

since

$$x = ut \qquad \partial x = u\partial t$$

and Eq. 7.11 may be rewritten as

$$\frac{\partial c}{\partial t} = K_z \frac{\partial^2 c}{\partial z^2} + W_s \frac{\partial c}{\partial z} \qquad (7.12)$$

Equation 7.12 describes the change of concentration of a

turbulent fluid parcel containing a discrete settling velocity, Ws, as a function of time. This linear partial differential equation was solved for the boundary conditions of no net sediment transport across the free surface and for no scour at the bottom for any given initial vertical sediment distribution. The solution for particle concentration as a function of depth and time (or distance downstream) for the case of dropout to zero concentration from an initially vertically uniform distribution is

$$c(z,t) = C_o\, e^{-0.5 W_s z (K_z)^{-1}}$$

$$\sum_{n=1}^{\infty} \frac{2\alpha_n^2\, e^{-(\alpha_n^2 K_z + 0.25\, W_s^2\, K_z^{-1})t}\, \psi_n}{(\alpha_n^2 + W_s/4K_z)\left((\alpha_n^2 + \frac{W_s^2}{4K_z^2})H + \frac{W_s}{K_z}\right)} \qquad (7.13)$$

where α_n are the real successive positive roots of the transcendental equation

$$2 \cot(H\alpha) = H\alpha/(W_s H/2K_z) - (W_s H/2K_z)/(H\alpha) \qquad (7.14)$$

and ψ is defined as

$$\psi_n = \cos(\alpha_n z) + \left(\frac{W_s}{2K_z\alpha_n}\right) \sin(\alpha_n z) \qquad (7.15)$$

Sayre and Chang integrated Eq. 7.10 over the vertical

to yield the ratio of the average concentration in the vertical to the initial average concentration.

$$(c/c_o) = 72\beta^2 e^{3\beta} \sum_{n=1}^{\infty} \frac{(-1)^{n-1}\, \alpha_n^2 \exp(-9\beta^2 + \alpha^2_n)\frac{K_z x U^*}{(6HU_o)}}{(9\beta^2 + \alpha_n^2 + 6\beta)(9\beta^2 + \alpha^2_n)^2} \qquad (7.16)$$

Where U^*, the shear velocity is approximated by Eq. 7.8, and β, the vertical dimensionless fall velocity is defined as

$$\beta = \frac{W_s}{kU^*} \qquad (7.17)$$

Equations 7.13, 7.14, 7.15 and 7.16 were computer coded to solve for the concentration distributions as a function of the vertical coordinate and time, and for the fallout rate respectively.

Numerical experiments were performed by WAPIC in order to simulate solutions to Eqs. 7.13 and 7.16 . A channel 30 feet deep was divided into 15 vertical grid cells with a 3x3 X-Y Eulerian grid matrix. Three thousand marker particles were horizontally centered in the exact middle of the X-Y matrix, and were equally spaced from the free surface to the bottom in order to develop an initially uniform concentration distribution for one column of vertical cells. A unidirectional X-flow field of 1.0 ft/sec was specified throughout the Eulerian grid. A

constant, uniform vertical diffusion coefficient was calculated by the relationships in Eqs. 7.7, 7.8, and 7.9, with a Manning friction factor of 0.020 yielding a turbulent diffusivity, Kz, of 0.09 ft^2/sec. The X-Y turbulent diffusion coefficients, Kx and Ky, were set identically to zero. The Eulerian grid was allowed to translate only in the X-direction with the mean velocity. The free surface was given a reflection boundary condition:

$$z_{NEW} = 2z_{\substack{\text{Reflective}\\\text{Boundary}}} - z_{OLD} \tag{7.18}$$

and the marker particles were removed from the computational field as they advected across the bottom.

For the initial simulation a settling velocity of 0.005 ft/sec was assigned to each particle. Figure 7.13 demonstrates the effect of WAPIC time step on the prediction of mass fallout rate as a function of distance downstream, for T = 60, 30 and 20 seconds. The observation is made, that as time step decreases, the WAPIC solution technique approaches the analytic solution. At time steps of 60 and 30 seconds the concentration field was found to oscillate about the analytic solution.

These results, plus the fact that WAPIC employs a space centered finite difference approximation to define the total pseudo velocity at the cell faces, suggested that a vertical numerical stability requirement of the following form should be utilized for marker particle movement (33)

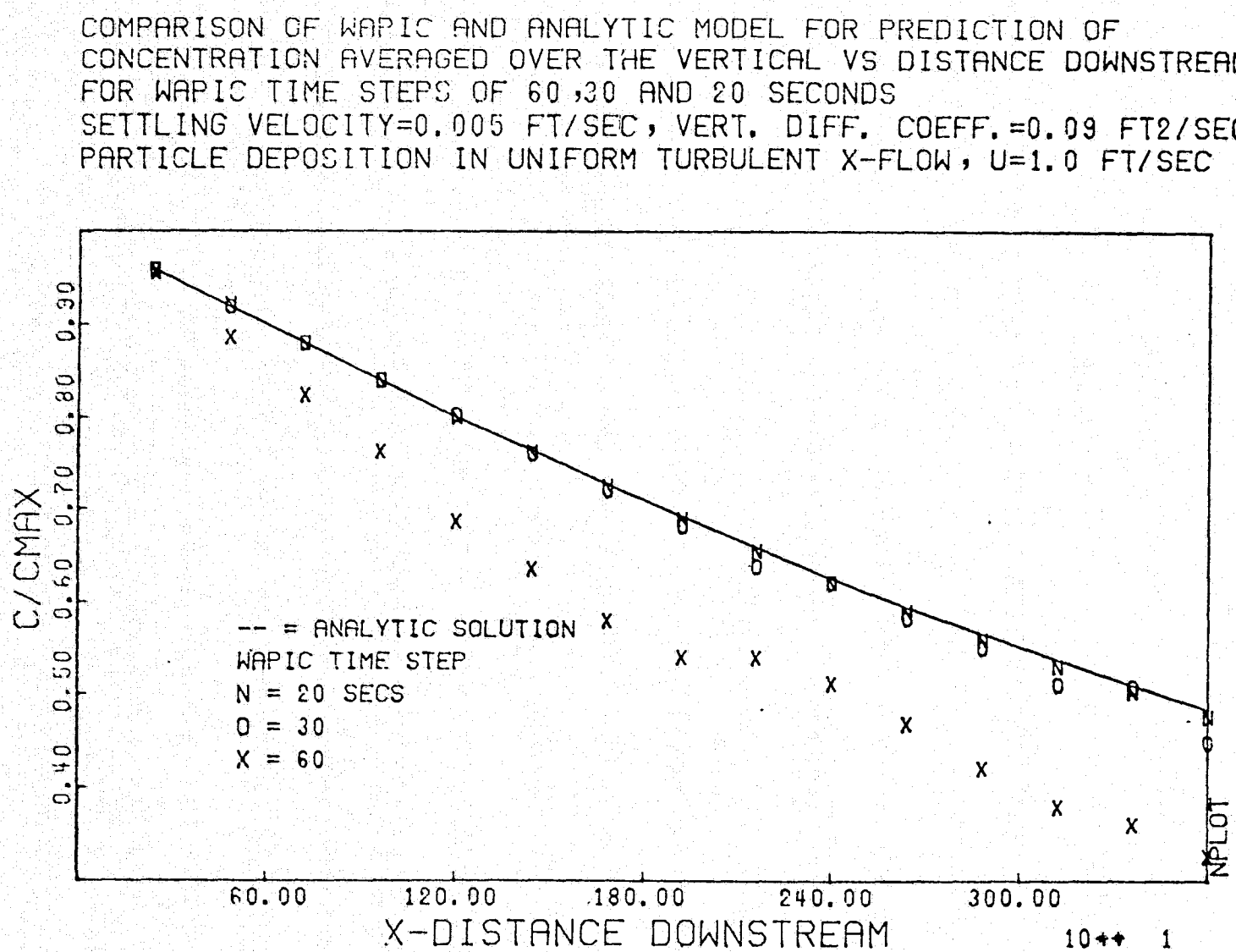

FIGURE 7.13 Comparison of WAPIC and Analytic Solution, Effect of WAPIC Time Step on the Prediction of Fallout Rate as a Function of Downstream Distance for a Singluar Particle Settling Rate

$$\text{Vertical Accuracy } \# = \left(\frac{W_s \Delta t}{\Delta z} + \frac{K_z \Delta t}{\Delta z^2}\right) \leq 0.5 \qquad (7.19)$$

Equation 7.19, which is a " Courant" dynamic stability requirement or time step restriction, states that for stability of the solution technique, a marker particle cannot be moved a distance greater than one-half a grid length per time step. Ws, can be visualized as a constant vertical advective velocity.

Table 7.2 details values of the vertical accuracy number (Equation 7.19) versus the WAPIC time step for values of Kz=0.09 ft^2/sec, Ws=0.005 ft/sec, and vertical grid size, ΔZ = 2.0 ft.

Time Step -sec.	Accuracy number
60	1.50
30	0.75
20	0.50

TABLE 7.2

Figure 7.14 details the development of an instability in the WAPIC predicted concentration field as a function of time or distance downstream. The instability starts at the free surface where the diffusion gradients first initiate, and then propagates through the vertical concentration field, until the whole concentration field oscillates at further distances downstream.

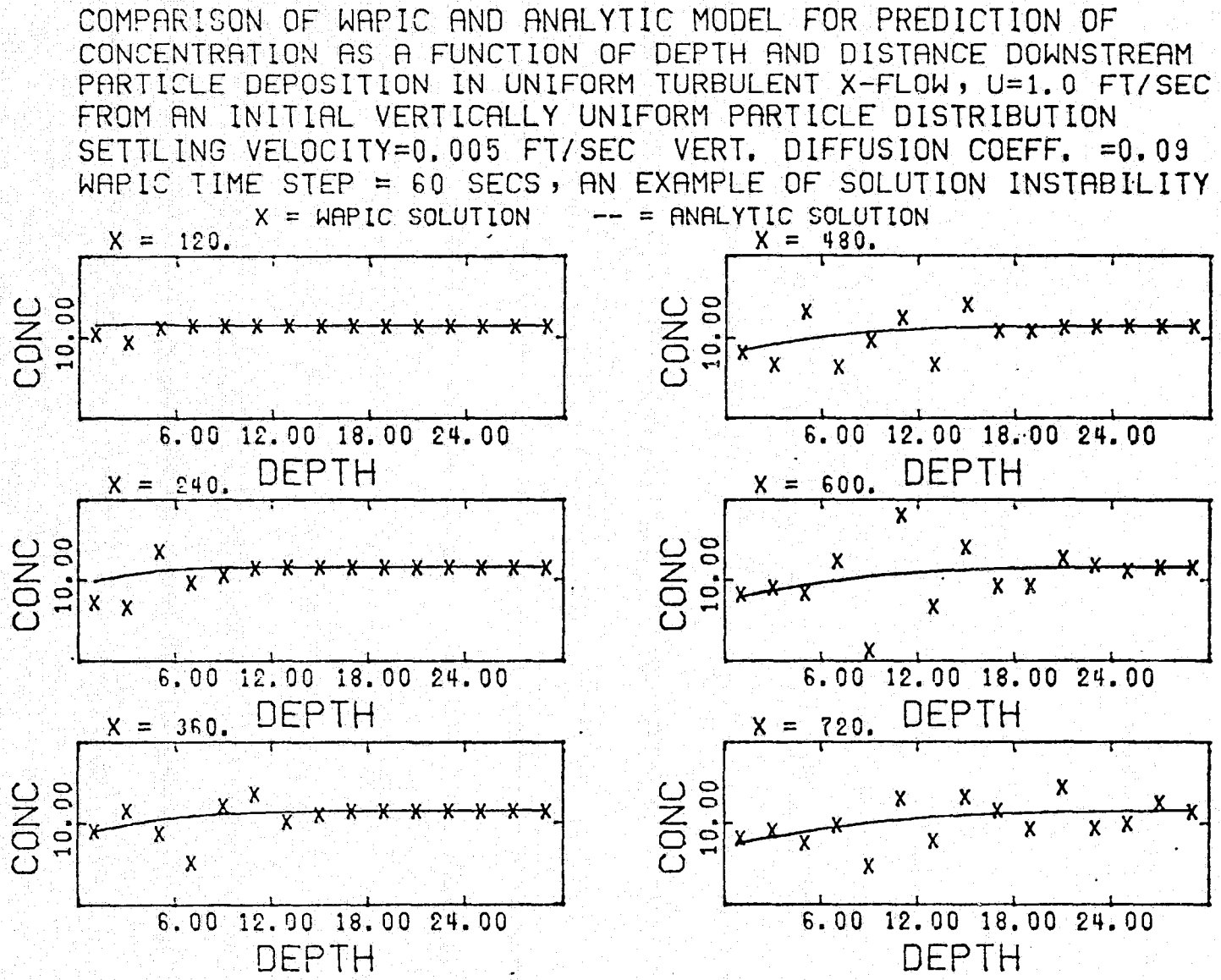

FIGURE 7.14 Development and Propagation of an Instability in the WAPIC Vertical Concentration Field for One Dimensional Sediment Transport with a Singular Particle Settling Rate

Figure 7.15 shows the predicted vertical concentration field, with a WAPIC time step equal to 20 seconds, or accuracy number of 0.5. The concentration oscillation has been effectively damped out and the technique predicts the concentration field within an absolute accuracy of 4.0 % .

Utilizing a time step of 20 seconds, WAPIC simulated the fallout rates of five particle settling velocities of 0.0005,0.001,0.005,0.008, and 0.01 ft/sec, with the same operating parameters used as above. Figure 7.16 details the fallout rates as a function of distance downstream. At the lower settling rates of 0.0005 and 0.001 ft/sec, the plots demonstrate that the fallout rate is essentially the settling velocity of the particles within a one hour time span from time T=0. This behavior indicates, for this case, that the smaller free fall settling velocities are rate limiting, not allowing the dominant diffusion process to come into action. As the free fall particle settling velocity increases relative to the particle diffusion velocities, for the diffusion value shown, the deposition rate decreases because concentration gradients develop near the free surface. The diffusion velocity acts to move the marker particles back into regions of depleted concentration which decreases the fallout rate.

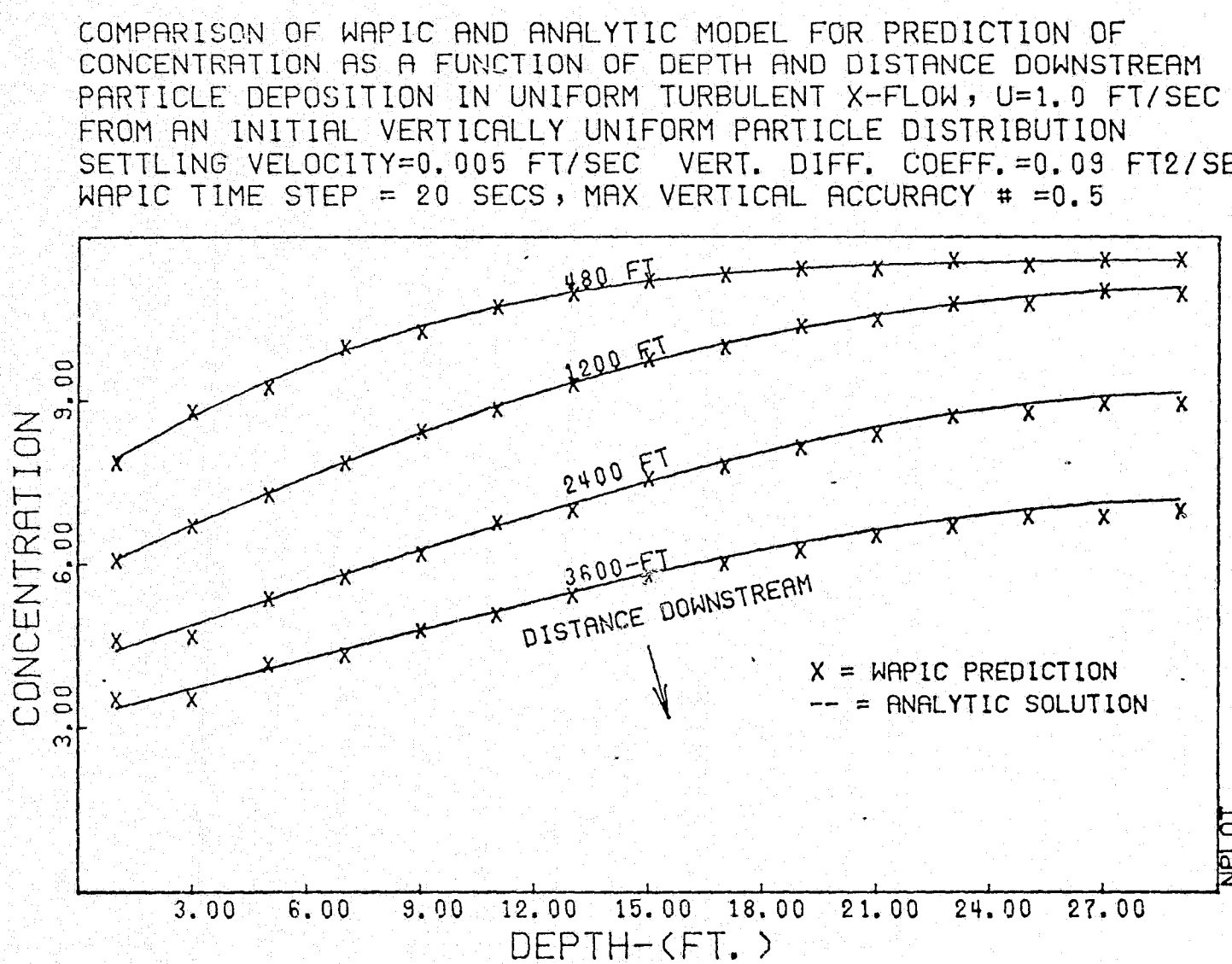

FIGURE 7.15 Damping of the Instability in the WAPIC Concentration Field by Use of the Accuracy Number Requirement

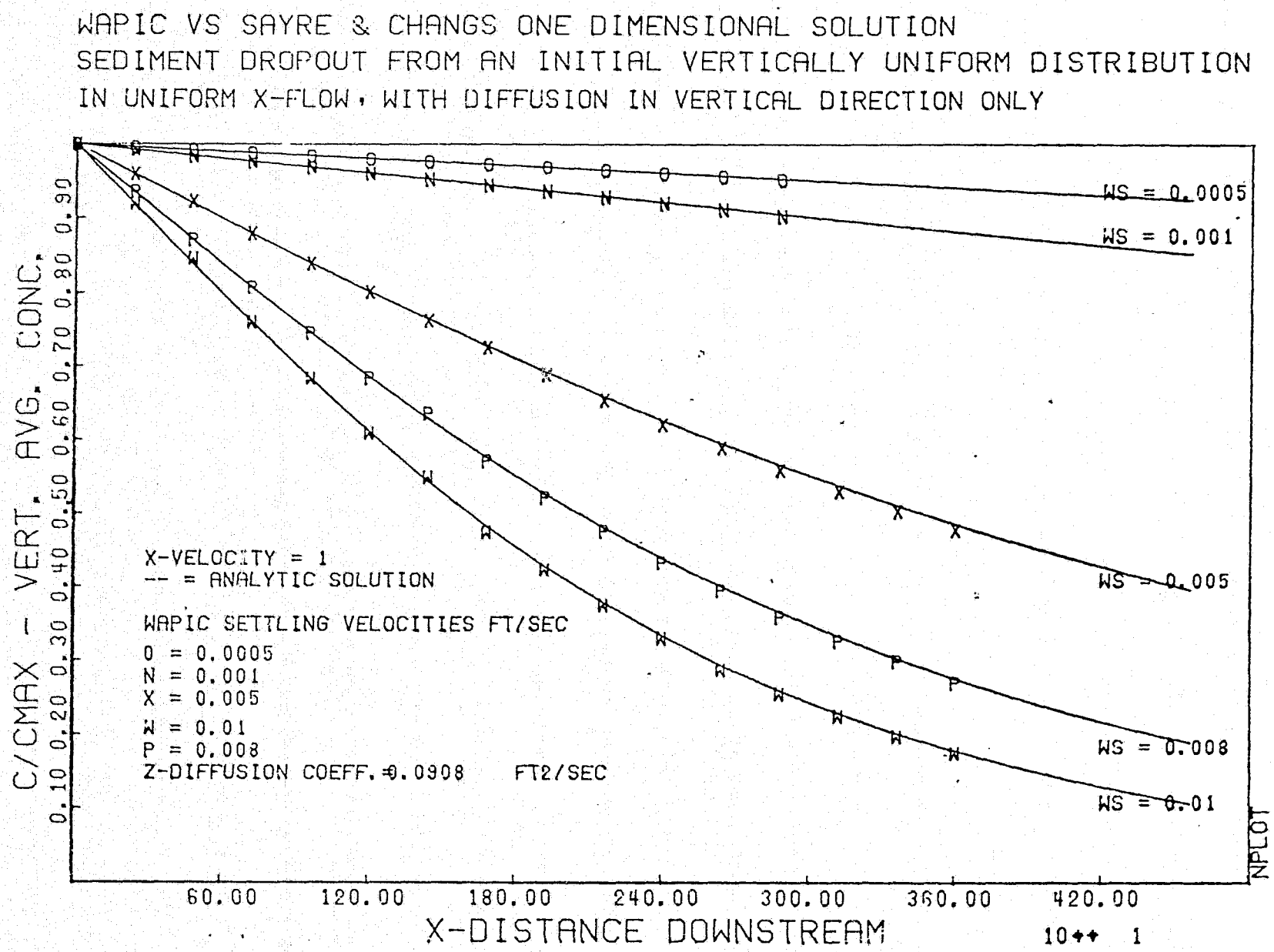

FIGURE 7.16 WAPIC Versus Sayre and Chang's One Dimensional Solution for Sediment Transport. Comparison with Five Different Sediment Fall Velocities

VIII. SIMULATION OF LONG TERM SEDIMENT TRANSPORT

A. Objectives and Background

As explained in Chapters II and III, WAPIC was designed to simulate the three dimensional long term turbulent diffusion and advection of dilute, neutrally and non-neutrally buoyant sedimentary and pollutant particulates in coastal and estuarine waters. The method was utilized to simulate the long term transport of a dilute suspended sediment cloud resulting from a barged waste release at Brown's Ledge in Rhode Island Sound. This area is currently being considered by the U. S. Army Corps of Engineers as a dump site for Fall River dredged spoil disposal (1). The dump site is a square nautical mile area, the center of which is located 41° 18.3′ N, 71° 04.1′ W in an area known as Brown's Ledge. (Figure 8.1) From Figure 8.2, which details the bathymetry at Brown's Ledge, it can be seen that the area surrounding the dump site is relatively shallow water ranging from 60 - 120 feet , the dump site being 100 to 110 feet deep.

Since this area is relatively shallow, the hypothesis is made that the short term transport phase of the dredged waste release would be entirely dominated by the entrainment phase (6). In other words, practically all of the sediment would descend directly to the bottom, with very little loss of material to the ambient current system. Gordon (74) in an observational study of dredged waste disposal in Puget Sound, found that the material left the barge with a "well defined mass falling with a maximum

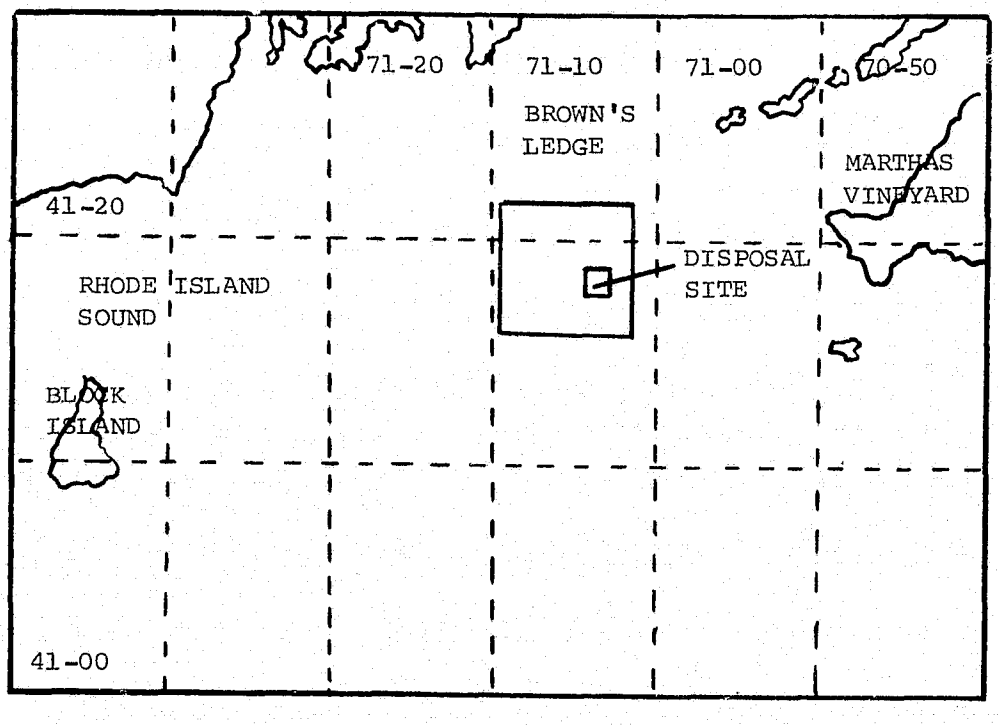

FIGURE 8.1 Geographic Location of Browns Ledge and the Proposed One Square Nautical Mile Dump Site

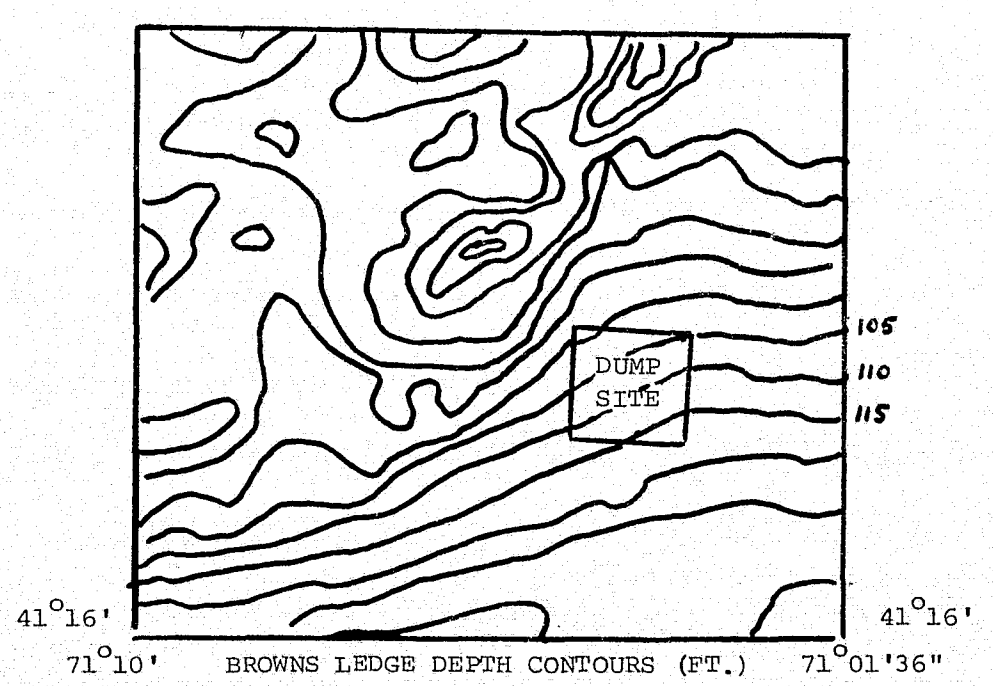

FIGURE 8.2 Depth Contours at Browns Ledge

velocity of approximately 6 ft/sec." Using this value as a representative estimate of the descent velocity of a waste cloud, at Brown's Ledge, the cloud would be expected to reach the bottom well within 60 seconds. Any sediment entrained in the water column would be due to the ambient turbulence, and the surge of the cloud as it lands on the bottom.

A very conservative engineering estimate can be made that no more than five percent of the instantaneous dump of bottom sediment would remain within the water column to be advected and diffused by the tidal and wind driven current fields. Since the average sea scow carries approximately 3000 cubic yards (2), and the typical specific density of Fall River sediment being 2.6, then approximately 10^8 grams (110 tons) of sediment would be entrained within the water column. If this cloud initially possessed a cylindrical shape 200 ft. in diameter and a vertical length of 35 feet, and the sediment were distributed evenly throughout at time T = 0, then a mean concentration of 3000 mg/liter (0.187 lb/ft^3) would be apparent. This value is within the limits of three percent by weight for dilute settling and transport of suspended sediment noted by Vanoi (44).

This suspended sediment will advect and diffuse with the tidal and wind driven currents in Rhode Island Sound. As described by Saila et. al. (2), two significant field studies of the hydrodynamics of Rhode Island Sound have been accomplished. The non-tidal wind driven circulation was investigated by Cook (75) in 1966, using wind drift

bottles and sea bed drifters to determine upper and lower layer net drift. His generalized net drift data for Rhode Island Sound are detailed in Table 8.1.

SEASON	SURFACE DRIFT	BOTTOM DRIFT
Spring	N and E	NW
Summer	N	NW
Autumn	S	N
Winter	S	N
SPEED RANGE	1.1 to 7.6 n.m./day	0.05 to 1.6 n.m./day

Table 8.1 Cook's 1967 Study of Non-Tidal Net Drift in Rhode Island Sound

Shonting (76) in 1967 utilized an array of current meters to perform a 13 day study of the horizontal current patterns within a square mile area in Rhode Island Sound. Shonting found that tidally driven inertial flows combined with tidal motions dominate the current regimes and that mean speeds in the upper layer of current motion did not exceed 0.50 knots, and that turbulent eddies were present having scales less than a kilometer.

Hurlburt and Spaulding (8) applied a two dimensional tidally driven hydrodynamic model to predict current patterns and magnitudes in Rhode Island Sound - Block Island Sound - Buzzards Bay Complex. An interesting result of this modeling effort was the indication of extremely weak tidal currents in Rhode Island Sound, especially in the region of the proposed dump site. Figures 8.3 A, B, C,

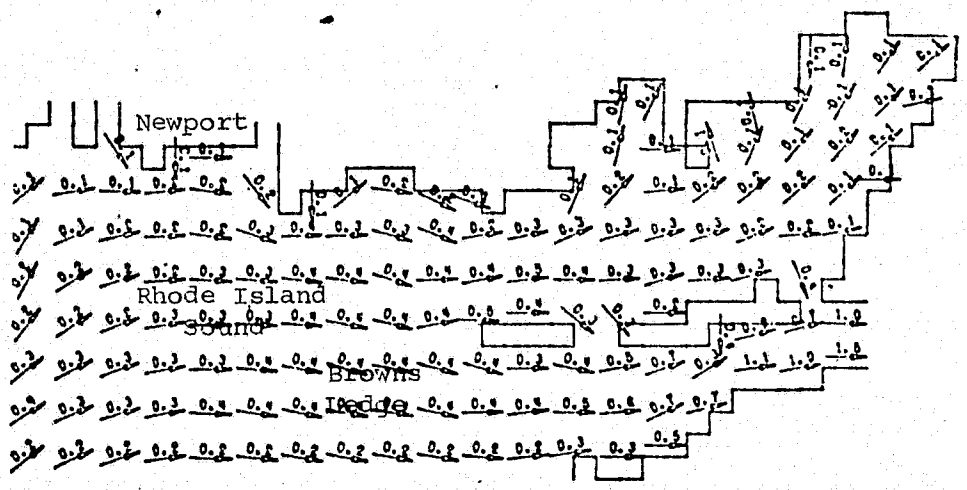

TIDAL CURRENTS IN KNOTS ZERO HOURS
AFTER HIGH WATER AT NEWPORT, RI

FIGURE 8.3A Two Dimensional Vertically Averaged Velocity Vectors in Rhode Island Sound, 0.0 Hours After High Water at Newport, R.I.

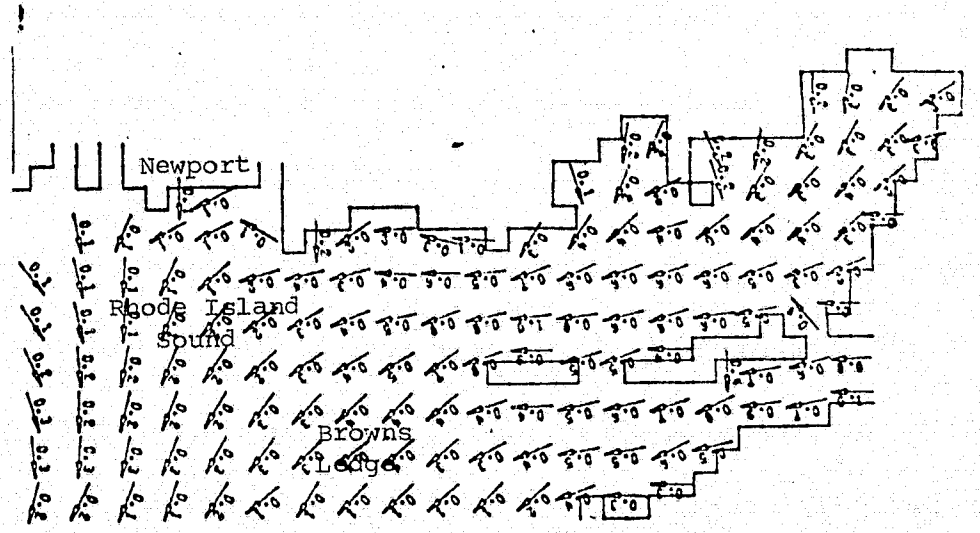

TIDAL CURRENTS IN KNOTS FOUR HOURS
AFTER HIGH WATER AT NEWPORT, RI

FIGURE 8.3B Two Dimensional Vertically Averaged Velocity Vectors in Rhode Island Sound, 4.0 Hours After High Water at Newport, R.I.

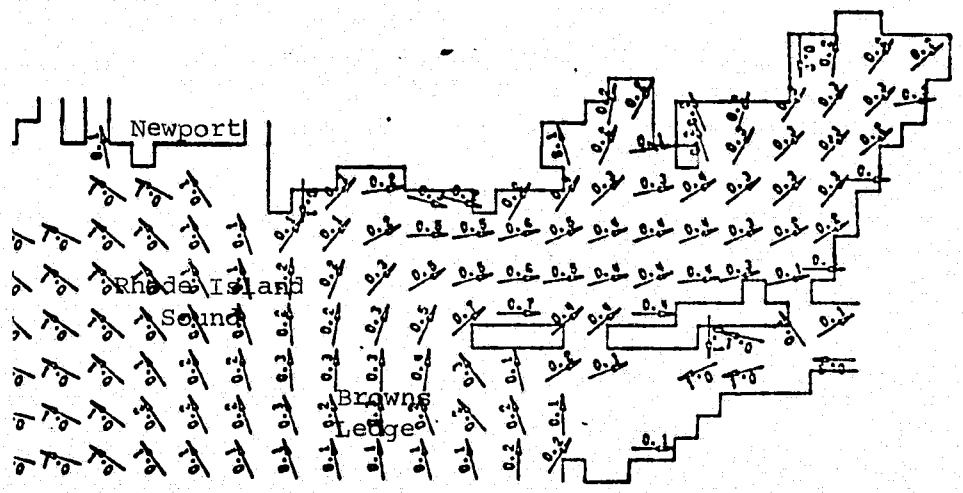

TIDAL CURRENTS IN KNOTS EIGHT HOURS
AFTER HIGH WATER AT NEWPORT, RI

FIGURE 8.3C Two Dimensional Vertically Averaged Velocity Vectors in Rhode Island Sound, 8.0 Hours After High Water at Newport, R.I.

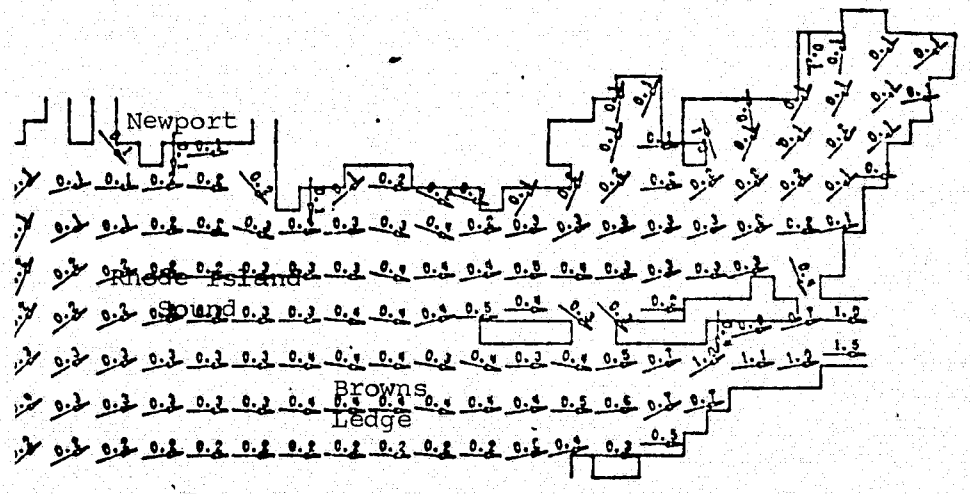

TIDAL CURRENTS IN KNOTS TWELVE HOURS
AFTER HIGH WATER AT NEWPORT, RI

FIGURE 8.3D Two Dimensional Vertically Averaged Velocity Vectors in Rhode Island Sound, 12.0 Hours After High Water at Newport, R.I.

D detail tidal currents in Rhode Island Sound, referenced to slack water at Newport, Rhode Island. These figures show that the vertically averaged tidal currents range from 0.1 to 0.4 knots during the twelve hour tidal cycle.

Utilizing data from this model, an average net drift in the proposed disposal area was found to be approximately 0.023 knots or 0.55 n.m./day, in a direction measured 110 CW. from true north (almost ESE). The magnitude of this value is within range of values found by Saila et. al. (2) in July, 1970 of 0.03 - 0.08 knots net drift with a general southeast to southerly direction.

B. Procedure of Application

The transformed version of WAPIC was coupled to Spaulding and Hurlburt's (8) tidally driven two dimensional vertically averaged hydrodynamic model through the use of a two dimensional velocity processor. As explained previously, the velocity processor was required to interpolate advective velocities from the square nautical mile meshes to the initially smaller, translating and expanding three dimensional WAPIC Eulerian velocity grid.

In order to adjust the hydrodynamic velocities with experimentally reported values for net drift at Brown's Ledge, a correction procedure was employed (77). The procedure was to subtract from the hydrodynamic velocity vectors, in the immediate Brown's Ledge area, the net tidal drift (calculated from the 12 hour average) at the proposed dump site. Subsequently, the net drift velocity vector was

added to the new velocity components with a correction for the variation of bottom depth relative to the depth at the area of the experimentally determined net (wind and tidal) drift. The overall effect was to subtract out the model net tidal drift, and add the total net wind and tidal drift (based on field data) in the area to produce a velocity field yielding a net drift in the direction desired. The total net drift chosen for this particular set of simulations was 0.7 n.m. day in the ENE direction (77).

Seven particular simulations were performed to illustrate the diffusive and advective patterns of mass transport in the area. The first three cases utilized marker particles with neutral buoyancy and constant horizontal diffusion coefficients of 50.0 and 100.0 ft^2/sec for the first two and scale dependent horizontal diffusion coefficients for the third (Table 8.2). Four additional simulations of vertical fallout of sediment were made by assigning settling velocities to the individual Lagrangian marker particles. Various mean sediment diameters and a specific density of 2.6 for Fall River sediment (1) were assigned to each marker to produce free fall settling velocities with the use of Eq. 4.13.

All four of the marker particle settling velocity studies utilized constant horizontal diffusion coefficients of 100.0 ft^2/sec. These four simulations were divided into two sets of two simulations. The differing variable in each simulation of both sets was the magnitude of the vertical diffusion which was 0.0001 and 0.01 ft^2/sec

	X-Y GRID LENGTHS FT.		DIFFUSION COEFFICIENTS FT^2/SEC		INITIAL X,Y,η STANDARD DEVIATIONS FT.			# OF MARKER PART.	PARTICLE DIAMETERS FT.
	X,	Y	K_X, K_Y	K_Z	σ_x	σ_y	σ_η		N.B. = NEUTRALLY BUOYANT
1.	400		50.	.0001	800.	800.	$\Delta\eta$	3000	N.B.
2.	200.		100.	.0001	400.	400.	$\Delta\eta$	3000	N.B.
3.	200.		Scale Dependent	.0001	400.	400.	$\Delta\eta$	3000	N.B.
4.	200.		100.	.0001	400.	400.	$\Delta\eta$	2500.	0.000083 FT (0.0025 cm)
5.	200.		100.	.01	400.	400.	$\Delta\eta$	2500.	0.00083 FT
6.	200.		100.	.0001	400.	400.	$\Delta\eta$	2500.	0.00005, 0.000083 0.00016, 0.0002 0.00028 FT
7.	200.		100.	.01	400.	400.	$\Delta\eta$	2500.	0.00005, 0.000083 0.00016, 0.0002 0.00028 FT

TABLE 8.2 Operating Parameters for Browns Ledge Simulation of Long Term Transport of Sediment

respectively. The first set of simulations considered the transport of a single particle diameter of 0.000083 ft (0.0025 cm), which yields a settling velocity of 0.003 ft/sec by Eq. 4.13. The second set simulates the transport of five different particle diameters of 0.00005, 0.000083, 0.00016, 0.00020, and 0.00028 ft. (0.0015, 0.0025, 0.0040, 0.0060, and 0.0085 cm.) which yielded settling velocities of 0.001, 0.003, 0.008, 0.117, and 0.026 ft/sec respectively.

The simulations of a single and five different particle fall velocities demonstrated the effects of choosing a single average particle diameter or fall velocity to represent the turbid cloud as opposed to a spectrum of particle diameters. The variation of the vertical diffusion coefficient was used to determine the effect of the vertical turbulence scale versus the particle settling rate on the fall velocity of the total particle cloud.

For each of the seven simulations, the initial particle distribution was three dimensionally Gaussian in a 15x15x10 X-Y-η Eulerian grid. The particle cloud was placed directly above the shelf at Brown's Ledge, just slightly to the northeast of the proposed disposal site. This location was chosen for simulation, because of the interesting variation in bottom topography (Figure 8.2) and the economy of simulating particle fallout in 60-70 foot depths as opposed to 100 - 120 foot depths at the disposal site.

The center of mass of the particle cloud was placed approximately 20 feet deep, the cloud possessing a vertical range of fifteen feet. All four settling velocity cases also utilized a 0.7 n.m./day net wind drift in the ENE direction. The negatively buoyant particle simulations were run until more than 95 per cent of the marker particles had fallen to the bottom.

C. Results and Graphics of Simulations

1. K_x, K_y = 50 ft²/sec, Neutrally Buoyant.

This neutrally buoyant simulation was run for approximately 15 hours during which an initial maximum concentration of 3000 mg/liter decayed to 1-5 mg/liter levels for constant horizontal and vertical diffusion coefficients of 50.0, and 0.0001 ft²/sec respectively.

Figure 8.4 A details the translation and expansion of an initially square nautical mile WAPIC grid in time through the Sound waters in approximate three hour time steps. Figures 8.4 B, C, D, E, F, G illustrate two dimensional X-Y concentration contours at vertical levels of 4, 5, 6 and 7 at different times in the 15 hour simulation. Concentrations were plotted at these levels because they contained the maximum particle densities. By time T = 12420 sec., Fig. 8.4 C, the original WAPIC grid cell length had expanded from 400 to 781.2 feet. The skewness in the cloud was evident as the cloud grew large enough to feel the shear in the advective tidal velocities. By time T = 41,100 secs., Fig. 8.4 G, the WAPIC grid had

translated and expanded to the lower edge of the advective velocity field and had stopped expanding and translating, while the particle cloud was no longer located in the center of the Eulerian WAPIC grid .

2. K_x, K_y = 100.0 ft^2/sec, Neutrally Buoyant

This second neutrally buoyant marker particle simulation utilized horizontal and vertical diffusion coefficients of 100.0 and 0.0001 ft^2/sec respectively, and an initial X-Y grid size of 200 feet. Since the horizontal diffusion coefficients had doubled, the background levels were reached in less than half the time of the previous simulation. Figure 8.5 A details the two dimensional translation and expansion of the horizontal WAPIC grid at times T = 0, 1, 3, 5, 6, and 7 hours after slack tide. This plot demonstrated a net drift of the marker particle cloud in an ENE direction, with the original area expanding to more than 36 times its original size. Figures 8.5 B, C, D detail two dimensional concentration contours at various simulation times. After six hours, (concentration contour plots are not given at T = 21600 sec.), the maximum concentration level had dropped to the 1-5 mg/liter level, as compared to fifteen hours for the previous simulation.

3. Scale Dependent, Neutrally Buoyant

A simulation was done to test WAPIC'S horizontal scale dependent diffusion coefficient calculation procedure. The horizontal diffusion coefficients were calculated by Leendertse's formulation, Eq. 6.13 a. This equation approximates the total diffusion coefficient as the sum of

Elder's diffusion coefficient plus scale dependent diffusion due to the wind. At each time step, WAPIC calculated the horizontal standard deviations and an updated K_{wind} by Eqs. 6.13 e, f.

An initial grid size of 200 feet was utilized with an initial maximum concentration of 1500 mg/liter. After approximately 5.0 hours of simulation, concentration levels had fallen to background values of 1-5 mg/liter. Figure 8.6 A details the horizontal grid expansions and translations at T = 0, 1.0, 1.8, 2.6, 3.6, and 4.6 hours. Again, the net drift of the particle cloud was towards the ENE, as would be expected.

Figures 8.6 B and C show two dimensional concentration contours for an X-Y plane through the maximum concentration level at various times. The maximum concentration stays at the same vertical level. The values of the X-Y grid lengths, latitude and longitude of the WAPIC grid origin for each time level of concentration plot are given at the right hand side of Figs. 8.6 B, C in descending time order. In comparison with the two previous simulations, the utilization of the scale dependent horizontal diffusion coefficient approximation, accelerated the transport of the cloud concentration to background levels of entrained sediment.

4. Single Settling Rate, K_z = 0.0001 ft^2/sec

The fourth simulation utilized 2500 markers, each with a free fall velocity of 0.003 ft/sec in a tidal velocity field, with Fickian horizontal and vertical diffusion

coefficients of 100.0 and 0.0001 ft^2/sec respectively. Figure 8.7 A details the expansion and translation of the horizontal grid at times T = 0, 1, 3, and 5 hours after high water. Figures 8.7 B, C, D illustrate two dimensional concentration contours for an X-Y plane (for a given vertical level) passing through the maximum concentration at various times. These figures illustrate the descent of the regions of maximum cloud concentration with increasing vertical levels. Figures 8.7 E, F, G, H demonstrate the physical vertical descent of the marker particle cloud to the bottom. These are X-Z, and Y-Z planar views of the marker particle cloud in space. The axes are in units of feet (depth) and dimensionless horizontal grid distance. The intersection of a plane passing through the cloud's center of mass and intersecting the bottom, in either the X-Y direction, yields a bottom topographic line for referencing the marker particles. One out of ten of the marker particles were plotted.

These figures show the physical descent and horizontal expansion of the marker particle cloud through time. Figure 8.7 H displays the final descent of the cloud at T = 5.19 hours to the bottom. Particles below the bottom topographic line were not below ground, but were just below the vertical level of the intersection of the vertical plane and the bottom.

Figure 8.7 I details the vertical depth and horizontal translation of the center of mass of the particle cloud from T = 0, and the percent mass deposited of the marker

particle cloud as a function of time. The deposition rate was nearly constant from time T = 3.0 to 5.0 hours, then decreased when the particles began to reach the bottom and were diffused and advected at a nearly constant vertical level. After 6.5 hours, more than 95 pecent had been deposited. The X-Y coordinates of the center of mass of the cloud translated in an ENE direction. The slopes of the first two plots of Fig. 8.7 I record the vertical and horizontal velocities of the center of mass while the third slope was the actual deposition rate.

5. Single Settling Rate, K_z = 0.01 ft^2/sec

The fifth simulation was exactly the same as the fourth except a vertical diffusion coefficient 100 times larger, K_z = 0.01 ft^2/sec, was utilized. In Fig. 8.8 A, the grid translated towards the East, with a net displacement of the grid origin in the ESE direction after 6.5 hours of simulation. Figure 8.8 B details horizontal plots of the concentration contours, and 8.8 C, D, E, F show the vertical descent of the marker particle cloud. Within a time span of four to six hours following the release, Figure 8.8 G, a lower particle deposition rate was evident as compared to that of Fig. 8.7 I. The plots of the vertical positions of the center of mass for the above two figures were almost identical. The initial effect of the higher diffusion coefficient in case 5 was to increase the deposition rate (more vertical spread), but as the center of mass of the cloud reached the bottom, the effect was to retard the fallout rate from that found in case 4.

Interestingly, both case 4 and 5 reached the 95 percent mass deposited level at the same time.

6. Five Settling Rates, K_z = 0.0001 ft²/sec

The sixth simulation utilized five different marker particle settling rates (i.e., diameters) with constant horizontal and vertical diffusion coefficients of 100.0 and 0.0001 ft²/sec respectively. The 2500 marker particles were evenly divided into groups of 500 for each particle diameter. All particles were assumed to possess the same specific density of 2.6.

Figure 8.9 A shows the horizontal translation and expansion of the WAPIC grid at times T = 0, 2, 4 hours. Figures 8.9 B, C, show the concentration contours for the maximum cloud concentrations at various times, T = 0, 1.12, 1.81, 2.16 hours. Figures 8.9 D, E, F again illustrate the vertical descent of the marker particle cloud to the bottom. Figure 8.9 G in comparison with Fig. 8.7 F, both at the approximate time of T = 2.2 hours, demonstrated a much greater vertical spread in particle position due to the fact that there were five particle settling rates, with three velocities greater than the settling rate in case 4. In case 6, the vertical particle movements were dominated by the magnitudes of the settling velocities which overshadowed the diffusive vertical flux.

In Fig. 8.9 H, the particle cloud deposited its mass in less than 2.5 hours and moved no further than 0.7 nautical miles to the ENE of the original position. Figure 8.9 H further demonstrated that the settling velocity of

the center of mass of the cloud varied slightly with time.

7. Five Settling Rates, K_z = 0.01 ft²/sec

The seventh, and final simulation of particulate transport at Brown's ledge was the same as the sixth except that a constant vertical diffusion coefficient of 0.01 ft²/sec was utilized. The purpose of using this larger coefficient was to determine the effect of the magnitude of the vertical turbulence scale relative to the settling rates on the overall fallout rate of the cloud. Figures 8.10 A, B, C, D, E, F, G relative to Figs. 8.9 of case 6, demonstrate that there was very little difference between the two simulations as far as concentration, center of mass, and fallout rates were concerned. This behavior was due to the fact that the magnitudes of sixty percent of the particle settling velocities were greater than the diffusion velocities of the particles. In other words, for cases six and seven, the free fall velocities dominated the vertical scale of motion. These simulations demonstrate that adequate resolution of particulate fallout from a suspended sediment cloud requires not only knowledge of the vertical scale of turbulence but also the distribution of sediment diameters and densities (fall velocities).

COUPLING WAPIC TO 2-D VERTICALLY AVG. HYDRODYNAMIC TIDAL MODEL
TRANSLATION AND EXPANSION OF 15X15 X-Y GRID AROUND AN INITIALLY
3-D GAUSSIAN CLOUD OF NEUTRALLY BUOYANT MARKER PARTICLES
WITH CONSTANT X-Y ,Z DIFF. COEFFICIENTS OF 50.0 ,0.0001 FT2/SEC
GRID MOVEMENTS IN THREE HOUR STEPS FROM TIME T=0 ,AT SLACK TIDE
INITIAL X-Y TOTAL GRID SPAN OF 6000 FT.

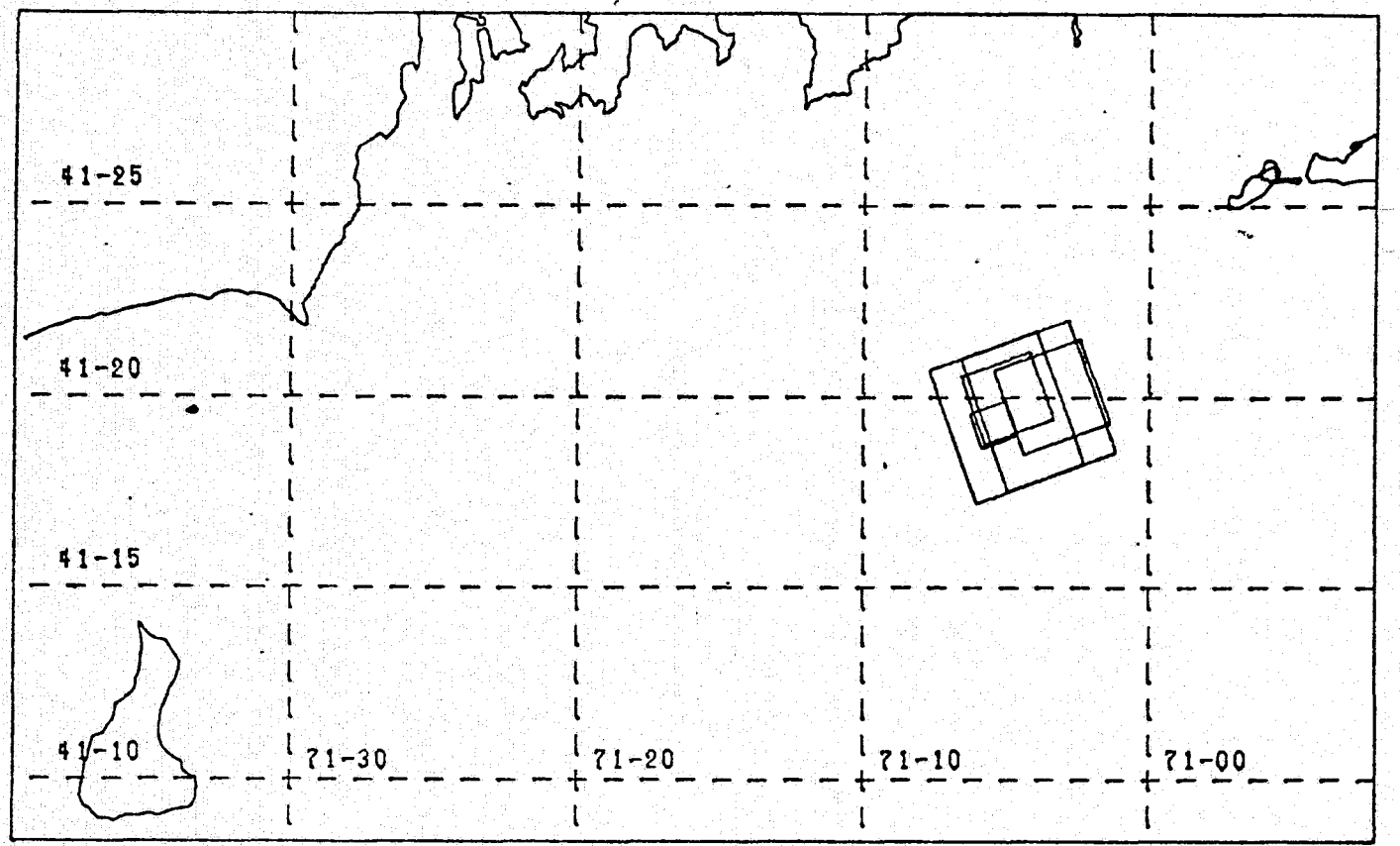

FIGURE 8.4A Long Term Transport of Neutrally Buoyant Particle at Brown's Ledte with Constant Horizontal and Vertical Dispersion Coefficients of 50, 0, 0.0001 FT^2/SEC. Two Dimensional Plot of the Expansion and Translation of the Horizontal Grid

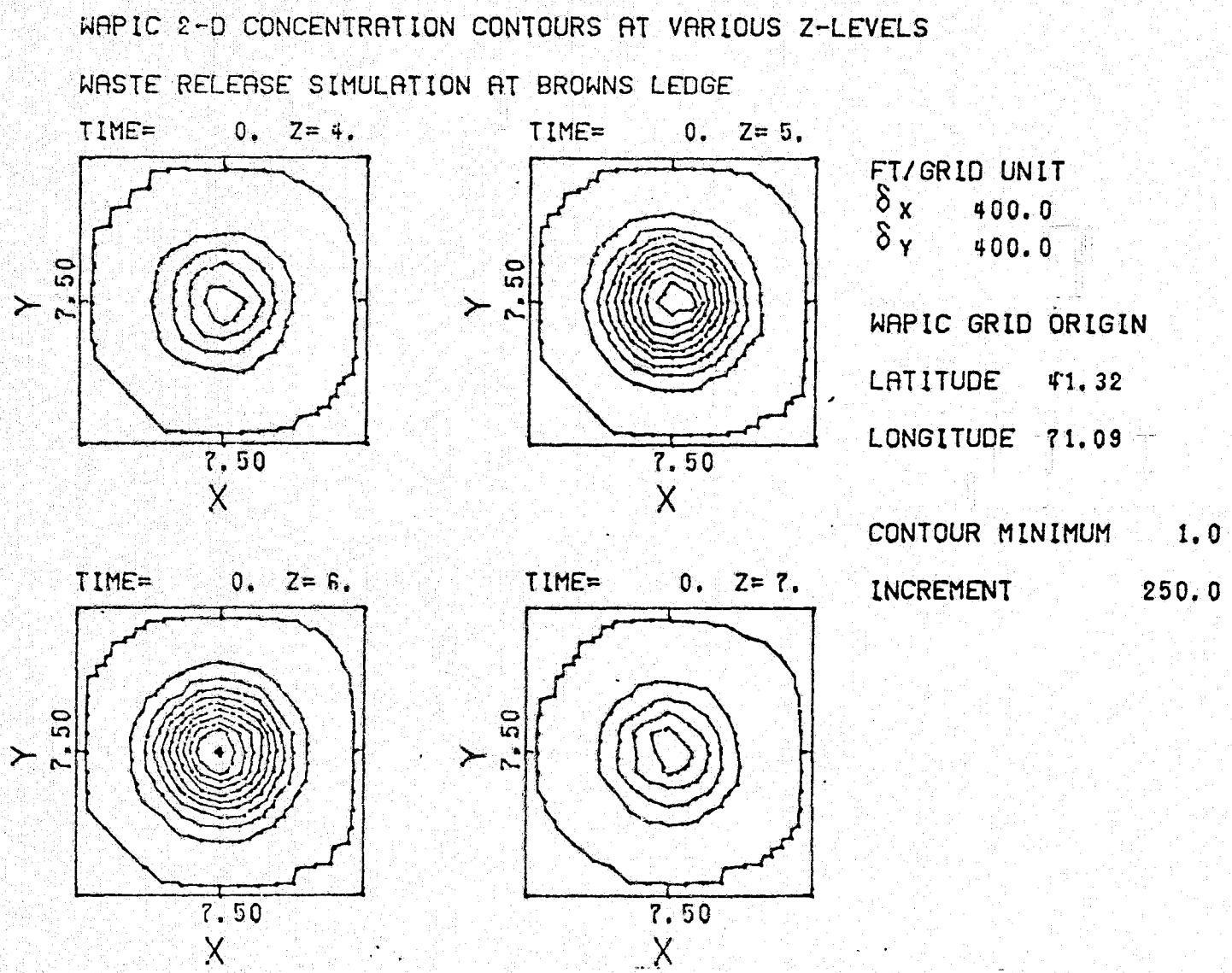

FIGURE 8.4B Long Term Transport of Neutrally Buoyant Particle at Brown's Ledge with Constant Horizontal and Vertical Dispersion Coefficient of 50, 0.0001 FT^2/SEC. T = 0.0 Secs, Horizontal Concentration Contours

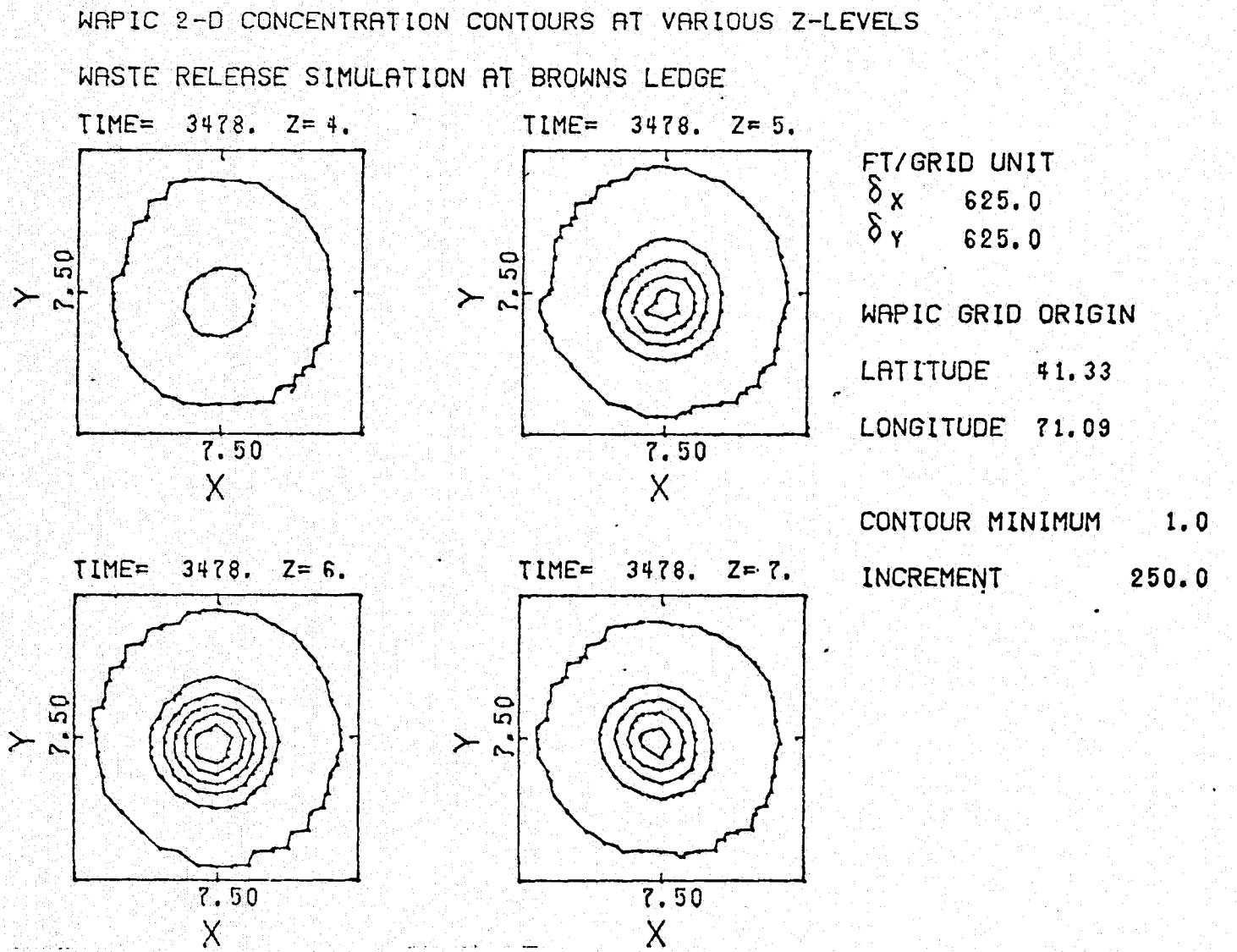

FIGURE 8.4C Long Term Transport of Neutrally Buoyant Particle at Brown's Ledge with Constant Horizontal and Vertical Dispersion Coefficient of 50, 0.0001 FT^2/SEC. T = 3478 Secs. Horizontal Concentration Contours

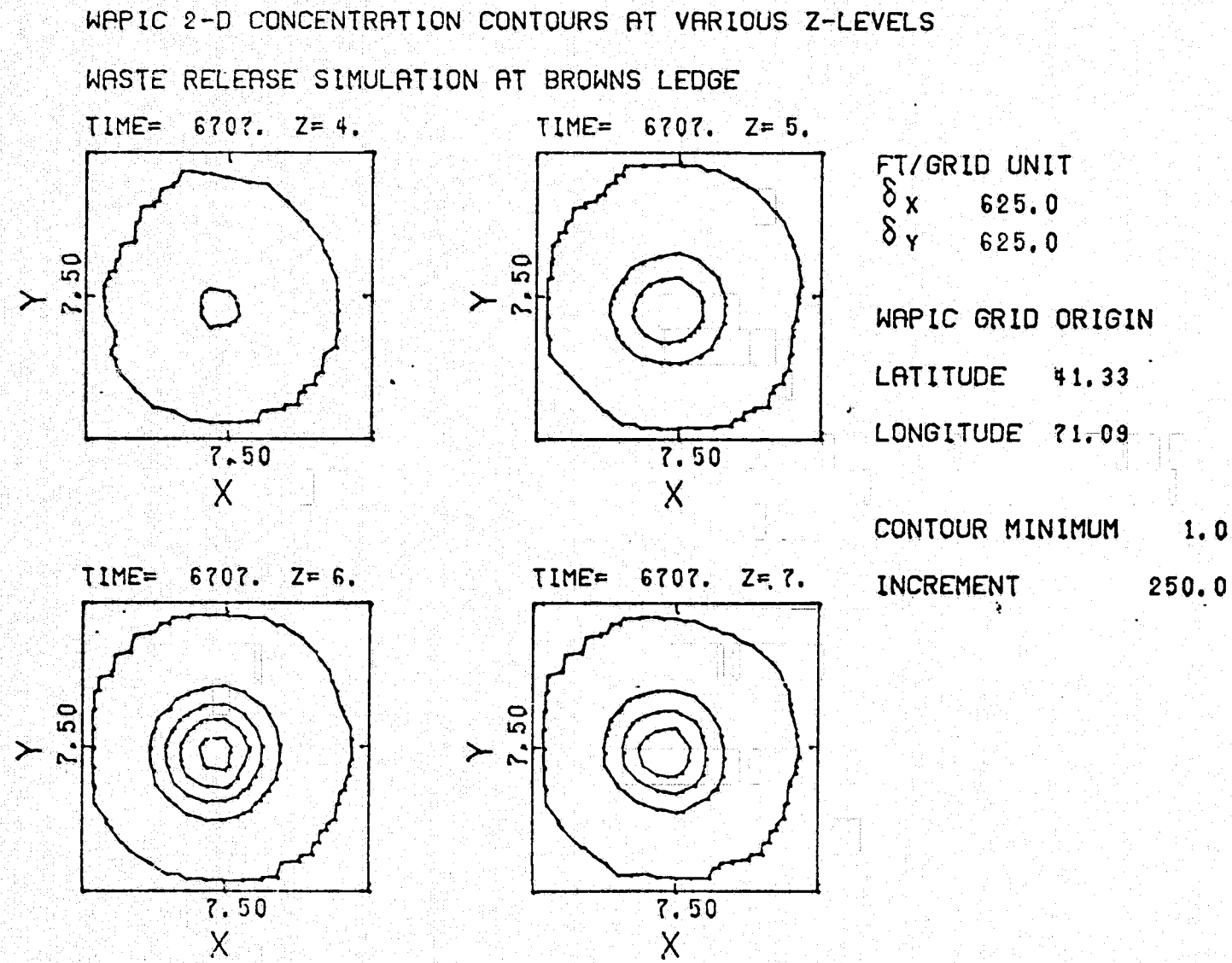

FIGURE 8.4D Long Term Transport of Neutrally Buoyant Particle at Brown's Ledge with Constant Horizontal and Vertical Dispersion Coefficient of 50, 0.0001 FT^2/SEC. T = 6707 Sec. Horizontal Concentration Contours

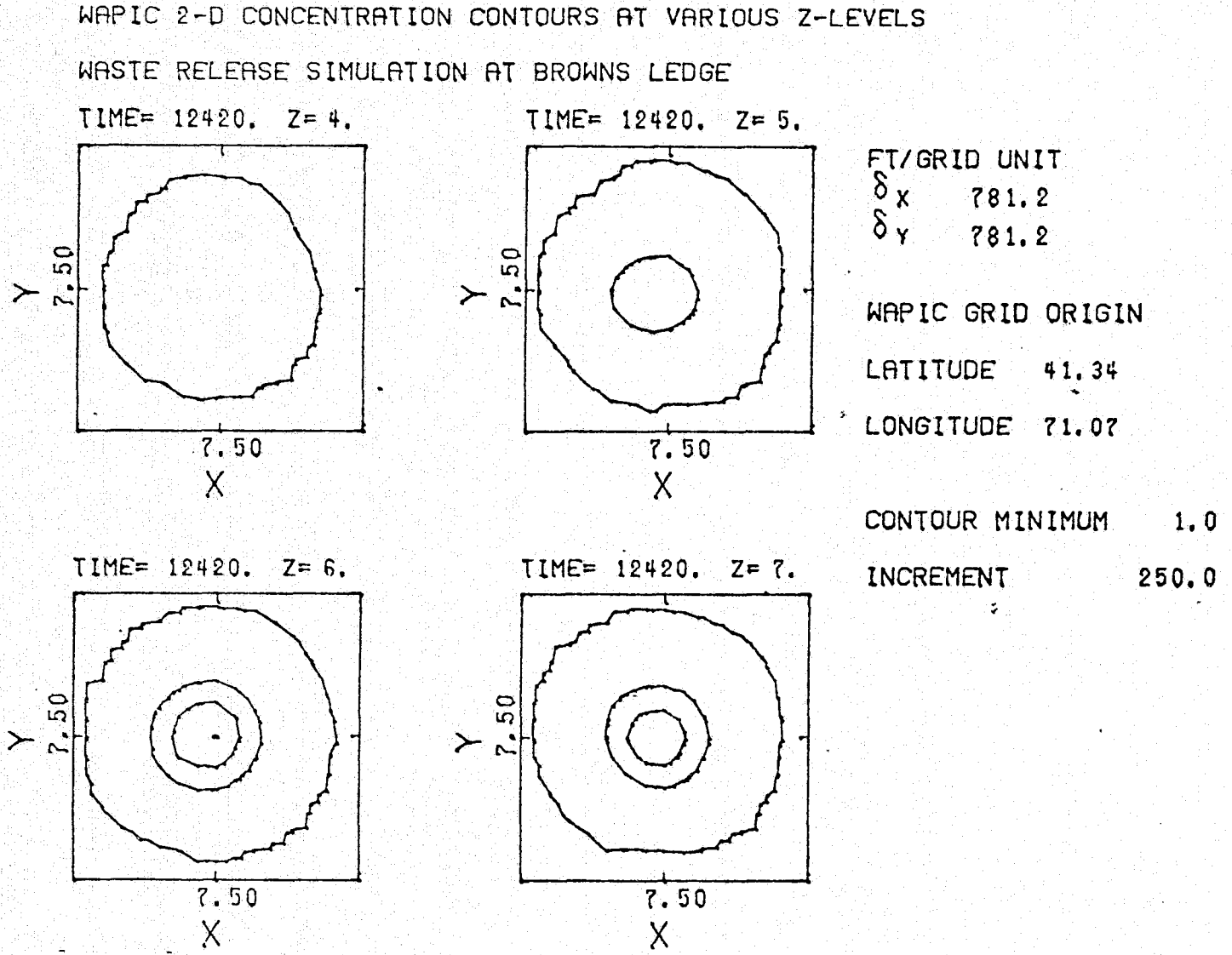

FIGURE 8.4E Long Term Transport of Neutrally Buoyant Particle at Brown's Ledge with Constant Horizontal and Vertical Dispersion Coefficient of 50, 0.0001 FT^2/SEC. T = 12420 Sec. Horizintal Concentration Contours

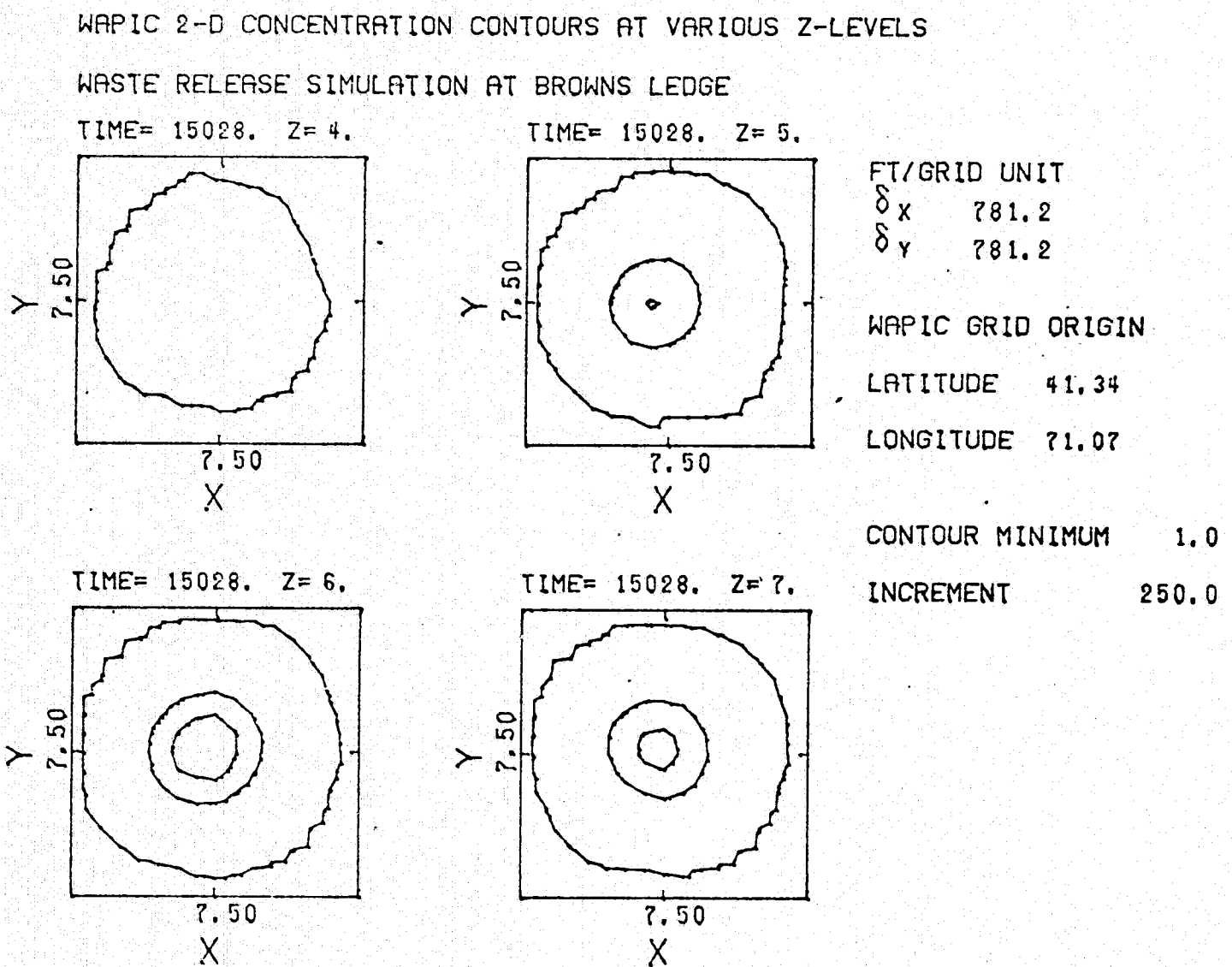

FIGURE 8.4F Long Term Transport of Neutrally Buoyant Particle at Brown's Ledge with Constant Horizontal and Vertical Dispersion Coefficient of 50, 0.0001 FT^2/SEC. T = 15028 Sec. Horizontal Concentration Contours

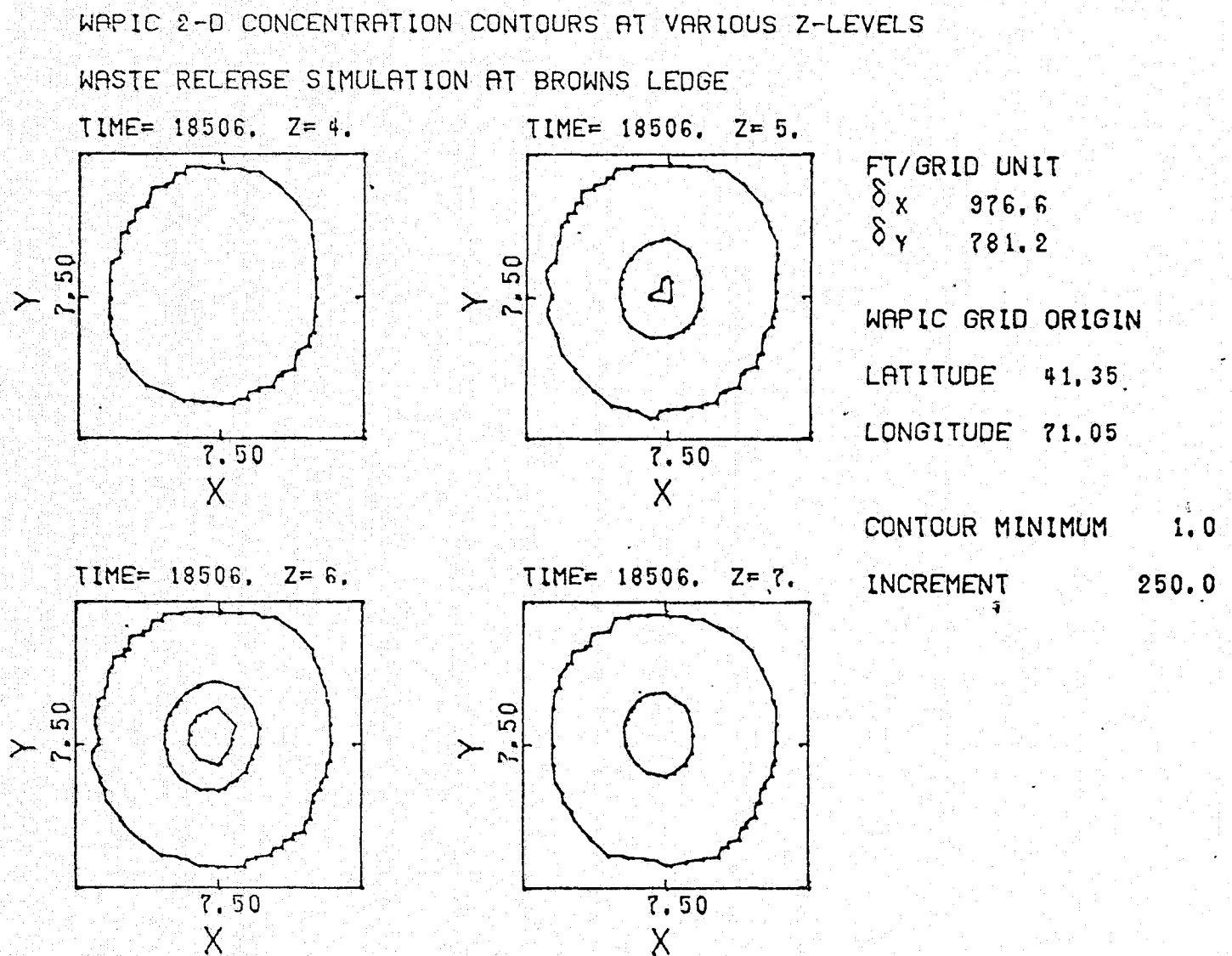

FIGURE 8.4G Long Term Transport of Neutrally Buoyant Particle at Brown's Ledge with Contant Horizontal and Vertical Dispersion Coefficient of 50, 0.0001 FT^2/SEC. T = 18506 Sec. Horizontal Concentration Contours

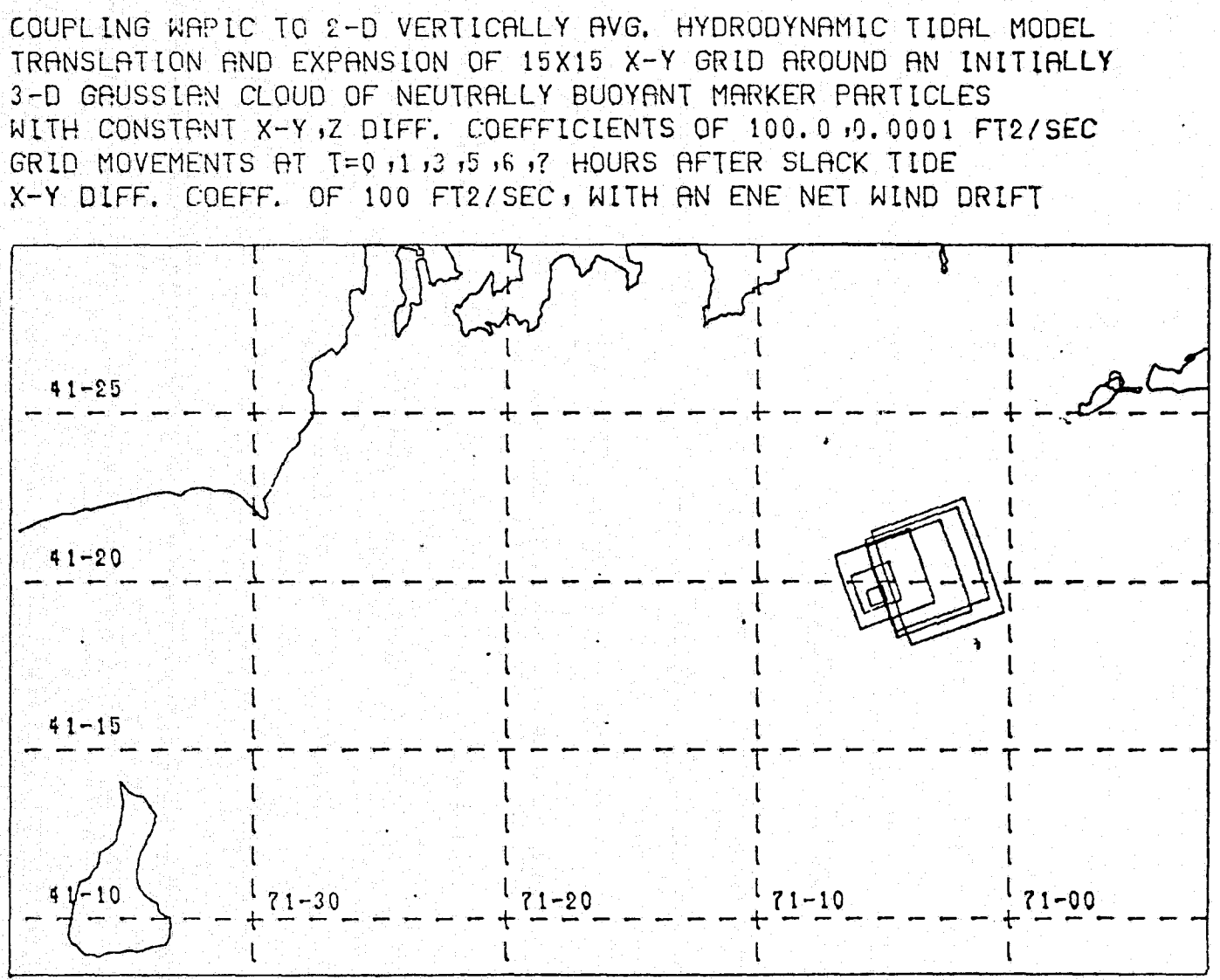

FIGURE 8.5A Long Term Transport of Neutrally Buoyant Particles at Brown's Ledte with Constant Horizontal and Vertical Dispersion Coefficients of 100.0, 0.001 FT^2/SEC. Two Dimensional Plot of Expansion and Translation of Horizontal Grid

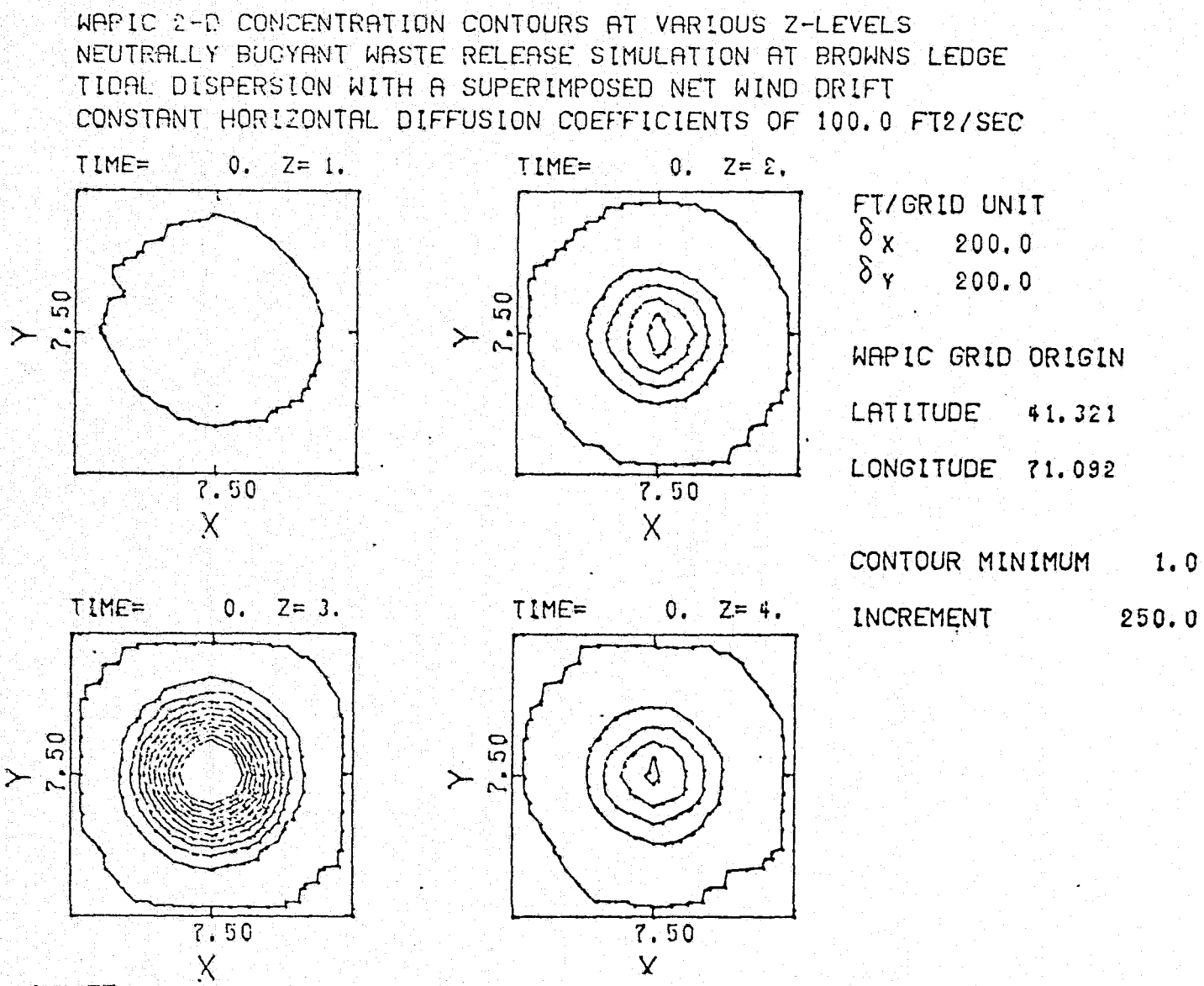

FIGURE 8.5B Long Term Transport of Neutrally Buoyant Particles at Brown's Ledge with Constant Horizontal and Vertical Dispersion Coefficients of 100.0, 0.001 FT^2/SEC. Two Dimensional Plot of Expansion and Translation of Horizontal Grid. T = 0.0 Sec., Concentration Contours

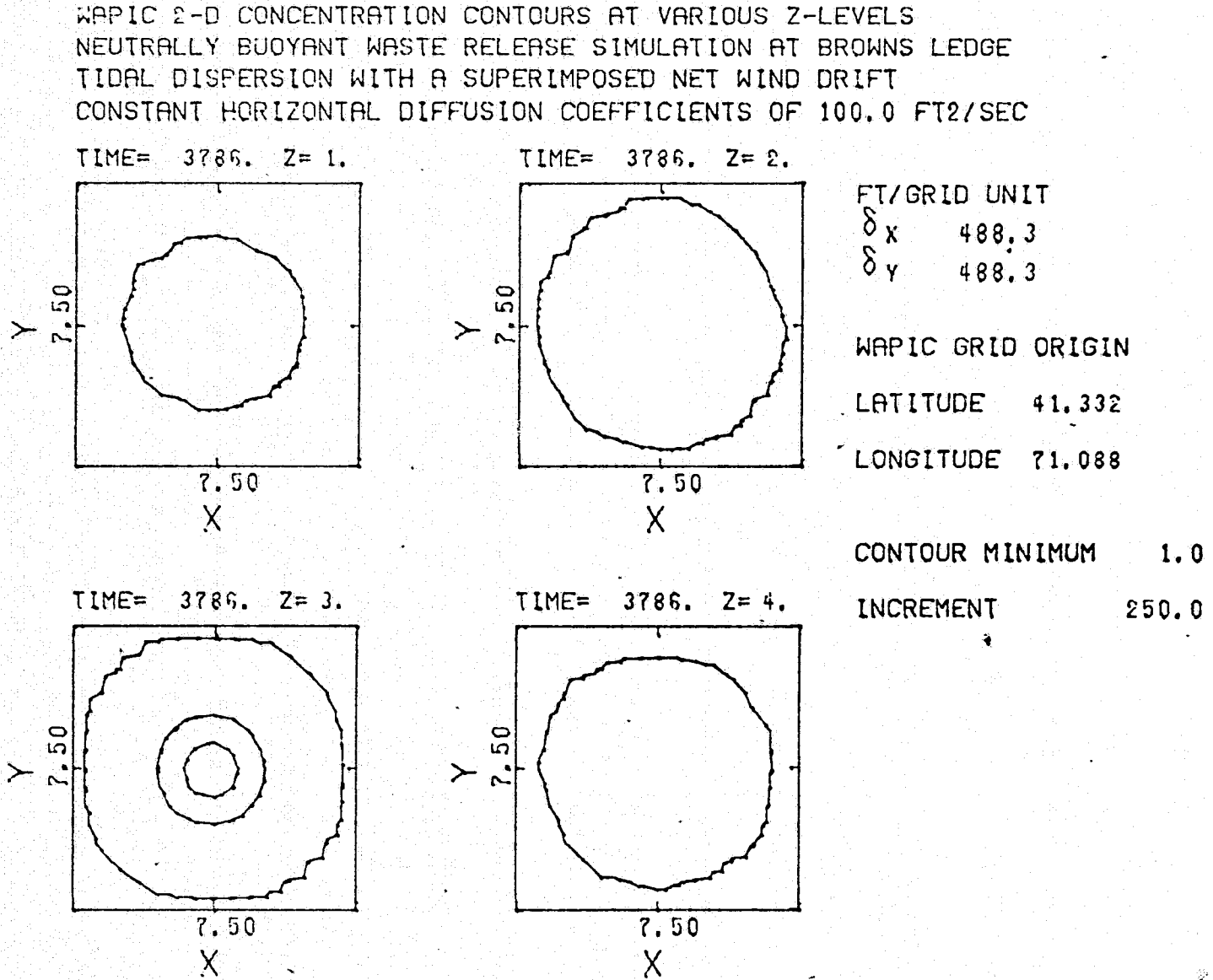

FIGURE 8.5C Long Term Transport of Neutrally Buoyant Particles at Brown's Ledge with Constant Horizontal and Vertical Dispersion Coefficients of 100.0, 0.001 FT^2/SEC. Two Dimensional Plot of Expansion and Translation of Horizontal Grid. T = 3786 Sec., Concentration Contours

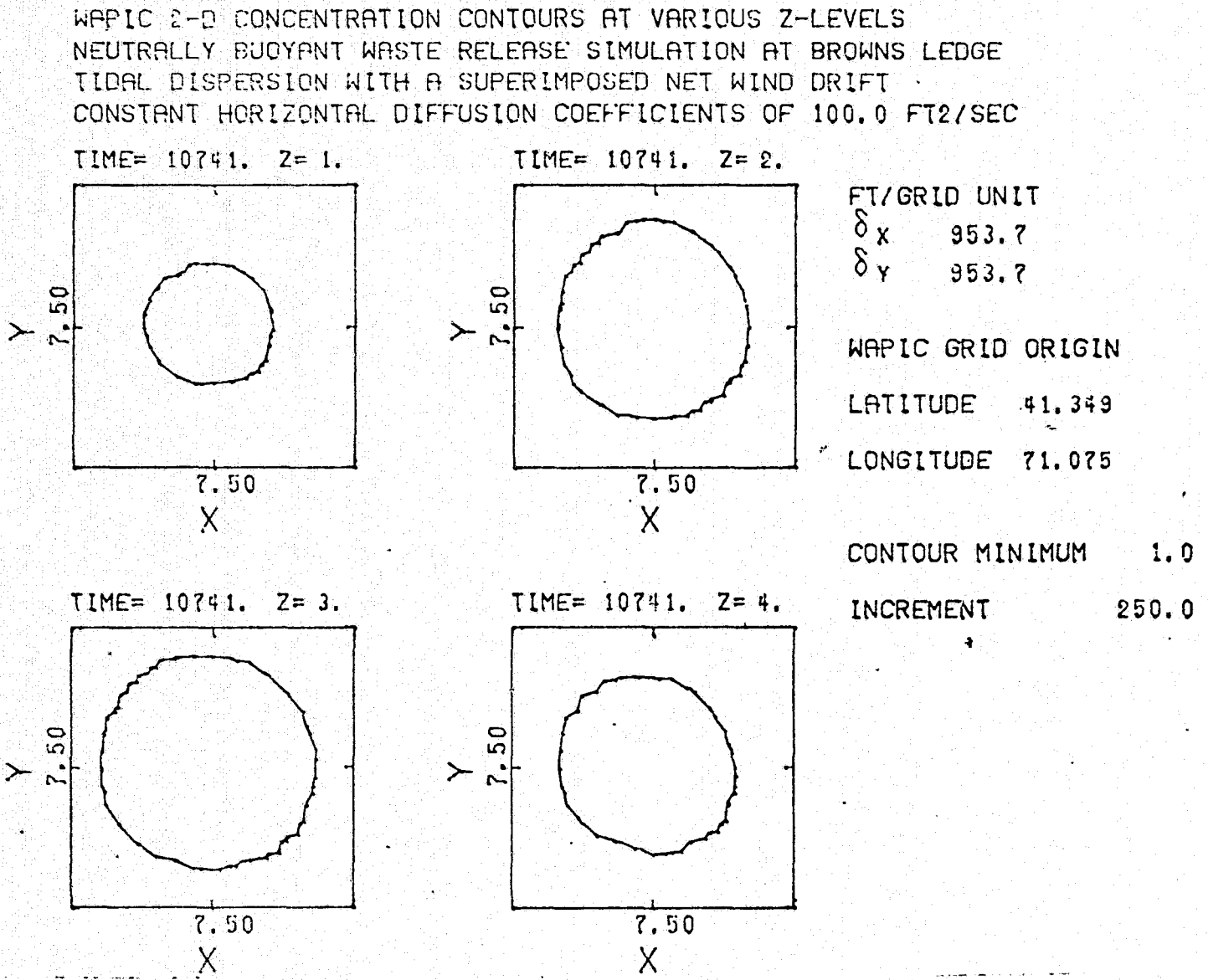

FIGURE 8.5D Long Term Transport of Neutrally Buoyant Particles at Brown's Ledge with Constant Horizontal and Vertical Dispersion Coefficients of 100.0, 0.001 FT^2/SEC. Two Dimensional Plot of Expansion and Translation of Horizontal Grid. T = 10741 Sec., Concentration Contours

COUPLING WRPIC TO 2-D VERTICALLY AVG. HYDRODYNAMIC TIDAL MODEL
TRANSLATION AND EXPANSION OF 15X15 X-Y GRID AROUND AN INITIALLY
3-D GAUSSIAN CLOUD OF NEUTRALLY BUOYANT MARKER PARTICLES
WITH SCALE DEPENDENT X-Y DIFF. COEFF, Z. COEFF.=0.01 FT2/SEC:
GRID MOVEMENTS AT T=0 ,1.0 ,1.8 ,2.6 ,3.6 ,4.6 HRS. , FROM SLACK TIDE
INITIAL X-Y TOTAL GRID SPAN OF 3000 FT.

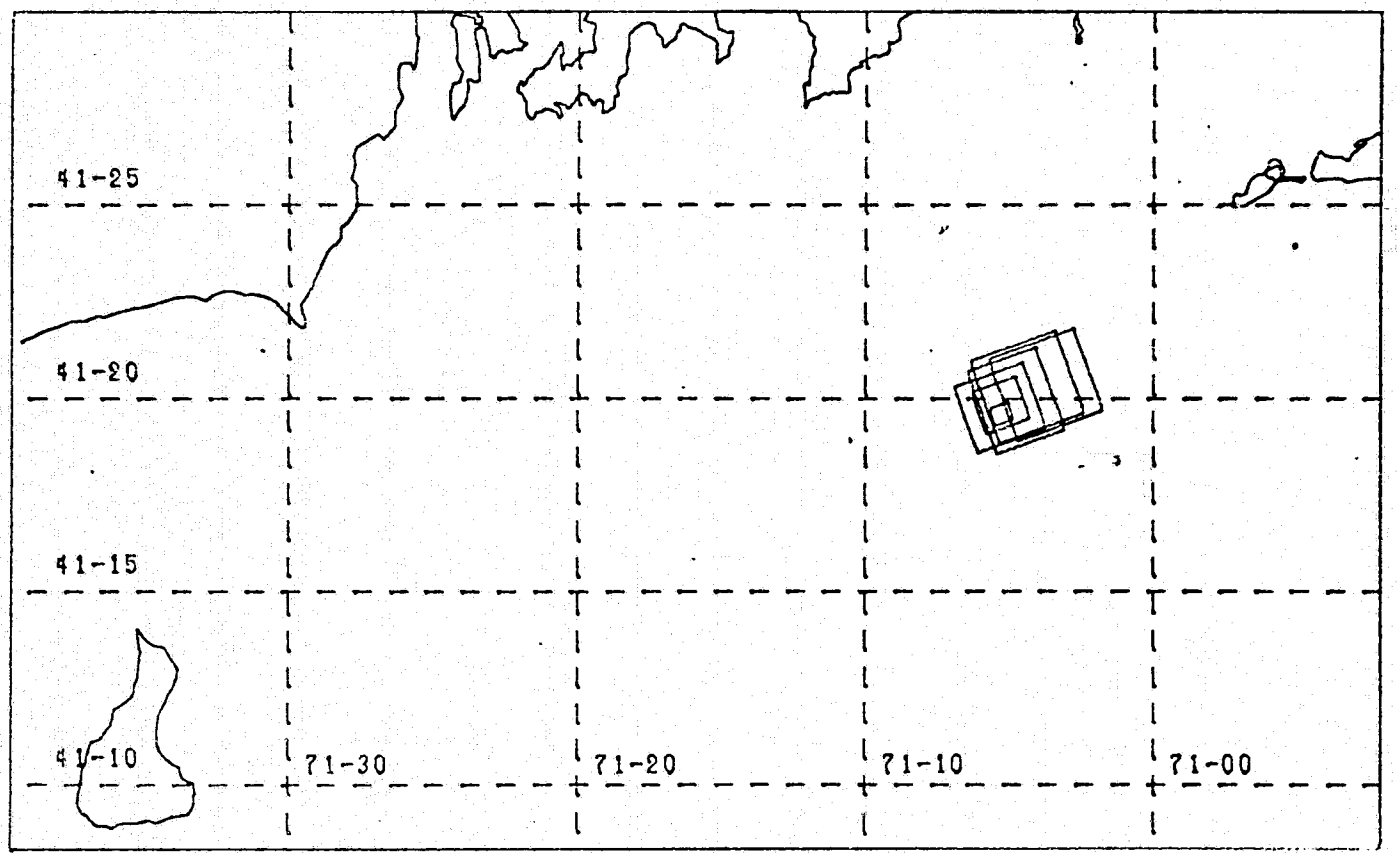

FIGURE 8.6A Long Term Transport of Neutrally Buoyant Particle at Brown's Ledge with Scale Dependent Horizontal Diffusion Dispersion Coefficients, and Vertical Dispersion Coefficient = 0.01 FT^2/SEC. Two Dimensional Plot of Expansion and Translation of Horizontal Grid.

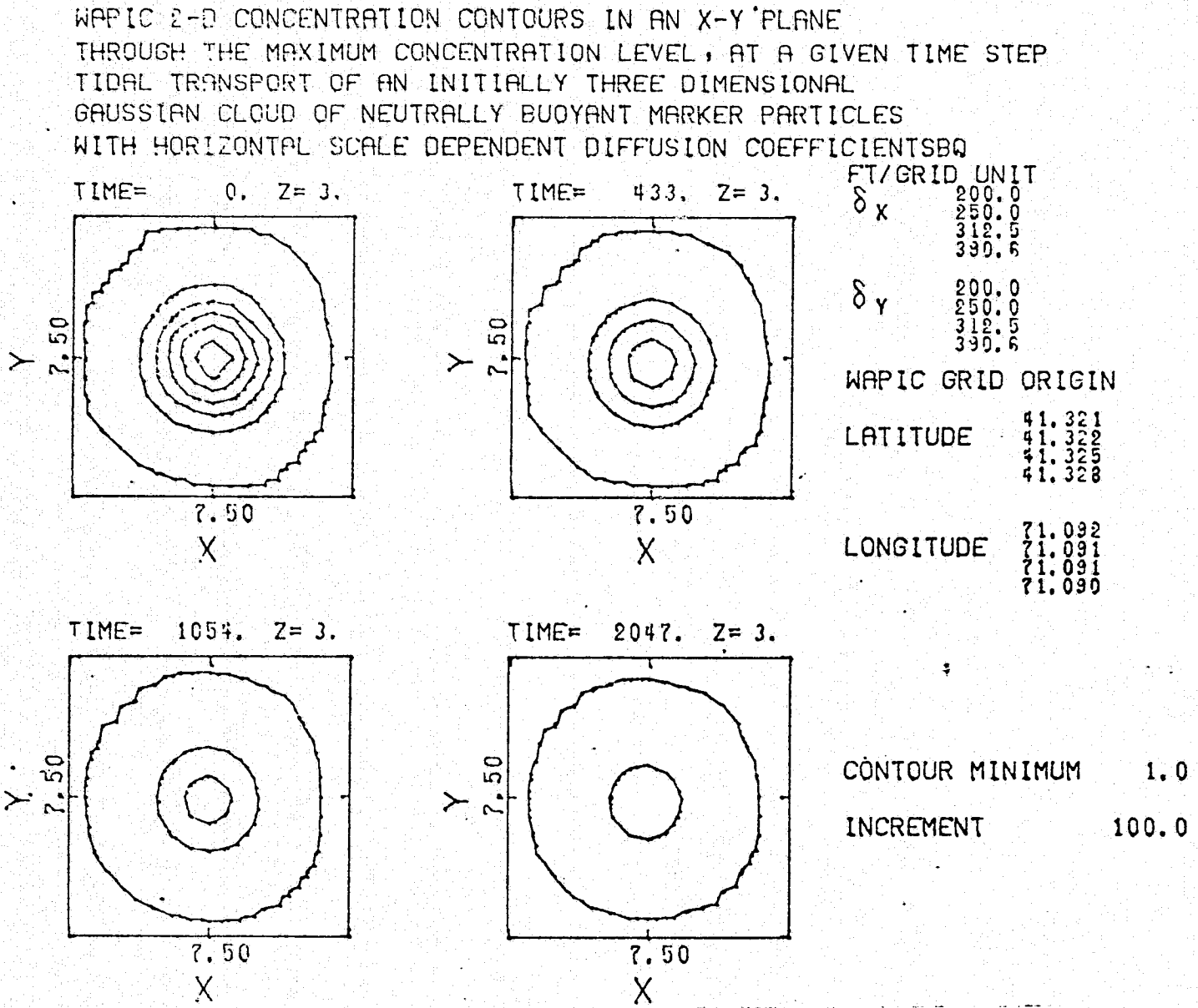

FIGURE 8.6B Long Term Transport of Neutrally Buoyant Particle at Brown's Ledge with Scale Dependent Horizontal Diffusion Dispersion Coefficients, and Vertical Dispersion Coefficient = 0.01 FT^2/SEC. Concentration Contours at T = 0.0, 433.0, 1054.0, 2047.0 Secs

WAPIC 2-D CONCENTRATION CONTOURS IN AN X-Y PLANE
THROUGH THE MAXIMUM CONCENTRATION LEVEL, AT A GIVEN TIME STEP
TIDAL TRANSPORT OF AN INITIALLY THREE DIMENSIONAL
GAUSSIAN CLOUD OF NEUTRALLY BUOYANT MARKER PARTICLES
WITH HORIZONTAL SCALE DEPENDENT DIFFUSION COEFFICIENTSBQ

TIME= 3662. Z= 3.

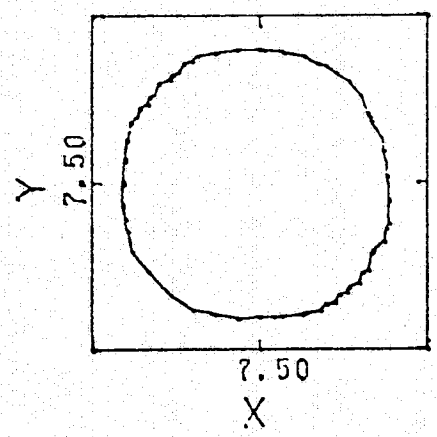

FT/GRID UNIT

δ_X 488.3
762.9

δ_Y 488.3
762.9

WAPIC GRID ORIGIN

LATITUDE 41.332
41.338

LONGITUDE 71.088
71.084

TIME= 6394. Z= 3.

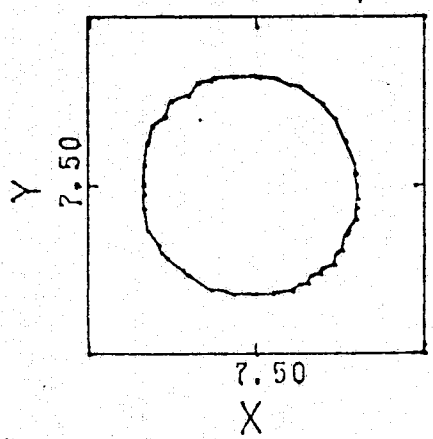

CONTOUR MINIMUM 1.0

INCREMENT 100.0

FIGURE 8.6C Long Term Transport of Neutrally Buoyant Particle at Brown's Ledge with Scale Dependent Horizontal Diffusion Dispersion Coefficient, and Vertical Dispersion Coefficient = 0.01 FT^2/SEC. Concentration Contours at T = 3662, 6394 Secs.

COUPLING WAPIC TO 2-D VERTICALLY AVG. HYDRODYNAMIC TIDAL MODEL
TRANSLATION AND EXPANSION OF 15X15 X-Y GRID AROUND AN INITIALLY
3-D GAUSSIAN CLOUD WITH A SINGLE PARTICLE SETTLING RATE
WITH CONSTANT X-Y,Z DIFF. COEFFICIENTS OF 100. ,0.0001 FT2/SEC
GRID MOVEMENTS AT 1 ,3 ,5 HOURS AFTER TIME T=0 , AT SLACK TIDE
INITIAL X-Y TOTAL GRID SPAN OF 3000 FT.

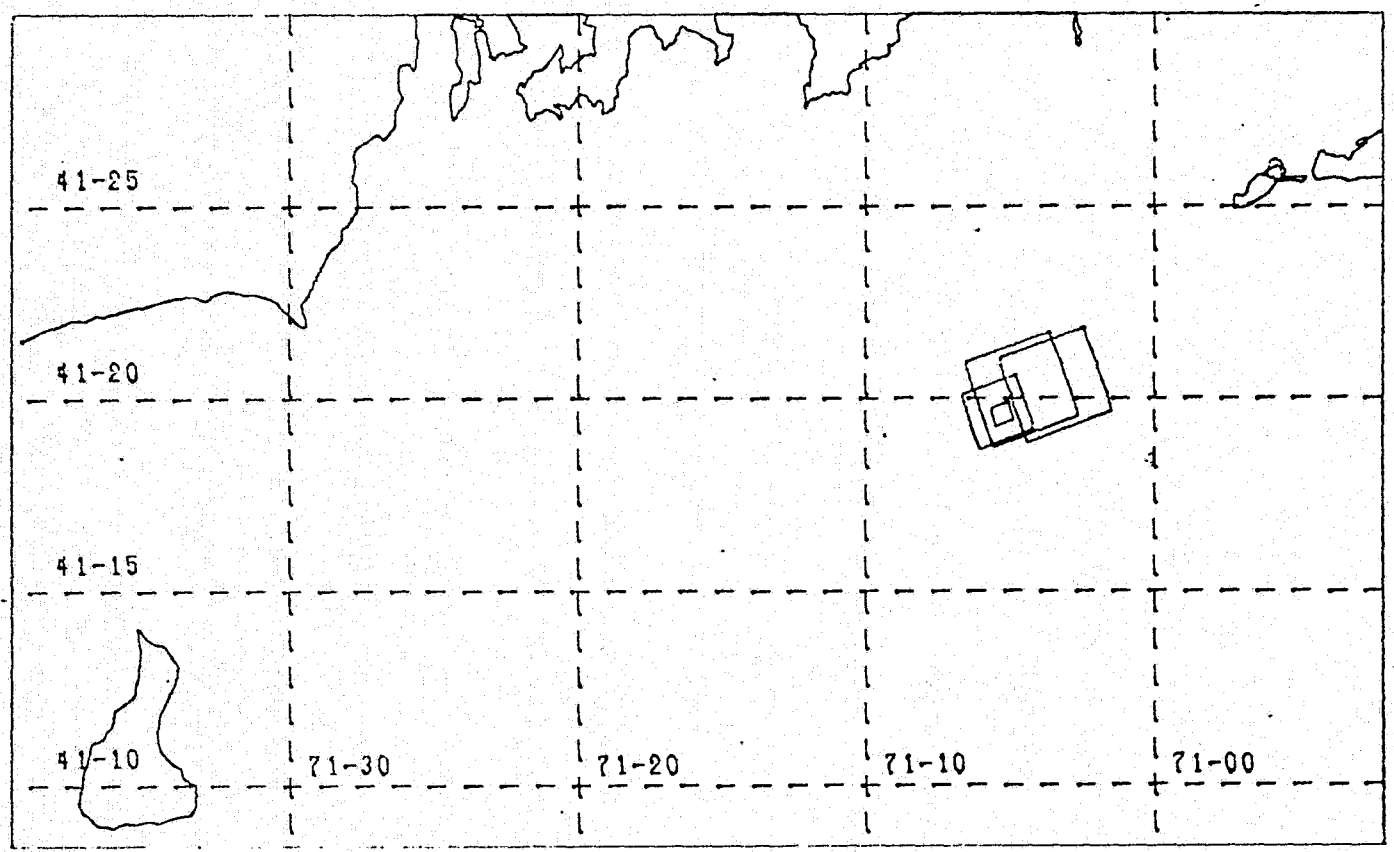

FIGURE 8.7A Long Term Transport of Sedimentary Particle with a Single Particle Settling Rate, with Constant Horizontal and Vertical Dispersion Coefficients of 100.0, 0.0001 FT^2/SEC, W_s = 0.003 FT^2/SEC. Two Dimensional Plot of Expansion and Translation of Horizontal Grid

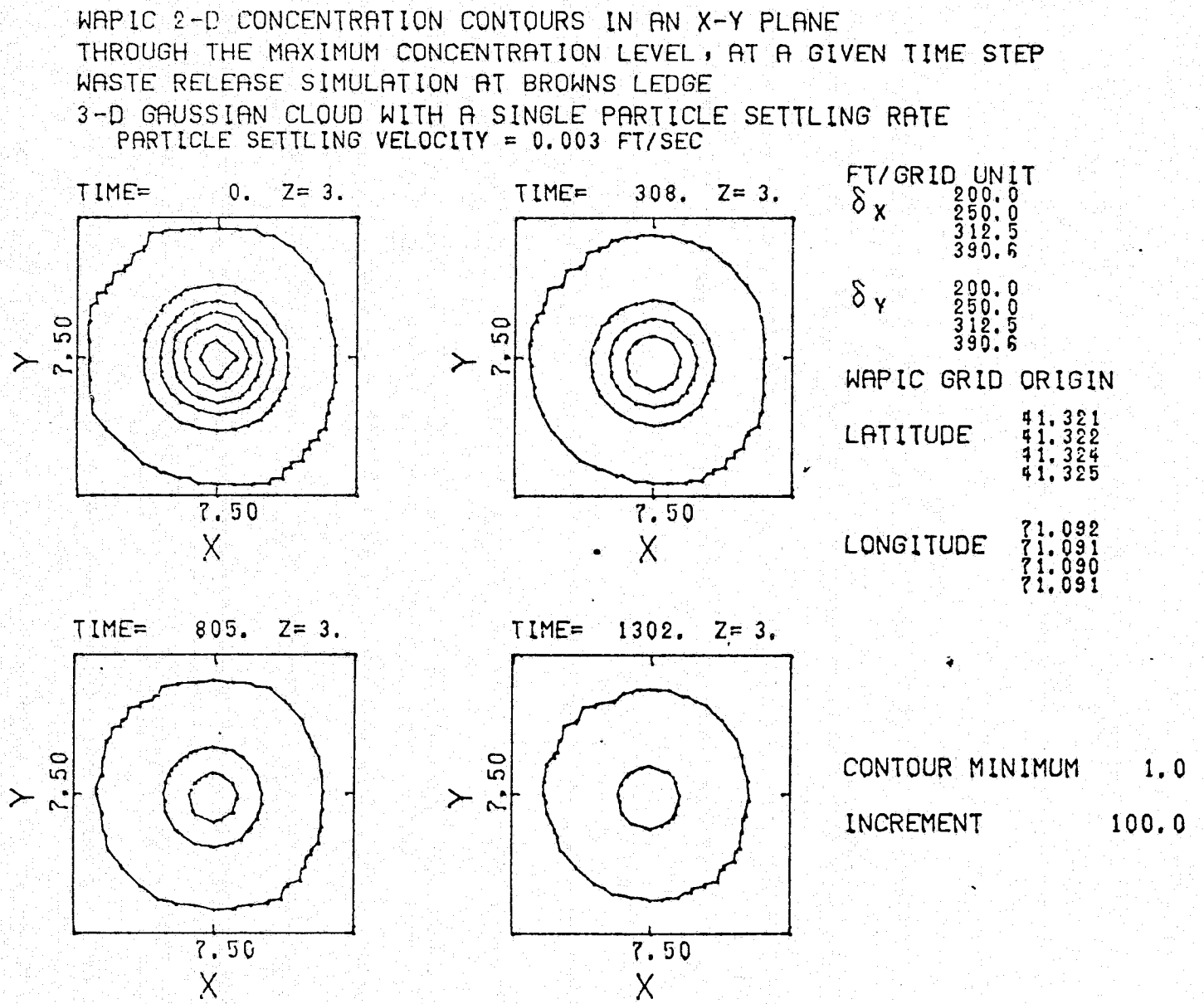

FIGURE 8.7B Long Term Transport of Sedimentary Particle with a Single Particle Settling Rate, with Constant Horizontal and Vertical Dispersion Coefficients of 100.0, 0.0001 FT^2/SEC, W_s = 0.003 FT/SEC. Concentration Contours at T = 0.0, 308, 805, 1302 Secs

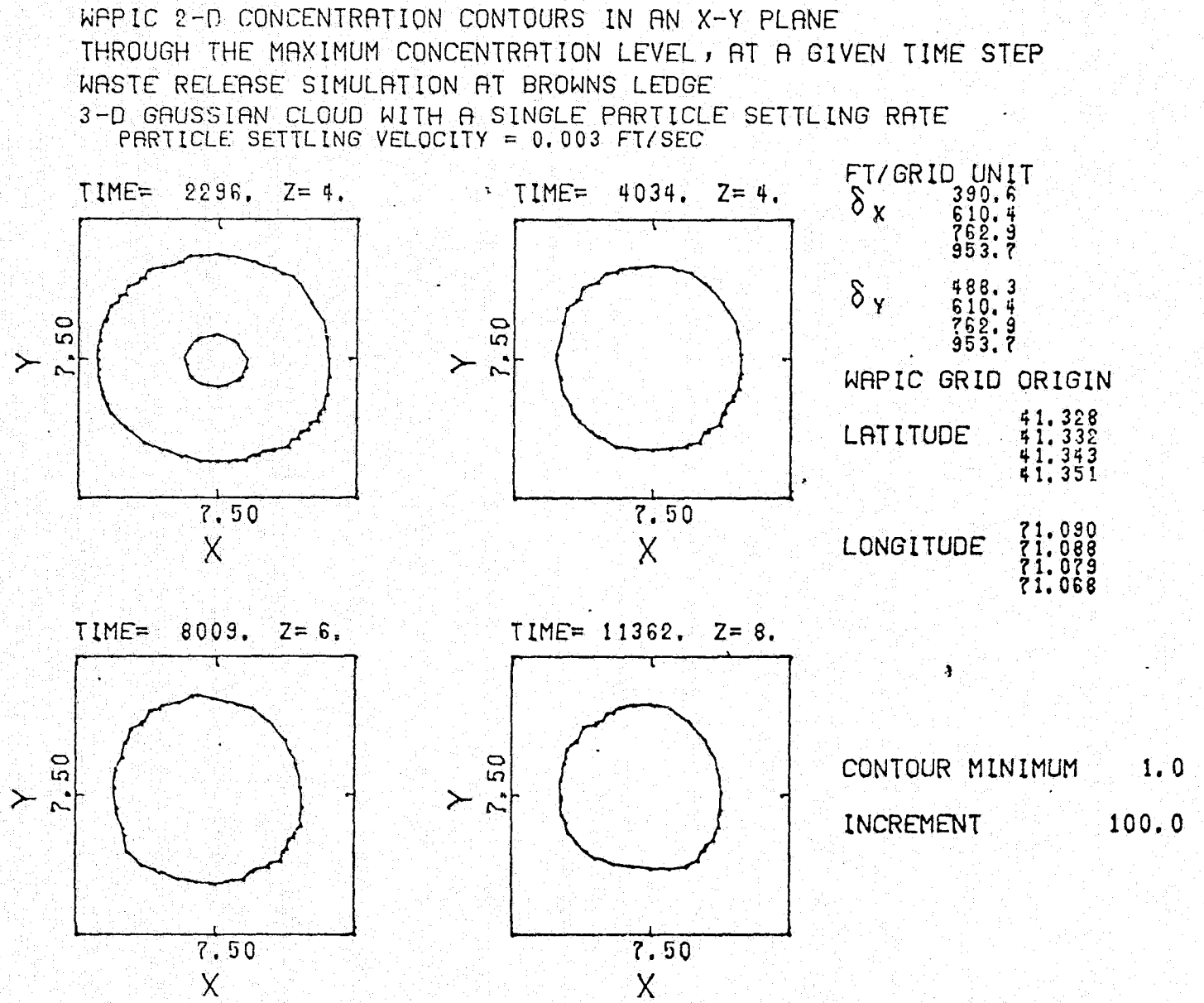

FIGURE 8.7C Long Term Transport of Sedimentary Particle with a Single Particle Settling Rate, with Constant Horizontal and Vertical Dispersion Coefficients of 100.0, 0.0001 FT^2/SEC, w_s = 0.003 FT/SEC. Concentration Contours at T = 2296, 4304, 8007, 11362 Secs

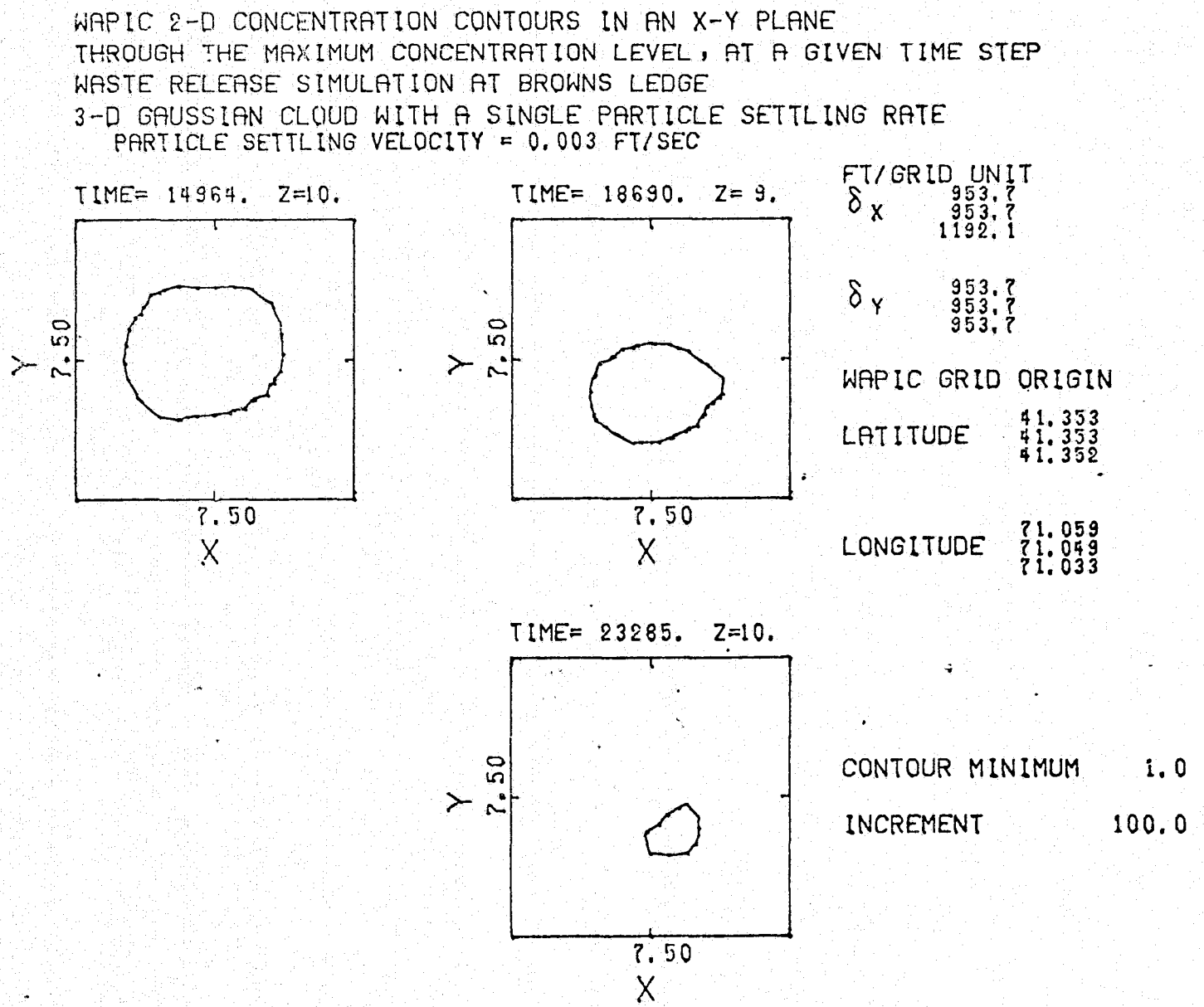

FIGURE 8.7D Long Term Transport of Sedimentary Particle with a Single Particle Settling Rate, with Constant Horizontal and Vertical Dispersion Coefficients of 100.0, 0.0001 FT^2/SEC, W_s = 0.003 FT/SEC. Concentration Contours at T = 14964, 18690, 23285 Sec

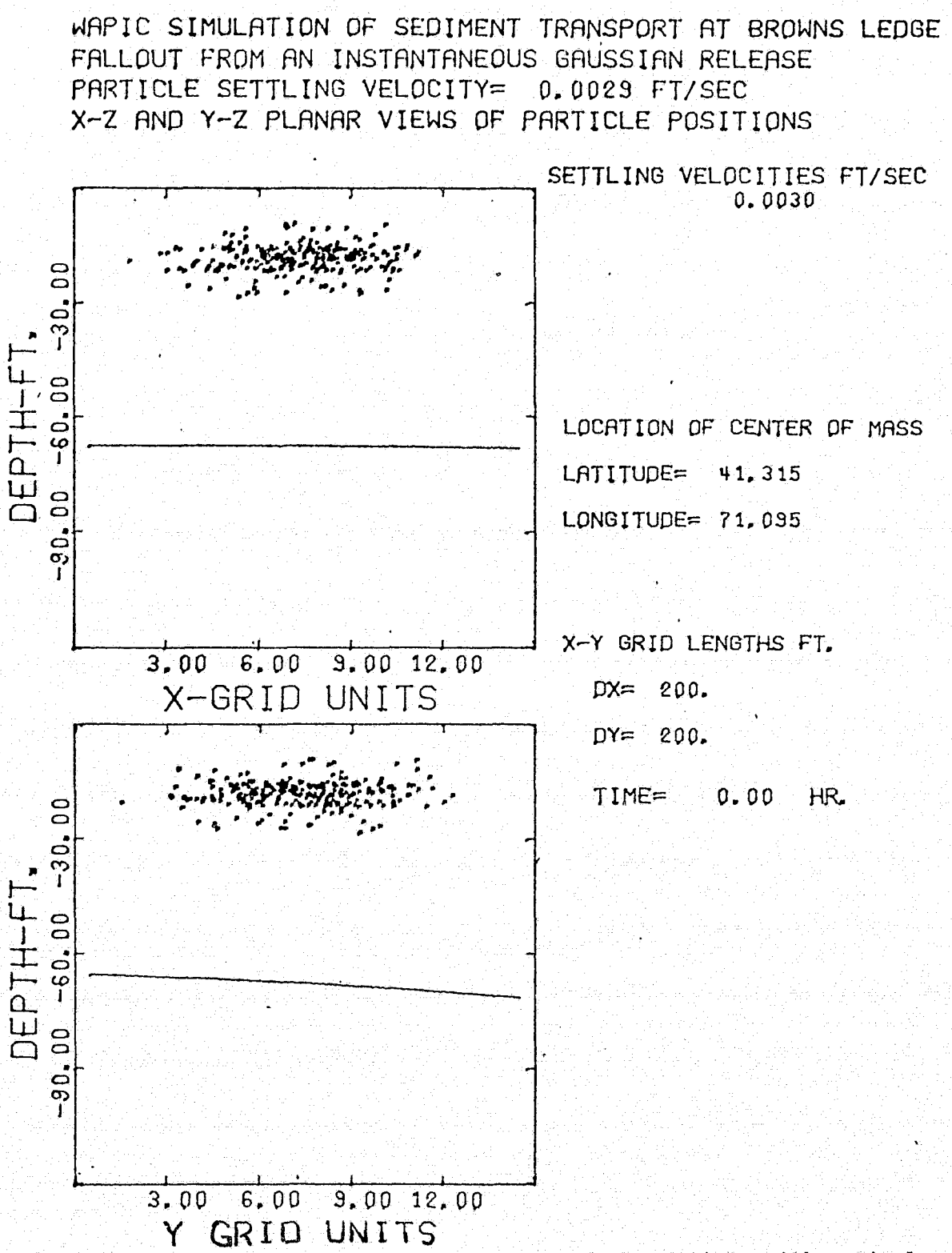

FIGURE 8.7E Long Term Transport of Sedimentary Particle with a Single Particle Settling Rate, with Constant Horizontal and Vertical Dispersion Coefficients of 100.0, 0.0001 FT^2/SEC, W_s = 0.003 FT/SEC; X-Y, Y-Z Planar View of Particle Cloud, T = 0.0 Hours

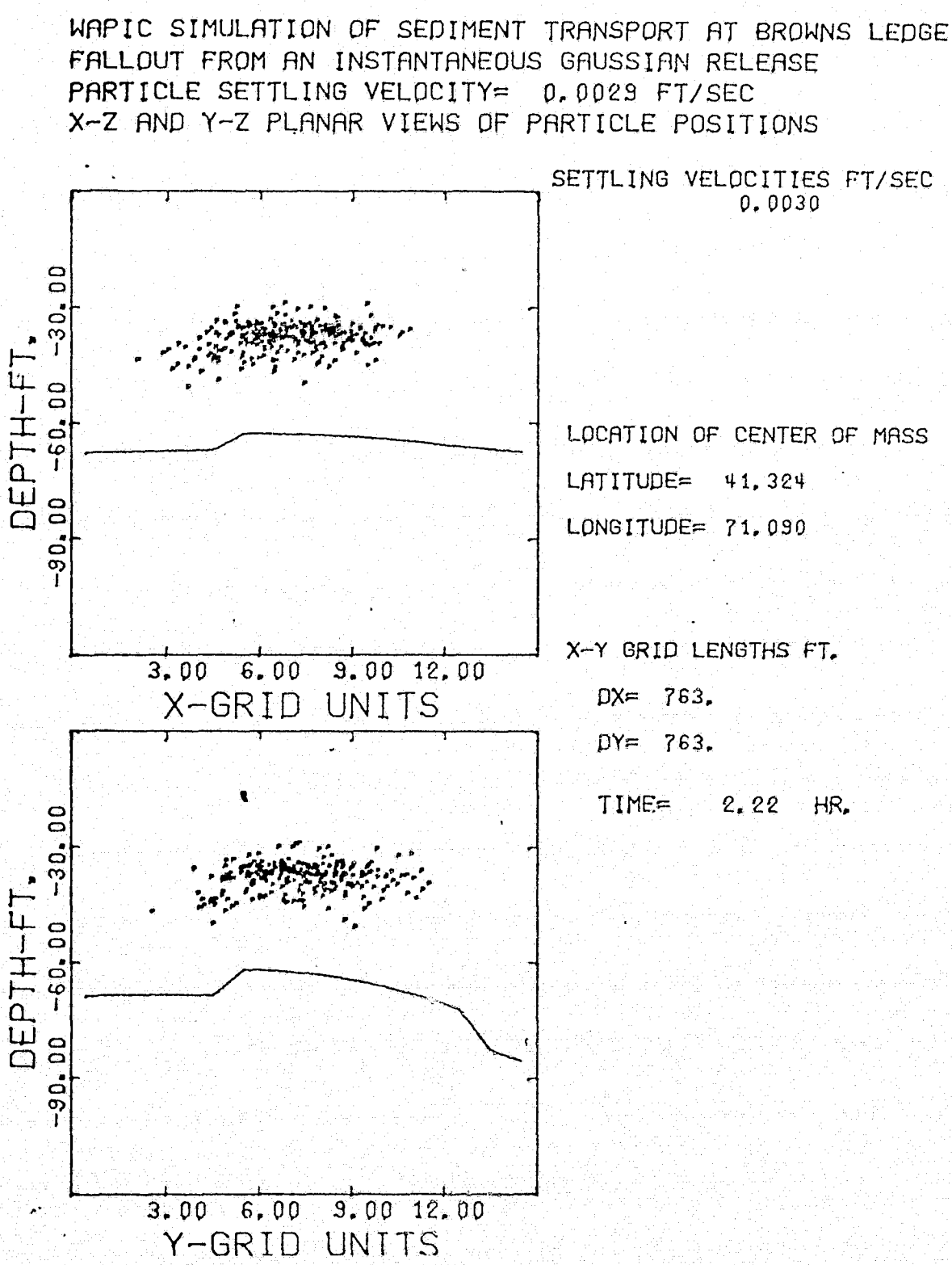

FIGURE 8.7F Long Term Transport of Sedimentary Particle with a Single Particle Settling Rate, with Constant Horizontal and Vertical Dispersion Coefficients of 100.0, 0.0001 FT^2/SEC, W_s = 0.003 FT/SEC; X-Y, Y-Z Planar View of Particle Cloud, T = 2.2 Hours

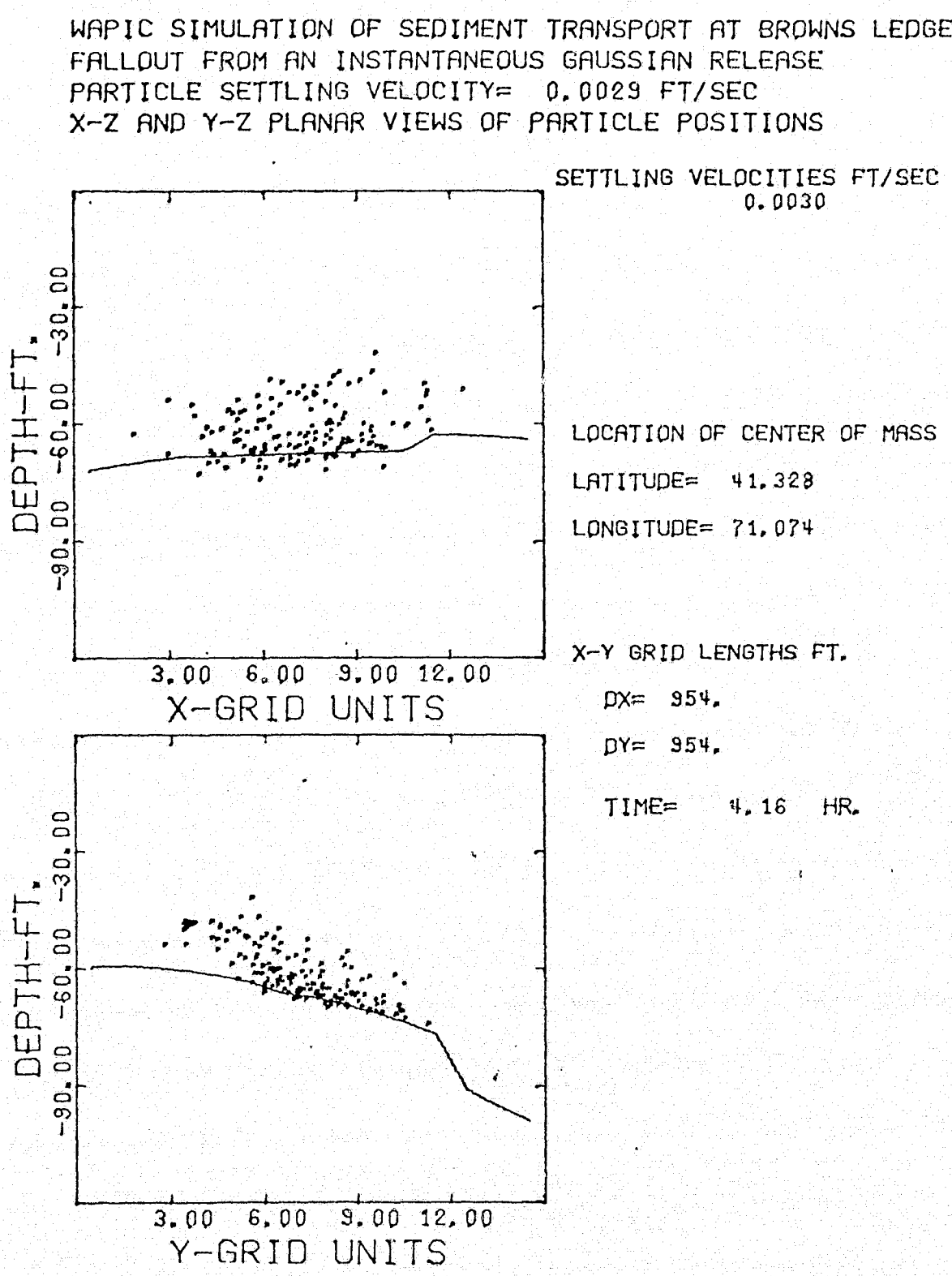

FIGURE 8.7G Long Term Transport of Sedimentary Particle with a Single Particle Settling Rate, with Constant Horizontal and Vertical Dispersion Coefficients of 100.0, 0.0001 FT^2/SEC, W_s = 0.003 FT/SEC; X-Y, Y-Z Planar View of Particle Cloud, T = 4.6 Hours

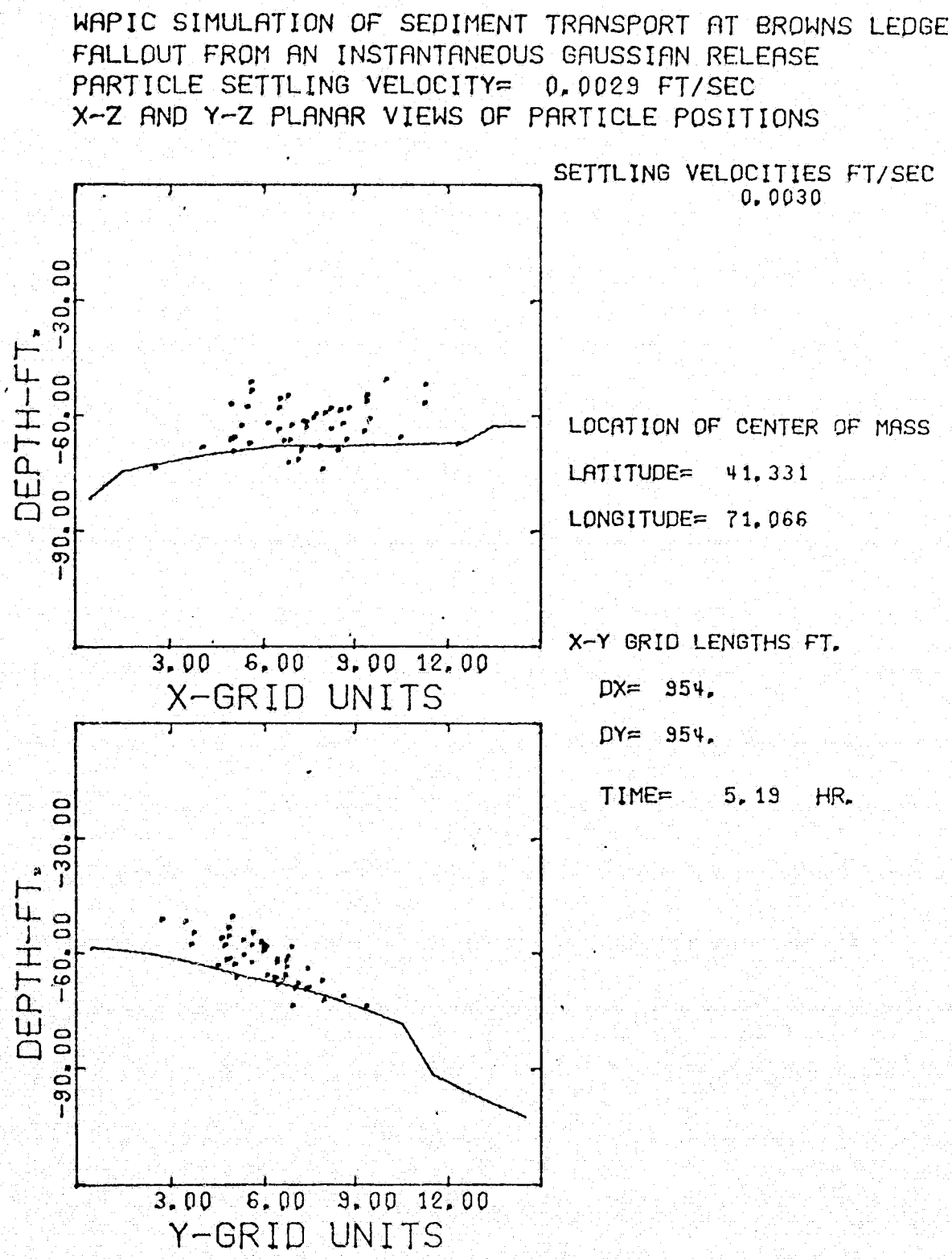

FIGURE 8.7H Long Term Transport of Sedimentary Particle with a Single Particle Settling Rate, with Constant Horizontal and Vertical Dispersion Coefficients of 100.0, 0.0001 FT^2/SEC, W_s = 0.003 FT/SEC; X-Y, Y-Z Planar View of Particle Cloud, T = 5.19 Hours

WAPIC SIMULATION OF SEDIMENT FALLOUT AT BROWNS LEDGE
FOR A SINGULAR PARTICLE SETTLING VELOCITY
THE X,Y,Z POSITIONS OF CENTER OF MASS, AND % OF MASS
REMAINING IN THE PARTICLE CLOUD AS A FUNCTION OF TIME

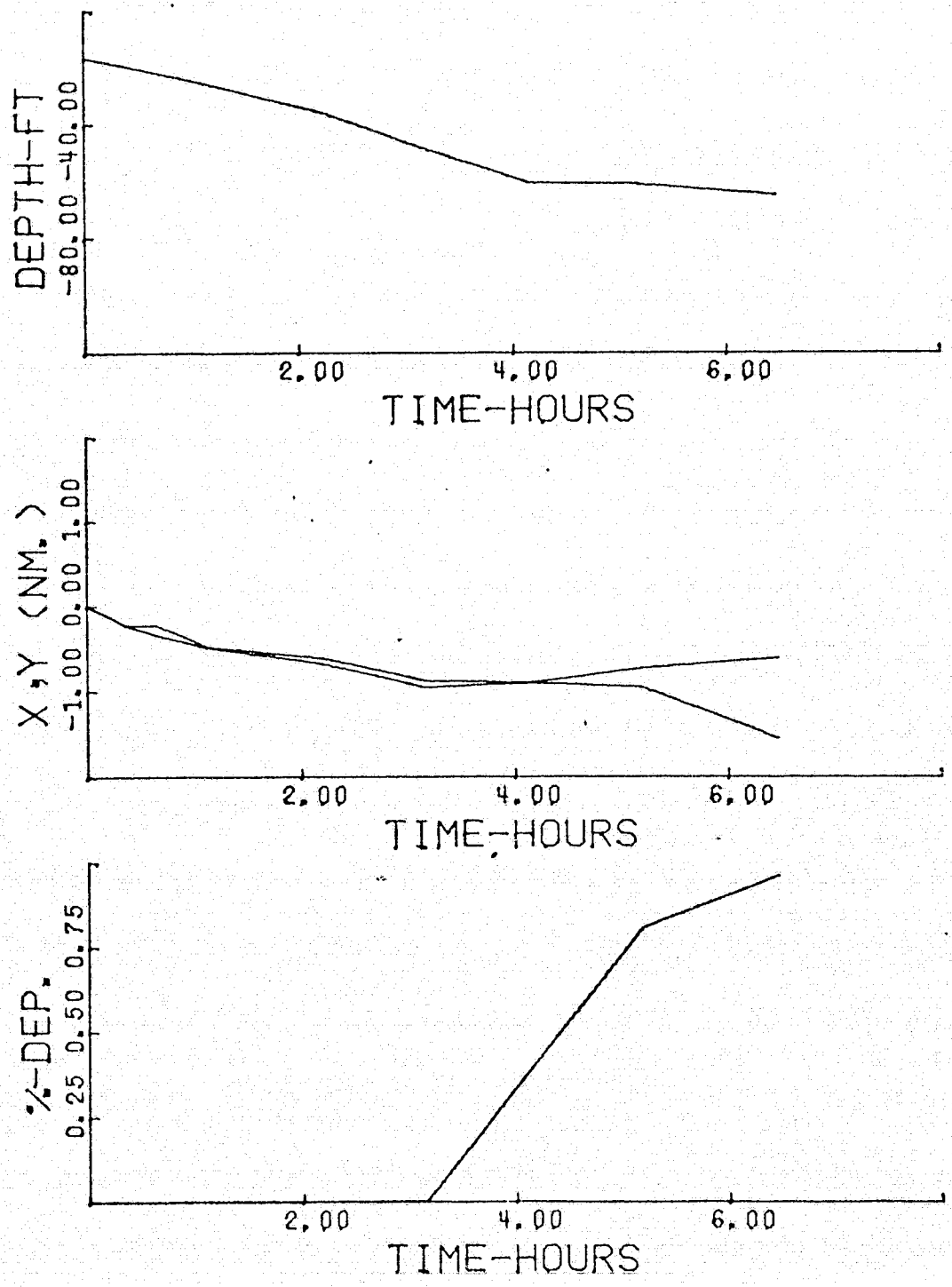

FIGURE 8.7I Long Term Transport of Sedimentary Particle with a Single Particle Settling Rate, with Constant Horizontal and Vertical Dispersion Coefficients of 100.0, 0.0001 FT^2/SEC, W_s = 0.003 FT/SEC; X-Y-Z Positions of Center of Mass and Percent Mass

COUPLING WAPIC TO 2-D VERTICALLY AVG. HYDRODYNAMIC TIDAL MODEL
TRANSLATION AND EXPANSION OF 15X15 X-Y GRID AROUND AN INITIALLY
3-D GAUSSIAN CLOUD WITH A SINGLE PARTICLE SETTLING RATE
WITH CONSTANT X-Y,Z DIFF. COEFFICIENTS OF 100. ,0.01 FT2/SEC
GRID MOVEMENTS AT T=0 ,1.2 ,3.6 ,6.5 HOURS FORM SLACK TIDE
INITIAL X-Y TOTAL GRID SPAN OF 3000 FT.

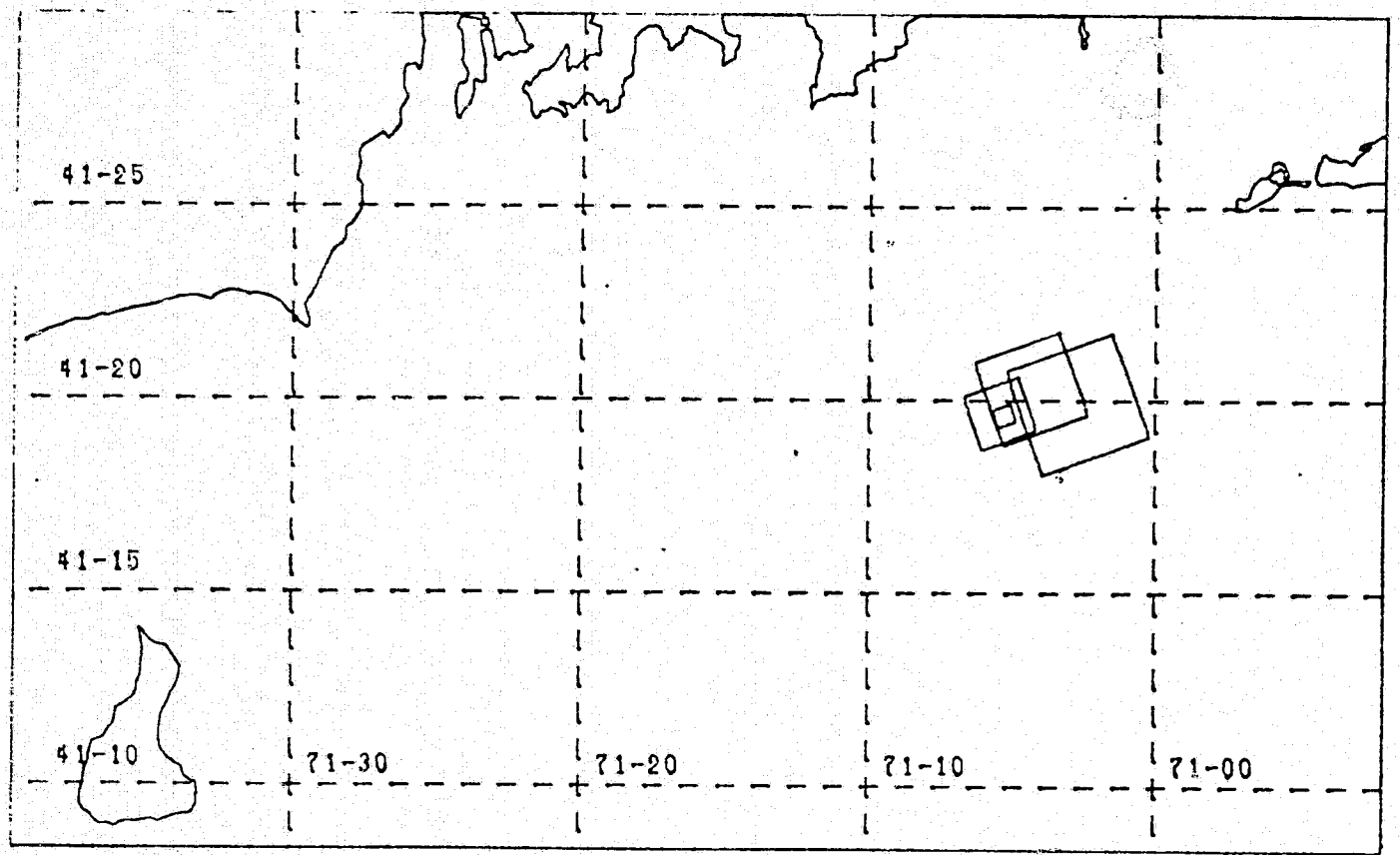

FIGURE 8.8A Long Term Transport of a Sedimentary Particle with a Single Particle Settling Rate, with Constant Horizontal and Vertical Dispersion Coefficients of 100.0, 0.01 FT^2/SEC. W_s = 0.003 FT/SEC; Two Dimensional Plot of Expansion and Translation of the Horizontal Grid

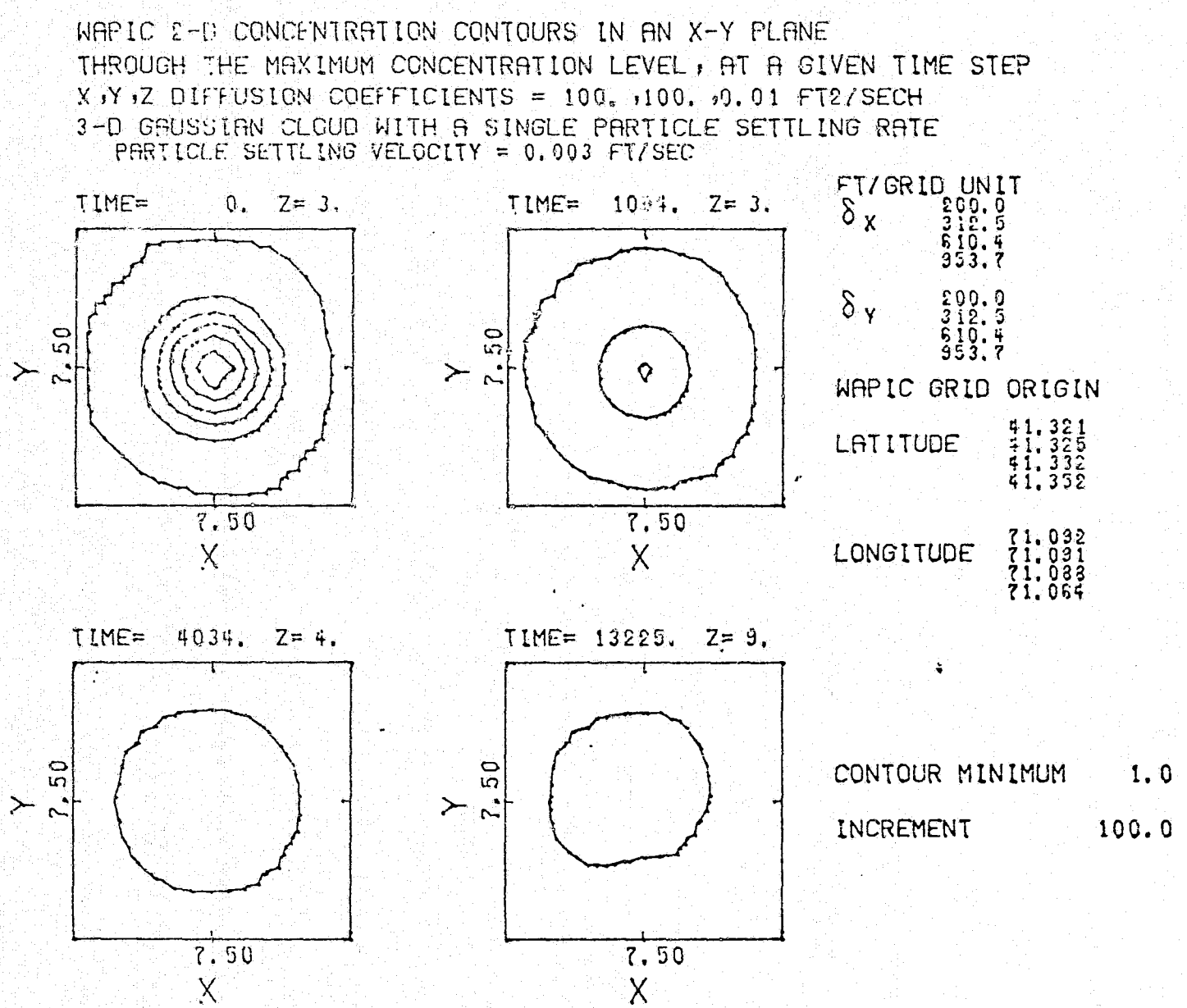

FIGURE 8.8B Long Term Transport of Sedimentary Particle with a Single Particle Settling Rate, with Constant Horizontal and Vertical Dispersion Coefficients of 100.0, 0.01 FT^2/SEC. W_s = 0.003 FT/SEC. Concentration Contours T = 0.0, 1054, 4034.0, 13,225, Sec

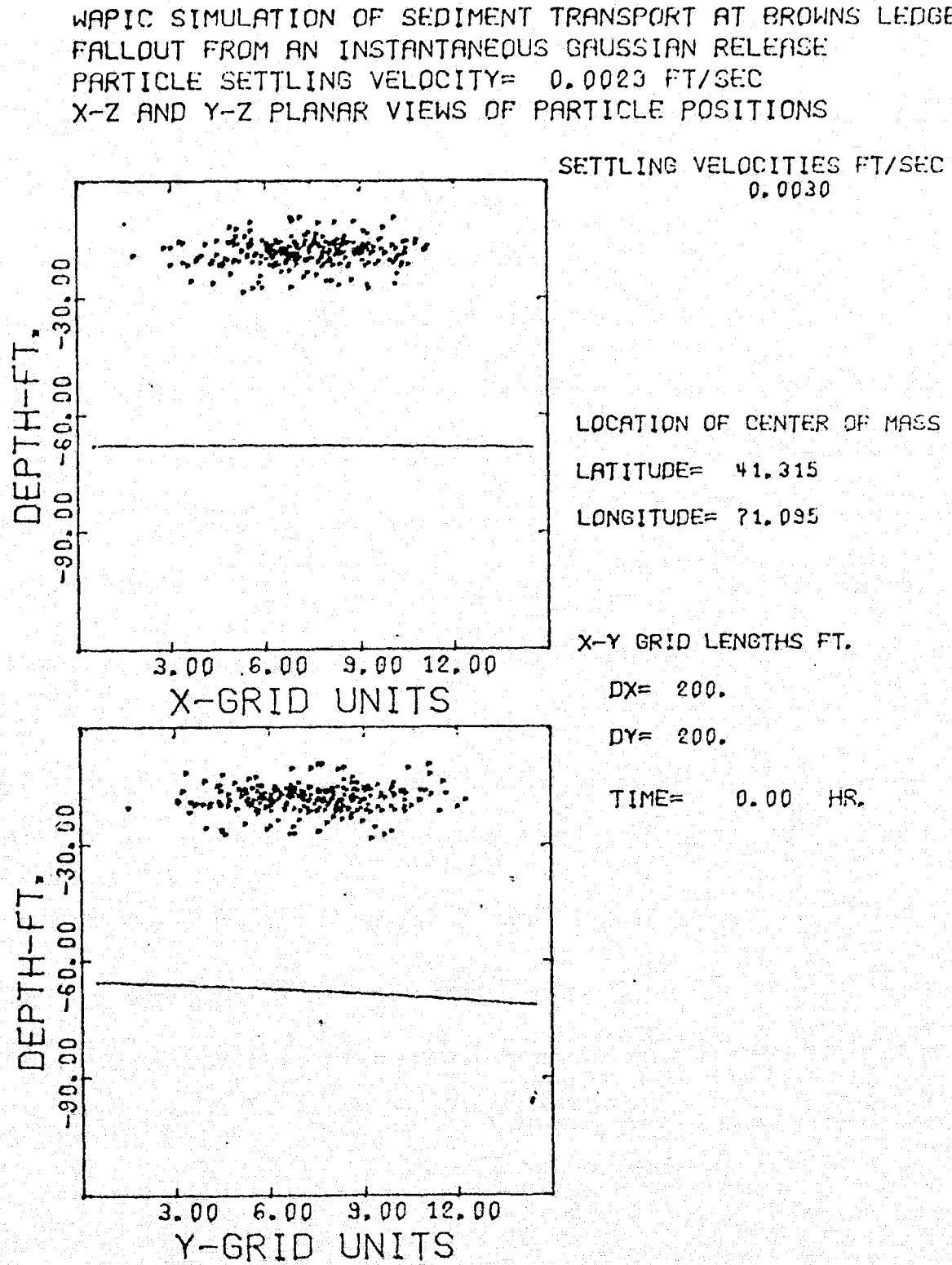

FIGURE 8.8C Long Term Transport of Sedimentary Particle with a Single Particle Settling Rate, with Constant Horizontal and Vertical Dispersion Coefficients of 100.0, 0.01 FT^2/SEC. W_s = 0.003 FT/SEC. X-Z, Y-Z Planar Views of Particle Cloud, $\bar{T}$ = 0.0 Hour

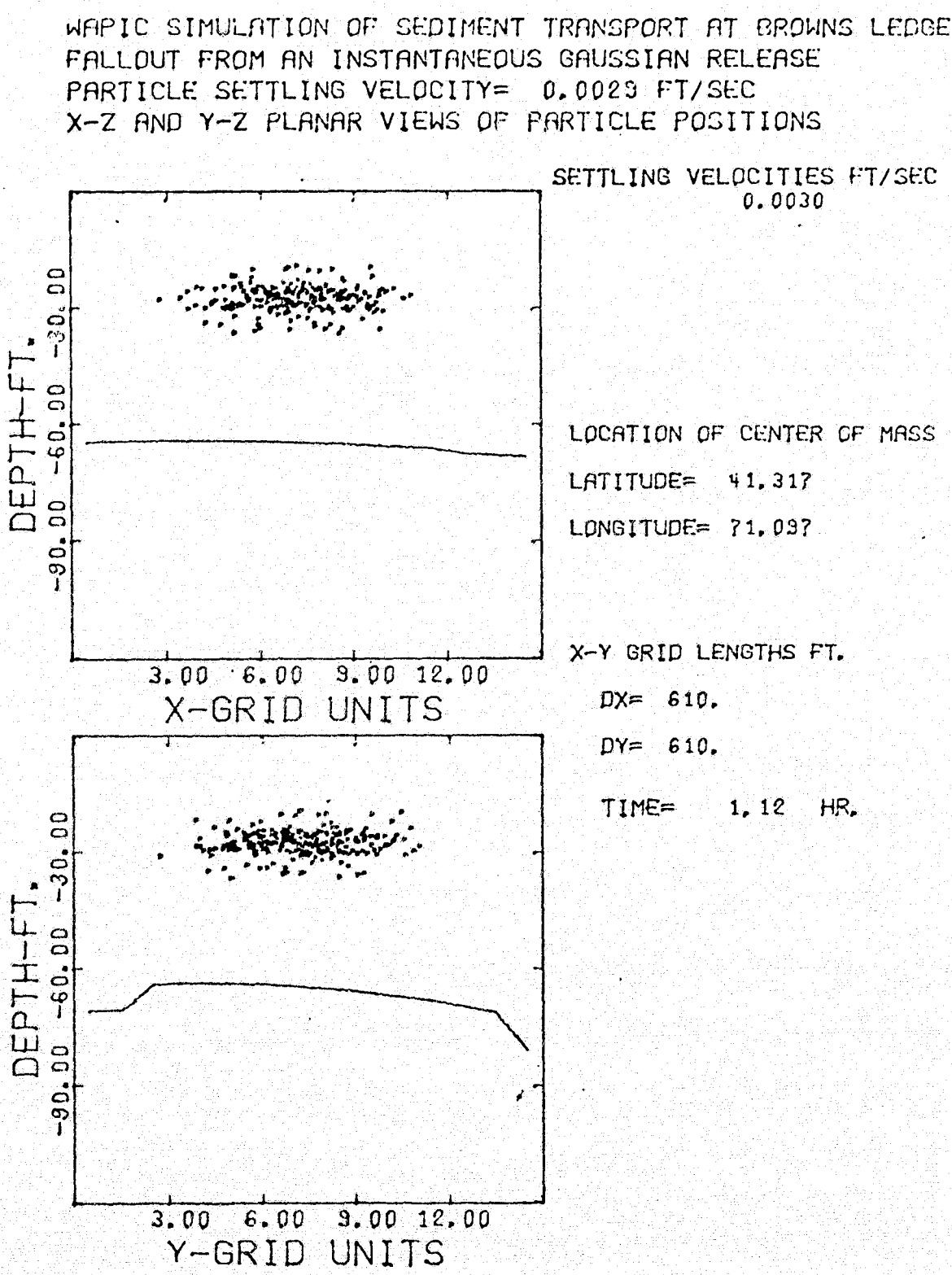

FIGURE 8.8D Long Term Transport of Sedimentary Particle with a Single Particle Settling Rate, with Constant Horizontal and Vertical Dispersion Coefficients of 100.0, 0.01 FT^2/SEC. W_s = 0.003 FT/SEC. X-Z, Y-Z Planar Views of Particle Cloud, T = 1.12 Hour

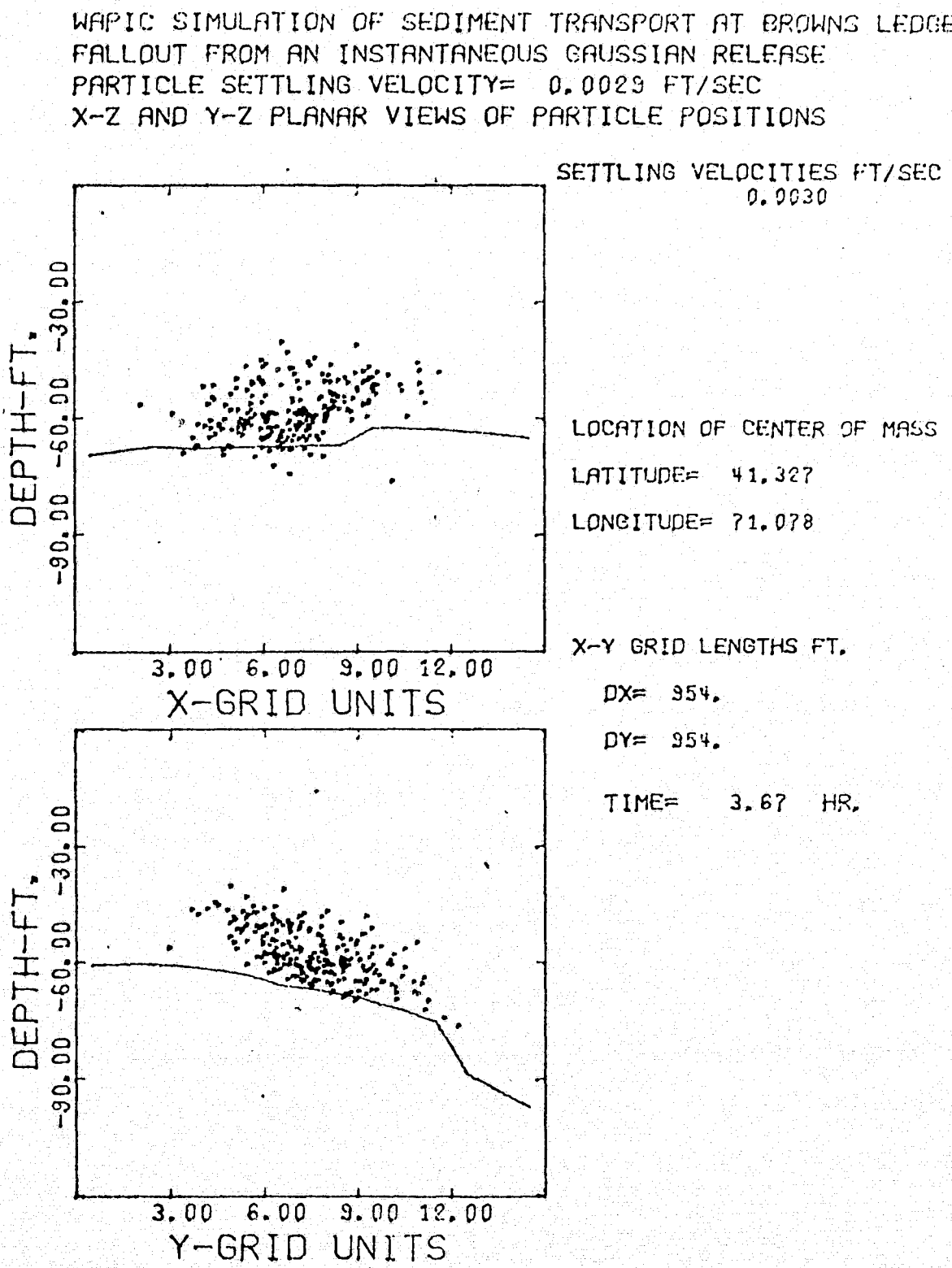

FIGURE 8.8E Long Term Transport of Sedimentary Particle with a Single Particle Settling Rate, with Constant Horizontal and Vertical Dispersion Coefficients of 100.0, 0.01 FT^2/SEC. W_s = 0.003 FT/SEC. X-Z, Y-Z Planar Views of Particle Cloud, T = 3.67 Hours

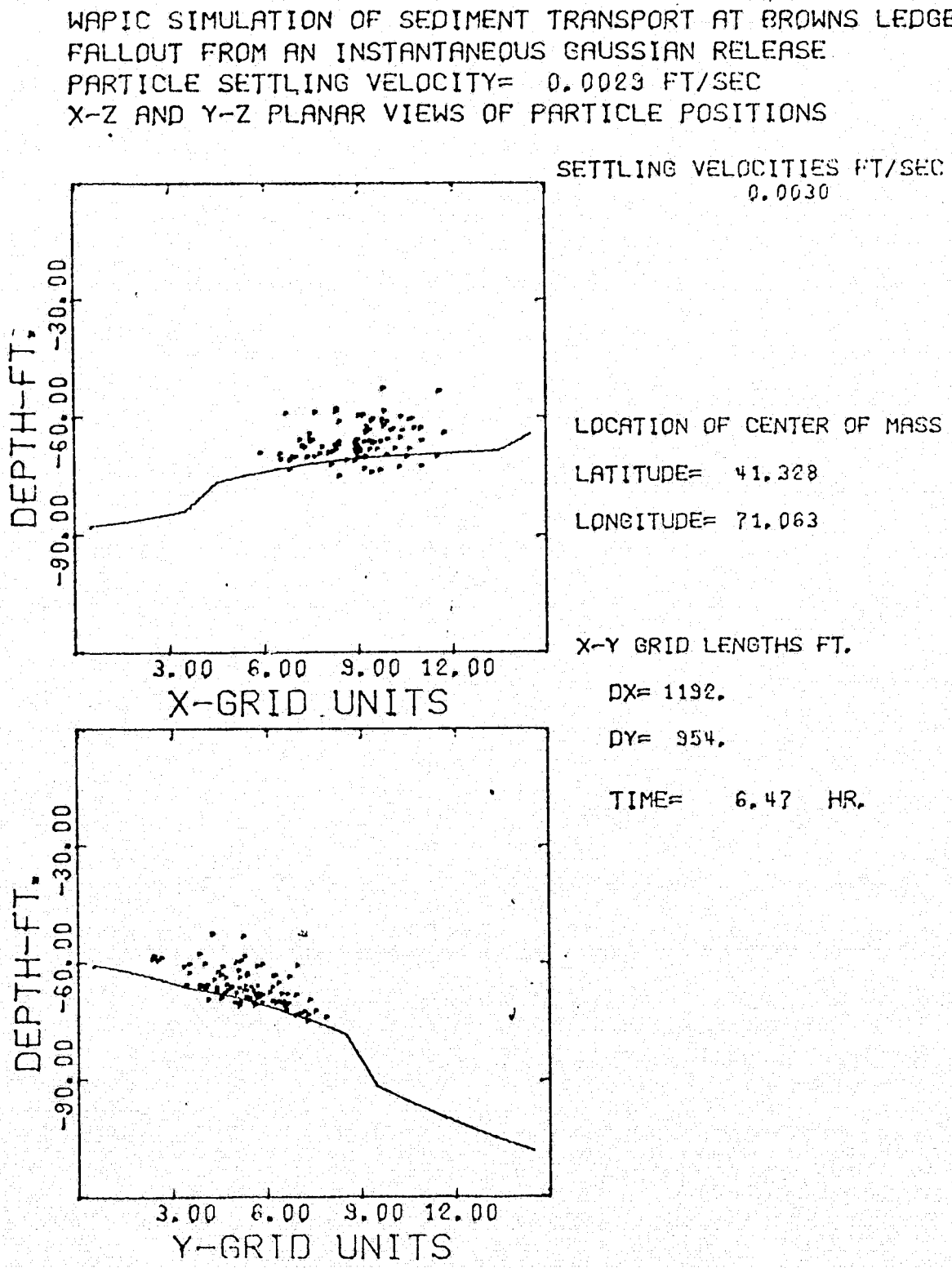

FIGURE 8.8F Long Term Transport of Sedimentary Particle with a Single Particle Settling Rate, with Constant Horizontal and Vertical Dispersion Coefficients of 100.0, 0.01 FT^2/SEC. W_s = 0.003 FT/SEC. X-Z, Y-Z Planar Views of Particle Cloud, $\bar{T}$ = 6.47 Hours

WAPIC SIMULATION OF SEDIMENT FALLOUT AT BROWNS LEDGE
FOR A SINGULAR PARTICLE SETTLING VELOCITY
THE X,Y,Z POSITIONS OF CENTER OF MASS, AND % OF MASS
REMAINING IN THE PARTICLE CLOUD AS A FUNCTION OF TIME

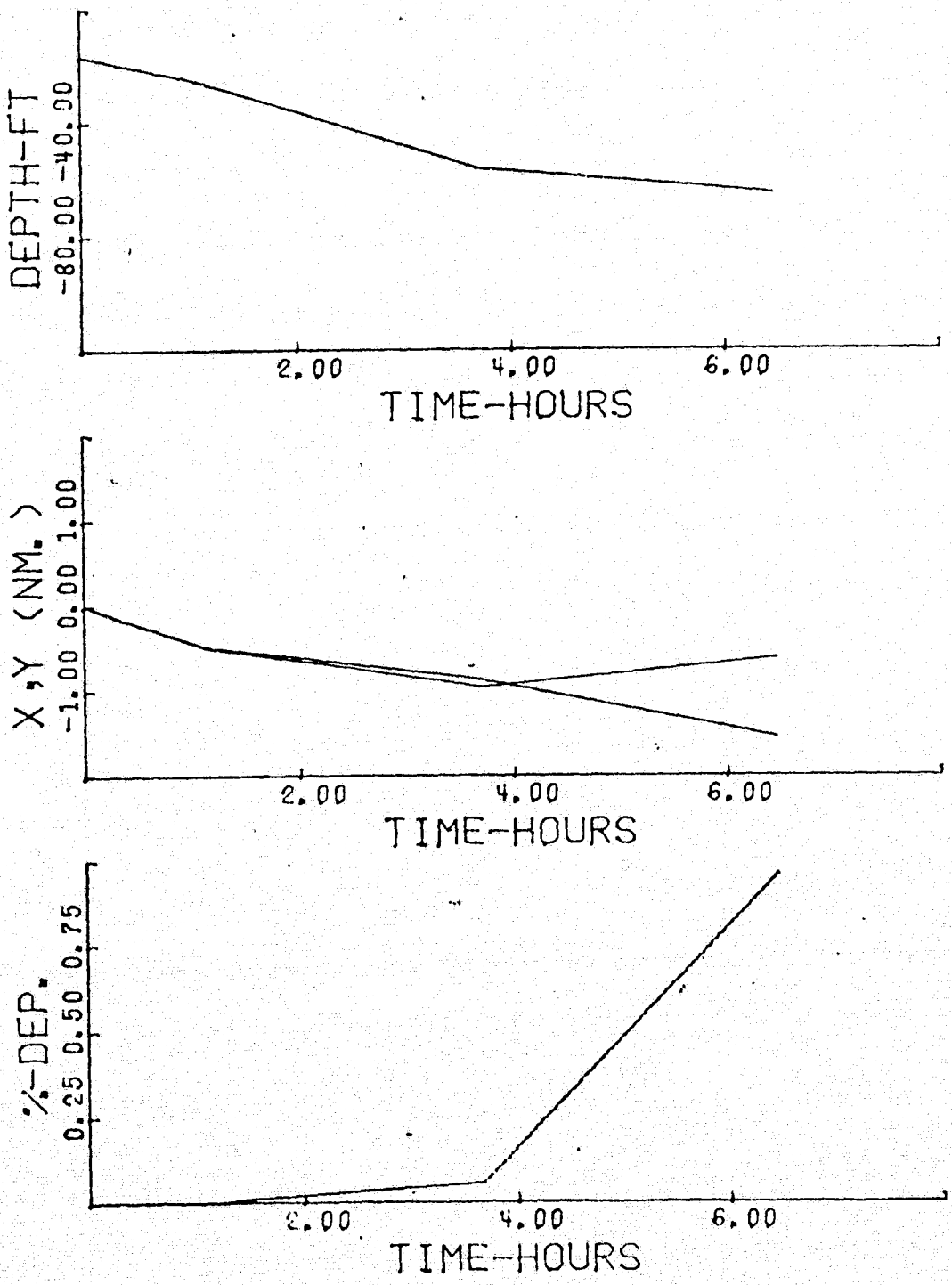

FIGURE 8.8G Long Term Transport of Sedimentary Particle with a Single Particle Settling Rate, with Constant Horizontal and Vertical Dispersion Coefficients of 100.0, 0.01 FT^2/SEC. W_s = 0.003 FT/SEC. X-Y-Z Positions of the Center o f Mass and Percent Mass Remaining in the Particle Cloud as a Function of Time

COUPLING WAPIC TO 2-D VERTICALLY AVG. HYDRODYNAMIC TIDAL MODEL
TRANSLATION AND EXPANSION OF 15X15 X-Y GRID AROUND AN INITIALLY
3-D GAUSSIAN CLOUD WITH 5 MARKER PARTICLE SETTLING RATES
WITH CONSTANT X-Y,Z DIFF. COEFFICIENTS OF 100. ,0.0001 FT2/SEC
GRID MOVEMENTS IN 2 HOUR STEPS FROM TIME T=0 , AT SLACK TIDE
INITIAL X-Y TOTAL GRID SPAN OF 3000 FT.

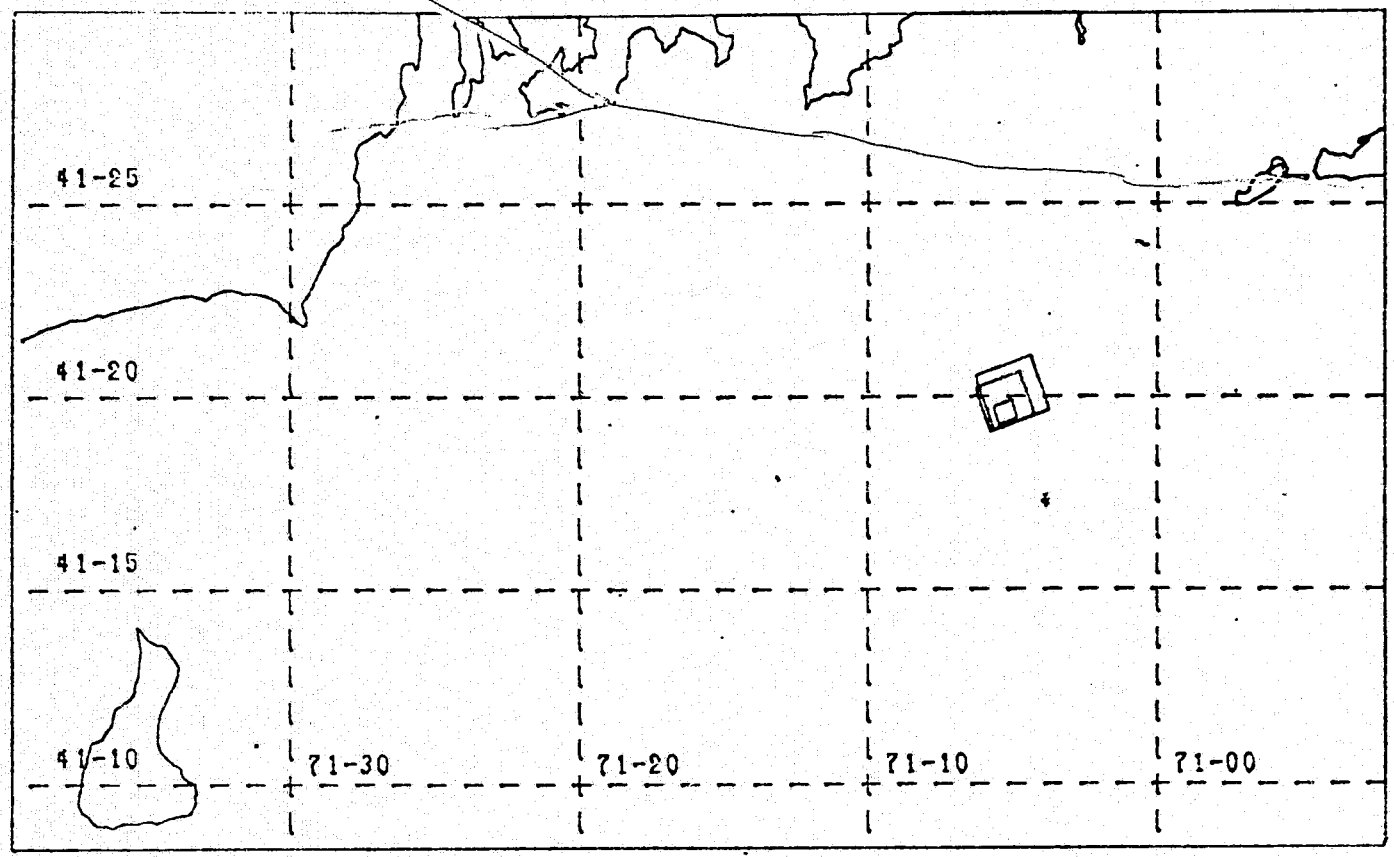

FIGURE 8.9A Long Term Transport of a Sediment Cloud with Five Different Settling Velocities, with Horizontal and Vertical Diffusion Coefficients of 100.0, 0.0001 FT^2/SEC, W_s = 0.002, 0.003, 0.008, 0.017, 0.026 FT/SEC. Two Dimensional Plot of Expansion and Translation of the Horizontal Grid

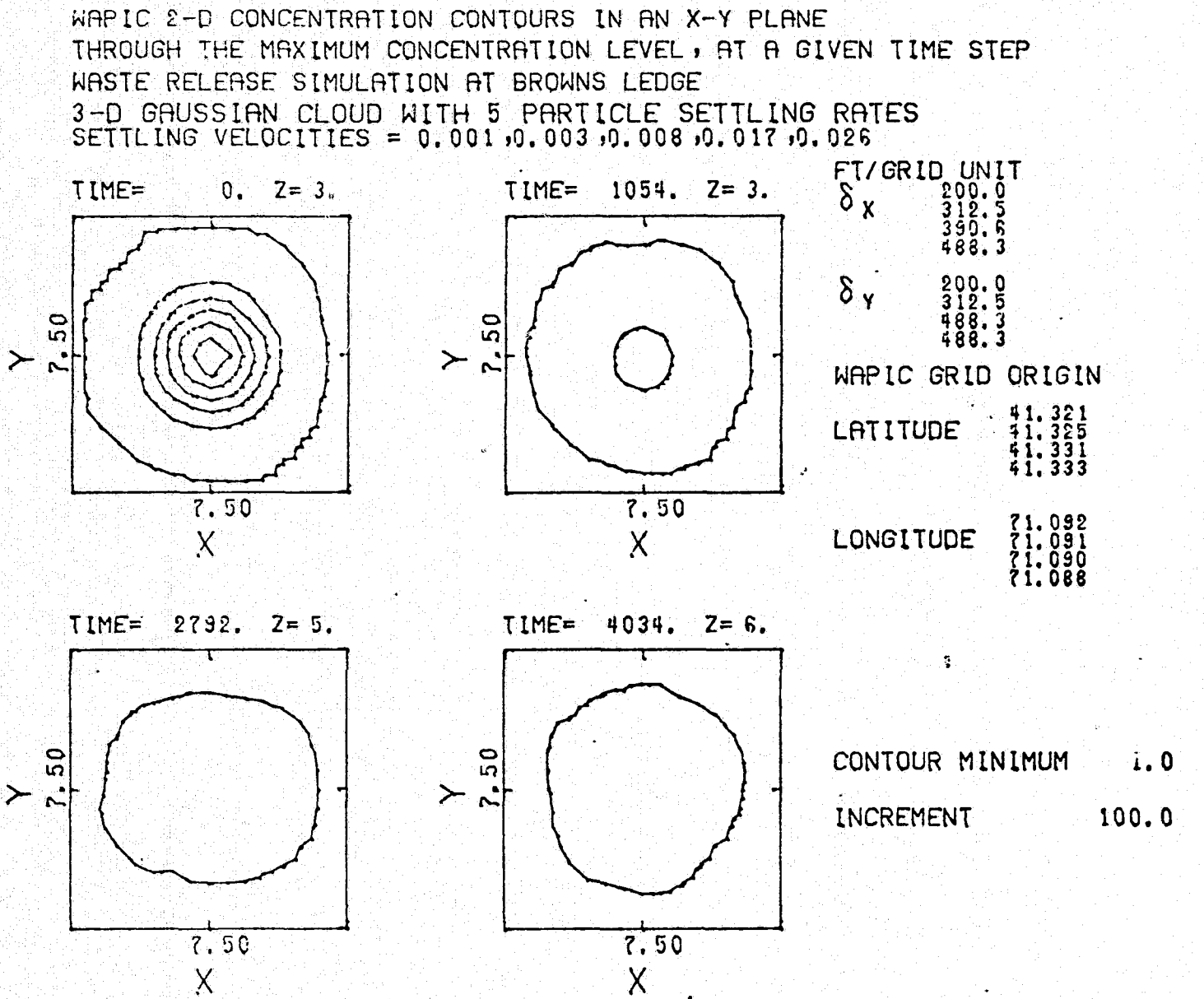

FIGURE 8.9B Long Term Transport of a Sediment Cloud with Five Different Settling Velocities, with Horizontal and Vertical Diffusion Coefficients of 100.0, 0.0001 FT^2/SEC, W_s = 0.002, 0.003, 0.008, 0.017, 0.026 FT/SEC. Concentration Contours T = 0.0, 1054, 2792, 4034, Secs.

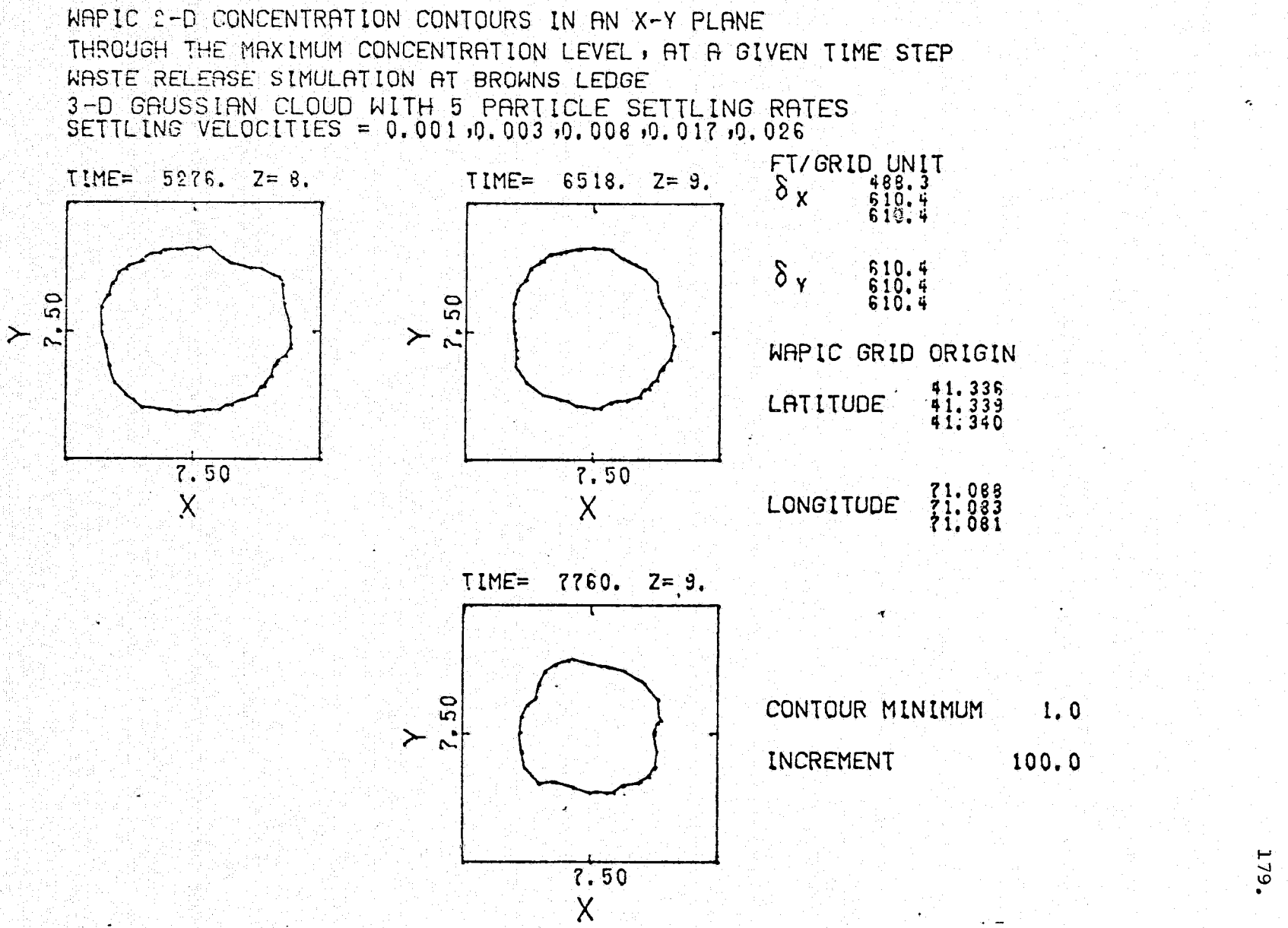

FIGURE 8.9C Long Term Transport of a Sediment Cloud with Five Different Settling Velocities, with Horizontal and Vertical Diffusion Coefficients of 100.0, 0.0001 FT^2/SEC, W_s = 0.002, 0.003, 0.008, 0.017, 0.026 FT/SEC. Concentration Contours T = 5276, 6518, 7760 Secs.

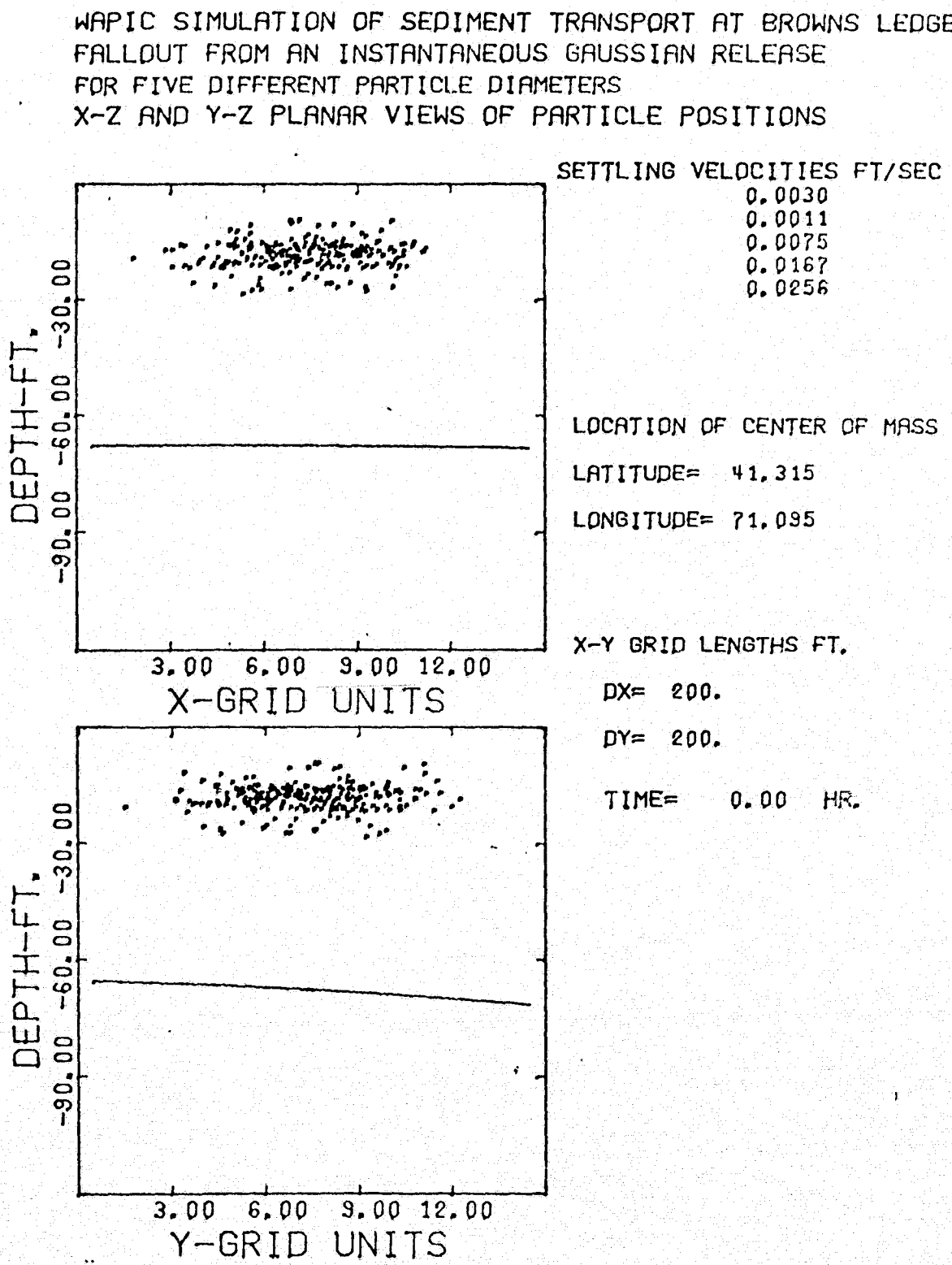

FIGURE 8.9D Long Term Transport of a Sediment Cloud with Five Different Settling Velocities, with Horizontal and Vertical Diffusion Coefficients of 100.0, 0.0001 FT^2/SEC, W_s = 0.002, 0.003, 0.008, 0.017, 0.026 FT/SEC. X-Z, Y-Z Planar Views of Particle Cloud, T = 0.0 Hour

WAPIC SIMULATION OF SEDIMENT TRANSPORT AT BROWNS LEDGE
FALLOUT FROM AN INSTANTANEOUS GAUSSIAN RELEASE
FOR FIVE DIFFERENT PARTICLE DIAMETERS
X-Z AND Y-Z PLANAR VIEWS OF PARTICLE POSITIONS

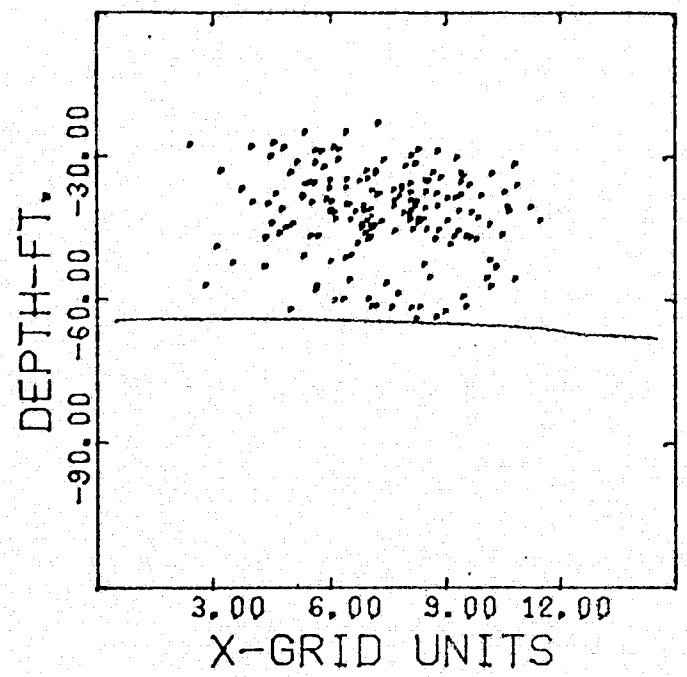

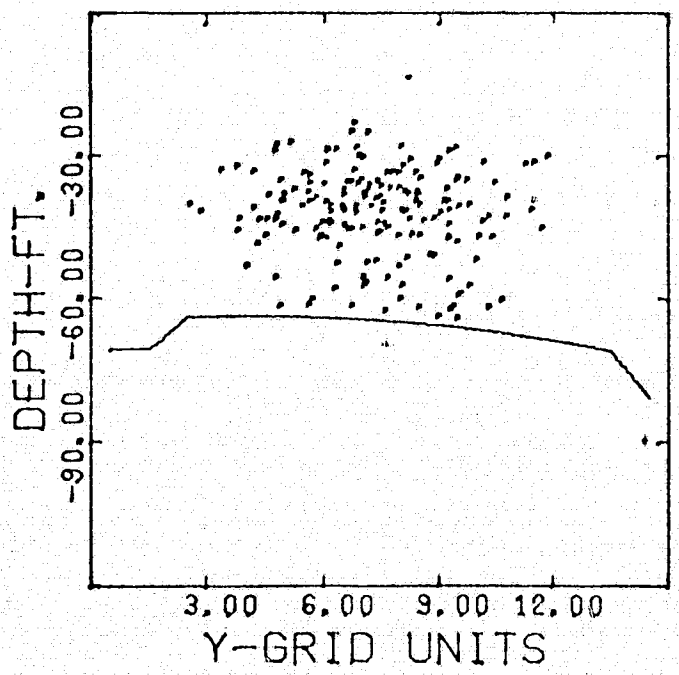

SETTLING VELOCITIES FT/SEC
0.0030
0.0011
0.0075
0.0167
0.0256

LOCATION OF CENTER OF MASS

LATITUDE= 41.320

LONGITUDE= 71.035

X-Y GRID LENGTHS FT.

DX= 488.

DY= 488.

TIME= 1.12 HR.

FIGURE 8.9E Long Term Transport of a Sediment Cloud with Five Different Settling Velocities, with Horizontal and Vertical Diffusion Coefficients of 100.0, 0.0001 FT^2/SEC, W_s = 0.002, 0.003, 0.008, 0.017, 0.026 FT/SEC. X-Z, Y-Z Planar Views of Particle Cloud, T = 1.12 Hours

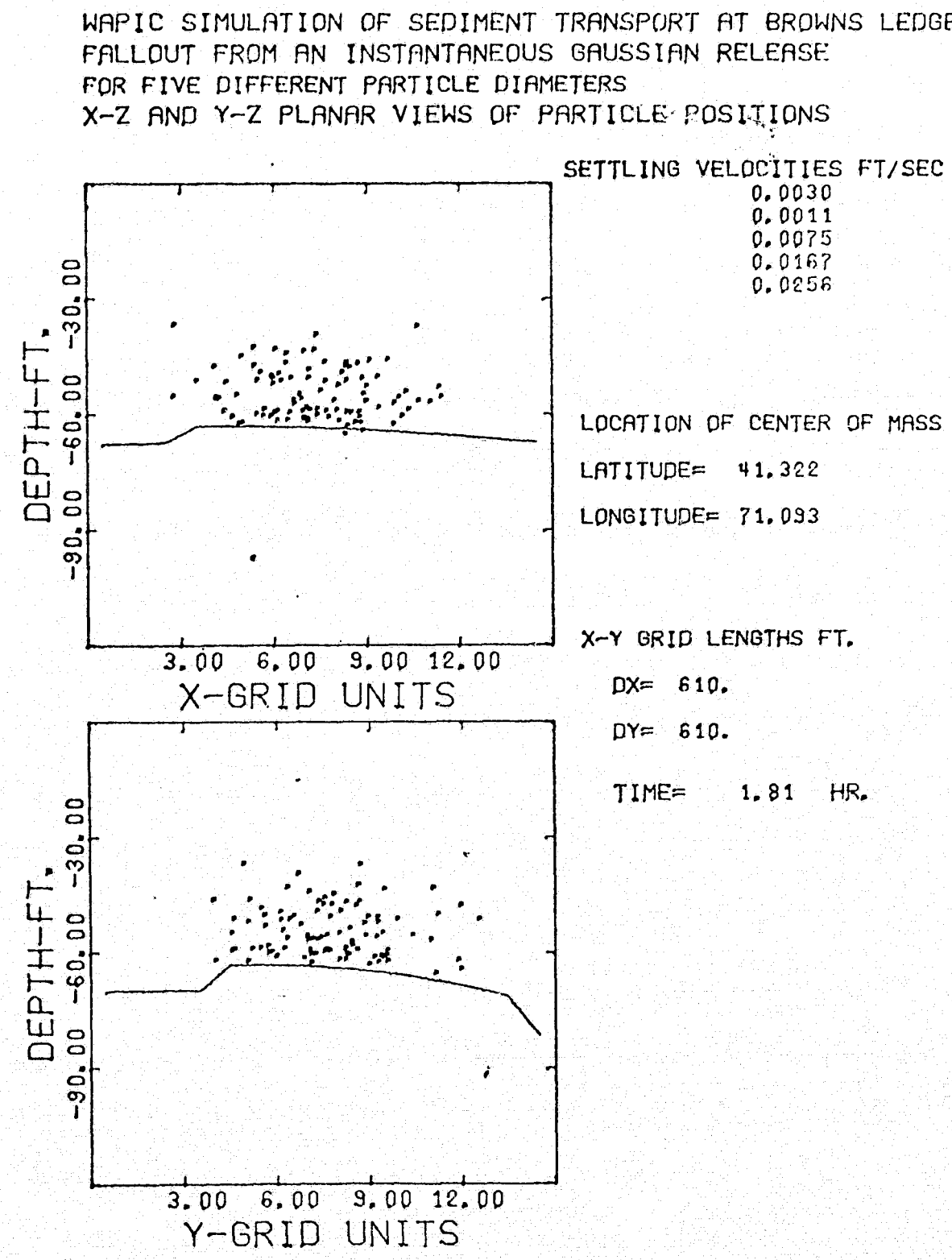

FIGURE 8.9F Long Term Transport of a Sediment Cloud with Five Different Settling Velocities, with Horizontal and Vertical Diffusion Coefficients of 100.0, 0.0001 FT^2/SEC, W_s = 0.002, 0.003, 0.008, 0.017, 0.026 FT/SEC. X-Z, Y-Z Planar Views of Particle Cloud, T = 1.81 Hours

WAPIC SIMULATION OF SEDIMENT TRANSPORT AT BROWNS LEDGE
FALLOUT FROM AN INSTANTANEOUS GAUSSIAN RELEASE
FOR FIVE DIFFERENT PARTICLE DIAMETERS
X-Z AND Y-Z PLANAR VIEWS OF PARTICLE POSITIONS

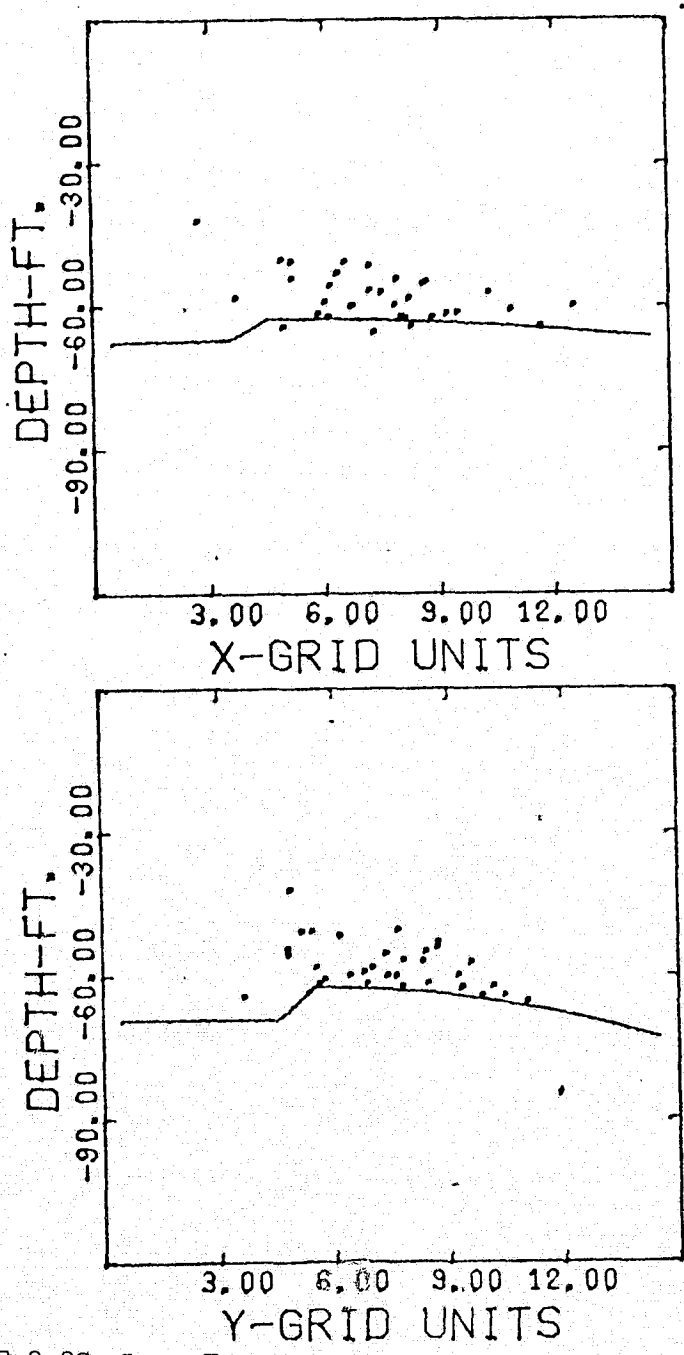

SETTLING VELOCITIES FT/SEC
0.0030
0.0011
0.0075
0.0167
0.0256

LOCATION OF CENTER OF MASS

LATITUDE= 41.323

LONGITUDE= 71.091

X-Y GRID LENGTHS FT.

DX= 610.

DY= 610.

TIME= 2.16 HR.

FIGURE 8.9G Long Term Transport of a Sediment Cloud with Five Different Settling Velocities, with Horizontal and Vertical Diffusion Coefficients of 100.0, 0.0001 FT^2/SEC, W_s = 0.002, 0.003, 0.008, 0.017, 0.026 FT/SEC. X-Z, Y-Z Planar Views of Particle Cloud, T = 2.16 Hours

WAPIC SIMULATION OF SEDIMENT FALLOUT AT BROWNS LEDGE
FOR A SINGULAR PARTICLE SETTLING VELOCITY
THE X,Y,Z POSITIONS OF CENTER OF MASS, AND % OF MASS
REMAINING IN THE PARTICLE CLOUD AS A FUNCTION OF TIME

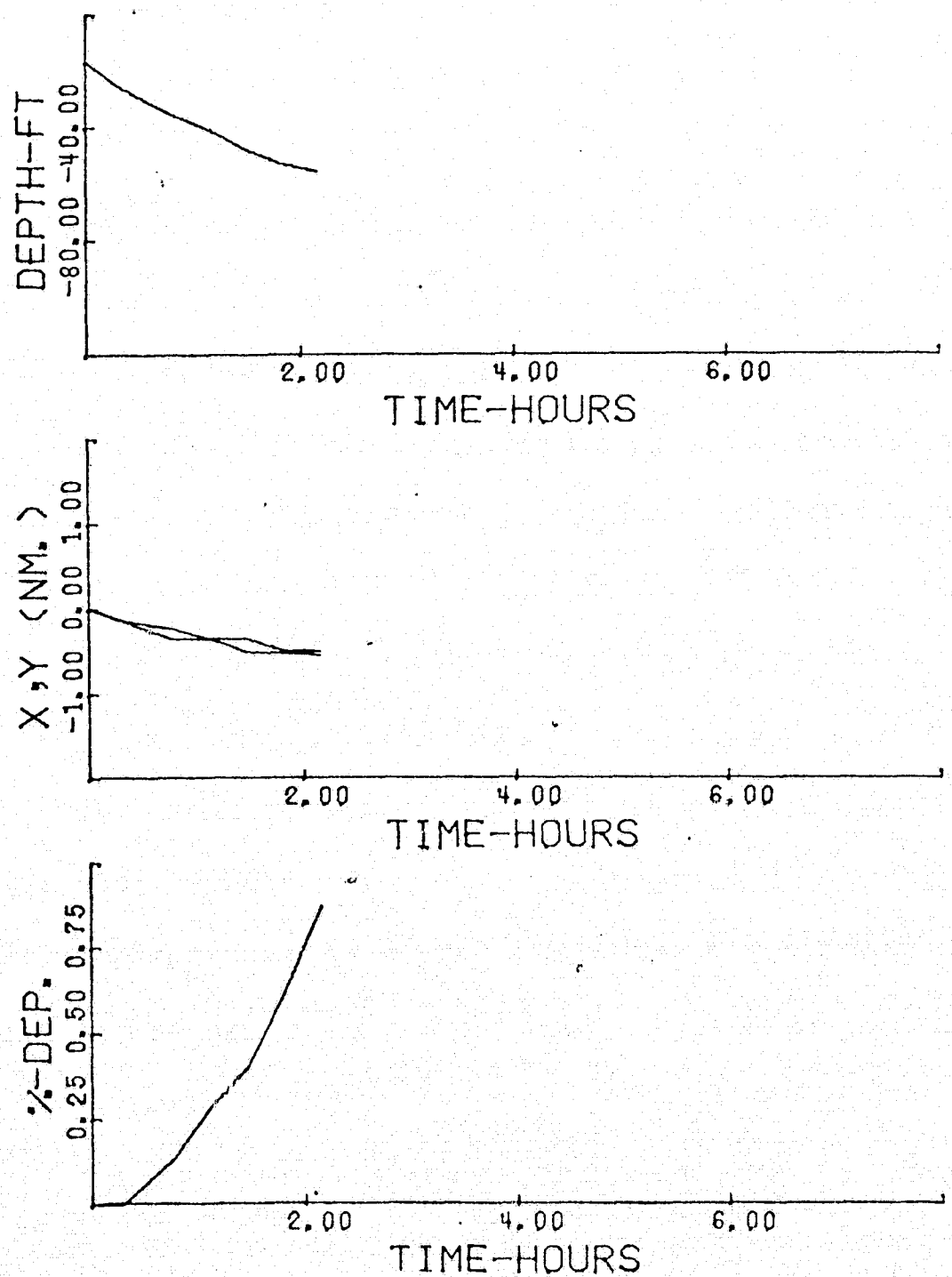

FIGURE 8.9H Long Term Transport of a Sediment Cloud with Five Different Settling Velocities, with Horizontal and Vertical Diffusion Coefficients of 100.0, 0.0001 FT^2/SEC, W_s = 0.002, 0.003, 0.008, 0.017, 0.026 FT/SEC. X-Y-Z Positions of the Center of Mass and Percent Mass Remaining in the Particle

COUPLING WASIC TO 2-D VERTICALLY AVG. HYDRODYNAMIC TIDAL MODEL
TRANSLATION AND EXPANSION OF 15X15 X-Y GRID AROUND AN INITIALLY
3-D GAUSSIAN CLOUD WITH 5 MARKER PARTICLE SETTLING RATES
WITH CONSTANT X-Y,Z DIFF. COEFFICIENTS OF 100. ,0.01 FT2/SEC
GRID MOVEMENTS IN 1 HOUR STEPS FORM TIME T=0 , AT SLACK TIDE
INITIAL X-Y TOTAL GRID SPAN OF 3000 FT.

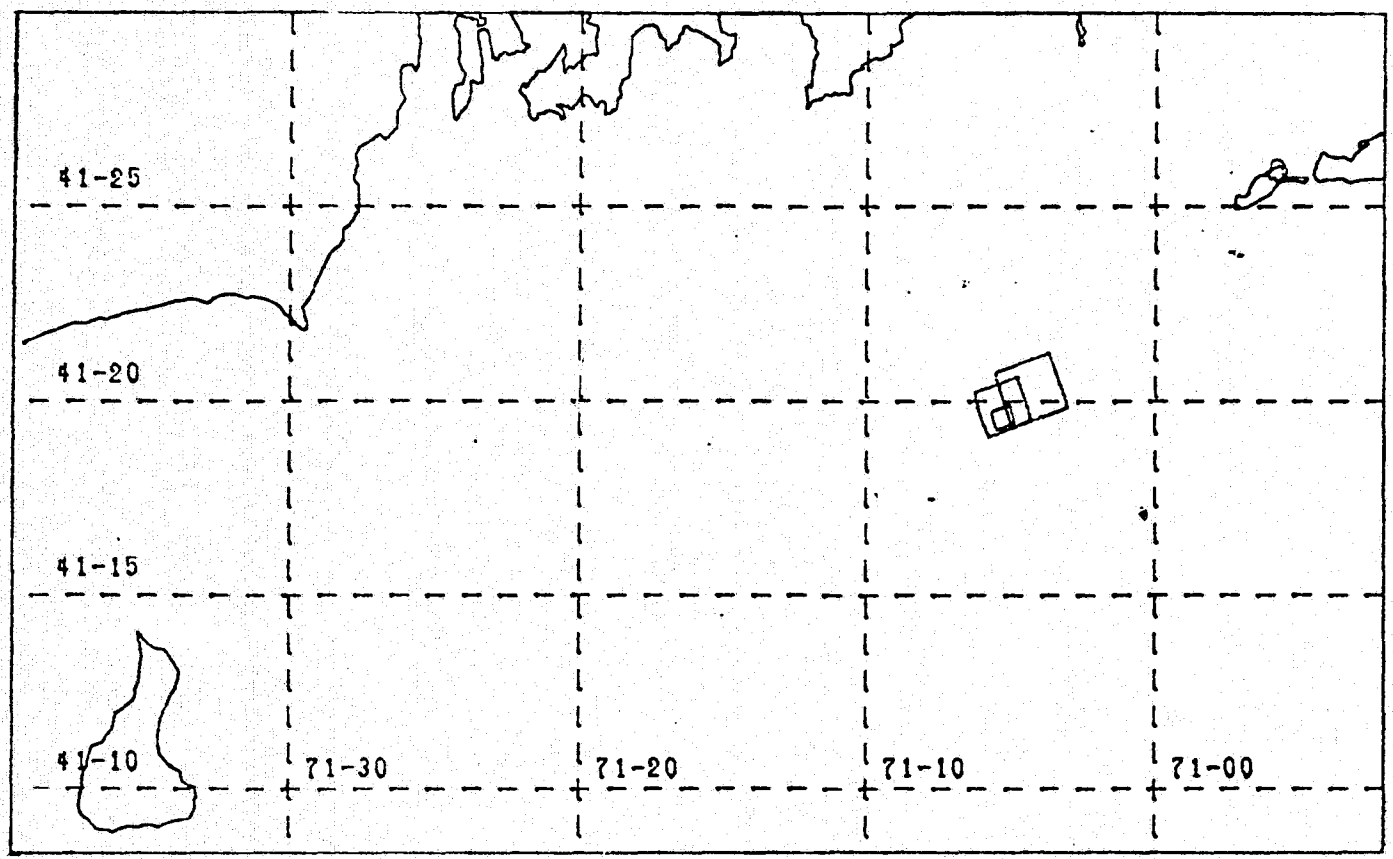

FIGURE 8.10A Long Term Transport of a Sediment Cloud with Five Different Settling Velocities, with Horizontal and Vertical Diffusion Coefficients of 100.0, 0.01 FT^2/SEC, W_s = 0.001, 0.003, 0.008, 0.017, 0.026 FT/SEC. Two Dimensional Plot of Expansion and Translation of the Horizontal Grid

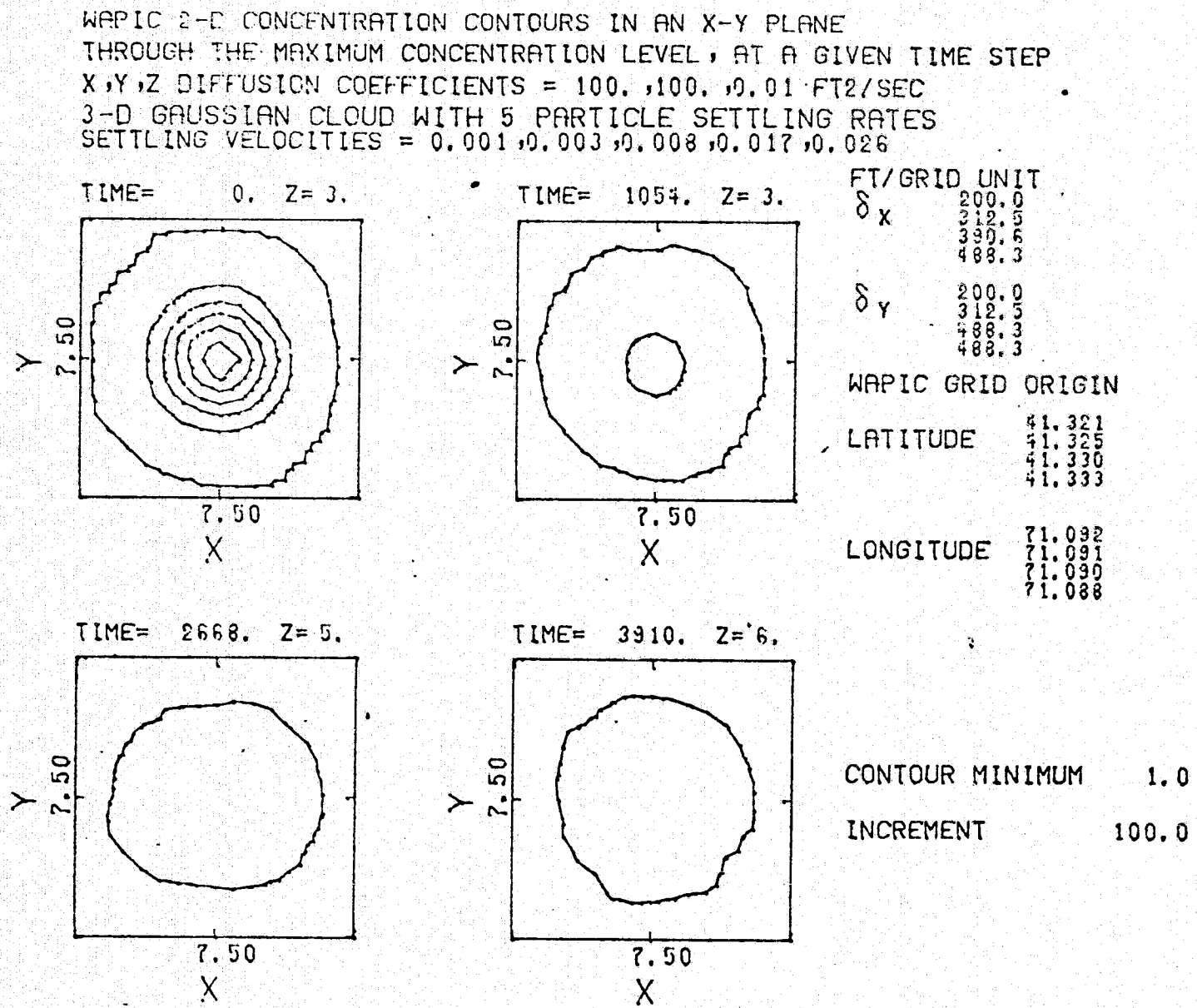

FIGURE 8.10B Long Term Transport of a Sediment Cloud with Five Different Settling Velocities, with Horizontal and Vertical Diffusion Coefficients of 100.0, 0.01 FT^2/SEC, W_s = 0.001, 0.003, 0.008, 0.017, 0.026 FT/SEC. Concentration Contours T = 0.0, 1054, 3910 Sec

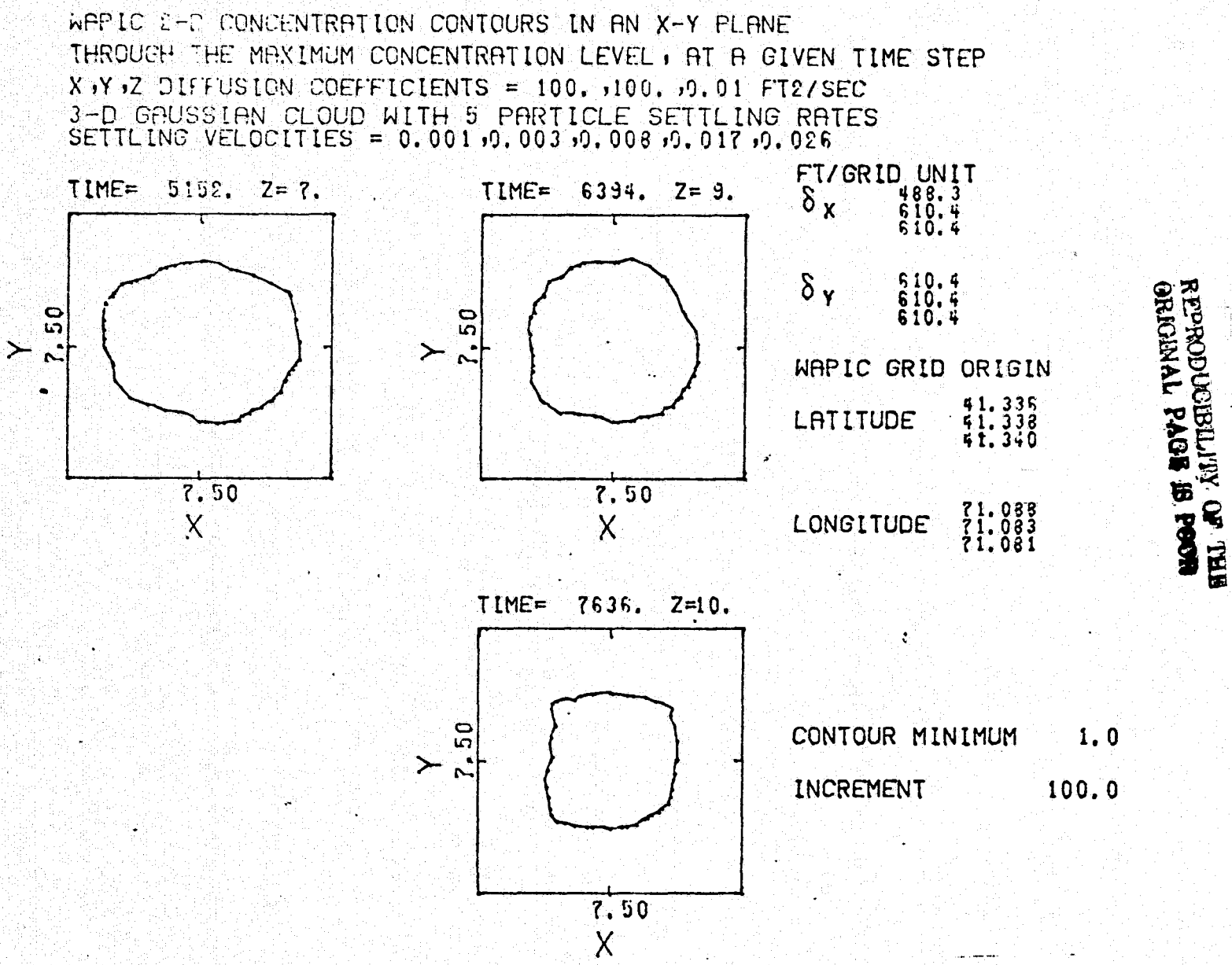

FIGURE 8.10C Long Term Transport of a Sediment Cloud with Five Different Settling Velocities, with Horizontal and Vertical Diffusion Coefficients of 100.0, 0.01 FT^2/SEC, W_s = 0.001, 0.003, 0.008, 0.017, 0.026 FT/SEC. Concentration Contours T = 5152, 6394, 7636 Secs

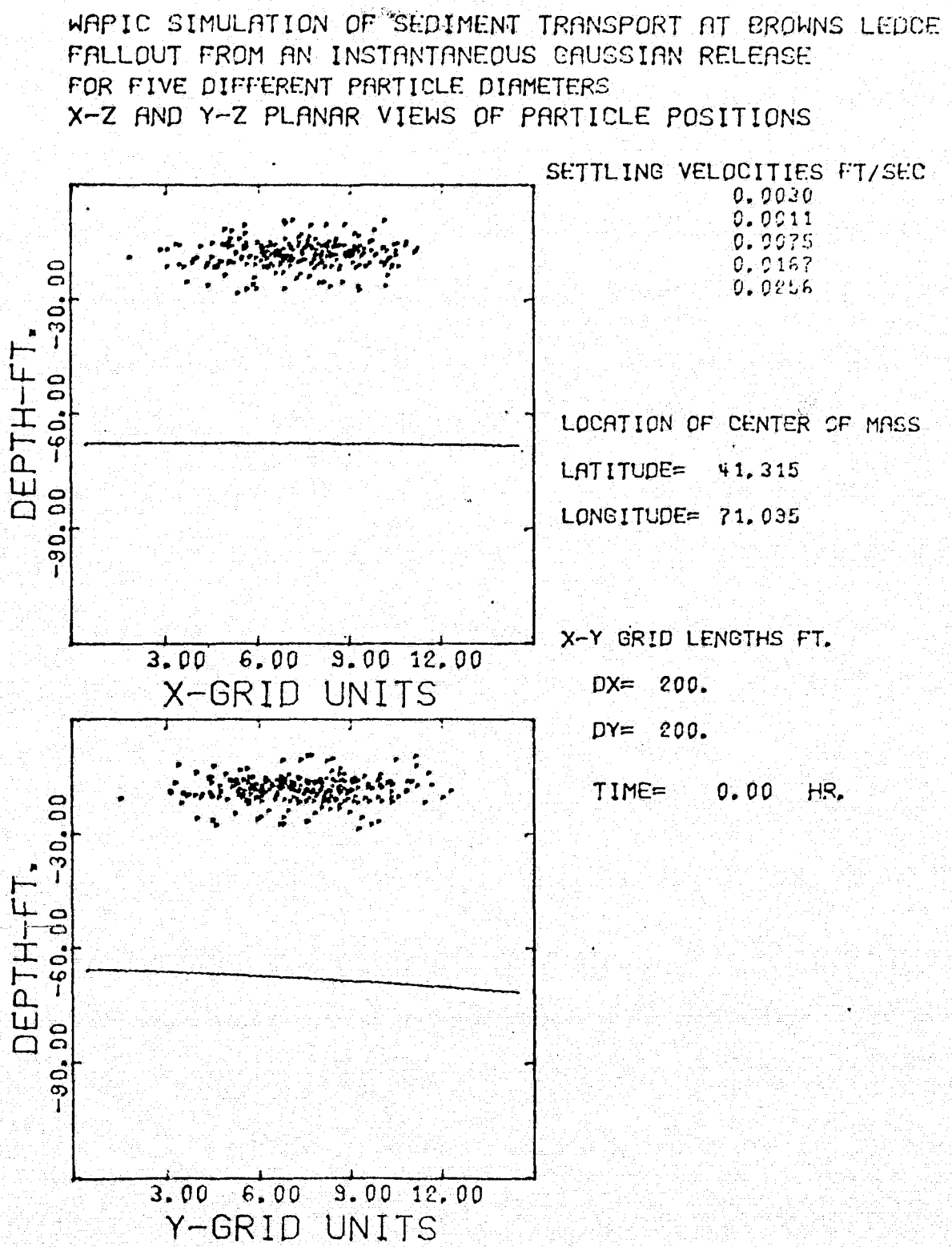

FIGURE 8.10D Long Term Transport of a Sediment Cloud with Five Different Settling Velocities, with Horizontal and Vertical Diffusion Coefficients of 100.0, 0.01 FT^2/SEC, W_s = 0.001, 0.003, 0.008, 0.017, 0.026 FT/SEC. X-Y, Y-Z Planar Views of Particle Cloud, T = 0.0 Hour

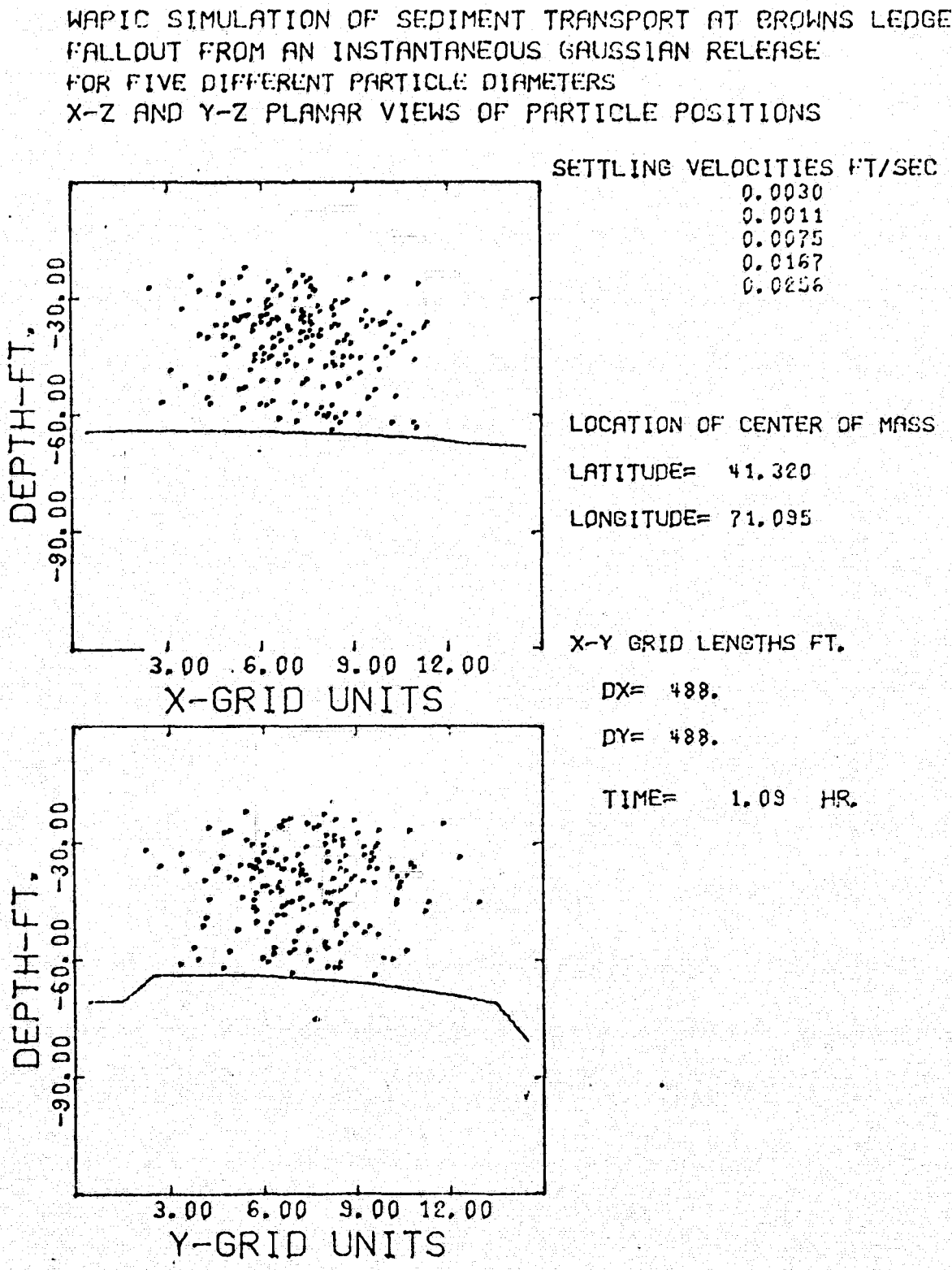

FIGURE 8.10E Long Term Transport of a Sediment Cloud with Five Different Settling Velocities, with Horizontal and Vertical Diffusion Coefficients of 100.0, 0.01 FT^2/SEC, W_s = 0.001, 0.003, 0.008, 0.017, 0.026 FT/SEC. X-Z, Y-Z Planar Views of Particle Cloud, T = 1.09 Hour

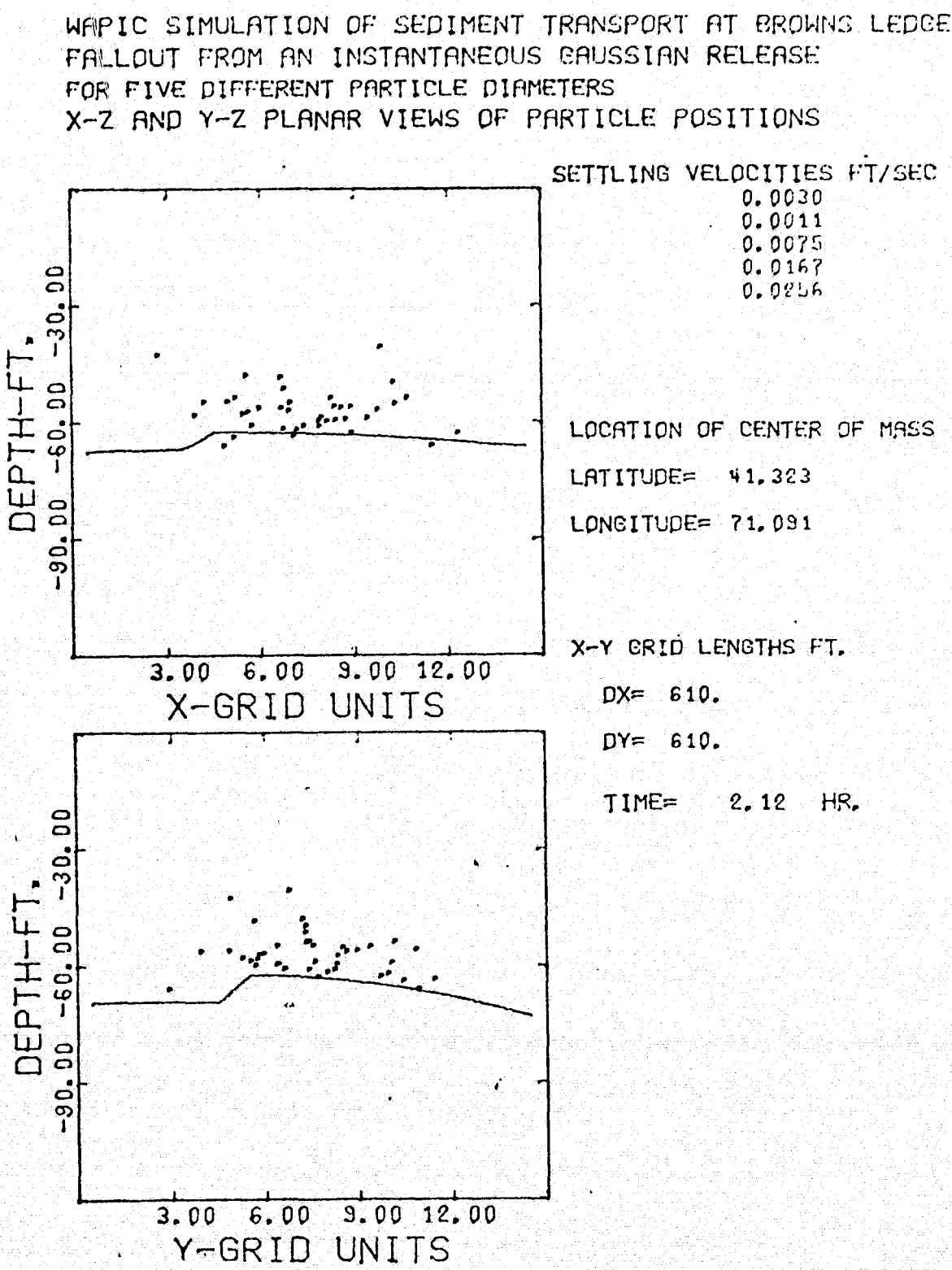

FIGURE 8.10F Long Term Transport of a Sediment Cloud with Five Different Settling Velocities, with Horizontal and Vertical Diffusion Coefficients of 100.0, 0.01 FT^2/SEC, W_s = 0.001, 0.003, 0.008, 0.017, 0.026 FT/SEC. X-Z, Y-Z Planar Views of Particle Cloud, T = 2.12 Hours

WAPIC SIMULATION OF SEDIMENT FALLOUT AT BROWNS LEDGE
FOR A SINGULAR PARTICLE SETTLING VELOCITY
THE X,Y,Z POSITIONS OF CENTER OF MASS, AND % OF MASS
REMAINING IN THE PARTICLE CLOUD AS A FUNCTION OF TIME

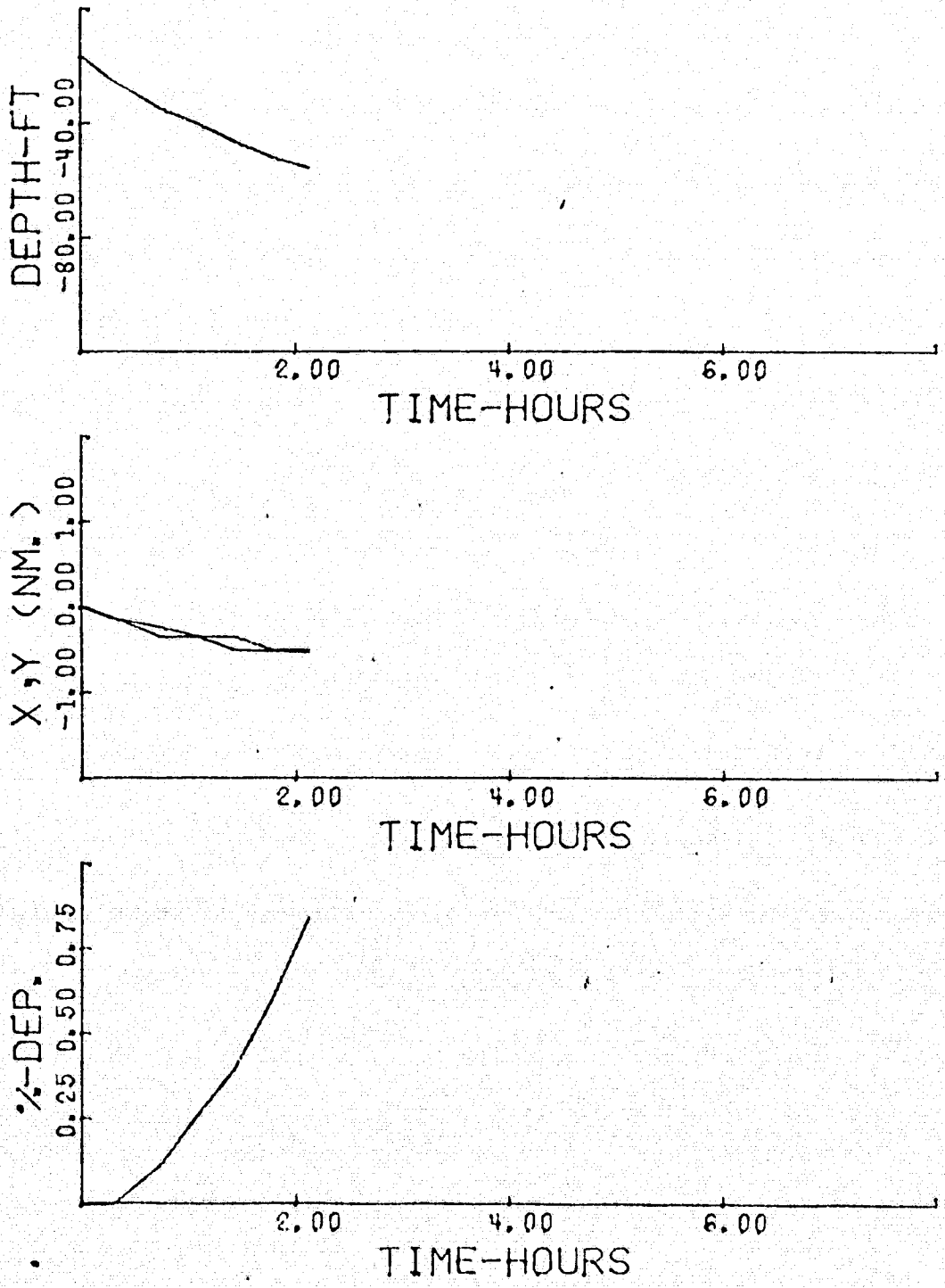

FIGURE 8.10G Long Term Transport of a Sediment Cloud with Five Different Settling Velocities, with Horizontal and Vertical Diffusion Coefficients of 100.0, 0.01 FT^2/SEC, W_s = 0.001, 0.003, 0.008, 0.017, 0.026 FT/SEC. X-Y-Z Positions of the Center of Mass and Percent Mass Remaining in the Particle Cloud as a Function of Time

IX. SUMMARY, CONCLUSIONS, RECOMMENDATIONS

WAPIC, a three dimensional Lagrangian marker particle in Eulerian finite difference cell technique for simulating the incompressible mass transport equation, has been developed. The method was verified against five analytic solutions and subsequently applied to the prediction of long term tidal transport of suspended sediment from an instantaneous barge disposal of dredged sediment waste at Brown's Ledge.

A. Verification Studies

The procedure was found, when utilizing a horizontal standard deviation to grid spacing ratio of 2.0, to accurately predict to within an absolute value of 6 % , the analytic concentration values for three dimensional unbounded turbulent transport of an initially Gaussian release in uniform steady unidirectional flow and steady uniformly sheared unidirectional flow.

WAPIC was applied in the simulation of long term transport of continuous Gaussian releases in a steady unidirectional turbulent flow field. Comparison with analytic concentration values were poor because of inadequate numbers of marker particles to represent the initial Gaussian particle distributions. In general, WAPIC, in its present form, is impractical for simulations of continuous waste releases, because of the excessive amounts of computer or auxiliary storage required for the

large number of marker particles necessary for adequate spatial representation of the succession of Gaussian releases. An accurate representation of the diffusive behavior of the continuous waste release may require on the order of 30 to 50 thousand marker particles in order to perform a two hour real time simlation.

WAPIC was verified against an analytic solution for turbulent transport of an instantaneous release in uniform plug channel flow. Predicted concentration values were within 5 % of the analytic values in the center of the channel. This simulation demonstrated the utility of WAPIC'S reflection boundary conditions and procedures for selective translation and expansion of the Eulerian finite difference grid.

WAPIC successfully simulated Dobbins' (73) one dimensional mass transport solution for fallout of an initially vertically uniform sediment distribution with a single vertical settling velocity in a steady turbulent channel flow field. The significance of this simulation was the verification of WAPIC'S ability to accurately predict the vertical concentration and fallout rates of negatively buoyant particles in a turbulent flow field. Vertical concentration values and particle deposition rates were all within 5 % accuracy for five different particle settling velocity cases. The Courant dynamic stability or time step restriction which is utilized in Eulerian finite difference schemes, was found to be a valid accuracy requirement for the WAPIC Eulerian finite difference -

Lagrangian marker particle algorithm.

B. Simulations At Brown's Ledge

Seven simulations of long term transport of suspended sediment resulting from an instantaneous disposal of dredged waste at Brown's Ledge in Rhode Island Sound were performed. A two dimensional vertically averaged tidal hydrodynamic model was successfully coupled through the use of a velocity processor to WAPIC. For all seven neutrally and non-neutrally buoyant suspended sediment simulations, the initial plume of hypothetical maximum concentrations of 1500 to 3000 mg/liter dropped to ambient background concentration levels of 1-5 mg/liter in less than two tidal cycles in approximately 60 to 120 feet of water.

The center of mass of the turbid cloud for all four negatively buoyant simulations was "conservatively" placed relatively close to the surface at a depth of twenty feet. In reality, the center of mass of the turbulent cloud would probably be located much closer to the bottom. The suspended sediment cloud would be produced by turbulent entrainment or mixing with the water column as the initial release descends and by the vertical upward momentum surge of the spoil cloud following the impact at the bottom (77). For the given release area shown, provided the vertical turbulent diffusion coefficients and free fall velocities are representative, the entrained cloud of sediment would settle to the bottom or diffuse to background levels in a

much shorter time span than shown in these simulations. The particle clouds were also conveniently placed near the surface for visual demonstration of the vertical descent of the clouds to the bottom.

The most important aspect of these simulations is that the long term horizontal and vertical transport of a spectrum of particle settling velocities can now be modeled, provided the ambient current field, horizontal and vertical turbulence levels, and physical characteristics of the suspended sediment are accurately known.

C. Recommendations

WAPIC, in its present form, may simulate the long term transport of an instantaneous release of sewage or pollutants from an outfall in a tidally dominated estuarine environment. Of interest would be the coupling of WAPIC to a three dimensional finite difference advective velocity field. Gordon (36) has developed a three dimensional finite difference hydrodynamic model for the Providence River. Utilizing the strictly Eulerian (non translating and expanding) version of WAPIC, the two models may be combined for the prediction of pollutant transport. At present the WAPIC velocity interpolation scheme is only two dimensional. Should WAPIC be coupled to a three dimensional hydrodynamic field, and the Eulerian grid system expands and translates in either two or three dimensions, then a three dimensional velocity interpolation

scheme will be required.

A field verification of the WAPIC mass transport procedure in a tidally driven environment is necessary in order to determine the actual predictive capabilities. A search for a suitable field study of long term pollutant or sediment transport with an adequate data base of advective field velocity vectors, tide heights, and suspended constituent levels for testing the procedure should be undertaken.

WAPIC is suitable for predicting the long term transport of dilute suspended sediment, but does not address the short term aspects of the descent, impact, and spreading surge of the negatively buoyant sediment or pollutant cloud. A two phase short term hydrodynamic model would be of value to produce the initial sediment distribution for WAPIC'S long term transport simulation. A suitable simulation technique might be a hybrid ALE, (Alternating Eulerian Lagrangian), PIC, (Particle In Cell), incompressible hydrodynamic technique. The PIC method is well suited for simulating the hydrodynamics of incompressible two phase flow situations.

WAPIC may be utilized for simulating the erosion and entrainment of sediment from the bottom boundary layer. A " Shields" critical shear velocity criteria (78) for entrainment of sediment might be considered. The vertically transformed, horizontally expanding and translating version of WAPIC coupled to a two or three

dimensional hydrodynamic velocity field might be used to study the sediment erosion and deposition patterns within an estuarine environment.

BIBLIOGRAPHY

1. Fall River Harbor Improvement Dredging Project and Fall River/Providence River Harbor Dredging Actions with Ocean Disposal at Browns Ledge. Graduate School of Oceanography, University of Rhode Island. Draft Environmental Impart Statement, U. S. Army Corp of Engineers, New England Division, 1976.

2. Saila, S. B., Pratt, S. D., Polgar, T. T., Dredge Spoil Disposal in Rhode Island Sound, Marine Technical Report No. 2, University of Rhode Island, 1972.

3. Sissenwine, M. P., S. B. Saila, Rhode Island Sound Dredge Spoil Disposal and Trends in Floating Trap Fishery, Marine Reprint No. 30, University of Rhode Island, 1975.

4. Johnson, B. H., Investigation of Mathematical Models For the Physical Fate Prediction of Dredged Material. Office of Dredged Material Research. U. S. Army Engineer Waterways Experiment Station, Hydraulics Laboratory. Tech. Report D-74-2, March 1974.

5. Koh, R., and Y. Chang, Mathematical Model for Barged Ocean Disposal of Wastes, EPA-66012-73 029, December 1973.

6. Krishnappan, B. G., Dispersion of Granular Material Dumped in Deep Water Scientific Series No. 55, Canada Centre for Inland Waters, Burlington, Ontario, 1975.

7. Hunter, D., and M. Spaulding, "Development of a Three Dimensional Numerical Water Quality Model for Continental Shelf Applications", Department of Ocean Engineering, University of Rhode Island, NSG-1008, 1975.

8. Hurlbut, S. and M. Spaulding, "Application of a Two Dimensional Hydrodynamic and Constituent Transport Model to Block Island Sound - Rhode Island Sound - Buzzards Bay Complex, Symposium on Modeling of Transport Mechanisms in Ocean and Lakes, Canada Centre for Inland Waters, Burlington, Ontario, 1975.

9. Gordon, R. B., and M. Spaulding, "A Bibliography of Numerical Models for Tidal Rivers, Estuaries, and Coastal Waters," University of Rhode Island, Marine Technical Report 32, Ocean Engineering, NOAA Sea Grant, 1974.

10. Fischer, H. B., Mixing and Dispersion in Estuaries, Annual Review of Fluid Mechanics, 8:107-131.

11. Spaulding, M. L., Brown, G. A., F. M. White, Applying a Water Quality Model to Pollution Management, Marine Technical Report 26, University of Rhode Island.

12. Hess, K. W., and F. M. White, Modelling the Dispersal of a Marked Fluid in Narragansett Bay. Marine Technical Report No. 38, University of Rhode Island.

13. Harlow, Francis, H., "The Particle-in-Cell Computing Method for Fluid Dynamics", Methods in Computational Physics. 3:310-343., 1964.

14. Fischer, H. B., A Lagrangian Method for Predicting Pollutant Dispersion in Bolinas Lagoon, Marin County, California. U. S. Geol. Survey Paper S82-B, 1972.

15. Wallis, I. G., Lagrangian Models of Waste Transport for Estuaries and Tidal Inlets. Geophysical Fluid Dynamics Laboratory, Monash University, Clayton, Victoria, Australia, September 1974.

16. Roache, P. J., Computational Fluid Dynamics, Hermosa Publishers, Alberquerque, New Mexico, 1972.

17. Pritchard, D. W., Hydrodynamic Models Chapter II, Estuarine Modeling An Assessment, Tracor. Inc., Austin, Texas, 1972.

18. Hess, K. W. and F. M. White, A Numerical Tidal Model of Narragansett Bay. Marine Technical Report No. 20, University of Rhode Island, 1974.

19. Leendertse, J. J., and E. C. Gritton, "A Water Quality Simulation Model for Well Mixed Estuaries and Coastal Seas, Vol. II: Computational Procedures, The Rand Corporation, July 1971.

20. Spaulding, M. L., "Two Dimensional, Laterally Integrated Estuarine Numerical Water Quality Model," Ph. D. Thesis, Department of Mechanical Engineering and Applied Mechanics, University of Rhode Island, October 1972.

21. Wang, H. P., "A Three Dimensional Finite Element Model of Circulation in Block Island Sound.," Ph. D. Thesis, Department of Mechanical Engineering, University of Rhode Island, 1976.

22. Leimkuhler, W. F., "A Two Dimensional Finite Element Dispersion Model" Massachusetts Institute of Technology, Department of Civil Engineering, 1974.

23. Krone, R. B., and C. R. Ariathurai, "Applications of Sediment Transport Models." Department of Civil Engineering, University of California, Davis, 1976.

24. Evans, M. E., and Harlow, F. H., "The Particle-in-Cell Method for Hydrodynamic Calculations". Los Alamos Scientific Lab., Report No. LA-2139.

25. Sklarew, R. C., "A New Approach: The Grid Model of Urban Air Pollution" Paper presented at the 63rd Annual Meeting of the Air Pollution Control Association, St. Louis, Missouri, June 1970.

26. Hotchkiss, R. S., "The Numerical Calculation of Three Dimensional Flows of Air and Particulates About Structures." Los Alamos Scientific Laboratory, LA-DC-13071, 1971.

27. Hirt, C. W., and J. L. Cook, Calculating Three Dimensional Flows about Structures and Over Rough Terrain", Journal of Computational Physics, 9, pg. 290-302, 1972.

28. Lange, R., ADPIC - A Three Dimensional Computer Code for the Study of Pollutant Dispersal and Deposition Under Complex Conditions. Lawrence Livermore Lab, University of California, URCL-51462, October 1973.

29. Lange, R. and J. B. Knox, "Adaptation of a Three Dimensional Atmospheric Transport Diffusion Model to Rainout Assessments", Lawrence Livermore Lab. University of California, URCL-75731, September 1974.

30. Knox, J. B., Hardy, D. M., and C. A. Sherman, Aquatic and Atmospheric Simulation, Lawrence Livermore Lab. , University of California, URCL-51405 Rev. 1, June 1973.

31. Hirt, C. W., A. A. Amsden, and J. L. Cook, An Arbitrary Lagrangian-Eulerian Computing Method for All Flow Speeds.

32. Spaulding, M., "Numerical Modeling of Pollutant Transport Using a Lagrangian Marker Particle Technique", NASA Langley Research Center, Hampton, VA NASA TMX-73938, August 1976.

33. Csanady, G. T., Turbulent Diffusion in the Environment, D. Reidel Pub. Company, 1974.

34. Bird, R., Stewart, W., and E. Lightfoot, Transport Phenomena, John Wiley and Sons, New York, 1960.

35. Spaulding, M. "Derivation of a Three-Dimensional Numerical Water Quality Model for Estuary and Continental Shelf Application," NASA Technical Memo, X-71930, 1973.

36. Gordon, R. B., "A Three Dimensional Numerical Model of Circulation and Salinity Distribution for Estuarine and Coastal Applications," Thesis in Progress, Department of Ocean Engineering, University of Rhode Island, 1976.

37. Forester, C. K., "A Method of Time Centering the Lagrangian Marker Particle Computation," Journal of Computational Physics, 4, pg. 269 - 714, 1973.

38. Dobson, R. S., Some Applications of a Digital Computer to Hydraulic Engineering Problems. Technical Report 80, Department of Civil Engineering, Stanford University, 1967.

39. Himmerle, W. J., Computer Generation of Uniform and Normal Random Numbers. Class Notes from Computer Science 552, Department of Computer Science and Experimental Statistics, University of Rhode Island, 1975.

40. Watson, R. L., Modified Rubey's Law Accurately Predicts Sediment Settling Velocities, Water Resources Research, Vol. 5, NVS, pp. 1147-50, 1969.

41. Rubey, W. W., Settling Velocities of Gravel, Sand and Silt Particles, American Journal Science Ser. 5, 25, 325-38, 1933.

42. Leendertse, J. J., "Aspects of a Computational Model for Long Period Water Wave Propagation," The Rand Corporation, RM-5294, PR, May 1967.

43. Yevjevich, V., "Probability and Statistics in Hydrology" Water Resources Publications, Fort Collins, Colorado, 1972.

44. Vanoi, V. A., Experiments on the Transportation of Suspended Sediments American Geophysical Union, 1941.

45. Brush, L. M. Jr., Exploratory Study of Sediment Diffusion, Journal of Geophysical Research, V. 67, No. 4, pp. 1427-35., 1962.

46. Milano, V., Turbulence Effects on Settling and Transport of Solid Particles in Suspension, Institute of Hydraulics, University of Pisa, Pisa, Italy, Publication No. 1515, Series 31, pp. 447-475, Also, NASA TT-F-16907, Translated Tech. Report N76-19375.

47. Holley E., Unified View of Diffusion and Dispersion, ASCE Journal, HYD., March, 1969.

48. Von Karman, T., Some Aspects of the Turbulence Problem, Proc., Fourth International Cong. for Applied Mechanics, Cambridge, MA 1934.

49. Taylor, G. I., Diffusion by Continuous Movements, London Math. Soc. Proc. Ser. 2, Vol. 20, pp. 196-211, 1921.

50. Batchelor, G. K., The Applications of Similarity Theory of Turbulence to Atmospheric Diffusion, Q. J. Royal Meterological Society, 76, 328, 1950.

51. Batchelor, G. K., Diffusion in a Field of Homogeneous Turbulence: II The Relative Motion of Particles, Cambridge Phil Soc., Proc. 48:345, 1952.

52. Stommel, H. Horizontal Diffusion Due to Oceanic Turbulence, Journal Marine Research, 8:199, 1949.

53. Sayre, W. W., and F. M. Chang, A Laboratory Investigation of Open-Channel Dispersion Processes for Dissolved, Suspended, and Floating Dispersants. Geological Survey Professional Paper, 433-E, U. S. Department of Interior.

54. Yotasukura, N., Smoot, G. J. and D. I. Cahal, Dispersion in Open Channel Flow, U. S. Geological Survey, Open File Report, 1964.

55. Glover, R. E., Dispersion of Dissolved or Suspended Matter in Flowing Streams, U. S. Geological Survey Professional Paper, 433-B, 1964.

56. Godfrey, R. G., and Frederick, B. J., Dispersion in Natural Streams, U. S. Geological Survey Open File Report, 1964.

57. Yudelson, J., A Survey of Ocean Diffusion Studies and Data, Cal. Tech. Memorandum 67-2, September 1967.

58. Okubo, A., Oceanic Diffusion Diagrams, Deep Sea Research, 18, 789, August 1971.

59. Elder, J., The Dispersion of a Marked Fluid in Turbulent Shear Flow, Journal of Fluid Mechanics, 5-4, 554, May 1959.

60. Holley, E., Harleman, D., and H. Fischer, Dispersion in Homogeneous Estuary Flow, ASCE Journal, HYD, 1691, August 1970.

61. Leendertse, J. J., A Water Quality Simulation Model for Well Mixed Estuaries and Coastal Seas: Volume I, Principles of Computations, RM-6230-RL, Santa Monica, California, February 1970.

62. Pritchard, D., "The Movement and Mixing of Contaminants in Tidal Estuaries, Proceedings, First International Conference on Waste Disposal in the Marine Environment, E. A. Pearson, Ed., 1970.

63. Lang muir, I., Surface Motion of Water Induced by Wind. Science, 87, 119, 1938.

64. Scott, J. T., Meyer, G. E., Stewart, R., and E. G. Walther, On the Mechansims of Langmuir Circulations and Their Role in Epilimnion Mixing. Limmol. Oceanog., 14: 493-503.

65. Faller, A. J., The Generation of Langmuir Circulations by the Eddy Pressures of Surface Waves. Limnol. and Oceanog. 14, 504-513.

66. Faller, A. J., Oceanic Mixing and the Langmuir Circulations" Technical Note BN 863, Institute for Fluid Dynamics and Applied Mathematics. University of Maryland, College Park, March, 1971.

67. Murray, S. T., Settling Velocities and Vertical Diffusion of Particles in Turbulent Water, Journal of Geophysical Research, Vol. 75, No. 9 March, 1970.

68. Quesada, A. F., and M. A. MacLeod, The Determination of Diffusion Coefficients in Shearing Flow by Chemical Tracer Techniques. Proc. Symp. Air Pollution, Turbulence and Diffusion, pp. 384-391, New Mexico, 1972.

69. Carter, H. H. and A. Okubo, A Study of the Physical Processes of Movement and Dispersion in the Cape Kennedy Area. Final Report, U. S. Atomic Energy Comm. Contract No. AT(30-2)-2973

70. Okubo, A., and M. J. Karwiet, Diffusion From a Continuous Source In A Uniform Shear Flow, Contribution 139 of the Chesapeake Bay Institute and Department of Earth and Planetary Sciences, John Hopkins University, NYO-3109-41, 1971.

71. Wnek , W. J. and E. G. Fochtman, Mathematical Model For Fate of Pollutants in Near-Shore Waters, Environmental Science and Technology, Vol. 6, No. 4, April 1972.

72. Cleary, R. W. and D. D. Adrian, Journal of the Environmental Engineering Division, ASCE Vol. 99, No. EE3, June 1973.

73. Dobbins, W. E., Effect of Turbulence on Sedimentation, Am. Soc. Civil Engineers Trans., Vol. 109, pp. 629-678.

74. Gordon, R., "Field Investigations at the Durvanish Water Way Site, Eliot Bay, Puget Sound, Washington", Dredged Material New-Notes-Reviews, Vol. D-76-4, August 1976.

75. Cook, G. S., "Non Tidal Circulation in Rhode Island Sound," Naval Underwater Weapons Research and Engineering Station, TM, No. 369, 1966.

76. Shunting, D. H., "Rhode Island Sound Square Kilometer Study 1967: Flow Patterns and Kinetic Energy Distribution", Journal of Geophysical Research, 74:13, 1967.

77. Hurlbut, S. and M. Spaulding, "Dispersion of Dredged Waste Plume at Brown's Ledge Site: Non Published Report Submitted to Clement Griscom, Division of Marine Resources, Ocean Engineering Department, University of Rhode Island, January 1976.

78. Shields, A., "Application of Similarity Principles and Turbulence Research To Bed Load Movement, Mitteil ungen der Preuss. Vers uchsanst. Fur Wasserbau and Schiffbau, Berlin, No. 26,1936.

APPENDIX A

Derivation of transformation identities (36)

$$\frac{\partial}{\partial x} = \frac{\partial}{\partial x}\Big)_{y,z,t} \qquad \frac{\delta}{\delta x} = \frac{\delta}{\delta x}\Big)_{y,\eta,t} \tag{A.1}$$

$$\frac{\delta A}{\delta c} = \frac{\partial A}{\partial c} + \frac{\partial A}{\partial z}\frac{\delta z}{\delta c} = \frac{\partial A}{\partial c} + \frac{\partial \eta}{\partial z}\frac{\delta z}{\delta c} + \frac{\partial A}{\partial \eta} \tag{A.2}$$

since

$$\frac{\partial A}{\partial z} = \frac{\partial \eta}{\partial z}\frac{\partial A}{\partial \eta} \tag{A.3}$$

Substituting for c, we define the derivative of A with respect to x, y, η, t in the x, y, η coordinate system as follows:

$$\frac{\delta A}{\delta t} = \frac{\partial A}{\partial t} + \frac{\delta \eta}{\delta z}\frac{\delta z}{\delta t}\frac{\partial A}{\partial \eta} \quad \text{from A.2} \tag{A.4}$$

define

$$\eta(x, y, z, t) = \frac{z - \xi(x,y,t)}{H(x, y, t)} \tag{A.5}$$

where

$$H(x, y, t) = \xi(x, y, t) + h(x, y) \tag{A.6}$$

$$\frac{\delta \eta}{\delta z} = \frac{\delta}{\delta z}\left[\frac{z - \xi}{H}\right] = \frac{1}{H} \tag{A.7}$$

$$\frac{\partial z}{\partial t} = \frac{\delta}{\delta t}\left[\eta H + \xi\right] = \frac{\delta}{\delta t}\left[(\eta + 1)\xi + \eta h\right] = (\eta + 1)\frac{\delta \xi}{\delta t} \tag{A.8}$$

APPENDIX A -- CONTINUED

so

$$\frac{\delta A}{\delta t} = \frac{\partial A}{\partial t} + \frac{1}{H}\left[(\eta + 1)\frac{\delta \xi}{\delta t}\right]\frac{\partial A}{\partial \eta} \qquad (A.9)$$

From A.2 for X-transformation

$$\frac{\delta A}{\delta x} = \frac{\partial A}{\partial x} + \frac{\delta \eta}{\delta z}\frac{\delta z}{\delta x}\frac{\partial A}{\partial \eta} \qquad (A.10)$$

$$\frac{\delta A}{\delta x} = \frac{\partial A}{\partial x} + \frac{1}{H}\left[(\eta + 1)\frac{\delta \xi}{\delta x} + \eta \frac{\delta h}{\delta x}\right]\frac{\partial A}{\partial \eta} \qquad (A.11)$$

Similiarly for Y-transformation

$$\frac{\delta A}{\delta y} = \frac{\partial A}{\partial y} + \frac{1}{H}\left[(\eta + 1)\frac{\delta \xi}{\delta y} + \eta \frac{\delta h}{\delta y}\right]\frac{\partial A}{\partial \eta} \qquad (A.12)$$

For z-term Transformation

$$\frac{\partial A}{\partial z} = \frac{\delta \eta}{\partial z}\frac{\partial A}{\partial \eta} = \frac{\partial}{\partial z}\left[\frac{z - \xi}{H}\right]\frac{\partial A}{\partial \eta} = \frac{1}{H}\frac{\partial A}{\partial \eta} \qquad (A.13)$$

so

$$\frac{\partial A}{\partial z} = \frac{1}{H}\frac{\partial A}{\partial \eta} \qquad (A.14)$$

APPENDIX B

VERTICAL TRANSFORMATION OF MASS TRANSPORT EQUATION

The transformation of the cartesian three dimensional mass transport equation may be accomplished using the transformation identities A. 9, 11, 12, 14 after Gordon (36). For convenience, the 3-D mass transport equation will be divided into seven (7) terms,

$$\underset{(a)}{\frac{\partial c}{\partial t}} + \underset{(b)}{U\frac{\partial c}{\partial x}} + \underset{(c)}{V\frac{\partial c}{\partial y}} + \underset{(d)}{W\frac{\partial c}{\partial z}} - \underset{(e)}{\frac{\partial}{\partial x}\left(K_x \frac{\partial c}{\partial x}\right)} - \underset{(f)}{\frac{\partial}{\partial y}\left(K_y \frac{\partial c}{\partial z}\right)} - \underset{(g)}{\frac{\partial}{\partial z}\left(K_z \frac{\partial c}{\partial z}\right)} = 0 \tag{B.1}$$

each term being transformed separately.

$$\frac{\partial c}{\partial t} = \frac{\delta c}{\delta t} \quad \frac{1}{H}\left[(\eta + 1)\frac{\delta \xi}{\delta t}\right]\frac{\partial c}{\partial \eta} \tag{B.2}$$

$$U\frac{\partial c}{\partial x} = U\left[\frac{\delta c}{\delta x} - \frac{1}{H}\left[(1+\eta)\frac{\delta \xi}{\delta x} + \eta\frac{\delta h}{\delta x}\right]\frac{\partial c}{\partial \eta}\right] \tag{B.3}$$

$$V\frac{\partial c}{\partial y} = V\left[\frac{\delta c}{\delta y} - \frac{1}{H}\left[(1+\eta)\right]\frac{\delta \xi}{\delta y} + \eta\frac{\delta h}{\delta y}\right]\frac{\partial c}{\partial \eta}\right] \tag{B.4}$$

Consider the total time derivative

$$\frac{d}{dt} = \frac{\partial}{\partial t} + U\frac{\partial}{\partial x} + V\frac{\partial}{\partial y} + W\frac{\partial}{\partial z} \tag{B.5}$$

Transforming this

$$\frac{d}{dt} = \frac{\delta}{\delta t} + U\frac{\delta}{\delta x} + V\frac{\delta}{\delta y} + \frac{W}{H}\frac{\partial}{\partial \eta} - \frac{1}{H}\cdot\left(\frac{\partial z}{\partial t} - U\frac{\partial z}{\partial x} + V\frac{\partial z}{\partial y}\right)\frac{\partial}{\partial \eta} \tag{B.6}$$

Defining a dimensionless vertical velocity

$$\omega = \frac{W}{H} - \frac{1}{H}\left(\frac{\partial z}{\partial t} + U\frac{\partial z}{\partial x} + V\frac{\partial z}{\partial y}\right) \tag{B.7}$$

APPENDIX B - EQUATIONS - CONTINUED

Thus

$$W = \omega H + \left(\frac{\partial z}{\partial t} + U \frac{\partial z}{\partial x} + V \frac{\partial z}{\partial y} \right) \tag{B.8}$$

$$w \frac{\partial c}{\partial z} = \left[\omega H + \left(\frac{\partial z}{\partial t} + U \frac{\partial z}{\partial x} + V \frac{\partial z}{\partial y} \right) \right] \frac{1}{H} \frac{\partial c}{\partial \eta} \tag{B.9}$$

$$\frac{\partial}{\partial x} \left[K_x \frac{dc}{\partial x} \right] = \frac{\delta}{\delta x} \left[K_x \left[\frac{\delta c}{\delta x} - \frac{1}{H} \left[1 + \eta \right] \frac{\delta \xi}{\delta x} + \eta \frac{\delta h}{\delta x} \right] \frac{\partial c}{\partial \eta} \right] \tag{B.10}$$

$$+ \text{H. O. T.}_x \quad (0)$$

$$\frac{\partial}{\partial y} \left[K_y \frac{\partial c}{\partial y} \right] = \frac{\delta}{\delta y} \left[K_y \left[\frac{\delta c}{\delta y} - \frac{1}{H} \left[1 + \eta \right] \frac{\delta \xi}{\delta y} + \eta \frac{\delta h}{\delta y} \right] \frac{\partial c}{\partial \eta} \right] \tag{B.11}$$

$$+ \text{H. O. T.}_y \quad (0)$$

$$\frac{\partial}{\partial z} \left[K_z \frac{\partial c}{\partial z} \right] = \frac{\partial}{\partial \eta} \frac{K_z}{H^2} \frac{\partial c}{\partial \eta} \tag{B.12}$$

Now the transformed terms in each dimension will be rearranged in each dimension.

[x - terms] - B. 3 without $U \frac{\partial c}{\partial \eta}$ term and B. 10

$$U \frac{\delta c}{\delta x} - \frac{\delta}{\delta x} \left[K_x \left[\frac{\delta c}{\delta x} - \frac{1}{H} \left[1 + \eta \right] \frac{\delta \xi}{\delta x} + \eta \frac{\delta h}{\delta x} \right] \frac{\partial c}{\partial \eta} \right] \tag{B.13}$$

assuming incompressibility expression B.13 may be rearranged as

APPENDIX B - EQUATIONS - CONTINUED

$$\frac{\delta}{\delta x}\left[\, U - \frac{K_x}{c}\left[\, \frac{\delta c}{\delta x} - \frac{1}{H}\left[1 + \eta\right]\frac{\delta \xi}{\delta x} + \eta\,\frac{\delta h}{\delta x}\,\right]\frac{\partial c}{\partial \eta}\,\right] c \qquad \text{(B.14)}$$

or

$$\frac{\delta}{\delta x}\,(U_T c) \qquad \text{where} \qquad \text{(B.15)}$$

$$U_T = U - \frac{K_x}{c}\left[\, \frac{\delta c}{\delta x} - \frac{1}{H}\left[1 + \eta\right]\frac{\delta \xi}{\delta x} + \eta\,\frac{\delta h}{\delta x}\,\right]\frac{\partial c}{\partial \eta} \qquad \text{(B.16)}$$

[y-Terms] Similarly

$$V_T = V - \frac{K_y}{c}\left[\, \frac{\delta c}{\delta y} - \frac{1}{H}\left[1 + \eta\right]\frac{\delta \xi}{\delta y} + \eta\,\frac{\delta h}{\delta y}\,\right]\frac{\partial c}{\partial \eta} \qquad \text{(B.17)}$$

and

$$\frac{\delta}{\delta y}\,(V_T\, c) \qquad \text{(B.18)}$$

[η - Terms]

Combining $\frac{\partial c}{\partial \eta}$ terms of B. 2, 3, 4 with B.9

Assuming

$$\frac{\partial \xi}{\partial t},\ \frac{\partial z}{\partial t},\ \frac{\partial z}{\partial x},\ \frac{\partial z}{\partial y},\ \frac{\delta \xi}{\partial x},\ \frac{\delta \xi}{\partial y} \ll \frac{\partial h}{\partial x}, \frac{\partial h}{\partial y}$$

with some rearrangement

$$\frac{\partial}{\partial \eta}\left[\, \omega - \frac{K_z}{H^2 c}\,\frac{\partial c}{\partial \eta} - \frac{\eta}{H}\left[U\,\frac{\delta h}{\delta x} - V\,\frac{\delta h}{\delta y}\,\right]\,\right] c \qquad \text{(B.19)}$$

which is equivalent to

$$\frac{\delta}{\delta \eta}\,\left[\omega_T\, c\right] \qquad \text{(B.20)}$$

$$\omega_T = \omega - \frac{K_z}{H^2 c} \cdot \frac{c}{\eta} - \frac{\eta}{H} \left[U \frac{\delta h}{\delta x} + V \frac{\delta h}{\delta y} \right] \qquad (B.21)$$

[T Terms]

$$\frac{c}{t} = \frac{\delta c}{\delta t} \qquad (B.22)$$

Combining B.15, 17, 20, 21

$$\frac{\delta c}{\delta t} + \frac{\delta}{\delta x} [U_T c] + \frac{\delta}{\delta y} [W_T c] + \frac{}{\eta} [\omega_T c] = 0 \qquad (B.23)$$

where U_T, V_T, and ω_T are defined by B.16, 18, and 20.

B.22 represents the vertically transformed total pseudo velocity form of the three dimensional mass transport equation.

VERTICAL TRANSFORMATION OF PARTICLE SETTLING VELOCITIES

Now that the vertical coordinate has been transformed into dimensionless η-space, the characteristic velocity has units of T^{-1} where

$$\frac{D\eta}{Dt} = \omega$$

Particle settling velocities must also be transformed using B.2

$$W_s = \omega_s H + \left(\frac{\partial z}{\partial t} + U\frac{\partial z}{\partial x} + V\frac{\partial z}{\partial y}\right)$$

ω_s = transformed vertical settling rate

assuming $\frac{\partial h}{\partial t}, \frac{\partial \eta}{\partial t}, \frac{\delta \xi}{\delta x}, \frac{\delta \xi}{\delta y}, \frac{\delta \xi}{\delta t} \rightarrow 0$

$$\omega_s = \frac{1}{H}\left[W_s - \left[(\eta + 1)\frac{\delta \xi}{\delta t} + U\left[(\eta + 1)\frac{\delta \xi}{\delta x} + \eta\frac{\delta h}{\delta x}\right]\right.\right. \qquad (B.24)$$

$$\left.\left. + V\left[(\eta + 1)\frac{\delta \xi}{\delta y} + \eta\frac{\delta h}{\delta y}\right]\right]\right]$$